Dynamic assembly, disassembly and bundling of the bacterial cell division protein FtsZ and YgfE (ZapA)

By

Xi Cheng (BSc, MSc)

A thesis submitted in partial fulfilment of the requirements for the degree of

Doctor of Philosophy in Chemistry

University of Warwick, Department of Chemistry

December 2011

Table of Contents

Acknowledgements

First, I am deeply indebted to my supervisors, Professor Alison Rodger, in Chemistry, Dr. Matthew Hicks, who is the former Senior Research Fellow in Chemistry and Dr. David Roper, in Biological Science. Their support, guidance and encouragement from the initial to the final level enabled me to develop an understanding of this project.

This project would not have been possible without the help from many other people. I wish to thank Dr. Tim Dafforn from Birmingham University. He has given ideas to this project and also allowed me to work in his group. At Birmingham University I performed the analytical ultracentrifugation and sedimentation assay, especially under the help of Ms. Rosemary Parslow and Dr. Yu-pin Lin.

I must not forget to thank Dr. James Covington and his PhD student Max Joseph who build the fantastic flow cell. Dr. Corinne Smith and Mr. Ian Portman in the imaging suite in Biological Sciences deserve a sincere thanks for their help with the electron microscope.

All my past and present lab buddies in the Biophysical Chemistry and Structural Biology, made it a convivial place to work. They inspired me in research and life through our interactions during the long hours in the lab. In particular, I would like to thank Dr. Raul Pacheco-Gomez, who spent much time in helping me to start this project when he was about to leave Warwick. I would also like to thank all the friends that I have made in UK for giving me company and encouragement when I was lonely, especially to Zijin Li, Yanzi Gou, and Yao Zhao.

My deepest gratitude goes to my parents, Minheng Cheng and Hongying Zhu, for their everlasting love and support throughout my life, especially to my research abroad. I owe my loving thanks to my boyfriend, now husband, Qian Dong, who has left China to join me in UK, and brought me more happiness since the beginning of my final year. Without him, it would have been certainly much harder to finish a PhD.

Declaration

I hereby declare that the research submitted in this thesis was conducted by myself under the supervision of Professor Alison Rodger at the Department of Chemistry, University of Warwick.

No part of this work has previously been submitted to be considered for a degree or other qualification. All sources of information have been specifically acknowledged in the form of references.

Some material contained within this thesis has been submitted for publication and a copy of the paper is bound at the end of the thesis:

Cheng, X., R. Pacheco-Gomez, M. R. Hicks, C. J. I. Smith, D. Roper, S. Addinal, A. Rodger, T. R. Dafforn "Tetramerisation of ZapA is required for FtsZ bundling." *Biochem. J.* submitted.

Abstract

The protein FtsZ is a tubulin-like GTPase, which plays an essential role in prokaryotic cell division. *In vivo* it assembles into a dynamic ring (the Z-ring) at the future site of cell division on the inner surface of the cytoplasmatic membrane. The Z-ring then serves as a scaffold which recruits all other division proteins to form the cytokinetic machinery. The constriction of the ring facilitates the separation of two daughter cells.

In vitro, FtsZ polymerizes in the presence of GTP to form single-stranded protofilaments. It is assumed that FtsZ association and assembly reactions studied *in vitro* will play an important role in understanding the mechanism of Z-ring assembly and disassembly *in vivo*. In this work, we therefore have studied the dynamics of FtsZ polymerization *in vitro,* especially the bundling induced with YgfE.

YgfE, the putative *Escherichia coli* ZapA orthologue, is one of these division proteins recruited by FtsZ. It acts to enhance lateral associations between FtsZ fibres to form larger bundles. In this study, we have demonstrated that YgfE exists as a tetramer in solution at the concentrations reported in this study, and the bundling activity is exerted more efficiently on preformed FtsZ protofilaments. We also investigate the importance of the tetramerisation of YgfE on function. A number of mutant forms of ZapA were generated with the aim of disrupting the dimer:dimer interface. Using those mutants we show that tetramerisation is a requirement for both FtsZ bundling, and GTPase modulation activities.

In addition, a novel technique, continuous channel flow linear dichroism (LD) spectroscopy, has been first developed in this work. LD is a simple spectroscopy technique for structural characterization of long biomacromolecules in solutions. Continuous channel flow Flow LD has overcome the limitation of Couette flow LD due to the time required to assemble and fill the cell.

List of Abbreviations

Abbreviation	Meaning
A_{xxx}	absorbance at wavelength xxx nm
AFM	atomic force microscopy
APS	ammonium persulfate
ATP	adenosine-5'-triphosphate
AUC	analytical ultracentrifugation
B. subtilis	*Bacillus subtilis*
C	Cytosine
CBB	Coomassie brilliant blue
CD	circular dichroism
ct	calf thymus
DAPI	4',6-diamidino- 2-phenylindole
DEAE	Diethylaminoethyl
DLS	dynamic light scattering
DNA	deoxyribonucleic acid
DNase I	deoxyribonuclease I
DTT	Dithiothreitol
EB	ethidium bromide
E. coli	*Escherichia coli*
EDTA	ethylenediaminetetraacetic acid
EM	electron microscopy
G	Guanine
GFP	green fluorescent protein
GDP	guanosine-5'-diphosphate
GTP	guanosine-5'-triphosphate

Continued on next page

Abbreviation	Meaning
GTP-γS	guanosine-5'-O-[gamma-thio]triphosphate
HEPES	N-(2-hydroxyethyl)piperazine-N'-(2-ethanesulfonic acid)
IMAC	immobilised metal affinity chromatography
IPTG	isopropyl-β-D-thiogalactopyranoside
ITC	isothermal titration calorimetry
kDa	kiloDalton
LD	linear dichroism
LB	Luria-Bertani broth
MES	2-morpholinoethanesulfonic acid
MESG	2-amino-6-mercapto-7-methylpurine/methylthioguanosine
MOPS	3-(N-morpholino)propanesulfonic acid
NMR	nuclear magnetic resonance
OD_{xxx}	optical density at wavelength xxx nm
PAGE	polyacrylamide gel electrophoresis
pH	$-\log_{10} [H^+]$
P_i	inorganic phosphate
PCS	photon correlation spectroscopy
PNP	purine nucleoside phosphorylase
RNA	ribonucleic acid
rpm	revolutions per minute
R.S.D.	relative standard deviations
SDS	sodium dodecyl sulphate
TEM	transmission electron microscopy
TEMED	N,N,N',N'-tetramethylethylenediamine
Tris	Tris (hydroxymethyl)aminomethane
U	unit

Continued on next page

Abbreviation	Meaning
UA	uranyl acetate
UV/Vis	ultra-violet/visible spectroscopy
v/v	volume to volume ratio
WT	wild type
w/v	weight to volume ratio
w/w	weight to weight ratio
β-ME	β-mercaptoethanol
×g	times the acceleration of gravity

Standard 3 and 1 letter amino acid abbreviations

Amino Acid	3 Letter Code	1 Letter Code
Alanine	Ala	A
Arginine	Arg	R
Asparagine	Asn	N
Aspartic Acid	Asp	D
Cysteine	Cys	C
Glutamine	Gln	Q
Glutamic Acid	Glu	E
Glycine	Gly	G
Histidine	His	H
Isoleucine	Ile	I
Leucine	Leu	L
Lysine	Lys	K
Methionine	Met	M
Phenylalanine	Phe	F
Proline	Pro	P
Serine	Ser	S
Threonine	Thr	T
Tryptophan	Trp	W
Tyrosine	Tyr	Y
Valine	Val	V

This thesis is dedicated to my father, Minheng Cheng

to my mother, Hongying Zhu

to my boyfriend now husband, Qian Dong

CHAPTER 1 – INTRODUCTION

FtsZ is an essential cell division protein in *Escherichia coli* (*E. coli*). In living bacteria, FtsZ forms a ringlike structure (Z-ring) at the cell midpoint. Cell division coincides with a gradual contraction of the Z-ring. The aim of the work reported in this thesis was to study the assembly of FtsZ, and the functions of YgfE (an accessory cell division protein) modulating the FtsZ assembly *in vitro*. Therefore a summary of the literature review that is relevant to the research is reported in this chapter.

1.1 Prokaryotic cell division and the discovery of FtsZ

The cell cycle, or cell-division cycle, is the series of events that takes place in an orderly sequence in a cell leading to its duplication (replication) and division. The cell division is a vital process by which all living things reproduce. In unicellular species, such as bacteria and yeasts, each cell division produces a complete new organism as a way of reproduction. In multicellular species, cell division allows the organism to grow and develop by expanding the total number of cells, to repair and replace injured or worn-out cells, and in some cases, to make specialized cells for reproduction.

Prokaryotes such as bacteria use a relatively simple form of cell division called binary fission. When the parent cell grows to an appropriate size, the chromosome is replicated so that two exact copies of the genetic material exist inside the parent cell. These two molecules of DNA are attached to the cell's plasma membrane. One strand is attached to the membrane at one end of the cell, and the other strand is attached to the opposite end. Growth of the cell and the completion of DNA replication are coordinated with the formation of a septum, or invagination, of the

cell membrane, growing across the middle of the cell, which eventually divides the cell into two.

In order to allow correct partitioning of the newly replicated chromosomes into two daughter cells, cytokinesis requires spatial, temporal and quantitative controls. Spatial control involves the identification of the midpoint of the cell where the septum will form. Temporal and quantitative controls ensure that newly replicated chromosomes are equipartitioned (Lutkenhaus and Addinall 1997).

Inroads into the process of cell division, as with many other complex biological processes, have relied on genetics (de Boer, Cook and Rothfield 1990). The pioneering work of Hirota and others identified *E. coli* genes essential for cell division by the isolation of temperature-sensitive mutants that form filaments at the non-permissive temperature (Hirota, Ryter and Jacob 1968). These mutations were designated *fts* for 'filamenting temperature sensitive'. The list of such genes includes *ftsA*, *ftsL*, *ftsI*, *ftsQ*, *ftsN*, *ftsW*, *ftsK*, and *ftsZ* (Lutkenhaus and Addinall 1997). Evidence that has accumulated over the past few years from studies with bacterial cells indicates that FtsZ protein (filamenting temperature sensitive mutant Z) encoded by the *ftsZ* gene plays an important role in driving prokaryotic cell division, and functioning these spatial, temporal and quantitative controls.

The understanding of the molecular details of bacterial cell division began with the visualization of *E. coli* FtsZ in a ring structure (Bi and Lutkenhaus 1991). Immuno-gold electron microscopy showed a ring of concentrated FtsZ near the membrane in cells that were about to divide. As division proceeded, the FtsZ ring constricted and remained at the tip of the invaginating membrane. Levin and Losick were the first to view localized FtsZ by immunofluorescence (Levin and Losick 1996). They observed in both *Bacillus subtilis* (*B. subtilis*) and *E. coli* that the FtsZ ring was assembled very early in the cell cycle. Green fluorescent protein (GFP) has emerged as a powerful complement to immunofluorescence in the past few years

(Erickson 1997). Ma *et al.* used an FtsZ-GFP chimera to demonstrate the localization of FtsZ in *E. coli* (Ma, Ehrhardt and Margolin 1996). Sun and Margolin monitored the dynamics and assembly of FtsZ during the division cycle of live *E. coli* cells in real time by microculture of a merodiploid strain expressing GFP-tagged FtsZ (Sun and Margolin 1998). Due to the emergence of immunofluorescence and GFP to direct viewing the subcellular structures, as well as other development of microbiological, molecular and spectroscopic techniques to study protein-protein interactions, the function of FtsZ protein during cell division is gradually becoming clearer.

Figure 1.1 shows the dynamic behaviour of FtsZ in the bacterium *E. coli* during the cell division cycle. When a cell reaches an appropriate size, chromosome replication begins, and the replication origins move towards the cell poles until both set of daughter chromosomes are segregated. Near the end of this process, roughly coinciding with nucleoid segregation, the formation of the FtsZ ring, or simply the Z-ring, begins (den Blaauwen et al. 1999, Harry, Rodwell and Wake 1999, Lin, Levin and Grossman 1997, Quardokus and Brun 2002, Regamey, Harry and Wake 2000). The FtsZ protein starts to assemble into the Z-ring at a single point on the inner face of the cytoplasmic membrane at the cell centre, marking the future division site. Then it rapidly extends bidirectionally to form an arc and then a closed circle (Addinall and Lutkenhaus 1996). The Z-ring also serves as the scaffold to recruit at least ten other cell division proteins to assemble the cell-division machinery, including synthesizing the division septum (Margolin 2000, Rothfield, Justice and Garcia-Lara 1999, Weiss 2004). Although the ring maintains its shape and size for a large portion of the cell cycle (Weart and Levin 2003, den Blaauwen et al. 1999), individual FtsZ molecules in the ring are rapidly exchanged with cytoplasmic FtsZ (Stricker et al. 2002). When an unknown signal triggers cytokinesis, the Z-ring decreases in diameter at the leading edge of the septum, and contracts along with the cytoplasmic membrane (Addinall, Bi and Lutkenhaus 1996, Bi and Lutkenhaus 1991, Levin and Losick 1996). By the end of the septation

process the Z-ring has disassembled (Stricker et al. 2002), which result in the production of two separate newborn daughter cells.

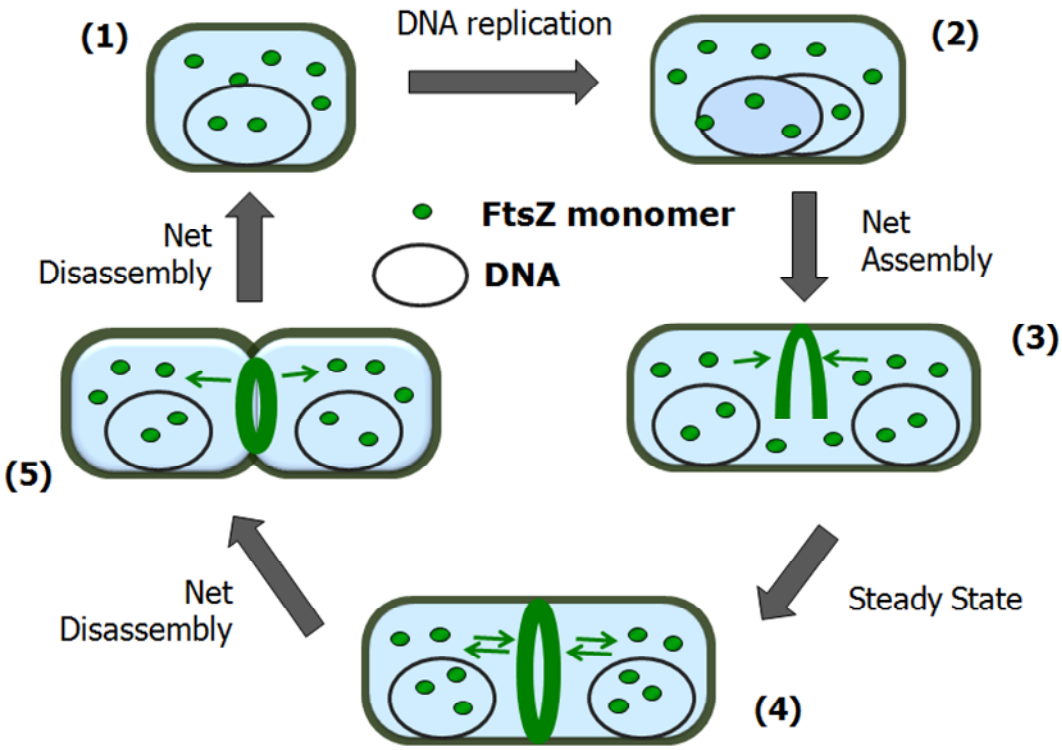

Figure 1.1 Dynamic behaviour of FtsZ in the bacterium *E. coli* during the cell division cycle. In step (1), newborn cells grown at low growth rates, contain a single chromosome in a structure known as a nucleoid. When the cell reaches an appropriate size, chromosome replication begins, and the replication origins move towards the cell poles until both daughter chromosomes are segregated (step (2)). Near the end of this process, the FtsZ protein starts to assemble into the Z-ring (green ring) on the inner face of the cytoplasmic membrane at the cell centre, marking the future division site (step (3)). In step (4), the Z-ring remains steady state, and recruits at least ten other proteins to assemble the cell-division machinery, which also synthesizes the division septum. During division (step (5)), contraction of the Z-ring and constriction of the outer membrane follow. The Z-ring decreases in diameter at the leading edge of the septum, which result in the production of two separate newborn daughter cells. Small green arrows indicate the assembly and disassembly of FtsZ subunits (Modified from (Lutkenhaus and Addinall 1997, Romberg and Levin 2003, Margolin 2005)).

There is thought to be a strong correlation between the Z-ring behaviour and the cell cycle succession. During different stages of the cell cycle, FtsZ exhibits a series of different behaviours: assembly to form the Z-ring at the mid-point of the cell, maintenance of the ring through continual subunit turnover, and constriction and disassembly of the ring. Small changes in FtsZ polymerization dynamics are able to trigger large and rapid changes in the whole cell division process. Thus FtsZ is the most comprehensively studied cell division protein in bacteria, and the study of dynamic assembly of FtsZ is fundamental to the regulation of bacterial cell division (Mukherjee and Lutkenhaus 1994, Erickson *et al*. 1996, Erickson 1995). Besides, FtsZ is thought to be an important new target for antibiotics. Specific inhibitors of FtsZ, the small synthetic antibacterials exemplified by PC190723, were found recently to protect against a lethal dose of *Staphylococcus aureus* in a mouse model of infection (Haydon et al. 2008).

1.2 Biochemical characterisation of FtsZ protein

Z-ring initiation, maintenance, and constriction are regulated, at least in part, by the modulation of FtsZ-assembly dynamics. Understanding FtsZ behavior *in vivo* will require the detailed analysis of FtsZ polymerization/depolymerization and structure *in vitro*.

1.2.1 Conservation of FtsZ

FtsZ is a 37- to 43-kDa protein, composed of between 352 and 383 amino acids. FtsZ is widely present in most of the major groups of bacteria and the auryarchaeal branch of the archaea. To date only one phylum of archaebacteria (*Crenarchaeota*) and three free-living species of bacteria (*Ureaplasma urealyticum*, *Prosthecobacter dejongii*, and *Pirellula sp.*) have been found to lack ftsZ genes (Vaughan *et al*. 2004, Glockner *et al*. 2003). In addition, eukaryotic organelles such as chloroplasts and some mitochondria also use FtsZ to divide (Gilson and Beech 2001, Osteryoung

2001, Rothfield et al. 1999, Margolin 2000). Elucidating the mechanism by which the Z-ring drives constriction is, therefore, critical to our understanding of cell division in prokaryotes and cytokinesis in eukaryotic organelles.

1.2.2 FtsZ is a homologue of tubulin

It was discovered in 1993–1995 that FtsZ was a bacterial homologue of eukaryotic tubulin, based both on a low degree of sequence identity (~10%) and a striking structural similarity (Erickson 1998, Erickson 1997). This possibility was first suggested by a short segment of its amino acid sequence in a glycine-rich loop, GGGTGTG, which is virtually identical to the tubulin signature motif, GGGTGSG (de Boer, Crossley and Rothfield 1992, Mukherjee, Dai and Lutkenhaus 1993, Lutkenhaus 1993, Raychaudhuri and Park 1992). A more extensive sequence alignment was presented by Mukherjee and Lutkenhaus, who identified a dozen additional completely conserved residues between all tubulins and FtsZ (Mukherjee and Lutkenhaus 1994). Despite the low level of sequence similarity, the tertiary structure of FtsZ is remarkably similar to that of tubulin, supporting the theory that these proteins have common ancestry (Erickson 1995, Löwe and Amos 1998, Nogales, Wolf and Downing 1998b, de Pereda et al. 1996).

1.2.3 FtsZ structures

The FtsZ subunit

Like tubulin, FtsZ binds and hydrolyses GTP (Mukherjee et al. 1993, de Boer et al. 1992, Raychaudhuri and Park 1992). FtsZ has strikingly similar protein folds and GTP-binding interactions to tubulin (Nogales et al. 1998a, Löwe and Amos 1998).

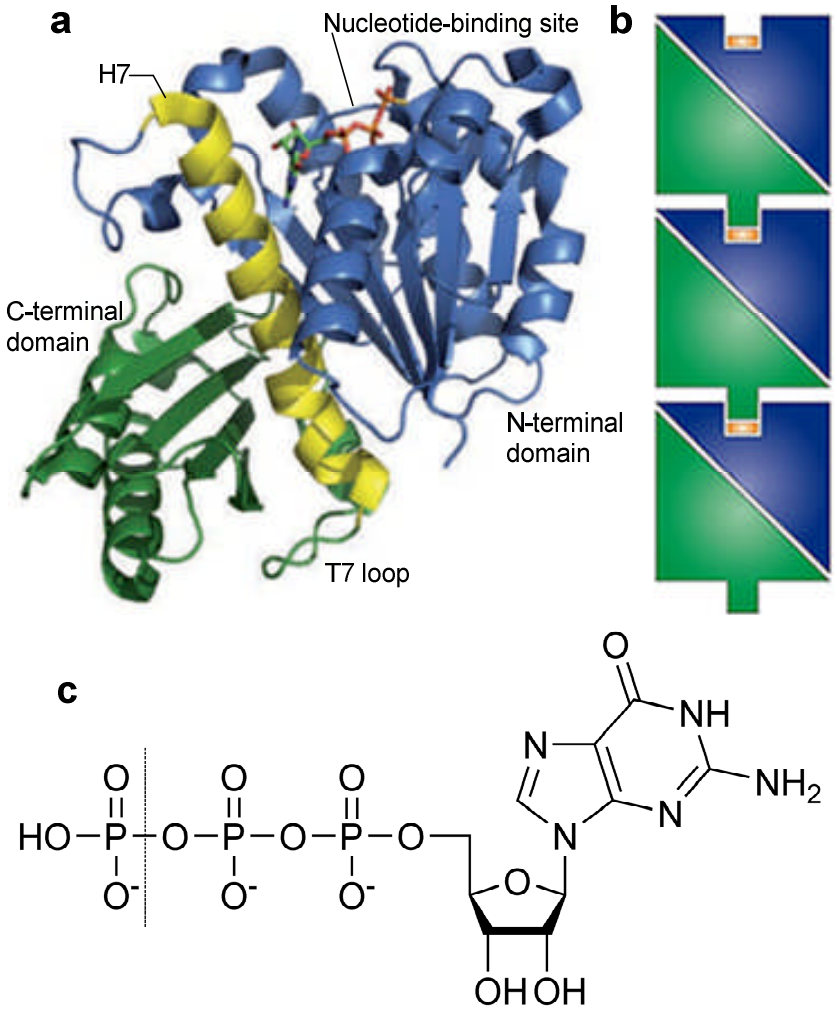

Figure 1.2.3 A model of forming FtsZ protofilament. (a) The crystal structure of a *B. subtilis* FtsZ monomer bound to GTP-γS (Protein Data Bank entry 2RHO). FtsZ comprises two globular domains that fold independently, separated by a central core helix, H7. The amino-terminal domain contains the tubulin signature motif, GGGTGTG, and forms the nucleotide-binding site. At the base of the carboxy-terminal domain, following H7, is the catalytic T7 or synergy loop. The extreme C-terminal tail, which is essential for interactions with other membrane-associated cell division proteins, is not visible in the crystal structure. (b) Similar to tubulin, FtsZ polymerizes into the head-to-tail linear protofilaments of individual subunits, shown in blue and green. Insertion of the T7 loop into the other subunit's nucleotide-binding site (orange) places two catalytic aspartate residues in the vicinity of the FtsZ γ-phosphate; these aspartate residues are thought to activate the GTPase activity of FtsZ by polarizing an attacking water molecule. (c) The chemical structure of GTP, in which the dashed line indicates where the γ-phosphate is cleaved. (Adams and Errington 2009).

The crystal structure of a *B. subtilis* FtsZ monomer (figure 1.2.3 a) shows that FtsZ comprises two globular domains that fold independently, separated by a central core helix, H7 (Adams and Errington 2009, Raymond et al. 2009, Oliva, Trambaiolo and Löwe 2007). The amino-terminal globular domain binds the bottom portion of the adjacent monomer in the protofilament, whereas the carboxy-terminal globular domain binds the top portion of the adjacent monomer in the protofilament. The GTP binding site, the amino acids that are best conserved between FtsZ and tubulin, is in N-terminal domain. At the base of the C-terminal domain, is the catalytic T7 or synergy loop. The extreme C-terminal (last 12 amino acids) is not required for assembly, but is essential for interactions with other membrane-associated cell division proteins, including FtsA and ZipA (Margolin 2005). Deletion of the C-terminal peptide blocks FtsZ function, probably by preventing its interaction with both ZipA and FtsA and hence the membrane (Ma and Margolin 1999).

The FtsZ polymers

Under standard assembly conditions and low FtsZ concentrations, GTP binding induces FtsZ self-assembly into the head-to-tail linear protofilaments of individual subunits, which resemble structures formed by tubulin (Oliva, Cordell and Löwe 2004, Mukherjee and Lutkenhaus 1994, Erickson et al. 1996, Löwe and Amos 1999, Erickson and Stoffler 1996, Romberg, Simon and Erickson 2001). It was noted that the protofilament spacing of approximately 42 Å is close to the 40 Å spacing in tubulin microtubules. The FtsZ T7 loop or synergy loop was thought to insert into the nucleotide-binding site of the other FtsZ subunit, thus placing the catalytic residues close to the γ-phosphate, thereby allowing nucleotide hydrolysis to proceed (Oliva et al. 2004, Scheffers et al. 2001, Adams and Errington 2009) (figure 1.2.3 b). The GTPase activity of FtsZ therefore depends on FtsZ polymerization (Scheffers et al. 2002).

Depending on the experimental conditions, FtsZ *in vitro* displays cooperative assembly (Romberg et al. 2001, Caplan and Erickson 2003, Chen et al. 2005, Wang

and Lutkenhaus 1993, Romberg and Mitchison 2004, Mukherjee and Lutkenhaus 1998) into a range of polymeric forms, from single-stranded protofilaments to mini rings, bundles, tubules and sheets (Mukherjee and Lutkenhaus 1994, Erickson et al. 1996, Bramhill and Thompson 1994, Popp et al. 2009). The Z-ring seen by light microscopy was thought to be 2–3 or 6–9 protofilaments thick, depending on the species and strain (Anderson, Gueiros-Filho and Erickson 2004, Chen and Erickson 2005), but how these protofilaments are associated with each other is unclear. It is likely that FtsZ protofilaments associating laterally to form bundles is important *in vivo* for the function of Z-ring (Margolin 2005). Cryo-electron microscopy tomography of *Caulobacter crescentus* cells suggests that the Z-ring *in vivo* might consists of a large number of short, overlapping protofilaments, rather than forming a continuous ring (Li et al. 2007). Recently, it has been proposed that FtsZ protofilament bundles seem to involve irregular weak association rather than a regular pattern of specific lateral bonds (Erickson 2009). In addition, electron microscopy and atomic force microscopy (AFM) show that the distances between pairs of protofilaments fluctuate under different conditions, and that their interaction is more of a loose association, suggesting that the lateral interactions between protofilaments are weak, plastic and heterogeneous (Mingorance et al. 2010, Mingorance et al. 2005, Sugimoto et al. 2010).

FtsZ bundling can be induced by several factors, such as macromolecular crowding (González *et al.* 2003), multivalent cations including DEAE dextran (Bramhill and Thompson 1994, Lu, Reedy and Erickson 2000), calcium (Lu et al. 2000, Mukherjee and Lutkenhaus 1999, Yu and Margolin 1997, Marrington et al. 2004b), and magnesium (Mukherjee and Lutkenhaus 1999, White et al. 2000, Marrington et al. 2004b), as well as cross-linking by other accessory cell division proteins (*e.g.* ZipA, YgfE) (Raychaudhuri 1999).

1.2.4 Dynamic assembly of FtsZ

During the cell cycle, the Z-ring goes through phases of net assembly, steady state turnover, and net disassembly. To understand these processes, it is necessary to study the behavior of pure FtsZ polymers' dynamics *in vitro*. FtsZ polymers, like tubulin microtubules, are dynamic in nature owing to GTP hydrolysis. In contrast to tubulin, the subunits of FtsZ are constantly cycling in and out of the polymers (Dajkovic and Lutkenhaus 2006, Chen et al. 2005, Chen and Erickson 2005, Mukherjee and Lutkenhaus 1998). Turnover of the Z-ring appears to be powered by FtsZ's GTP hydrolysis activity (Stricker et al. 2002).

As is the case with tubulin, the initial assembly of single-stranded FtsZ protofilaments occurs above a critical concentration of protein in solution that is around 0.5–1 μM (Wang and Lutkenhaus 1993, Mukherjee and Lutkenhaus 1998, Chen and Erickson 2005, Dajkovic, Mukherjee and Lutkenhaus 2008b). The existence of of a critical concentration indicates that polymerization of FtsZ is a cooperative process, meaning that the addition of FtsZ subunits to a growing polymer occurs with a higher affinity than an initial nucleation reaction. Cooperative assembly of FtsZ helps to limit the number of Z-rings in a cell by making polymer addition to a ring that already exists more favorable than initiation of a new ring elsewhere (Romberg and Levin 2003). *In vivo,* only about 30% of cellular FtsZ is assembled into the ring (Stricker et al. 2002), while some FtsZ protofilaments have been observed as clear dimers (Oliva et al. 2003, Löwe and Amos 1999).

However, the presence of only one binding interface for a new monomer to attach to an existing protofilament indicates an isodesmic (noncooperative) assembly mechanism (Rivas et al. 2000, Romberg et al. 2001), as does the appearance of single FtsZ protofilaments in electron micrographs without bundling factors. This raises the question of how FtsZ assembly can be cooperative if the basic polymer is a single-stranded protofilament. One set of experimental data are accounted for by a

model of cooperative polymerization with a dimer nucleus (Chen et al. 2005). To obtain cooperativity, it was thought that dimerization of FtsZ leads to sufficient conformational change in the FtsZ so that the subsequent addition of subunits occurs with a higher affinity (Dajkovic and Lutkenhaus 2006). Another model suggests that cooperativity can be accounted for by isodesmic assembly followed by cyclization. FtsZ initially assembles isodesmically into a straight protofilament, but after reaching a certain length the protofilaments are able to contact each other, which would cause the formation of additional lateral bonds, resulting in cooperativity (Margolin 2005, González et al. 2005). These possibilities need to be further investigated.

In the presence of GTP, FtsZ polymerizing into straight protofilaments is extremely rapid and displays little lag *in vitro* (Mukherjee and Lutkenhaus 1998, Chen et al. 2005). FtsZ assembly might be driven by the affinity between GTP-bound FtsZ monomers. GTP is subsequently hydrolysed by the active site formed between the two associated FtsZ monomers (Sossong et al. 1999, Scheffers et al. 2002). Recent data indicate that the nucleotide-binding site in FtsZ is accessible to the cytoplasm, which is rich in GTP (Oliva et al. 2004).

GTP hydrolysis during assembly is probably therefore balanced by rapid exchange of the GDP for the abundant GTP within the cell, which is resistant to depolymerization (Romberg and Mitchison 2004). The kinetics of GTP hydrolysis changes when FtsZ bundles are stabilized by calcium or DEAE dextran (Lu, Stricker and Erickson 1998, Mukherjee and Lutkenhaus 1999, Yu and Margolin 1997, Mingorance et al. 2001). A GTP regeneration system that extends the polymer lifetime of FtsZ has also been studied (Small and Addinall 2003).

Once GTP is exhausted due to hydrolysis, FtsZ protofilaments disassemble (Mukherjee and Lutkenhaus 1998, Chen and Erickson 2005, Stricker et al. 2002, Anderson et al. 2004, Marrington et al. 2004b). In addition, nucleotide hydrolysis

has been proposed to provide the force for constriction, whereby a nucleotide-dependent transition of conformational change from a straight, GTP-bound polymer to a curved, GDP-bound polymer can transmit mechanical work to the membrane (Li et al. 2007, Lu et al. 2000). However, the mechanism of force generation in bacterial cell division is complicated and remains controversial. Osawa's demonstration that Z-rings can impact a force on a tubular membrane *in vitro* (Osawa, Anderson and Erickson 2008), combined with the observation of both straight and curved filaments in *vivo* (Li et al. 2007), reinforces the possibility of force generation through the straight to curved conformational change of FtsZ polymers. However, other computational modeling predicts that the Z-ring undergoes a condensation transition from a low density state to a high-density state and generates a sufficient contractile force to achieve division. FtsZ GTP hydrolysis facilitates monomer turnover during the condensation transition, but does not directly generate forces (Lan et al. 2009).

1.3 Proteins that modulate FtsZ assembly

FtsZ is thought to be the first protein to localize to the site of future division in bacteria (Bi and Lutkenhaus 1991) (§ 1.1). It then assembles into the Z-ring, whose constriction gives rise to two equal daughter cells. The Z-ring also recruits other accessory cell division proteins, all of which play an important role in the progression and completion of cytokinesis. The number and diversity of proteins that are known to interact directly with FtsZ has grown steadily over the past decade. Some of these proteins are essential for survival but many are not, and there is considerable functional overlap in the group. The similarity of the polymerization dynamics of FtsZ and tubulin has afforded valuable insights into how the regulatory proteins might modulate FtsZ polymerization.

The polymerization of FtsZ is regulated by the accessory cell division proteins. Changes in FtsZ polymer structure or GTPase activity can alter the balance between

assembly and disassembly. Positive-acting factors promote Z-ring formation and stabilize the ring by concentrating FtsZ at the membrane, cross-linking separate protofilaments or facilitating the formation of stabilizing lateral interactions, as well as by preventing the disassembly of the polymer by inhibiting nucleotide hydrolysis.

After an unknown signal triggers ring contraction and disassembly, the presence of high levels of inhibitor proteins might help to antagonize the ring-stabilizing proteins and tip the balance towards disassembly beside the stimulation of GTP hydrolysis, although none of those inhibitor proteins is essential for Z-ring contraction or disassembly. These negative-acting factors that disassemble or destabilize the FtsZ polymer might do so by directly counteracting the mechanisms used by positive-acting factors — that is, by stimulating GTPase activity, facilitating disassembly by sequestering monomers or inhibiting the formation of lateral interactions.

In addition, some inhibitors ensure that cell division takes place at the right place and the right time. Estimates of the number of FtsZ monomers per *E. coli* cell vary between 3200 (Rueda, Vicente and Mingorance 2003) and 15,000 (Lu et al. 1998). The total endogenous FtsZ in the cell is approximately 10 μM (Osawa and Erickson 2005), which is significantly higher than the critical concentration (~1 μM) that is needed for protofilament assembly *in vitro*. This indicates that assembly inhibitors can keep FtsZ from initial assembly by preventing nucleotide binding, sequestering individual monomers or capping growing polymers, except at the right time and place. One such important inhibitory system is the Min system, which consists of the MinC, MinD and Min E proteins in *E. coli* (Raskin and de Boer 1999b, Hu et al. 1999).

Below we describe those accessory division proteins as two categories: stabilizing proteins and destabilizing proteins.

1.3.1 Stabilizing proteins

An essential requirement for the formation of the Z-ring is the attachment of FtsZ to the membrane. Recently, the lipids in the bacterial cell membrane were also shown to play a role in directing the FtsZ assembly at a particular position, *i.e.*, in the middle of the cell (Mileykovskaya and Dowhan 2005, Kuchibhatla, Bellare and Panda 2011). However, FtsZ does not seem to have any direct affinity for the membrane (Errington, Daniel and Scheffers 2003, Li et al. 2007, Erickson 2001). In *E. coli*, two other proteins can help to do this: FtsA and ZipA. FtsZ polymers are attached to the membrane through interaction of the conserved C-terminal tail of FtsZ with FtsA and/or ZipA. Experiments with a temperature-sensitive mutation on FtsA and ZipA have shown that both are essential for cell division (Pichoff and Lutkenhaus 2002, Hale and de Boer 1997). When both proteins are removed, the Z-ring does not form (Hale and de Boer 1999, Pichoff and Lutkenhaus 2002).

FtsA: FtsA is widely conserved throughout the bacteria (Margolin 2000), and is attached to the membrane through a carboxy-terminal amphipathic helix (Pichoff and Lutkenhaus 2005). FtsA binds directly to FtsZ (Din et al. 1998, Hale, Rhee and de Boer 2000, Haney et al. 2001) and recruits other cell division proteins to the Z-ring (Margolin 2000). In both *E. coli* and *B. subtilis* the ratio of FtsZ to FtsA must be maintained within a narrow range approximately 5 to 1 for cells to divide (Feucht et al. 2001, Rueda et al. 2003).This is exemplified by the fact that the toxic overproduction of either protein can be counteracted by overproduction of the other (Dai and Lutkenhaus 1992). The ability of FtsA to modulate FtsZ polymer stability *in vitro* has not yet been directly examined.

ZipA: ZipA is anchored to the membrane by an N-terminal transmembrane domain (Ohashi et al. 2002). Like FtsA, ZipA is also required for recruitment of other proteins to the septal site (Hale and de Boer 1999, Liu, Mukherjee and Lutkenhaus

1999, Margolin 2000). *In vitro*, ZipA promotes the assembly of FtsZ into thick bundles and sheets of protofilaments that are aligned laterally (Hale et al. 2000, Raychaudhuri 1999). Although ZipA is essential in *E. coli*, it is not widely conserved outside the Gamma-proteobacteria, which suggests that its role has either been replaced or become redundant (Hale and de Boer 1997).

Following FtsA and ZipA, other known cell division proteins are recruited. Although individually these proteins are not required for Z-ring assembly, their various roles in modulating the polymerization of FtsZ mean that the combined loss of certain regulatory proteins often produces a synthetic lethal division phenotype, the lethality due to a combination of two non-lethal mutations.

ZapA: ZapA is the accessory cell division protein that is the focus of this project. ZapA was first found in *B. subtilis*, but is conserved in a wide range of bacteria (Gueiros-Filho and Losick 2002). It is a small protein of about 10 kDa. The molecule is about 100 Å long containing roughly 50% coiled-coil structures. The crystal structure of ZapA from *Pseudomonas aeruginosa* shows it to be an anti-parallel tetramer with four globular domains at opposite ends of the coiled-coil stalk (Low, Moncrieffe and Löwe 2004).

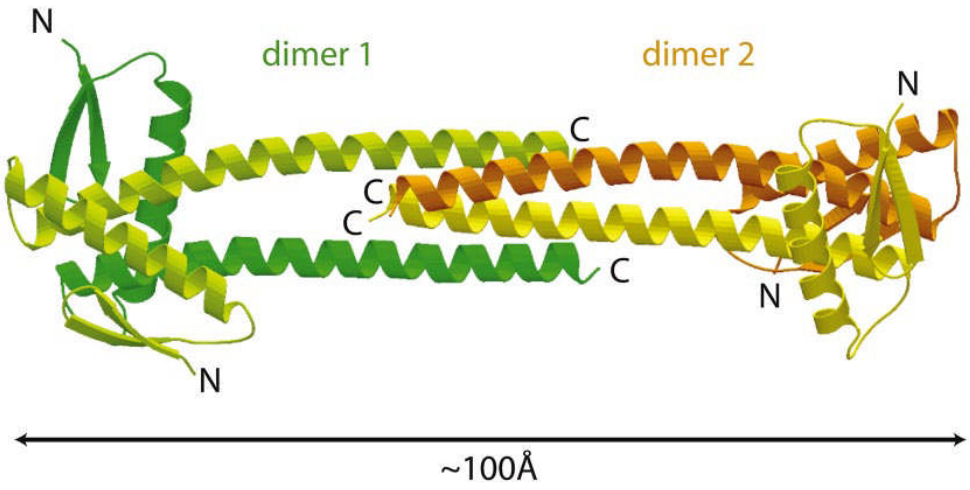

Figure 1.3.1 Crystal structure of ZapA from *Pseudomonas aeruginosa* (Löwe et al. 2004). Four molecules form a bone-like structure about 100 Å long.

In both *B. subtilis* and *E. coli*, ZapA is recruited to the divisome early. In *vitro*, ZapA binds directly with FtsZ and induces protofilaments to associate into large bundles, a property believed to be connected to its dimeric or tetrameric nature (Gueiros-Filho and Losick 2002, Small et al. 2007). The genetic experiments that originally identified ZapA (Gueiros-Filho and Losick 2002) suggest that *in vivo* this bundling activity may help stabilize Z-ring, though it is not known which parts of ZapA interact with FtsZ.

1.3.2 Destabilizing proteins

Min system: In *E. coli* and *B. subtilis* the best-characterized negative regulators of Z-ring assembly are the Min proteins, MinC, MinD, and MinE, which prevent the FtsZ ring forming anywhere in the cell except at the midcell. *In vivo*, the Min proteins have been found to form spatiotemporal patterns — the so-called Min oscillations (Pogliano 2008).

MinC, serves as an FtsZ inhibitor. It has two separate domains, each of which binds to FtsZ and promotes disassembly of FtsZ polymers and polymer bundles (Dajkovic et al. 2008a, Shen and Lutkenhaus 2009, Shiomi and Margolin 2007). MinD is an ATPase that binds to the membrane in its ATP form and is released from the membrane on ATP hydrolysis (Szeto et al. 2002, Hu, Gogol and Lutkenhaus 2002, Hayashi, Oyama and Morikawa 2001). MinD forms oligomers (Hu, Gogol and Lutkenhaus 2002, Suefuji, Valluzzi and RayChaudhuri 2002), and can form a complex with either MinC or MinE (Huang, Cao and Lutkenhaus 1996). Finally, MinE is a small protein, which is involved in preventing the formation of MinCD complexes in the middle of the cell. MinE forms a ring around the cell at the edge of the MinD zone (Raskin and de Boer 1999a, Raskin and de Boer 1997). It can bind to MinD and stimulates hydrolysis of its bound ATP in the presence of membranes. By doing so, MinE catalyzes the release of MinD from the membrane (Hsieh et al.

2010). As a result, MinD and MinE form zones that oscillate from one cell pole to the other. Because MinC binds to MinD, MinC oscillates in concert with MinD and therefore the concentration of the MinC inhibitor is lowest at mid-cell and highest at the poles, which directs FtsZ assembly at mid-cell and inhibits its assembly at the poles (Krebs, Goldstein and Kilpatrick 2009).

EzrA: EzrA is conserved throughout the low GC (G, guanine; C, cytosine) gram-positive bacteria, and has been identified as a negative regulator of Z-ring assembly (Levin, Kurtser and Grossman 1999). *In vitro*, it has been shown that EzrA inhibits FtsZ polymerization at two distinct levels (Levin et al. 1999, Haeusser et al. 2004, Chung et al. 2007): first, at the monomeric level, by reducing the affinity of FtsZ for GTP; and second, at the polymeric level, by increasing the rate of GTP hydrolysis, potentially by stabilizing the transition state of the hydrolysis reaction, and thereby promoting the disassembly of FtsZ polymers (Adams and Errington 2009).

SulA: SulA is a cell division inhibitor that becomes active under conditions of DNA damage (Huisman, D'Ari and Gottesman 1984, Huisman and D'Ari 1981), delaying cell division until chromosomes can be properly duplicated and partitioned. SulA both prevents the assembly of the Z-ring and facilitates the disassembly of existing Z-ring (Justice, Garcia-Lara and Rothfield 2000, Mukherjee, Cao and Lutkenhaus 1998, Bi and Lutkenhaus 1993). *In vitro* SulA binds directly to FtsZ and inhibits FtsZ assembly (Dajkovic et al. 2008b, Justice et al. 2000, Mukherjee et al. 1998, Cordell, Robinson and Löwe 2003, Higashitani, Higashitani and Horiuchi 1995, Trusca et al. 1998, Higashitani et al. 1997, Huang, Cao and Lutkenhaus 1996, Trusca and Bramhill 2002), as SulA significantly increases the critical concentration of FtsZ that is necessary for assembly without affecting its cooperative nature (Dajkovic et al. 2008b).

1.4 Aims of the project

1.4.1 The function of YgfE (ZapA) on FtsZ assembly

In the bacteria, cell division is regulated at the level of FtsZ assembly. The accessory cell division proteins affect the assembly, organization and stability of the Z-ring. However, how these proteins ensure the correct assembly of FtsZ into a Z-ring is unclear. The objective of the work presented here was to elucidate aspects of the mechanism by studying the interaction between FtsZ and three YgfE (ZapA) mutants *in vitro* with the long term goal of gaining a better understanding of the mechanism of cytokinesis for the majority of prokaryotes and some eukaryotic organelles. Besides, FtsZ is thought to be an important new target for antibiotics. There is now much emphasis on understading the mechanism of FtsZ polymerization, since inhibitors of this polymerization could constitute the new class of antibiotics.

1.4.2 Technical development for the study of FtsZ assembly dynamics

Some of the traditional techniques that have been used to study FtsZ assembly dynamics *in vitro* are summarized in this section. These techniques include right-angle light scattering, sedimentation (Bramhill and Thompson 1994), analytical ultracentrifugation (AUC) (Rivas et al. 2000, Sossong et al. 1999), electron microscopy (EM) (Bramhill and Thompson 1994, Erickson et al. 1996, Mukherjee and Lutkenhaus 1994), fluorescence microscopy (Yu and Margolin 1997), circular dichroism (CD) (Rivas et al. 2000) and isothermal titration calorimetry (ITC) (Caplan and Erickson 2003). Some of the disadvantages of these techniques range from not being quantitative, not being practical for kinetic assays, to not being useful for real time observations. Table 1.4.2 summarizes the main techniques that have traditionally been used for the study of FtsZ's biochemical activity, along with the limitations of each.

Table 1.4.2 Traditional techniques used for FtsZ's biochemical activity (Romberg and Levin 2003)

Method	Purpose	Main advantages	Main disadvantages
Right-angled light scattering	Monitoring the dynamics of FtsZ (polymerization /steady state / depolymerization) with/without other ligands	Easy Detection in real time	● Cannot distinguish increases in polymer mass from changes in polymer structure ● small polymers are under-reported
Sedimentation	Quantifying assembly	Easy	● Cannot distinguish increases in polymer mass from changes in polymer structure ● Cannot capture small polymers ● Cannot be used for kinetics
Analytical ultracentrifugation	Quantifying assembly	Quantitative	● Slow ● Not practical for kinetic assays
Electron microscopy	Direct visualizing polymers	High Resolution for viewing structures	● Cannot be used for real time observations ● May not be representative of what happens in solution ● Not quantitative
Fluorescence microscopy	Direct visualizing polymers	Visualization in real time	● Cannot view individual protofilaments ● Not quantitative
Circular dichroism	Determination of the secondary structure of FtsZ with or without other ligands	Quantitatively measure the effects of ligands on the FtsZ secondary structure	● Changes are small unless there is a big rearrangement of the protein structure
Isothermal titration calorimetry	Determination of thermodynamic parameters of interactions in solution	Quantitative	● Cannot be used for kinetics

Flow linear dichroism spectroscopy (LD) is a novel technique to study long biomolecules when the sample is aligned in an ordered fashion (Rodger et al. 2002). This technique has been used for the first time in recent work in the analysis of FtsZ dynamic assembly and the interaction with other ligands at Warwick (Dr. R. Marrington, Dr. R. Pacheco-Gomez). LD seems to be the ideal complement to other techniques for the study of the kinetics of FtsZ assembly in real time either with or

without other ligands/cations, since it polymerises from monomers into long, unbranched, linear polymers.

However, for the study of fast kinetics, LD has been limited by the time required to assemble and fill the cell. For currently available cells this process commonly takes around one minute. Therefore in this project, we first demonstrated a continuous channel flow-LD technique, which is developed to record the very first seconds of FtsZ polymerization, as well as the other fast reactions.

The work presented in the following chapters covers the study of the function of YgfE on the assembly of FtsZ, and the development of the continuous channel flow-LD that is suitable for collecting fast LD for the reaction of FtsZ polymerization.

CHAPTER 2 – MATERIALS AND METHODS I

(Molecular and Structural Biology)

2.1 Chemicals and reagents

All chemicals used were of analytical grade and only molecular grade biology water (0.1 μm filtered) or deionised water was used. Unless otherwise stated, the providers were: Sigma-Aldrich (USA), Calbiochem (USA), Fisher Scientific (USA), Fluka Chemika (Germany) or Helena Biosciences (UK).

2.2 Prokaryotic expression in *Escherichia coli*

Expression systems are designed to produce many copies of a desired protein within a host cell. In order to accomplish this, an expression plasmid vector is inserted into a host cell. This vector contains all of the genetic coding necessary to produce the protein, including a promoter appropriate to the host cell, a sequence which terminates transcription, and a sequence which codes for ribosome binding.

2.2.1 The pET expression system

The pET system is the most powerful system yet developed for the cloning and expression of recombinant proteins in *E. coli*, based on the T7 promoter-driven system originally developed by Studier and colleagues (Moffatt and Studier 1986, Rosenberg et al. 1987, Studier et al. 1990). The pET vectors are provided with resistance to ampicillin or kanamycin. Target genes are cloned in pET plasmids under control of the strong bacteriophage T7 promoter, which is not recognized by *E. coli* RNA polymerase, and therefore the T7 RNA polymerase must be added. Almost no expression occurs until a source of T7 RNA polymerase is provided. Usually, the host cell for this expression system has been genetically engineered to incorporate the gene for T7 RNA polymerase. When lactose or a molecule similar to

lactose (*e.g.* IPTG) is present inside the cell, transcription of the T7 RNA polymerase is activated, and quickly begins to transcribe the target gene which is then translated into the target protein. T7 RNA polymerase is so selective and active that almost all of the cell's resources are converted to target gene expression; the desired product can comprise more than 50% of the total cell protein a few hours after induction.

2.2.2 Plasmid vectors used in this project

In molecular biology, a vector is a DNA molecule used as a vehicle to transfer foreign genetic material into another cell. The most commonly used type of vector is a plasmid, which is a circular, double-stranded unit of DNA that replicates within a cell independently of the chromosomal DNA. Cells that have taken up the vector with antibiotic-resistant open reading frames can survive in growth media even when antibiotics are added. Thus the target genes cloned in plasmids can survive through antibiotic selection. Ampicillin is one of the most widely used antibiotics in gene cloning and protein expression for the selection of transformants. Ampicillin belongs to the penicillin group of antibiotics *i.e.* beta-lactam antibiotics. Unlike penicillin which is effective against only gram positive bacteria, ampicillin is also effective against gram negative bacteria, *e.g. E. coli.*

Table 2.2.2 shows the plasmid vectors used in this project:

Table 2.2.2 Plasmid vectors used in this project

Vector	Selection	Description
pET-FtsZ (*E. coli*)[&]	Ampicillin	pET expression system carrying the *ftsZ* open reading frame
pETDuet-ygfE (*E. coli*)[*]	Ampicillin	pETDuet-1 expression vector containing six-histidine tag and the *ygfE* open reading frame

[&] kindly donated by Dr. David I. Roper; * kindly donated by Dr. Stephen G. Addinnal

2.2.3 *E. coli* strains

E. coli are widely used in basic research studies as a host strain for the overproduction of proteins from cloned genes. An *E. coli* strain is a sub-group within the *E. coli* species that has unique characteristics that distinguishes it from other strains.

E. coli strain B834 (DE3) was used in this project to get protein expression. The protease-deficient hosts are methionine auxotrophs and allow high specific-activity labeling of target proteins with ^{35}S-methionine and selenomethionine for crystallography. B834 was infected by λDE3 for introduction of T7 RNA polymerase gene, and the resulting lysogen was termed *E. coli* B834 (DE3). λDE3 is a recombinant phage carrying the cloned gene encoding T7 RNA polymerase under control of the lacUV5 promoter, and thus, expression of T7 RNA polymerase is induced by inducers such as IPTG. Such strains are suitable for production of protein from target genes cloned in pET vectors by induction with IPTG. Genotype: F^- *ompT hsdS*$_B$(r_B^- m_B^-) *gal dcm met* (DE3).
(http://www.emdchemicals.com/b834de3-competent-cells/EMD_BIO-69041/p_FUKb.s1Oh6IAAAEjTBl9.zLX)

2.2.4 Preparation of competent cells for DNA transformation

Competent cells are those that possess more easily altered cell walls that DNA can be passed through easily. These cells readily incorporate foreign DNA. A cell that is not already competent can be made more competent through addition of calcium chloride and a heat shock.

Protocol

The required *E. coli* strain (B834 (DE3)) was quickly and lightly spread onto a Luria-Bertani broth (LB) agar plate containing no antibiotics using a sterile innoculating loop. The plate was then inverted and kept in an incubator at 37°C to allow the cells to grow overnight. On the following day, 2.5 ml of sterile LB medium was inoculated with a single colony from the LB plate. Then this LB medium was incubated at 37°C with shaking at 180 revolutions per minute (rpm) overnight. The entire overnight culture was used to inoculate 250 ml of LB medium containing 20 mM $MgSO_4$, which results in a 1:100 dilution. Cells were grown at 37°C in a 1 liter flask at 180 rpm until an optical density at 600 nm (OD_{600}) in a 1 cm cell reached 0.4–0.6 (typically 5–6 hours). The culture was then centrifuged to pellet the cells at 4,500×g at 4°C for 5 minutes. The cell pellet was then gently resuspended in 100 ml (0.4 volume based on the original culture volume) of ice-cold TFB1 buffer (30 mM potassium acetate, 10 mM $CaCl_2$, 50 mM $MnCl_2$, 100 mM RbCl and 15% (v/v) glycerol). For the remaining steps, the cells were kept on ice and all pipettes, tubes and flasks used are chilled. The resuspended cells were incubated at 4°C for 5 minutes and centrifuged at 4,500×g for 5 minutes before further resuspension in 10 ml (1/25 of the original culture volume) of ice-cold TFB2 (10 mM MOPS pH 6.5, 75 mM $CaCl_2$, 10 mM RbCl, 15% (v/v) glycerol). Competent cells were incubated on ice for 15–60 minutes and then aliquoted in 100 µl, frozen in liquid N_2 and stored at –80°C.

Note: The competent cells needed to be treated gently as they are highly sensitive to handling and elevated temperature. Most cells prepared this way are stable for at least 3 months.

2.2.5 Bacterial DNA transformation

Bacterial transformation means a process by which the genetic material carried by an individual cell is altered by incorporation of DNA from another organism into its genome. Briefly, to do a transformation is to insert a foreign DNA into another cell so that the cell expresses this new DNA.

Protocol

A 100 µl aliquot of chemically competent cells (§ 2.2.4) were thawed on ice on the day of use. 40 µl of competent cells were mixed gently with up to 1 µl of transforming plasmid DNA in a 1.5 ml eppendorf tube, and incubated on ice for 30 minutes. The volume of DNA solution should not exceed 5% of the volume of the competent cells or no more than 50 ng in a volume of 10 µl. The tube was then heated at 42°C in a preheated circulating water bath for 90 seconds. This step is a crucial step, since it enables the DNA to enter the competent cells. The eppendorf tube was immediately returned to ice and allowed to cool for 1–2 minutes. 300 µl of sterile LB was then added to the eppendorf tubes, which was then incubated at 37°C with shaking at 180 rpm for 30–45 minutes. This step allows the bacteria to recover and express the antibiotic resistance encoded by the plasmid. 100 µl of the transformed competent cells were spread onto LB agar plates containing the appropriate antibiotic. The plate was then inverted and kept in an incubator at 37°C to allow the cells growing overnight. The colonies typically appeared in 12–16 hours.

Notes: When handling frozen competent cells, it is important to keep them cool. Frozen cells are very sensitive to heat and must be kept on ice as much as possible.

Prior to spreading the transformed competent cells onto LB agar plates, a glass bent rod spreader was sterilized by dipping it into ethanol and then flamed by a Bunsen burner. The spreader was cooled to room temperature before spreading the transformed cells over the agar plate.

Transformed cells were plated at low density when selecting for resistance to ampicillin. The plates were incubated for less than 20 hours at 37°C in order to avoid ampicillin-sensitive satellite colonies that can inactivate the antibiotic in regions surrounding the colonies. After incubation, the plate was kept in the fridge at 4°C for less than three days before use.

2.3 Protein expression and purification

2.3.1 EcFtsZ

Escherichia coli FtsZ (EcFtsZ) was purified following the method described by Mukherjee and Lutkenhaus (Mukherjee and Lutkenhaus 1998). However, some modifications were introduced, which are detailed below.

Overproduction of EcFtsZ

To overproduce EcFtsZ, *E. coli* competent cells B834 (DE3) (§2.2.3) were transformed with the plasmid pETFtsZ (§ 2.2.2) which contains *ftsZ* open reading frame downstream of the high expression T7 promoter. 10 ml Luria-Bertani broth (LB) containing ampicillin (100 μg/ml) was inoculated with a fresh colony of the transformed B834 (DE3) and grown overnight with shaking at 37°C. The overnight culture was diluted into 1 litre of fresh LB medium with ampicillin (100 μg/ml) and grown at 37°C. At OD_{600} of 0.3, it was induced with 1 mM ITPG and the culture was grown for another 3–4 hours. The culture was then chilled and harvested at 7000 RPM for 15 minutes at 4°C and washed once with cold 10 mM Tris-HCl, pH 7.9, followed by another centrifugation at 4°C. The cell pellet was kept in –20°C.

Lysis of bacterial cells

In order to observe how effective the overexpression was from the crude cell lysates, a small scale culture was lysed instead of the whole bacterial cells. Cell pellets were thawed on ice, and a small amount of the pellet was collected and resuspended in 300 µl of buffer, which contains 50 mM Tris-HCl, pH 7.9, 50 mM KCl, 1 mM ethylendiaminetetraacetic acid (EDTA) and 10% glycerol (buffer A), in a 1.5 ml eppendorf. The resuspended pellet was then lysed by sonication in a MSE Soniprep device for 30 seconds at 20% power. The sonicated extract was then clarified by centrifugation in a bench-top centrifuge for 10 minutes at 13200×g at 4°C. Samples were analysed by sodium dodecyl sulfate–polyacrylamide gel electrophoresis (SDS–PAGE) (§ 2.4.1). If the crude cell lysates gave a big band around 40 kDa on gel, which corresponds to EcFtsZ, then the lysis for the large scale of bacterial cells was performed.

From this step onward all operations were done at 4°C unless otherwise mentioned. The major part of the culture pellet (see above) was resuspended in 20 ml of buffer A, and the culture was then put on the ice and lysed by sonication in the MSE Soniprep device (70% power, 1 minute) at an interval of 1 minute. The resulting extract was then centrifuged at 10,000×g for 10 minutes to remove unbroken cells and debris and the supernatant was centrifuged afterwards at 75,600×g for 90 minutes to remove the membrane fraction. The supernatant was then collected and 30% ammonium sulfate (16.6 g/100 ml of extract) was slowly added with stirring for 20 minutes. The ammonium sulphate precipitate was then recovered after centrifugation at 20,000×g for 10 minutes and resuspended extensively in buffer A. The resuspended pellet in buffer A was dialyzed overnight against buffer A with two changes of 1 litre each to remove ammonium sulfate. Ammonium sulfate fraction of EcFtsZ was monitored by SDS–PAGE (§ 2.4.1).

Purification of EcFtsZ by ion-exchange chromatography using DEAE-Sepharose

HiPrep 16/10 DEAE FF (GE Healthcare) is a prepacked, ready to use column (bed volume, 20 ml) for anion exchange chromatography. The matrix consists of a 6% highly cross-linked spherical agarose with a mean particle size of 90 µm. The charged group in the matrix is $–N^+(C_2H_5)_2H$ and it is stable over a pH range of 1 to 14 in the short term. EcFtsZ with an isoelectric point of 4.9 is negatively charged at pH 7.9 (after dialysis in buffer A). EcFtsZ will bind strongly to the positively charged matrix in low salt buffer. EcFtsZ can be eluted by increasing the salt gradient.

It is important to remark that rigorous cleaning was performed between purification runs as indicated by the manufacturer (http://sbio.uct.ac.za/Sbio/documentation/DEAE_agarose.pdf). This involved passing through the column a series of solutions at a flow rate of 5 ml/min: (i) 100 ml of 2 M NaCl (which removes ionically bound proteins), (ii) 50 ml of distilled water, (iii) 100 ml of 1 M NaOH solution (which removes hydrophobically bound proteins), (iv) 50 ml of distilled water, (v) 100 ml of 70% ethanol (which removes proteins, lipoproteins and lipids tightly hydrophobically bound to the column), (vi) 50 ml of distilled water. The column was then equilibrated with 100 ml of buffer A at a flow rate of 5 ml/min.

Then the dialyzed ammonium sulfate fraction was loaded onto the DEAE-Sepharose column, which was attached to an ÄKTA purifier (Amersham Biosciences). The dialysed and concentrated fraction was washed with 100 ml of buffer A (5 bed volumes) and eluted with 200 ml of a 50 mM–1 M KCl gradient at a flow rate of 0.2 ml/min. Fractions of 2 ml were collected. During purification, proteins passing through the column were monitored by the UV absorbance at 280 nm and the peak fractions of EcFtsZ eluted at around 200–250 mM KCl.

After that, EcFtsZ fractions were also monitored by SDS–PAGE to test the purity (§ 2.4.1). The fractions that appeared as a single band with little or no contamination as judged by SDS–PAGE were pooled together and dialysed extensively in buffer A (3 changes of 3 litres each). The protein concentration was determined by the Bio-Rad reagent (§ 2.4.2.2). The protein fractions were aliquoted in 100 µl and stored at –80 °C. Purified EcFtsZ stored in this way can be stable for at least 2 years with no apparent loss of GTPase or polymerization activities.

2.3.2 EcYgfE

E. coli YgfE (EcYgfE) was produced and purified following the method described by Addinall and Johnson (Addinall et al. 2005). Using this 3 step procedure, EcYgfE was able to be purified to 99% purity allowing crystallisation. The pETDuet-1 vector (Novagen) containing the gene encoding *E. coli* amino-terminal six-histidine tag YgfE was kindly donated by Dr. Stephen Addinall.

Overproduction of EcYgfE

E. coli competent cells B834 (DE3) (§2.2.3) were transformed with the high expression plasmid pETDuet-1 (§ 2.2.2). 10 ml Luria-Bertani (LB) containing ampicillin (100 µg/ml) was inoculated with a fresh colony of transformed B834 (DE3) and grown overnight with shaking at 37°C. The overnight culture was diluted into 1 litre of fresh LB medium with ampicillin (100 µg/ml) and grown at 37°C with shaking until OD_{600} reached approximately 0.5. Protein expression was induced by the addition of ITPG to a final concentration of 0.5 mM, and then the culture was grown for another 3–4 hours. Cells were harvested by centrifugation at 6400×g at 4°C for 15 minutes, and the pellet can be kept in –20°C freezer for several days.

Lysis of bacterial cells

In order to observe how effective the overexpression was from the crude cell lysates, a small scale culture was lysed instead of the whole bacterial cells. Cell pellets were thawed on ice, and a small amount of the pellet was collected and resuspended in 300 µl of buffer A (25 mM HEPES pH 8.0, 1 M NaCl and 10 mM imidazole) in a 1.5 ml eppendorf. The resuspended pellet was then lysed by sonication in a MSE Soniprep device for 30 seconds at 20% power. The sonicated extract was then clarified by centrifugation in a bench-top centrifuge for 10 minutes at 13200×g at 4°C. Samples were analysed by SDS–PAGE (§ 2.4.1). If the crude cell lysates gave a big band around 14 kDa on gel, which corresponds to EcYgfE, then the lysis for the remainder of the culture was performed.

The large portion of the cell pellet (see above) was resuspended in buffer A. The resuspended pellet was incubated on ice for 30 minutes with 2.5 mg/ml of chicken egg white lysozyme prior to lysis by sonication in a MSE Soniprep device for 2 minutes with a minute pause interval. The sonicated extract was clarified by centrifugation at 50,000×g at 4°C for 30 minutes and applied onto a 5 ml chelating sepharose (GE Healthcare) affinity gravity flow column charged with nickel.

Purification of EcYgfE on a Ni-sepharose column by immobilised metal affinity chromatography (IMAC)

The column was washed with 50 ml (10 column volumes) of buffer containing 25 mM HEPES, pH 8.0 and 20 mM EDTA to strip any nickel and contaminants from the column. It was followed by another wash with buffer containing 25 mM HEPES, pH 8.0 without EDTA. The column was then charged with nickel by equilibrating with 50 ml of 50 mM sodium acetate buffer pH 4.0 containing 25 mg/ml nickel chloride. The column was then washed with 50 mM sodium acetate buffer, pH 4.0 to remove any unbound nickel before being finally equilibrated with buffer A.

After equilibration, the fraction was loaded onto the column and extensively washed with 50 ml of buffer A, and 50 ml of buffer B (25 mM HEPES, pH 8.0, 1 M NaCl and 100 mM imidazole). EcYgfE was finally eluted with 50 ml of buffer C (25 mM HEPES pH 8.0, 1 M NaCl and 500 mM imidazole), and 5 ml of fractions were collected.

EcYgfE was monitored during purification by SDS–PAGE (§ 2.4.1) and the protein concentration of the fractions were assayed with the Bio-Rad reagent (§ 2.4.2.2). The pure EcYgfE was finally dialysed into a buffer containing 50 mM Tris-HCl, pH 7.9, 50 mM KCl, 1 mM EDTA and 10% glycerol (the same buffer used for EcFtsZ) with 3 changes of 3 litres each. The protein was then aliquoted into 100 µl samples and stored at –80 °C until needed for further studies.

2.4 Protein analysis

2.4.1 SDS-polyacrylamide gel electrophoresis (SDS-PAGE)

SDS-polyacrylamide gel electrophoresis (SDS-PAGE) is a commonly used technique to separate proteins according to their length of polypeptide chain or molecular weight.

General electrophoresis techniques cannot be used to measure the molecular weight of the biological molecules because the mobility of a substance in the gel is influenced by both charge and size. However, if the biological samples are treated so that they have a uniform charge, electrophoretic mobility then depends primarily on size.

In SDS-PAGE, the samples are treated with SDS (sodium dodecyl sulfate) combined with a reducing agent, such as β-mercaptoethanol (β-ME) or dithiothreitol (DTT). SDS is a strong anionic detergent which disrupts the secondary, tertiary and quaternary structures of the protein and leads to the formation of a linear

polypeptide chain. It provides a net uniform negative charge to the protein molecules, irrespective of the protein's own native charge. β-ME or DTT assists the protein denaturation by reducing all disulfide bonds. The protein samples are heated before loading into the polyarylamyde gel, which denatures the protein molecules further. To the denatured protein, SDS binds strongly along the polypeptide chain and provides a net negative charge to it. Generally, one SDS molecule binds per every two amino acid residues (Jones 1992). Now, the protein molecules migrate entirely on the basis of their size under the applied electric field.

Polyacrylamide gel consists of chains of polymerized acrylamide which are cross-linked by a bifunctional agent, *i.e.* N,N'-methylene-bis-acrylamide. These cross-links forms pores in the gel through which SDS-protein complexes pass. Small molecules can move through the polyacrylamide faster than big molecules. The porosity of the gel and thus the range of separation of SDS-polyacrylamide gels is determined by the degree of cross-linking and the concentration of acrylamide used to cast the gel that occurs during the polymerization reaction. The size of the pores decreases as the bisacrylamide:acrylamide ratio increases with 1:29 being the most common molar ratio. An acrylamide concentration of 12% with a molar ratio of bisacrylamide:acrylamide 1:29 allows a linear range of separation between 10 and 200 kDa and an acrylamide concentration of 15% allows separation between 3 and 100 kDa.

Discontinuous buffer system

Most protein separations are performed using a discontinuous buffer system, which was originally devised by Ornstein (Ornstein 1964) and Davis (Davis 1964) and modified by Laemmli (Laemmli 1970). Discontinuous buffer systems employ different buffers for tank and gel, and often two different buffers within the gel, with a third buffer in the tank. Discontinuous systems concentrate, or "stack" the protein samples into a very narrow zone prior to separation, which results in improved band sharpness and resolution. A very widespread discontinuous buffer system is the

tris-glycine or "Laemmli" system, in which the gel is divided into an upper "stacking" gel of low percentage of acrylamide (*i.e*. large pore size) at low pH (6.8) and a resolving gel with a pH of 8.8 with much smaller pores. Both gels contain only Cl^- as the mobile anion. The tank buffer has glycine as its anion, at a pH of 8.8.

When electrophoresis begins, glycine enters the stacking gel. Under the influence of the applied electric field, the anions (and negatively charged sample molecules) migrate toward the positive electrode (anode), the leading ion is Cl^- (high mobility and high concentration); glycinate is the trailing ion (low mobility and low concentration). As these two current carrying species separate, a region of low conductivity, with a consequent high voltage drop, is created between them, the proteins are thus compressed (stacked) into micrometer thin layers between Cl^- and glycinate. On reaching the resolving gel, the mobility of glycinate increases as it becomes fully ionized in the higher pH environment. As a result, glycinate moves along with Cl^-, leaving the SDS-protein complexes behind. The SDS-protein complexes now migrate towards the anode, according to their respective size. Due to the frictional resistance caused by the gel matrix, the proteins start getting separated. Smaller proteins migrate through the gel pores easily, whereas the larger proteins get retained by them.

Reagents

SDS-polyacrylmide gels

SDS-polyacrylmide gels generally consist of acrylamide, bisacrylamide, SDS, and a Tris-HCl buffer with adjusted pH. The resolving gel varies from 6–15% concentration of acrylamide depending on the requirements (12% and 15% gels were used in this project). Table 2.4.1 shows the components of the SDS-polyacrylmide gels used in this work.

Table 2.4.1 Components of the stacking gel and resolving gels

% Gel	Components	Volume (ml)
12% resolving gel	H_2O	3.3
	30% acryl-bisacrylamide mix	4.0
	1.5 M Tris-HCl (pH 8.8)	2.5
	10% SDS	0.1
	10% ammonium persulfate (APS)	0.1
	TEMED	0.004
15% resolving gel	H_2O	2.3
	30% acryl-bisacrylamide mix	5.0
	1.5 M Tris-HCl (pH 8.8)	2.5
	10% SDS	0.1
	10% ammonium persulfate (APS)	0.1
	TEMED	0.004
5% stacking gel	H_2O	3.4
	30% acryl-bisacrylamide mix	0.83
	1.5 M Tris-HCl (pH 6.8)	0.63
	10% SDS	0.05
	10% ammonium persulfate (APS)	0.05
	TEMED	0.005

Pre-made 30% (w/v) acrylamide and N,N'-methylene-bis-acrylamide (29:1) solutions were purchased from Sigma. The stock solutions were stored in dark glass bottles at room temperature to prevent the formation of acrylic and bisacrylic acid due to light and alkali. Tris buffers were prepared from Trizma base, and adjusted to the required pH (either 6.8 or 8.8). 10% (w/v) stock solution of sodium dodecyl sulfate (SDS) was prepared and stored at room temperature. For polymerizing the gel, ammonium persulfate (APS) and N,N,N',N'-tetramethylethylenediamine

gel, ammonium persulfate (APS) and N,N,N',N'-tetramethylethylenediamine (TEMED) were added. 10% (w/v) stock solution of APS was prepared, aliquoted in 1 ml, and stored at either 4 or –20°C. APS provides free radicals that cause polymerization of acrylamide and bisacrylamide. TEMED catalyse the formation of free radicals from APS. It is important not to add APS and TEMED until one is ready to pour the solution to form a gel.

Sample loading buffer

Generally, 5× sample loading buffer was prepared and mixed with protein samples (10 µl protein sample + 5 µl 5× sample loading buffer) for loading into the gel. The 1× sample loading buffer contained 62.5 mM Tris-HCl, pH 6.8, 10% glycerol, 2% SDS, 2.5% β-mercaptoethanol (β-ME) and 5% bromophenol blue.

Glycerol in the loading buffer increases the sample density, facilitating gel loading and preventing convective migration out of the sample wells. A small amount of bromphenol blue was added as a visual aid for sample loading and as a tracking dye, allowing easy monitoring of electrophoretic progress. β-ME assists the protein denaturation by reducing all disulfide bonds. Alternative, dithiothreitol (DTT) can be added. Also, five minutes of heating at 95°C was applied to the samples to further denaturate them.

While loading the protein samples onto the gel, protein molecular weight markers (also known as protein ladders), purchased from GE Healthcare were loaded into a separate well. These markers were used to estimate size of the proteins. Protein ladders consist of a mixture of proteins of predetermined size, and are commercially available.

Gel running buffer

In order to run the SDS-polyacrylamide gels, Tris-glycine (pH 8.3) is the buffer of choice. It is useful for separating proteins of a wide range (10–200 kDa). The gel

running buffer consists of 25 mM Tris, 192 mM glycine, and 0.1% SDS, pH 8.3. Generally, a 10× gel running buffer was prepared and stored at room temperature.

Protein stain to visualize the gel

For visualizing proteins, a gel is stained with Coomassie Brilliant Blue R-250 (CBB) (Wilson 1979, Wilson 1983). CBB is a sulfated trimethylamine dye. This anionic dye forms strong complexes with proteins by the virtue of the combination of van der Waals forces and electrostatic interactions with the NH_3^+ groups. CBB is a highly sensitive stain, which can detect as little as 50 ng of protein in the gel.

SDS-polyacrylamide gels are routinely stained in a solution containing 0.1% Coomassie Blue R250 (w/w), 30 % methanol and 5 % acetic acid. The acetic acid is used to fix the proteins in the gel, avoiding the proteins from being washed away while staining. The excess dye incorporated in the gel was removed by destaining with the same solution but without the dye. The proteins are detected as blue bands on a clear background.

SDS-PAGE protocol

Two glass plates and a spacer were assembled vertically on a Hoefer Mighty Small dual gel caster, and cleaned with 70% ethanol. 10 ml of the components of the resolving gel were mixed in a disposable plastic tube containing the desired concentration of acrylamide (12% or 15% gels in this study). 10% APS and TEMED were added to the resolving gel mixture to start the polymerization reaction. The mixture was then quickly poured into the gap between the two glass plates, and overlaid with ethanol preventing air from reaching the gel, which inhibits polymerization of the acrylamide and ensures that the gel surface is flat. After polymerization was complete, the ethanol was poured off, and carefully blotted with a piece of filter paper without damaging the gel surface. 5 ml of 5% stacking gel was then prepared, poured directly onto the surface of the polymerized resolving gel, and

a clean teflon comb was inserted carefully into the stacking gel solution, avoiding formation of any air bubbles.

While the stacking gel is polymerizing, 10 µl of the sample was added to 5 µl of 5× SDS gel-loading buffer, and heated at 95°C for 5 minutes to denature the proteins. After polymerization of the stacking gel, the teflon comb was carefully removed, and the top and bottom reservoirs were filled with running buffer. Each time the sample loading wells were fully filled with running buffer, and the wells were then washed by pipetting the running buffer to remove unpolymerised acrylamide. The samples as well as the protein markers were then loaded into the wells with a gel-loading tip. The electrical power supply was connected to the electrophoresis apparatus, and a constant voltage of 200 V was passed through the gel until the bromophenol blue dye in the gel-loading buffer reached the end of the gel, (usually 45 minutes approximately).

The gel was taken out and stained by immersing it in the CBB stain solution for 1 hour. The excess dye was allowed to destain by the same solution excluding the dye for about 2–10 hours. The destaining solution was changed two to three times in between. Destaining was stopped when the background of the gel was clear and the protein bands were sharply visible.

2.4.2 Protein concentration determination

The protein concentration was determined either using the Bio-Rad's colorimetric protein assay based on the Bradford method (1976) at 595 nm and/or a direct absorbance assay at 280 nm.

Absorbance at 280 nm

Absorbance assays (§ 3.1.1) are fast and convenient, since no additional reagents or incubations are required. However, there may be considerable error, especially for

unknowns or protein mixtures, because different proteins have widely varying absorption characteristics. The most common use for the absorbance assay is to monitor fractions from chromatography columns, or for a quick estimation where error in protein concentration is not a concern.

Protein concentration can be measured directly by the absorbance at 280 nm or 205 nm. The absorbance maximum at 280 nm (A_{280}) is mainly due to the aromatic amino acids tryptophan and tyrosine, and cystine, disulfide bonded cysteine residues, in protein solutions. The peptide bonds are primarily responsible for the maximum absorbance at 205 nm (A_{205}). The relationship of absorbance to protein concentration is linear. The A_{205} method can detect lower concentrations of protein, but is more susceptible to interference by reagents in the protein sample, so the A_{280} method is more commonly used.

The spectrophotometer was zeroed with the solvent blank, then 1 ml of protein sample was placed in a quartz window cuvette (1 cm path length) and the absorbance was read at 280 nm. If the A_{280} of the sample protein is higher than 1.5, the sample should be diluted in the same solvent and re-measured at 280 nm.

For pure proteins of known extinction coefficient, the concentration of protein was calculated according to the following equation:

$$[\text{Protein}] = [\boldsymbol{A_{280}} / (\boldsymbol{\varepsilon}\, \boldsymbol{l})] \times \text{dilution factor}$$

where ε is extinction coefficient, l is optical path length in cm. The units of the concentration are given by the units of the extinction coefficient × cm.

If the extinction coefficient is unknown, the theoretical extinction coefficient at 280 nm, ε_{280}, can be estimated if the protein sequence is known using the equation (Pace et al. 1995):

$\boldsymbol{\varepsilon_{280}}$ ($M^{-1}cm^{-1}$) = (Number of Tryptophan residues × 5500) + (Number of Tyrosine residues × 1490) + (Number of Cystine residues ×125)

Bio-Rad colorimetric assay

The Bio-Rad's colorimetric assay is an accurate assay for the determination of protein concentration and is based on the Bradford dye-binding method (Bradford 1976). This dye-binding assay is based on a differential colour change of an acidic dye (Coomassie Brilliant Blue G-250) in response to various protein concentrations. When the dye binds to proteins, the maximum absorbance changes from 465 nm to 595 nm. The Coomassie blue dye binds mainly to basic residues and aromatic amino acid residues.

For the standard assay, 10 µL of the protein solution was mixed with 200 µL of the protein assay dye, and 790 µL of sterile water in a 1.5 ml eppendorf. The mixture was incubated at room temperature for at least five minutes, and then transferred to a quartz cuvette (1 cm path length). The absorbance was measured at 595 nm. It should be noted that absorbance will increase over time and the samples should not be incubated at room temperature for more than 1 hour. In order to calculate the protein concentration, the instrument was calibrated to zero with a reference that lacks protein.

The comparison to a standard curve for the Bio-Rad protein assay gave a response of 0.1 absorbance units/1.95 µg of protein. The response is linear up to A_{595} = 0.6. If the absorbance measured is greater than 0.6 (Bradford 1976), the protein sample was

diluted and re-assayed. The absorbance at 595 nm was then introduced in the following formula to allow us to calculate the protein concentration in µg/ml:

[Protein] =

$(A_{595} / 0.1) \times 1.95 \times$ dilution factor $\times$ [1000 (total volume) / 10 (protein volume)]

EcFtsZ has no tryptophan residues and very few tyrosine residues. Thus, absorbance at 280 nm is not an accurate measurement for the concentration of FtsZ and the Bio-Rad colorimetric protein assay was performed for the FtsZ protein.

2.5 DNA analysis

DNA (deoxyribonucleic acid) solutions were made from a sodium salt of DNA (Sigma) by adding it into distilled water and allowing it to stand overnight until completely dissolved. DNA absorbs ultraviolet (UV) light around 260 nm due to the nitrogenous bases (purine and/or pyrimidine). The absorption profile of DNA can be used as a measure of the concentration and purity of a DNA sample (§ 3.1.1).

The concentration of calf thymus DNA (ct-DNA) in solution for this work was determined by measuring the absorbance at 260 nm. Before the measurement, the spectrophotometer was zeroed with water, and then 1 ml of DNA sample was placed in a small volume quartz cuvette (1 cm path length) and the absorbance was read at 260 nm. If the A_{260} of DNA was higher than 1.5, the sample was diluted and measured at 260 nm again.

The molar concentration of DNA was calculated according to the following equation:

$$[\text{DNA}] = [\boldsymbol{A_{260}} / (\boldsymbol{\varepsilon}\, \boldsymbol{l})] \times \text{dilution factor}$$

where ε is extinction coefficient, given as 6600 $M^{-1}cm^{-1}$ (per nucleotide or base) (Reichmann et al. 1954), l is optical path length in cm.

CHAPTER 3 – MATERIALS AND METHODS II

(Biophysical Chemistry)

The work reported in this thesis involves a range of biophysical chemistry techniques, including spectroscopic techniques such as ultraviolet (UV)/visible spectroscopy, light scattering, linear dichroism spectroscopy, and other techniques such as electron microscopy and analytical ultracentrifugation. This chapter summarizes the techniques used and where necessary details the method used.

3.1 Spectroscopic techniques

Spectroscopy is the study of the interaction between matter and light (electromagnetic radiation), and the spectroscopic data is often represented by a spectrum, a plot of radiation intensity measured as a function of wavelength. The interaction of radiation with matter can cause redirection of the radiation and/or transitions between the energy levels of the atoms or molecules. Because atoms and molecules have unique spectra, these spectra can be used to detect, identify and quantify chemicals.

There are many different types of spectroscopic techniques, utilizing a wide variety of different approaches to probing material properties, such as absorbance, reflection, emission, scattering, thermal conductivity, and refractive index. Also, different regions of the electromagnetic spectrum can provide different kinds of information as a result of such interactions. The spectroscopic techniques used in this project have been described below as well as the information that can be obtained from them.

3.1.1 UV/Visible spectroscopy

When an atom or molecule absorbs energy, electrons are promoted from their ground state to an excited state. So if sample molecules are exposed to light (electromagnetic radiation) having an energy that matches a possible electronic transition within the molecule, some of the light energy will be absorbed as the electron is promoted to a higher energy orbital. Different molecules or different parts of the same molecule can absorb radiation at different wavelengths. Absorption of light in the ultraviolet and visible regions is associated with the electronic transitions. These approximately may be described as being between the outermost atomic or molecular orbitals, generally between a bonding and an unfilled non-bonding orbital (n) or anti-bonding orbital (s*) with greater potential energy.

An optical spectrometer records the wavelengths at which absorption occurs, together with the degree of absorption at each wavelength. Absorbance (*A*) (or transmittance (*T*)) expresses the extent to which electromagnetic radiation is absorbed by a sample. If I_0 is the intensity of the incident radiation and *I* is intensity transmitted, the absorbance is given by (IUPAC):

$$A = -\log_{10}(I / I_0) = -\log_{10}(T)$$

The Beer-Lambert Law (Lambert 1760, Beer 1852), more commonly known as Beer's Law, states that the optical absorbance of an absorbing species in a transparent solvent varies linearly with both the sample cell path length and the absorbing species concentration.

$$A = \varepsilon c l$$

where ε is known as the extinction coefficient, c is the concentration of the absorbing species, and l is the cell path length, the length of the sample through

which the light passes. If l is measured in cm, and c in mol dm^{-3}, then ε has units of mol $^{-1}$ dm ^{3} cm^{-1}. Under defined conditions of solvent, pH and temperature the extinction coefficient for a particular compound is a constant at the specified wavelength.

One of the main applications of UV/visible spectroscopy in biochemistry is to measure the concentrations of protein or DNA solution (§ 2.4.2.1 & § 2.5). UV spectra of proteins are usually divided into the near UV (250–300 nm) and far UV (<250 nm) regions. The near UV region is also described as the aromatic region, where aromatic side-chains in proteins (phenylalanine, tyrosine and tryptophan) mainly contribute to be observed spectrum. The absorption in the far UV region is primarily dominated by transitions of the peptide backbone of the protein. For DNA, the UV absorbance from 200 to 300 nm is due exclusively to transitions of the nitrogenous bases (purine and/or pyrimidine). In this project, a Jasco V-660 spectrophotometer was used to collect UV/Visible spectra.

3.1.2 Circular dichroism

Circular dichroism (CD) is the differential absorption between left and right circularly polarized light (A_L and A_R) as a function of the wavelength. CD can be used for the measurement of chiral molecules or complexes as long as one of the interacting species is chiral, since the left and right circularly polarized light components are absorbed to different extents. All biological systems and many non-living ones are chiral. The main applications of CD spectroscopy in this project include determining conformational changes in proteins, or changes of protein folding as the result of ligand interactions as well as structural predictions when the crystal structures are not available. According to Beer-Lambert's law, the differential absorption is given by:

$$\Delta A = (A_L - A_R) = (\varepsilon_L - \varepsilon_R)\, c\, l = \Delta\varepsilon\, c\, l$$

where $\Delta\varepsilon$ is the differential molar extinction coefficient, c is the concentration (mol dm $^{-3}$) and l is the path length (cm).

Also, the recombined differentially absorbed circularly polarized light components produce radiation that is elliptically polarized (i.e., traces out an ellipse). A CD instrument reports the signal as either the difference in absorbance, ΔA, of the two components, $\Delta A = A_L - A_R$, or as the ellipticity in degrees, θ ($\theta = \tan^{-1}(b/a)$, where b and a are the minor and major axes of the resultant ellipse). There is a simple numerical relationship between ΔA and θ (θ in degrees), *i.e.* $\theta = 32.98\ \Delta A$. In this project, CD spectra were collected on a Jasco J-815 spectropolarimeter, and ellipticity θ were reported as results.

CD of proteins

Proteins are made up of amino acids which are intrinsically chiral (with the exception of glycine). Secondary structure motifs within the peptide sequence such as the α-helix and β-sheet impose additional chirality on the peptide sequence. At present the main use of CD in the study of proteins is as an empirical gauge of protein structure and conformation using the CD induced into the backbone peptide region from 190 nm to 240 nm. In the absence of any contributions to the CD from side chain transitions, this has proved to be a very successful approach. Distinctive CD spectra (figure 3.1.2.1) have been described for pure conformations such as the α-helix and β-sheet, β-turns, and also the random coil. The CD spectrum of a native protein is then the sum of the appropriate percentages of each component spectrum.

There are a range of different computer programs available for determining the percentage of different structural motifs from the CD spectrum. Generally, the algorithms use a library of well known peptide sequence or proteins with

well-defined secondary structures, and then a deconvolution of the data allows us to estimate the proportions of different secondary structure.

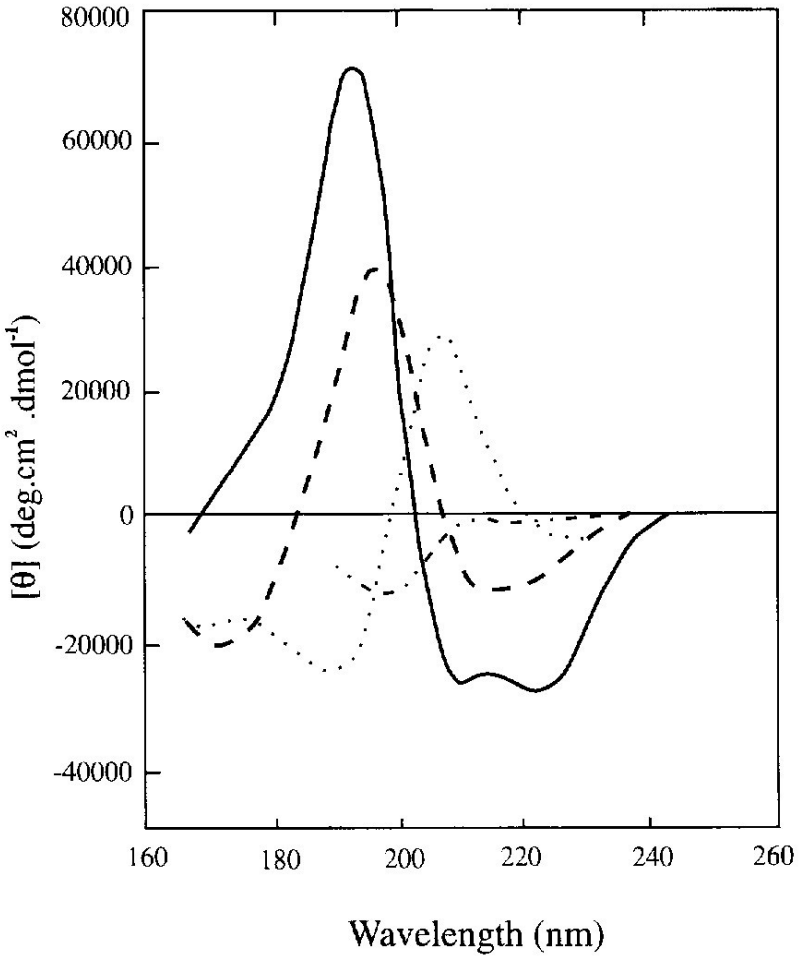

Figure 3.1.2.1 Far-UV CD spectra associated with various types of secondary structure of protein: solid curve, α-helix; long dashes, anti-parallel β-sheet; dots, type I β-turn, dots and short dashes, random coil (Johnson 1990).

α-helix: The α-helix is the dominant secondary structure in many proteins and on average accounts for about one-third of the residues in globular proteins. The α-helix is a well defined motif, and the CD spectrum is characterised by negative peaks at 222 nm and 208 nm with separate maxima of similar magnitude (corresponding to a $n \rightarrow \pi^*$ transition and part of the first $\pi \rightarrow \pi^*$ transition respectively) and a positive peak at 190 nm which corresponds to the remainder of the first $\pi \rightarrow \pi^*$ transition.

The helical length determines the intensity of the positive peak at 190 nm. The 208 nm peak is unique to the α-helix.

β-sheet: The CD spectra of β-sheets are not as well defined as α-helix due to the practical reason that they are less soluble in solvents with a good UV transmission and due to the intrinsic reason that β-sheets can be parallel or antiparallel and of varying lengths and widths. However, the common characteristics of CD spectra of β-sheet may shown to be a negative band at approximately 216 nm and a positive band near 195 nm.

β-turn: The label β-turn usually is used to include all possible turns in a protein, not simply the ones that enable a single strand to become an antiparallel β-sheet. Because of this range of structures, the CD of β-turns is not really well defined. A typical β-turn CD spectrum has a weak red-shifted negative band near 225 nm due to $n \rightarrow \pi^*$ transitions, a strong positive band between 200 nm and 205 nm corresponding to $\pi \rightarrow \pi^*$ transitions, and a strong negative band between 180 nm and 190 nm.

Random coil: When we refer to random coils, we refer to the parts of a folded protein that do not fit into any of the categories previously discussed, so not really random. The CD spectrum of a random coil protein is characterised by a strong negative band below 200 nm, a positive band at about 218 nm and sometimes a very weak negative band at 235 nm.

3.1.3 Linear dichroism

Linear dichroism (LD) spectroscopy is defined as the difference in absorption of light polarised parallel and perpendicular to an orientation axis by a sample (Rodger and Nordén 1997). For a sample to exhibit LD there is a requirement for the chromophores within the sample to be aligned in an ordered fashion. The resulting

LD measured when the sample is aligned then provides information on the alignment of the chromophores within the biological system. It is an ideal technique for studying classes of long biomacromolecules, such as DNA, fibrous proteins (FtsZ), membrane proteins and peptides in liposomes, and carbon nanotubes, for which it is intrinsically difficult to gain structural information by techniques such as NMR and X-ray diffraction because they are too large, too flexible or cannot be crystallized.

The LD of an oriented molecule can be calculated using the following equation:

$$LD = A_{//} - A_{\perp}$$

where $A_{//}$ is the absorbance parallel to the orientation axis and $A_{\perp}$ is the absorbance perpendicular to the orientation axis.

The LD signal generated therefore has two limits. For a chemical system whose electric transition is perfectly parallel to the orientation axis, as would be the case for a transition polarized parallel with the long axis of a rod shape molecule, then

$$LD = A_{//} - A_{\perp} = A_{//} > 0$$

Alternatively, if the polarization of the electric transition we are probing is perfectly perpendicular to the orientation direction, as would be the case for a pure short axis polarized transition of the molecule, then

$$LD = A_{//} - A_{\perp} = - A_{\perp} < 0$$

LD spectra may be collected using a converted CD spectropolarimeter. The circularly polarised light is converted to linearly polarised light by the addition of a

quarter wave plate. The plane polarised light passes then through the sample and interacts with the oriented molecules. In this project, LD measurements were performed at room temperature using a Jasco J-815 spectropolarimeter adapted for LD spectroscopy.

Alignment method

Different orientation methods are appropriate for different types of sample, for example stretched film for small molecules, flow orientation, squeezed gel and electric field orientation for larger molecules (Rodger 1993, Rodger et al. 2002, Nordén 1978, Johansson and Davidsson 1985)

The easiest orientation method is to flow samples. As with logs flowing down a stream, long molecules align in the flow. Biomolecules with a high aspect ratio (that is having one axis much longer than the orthogonally related axis) can be aligned using solution sheer flow. Flowing a solution through a thin channel is one way to achieve this. Because of the large volume of sample needed, it is only used in the fast injection LD (chapter 7) to record the fast kinetics. The Couette flow orientation system, derived from the independent inventions of Maurice Frédéric Alfred Couette and Henry Reginald Arnulph Mallock who in the late 1800s developed a method to measure viscosity based on shearing a liquid between coaxial cylinders (Couette 1890, Mallock 1888, Mallock 1896, Donnelly 1991), is the most widely used method of sample orientation for normal LD.

In Couette flow, the sample is placed between two cylinders at least one of which rotates. The velocity difference between the two cylinders gives rise to a shear force which orients the sample. The micro-volume Couette flow cell developed at Warwick (Marrington et al. 2005) is illustrated in figure 3.1.3. In this case the outer quartz capillary whose base is sealed with a plug of Araldite Rapide rotates, and the inner rod which is suspended vertically from the lid, remains stationary. An annular

gap of ~0.25 mm between the quartz rod suspended from the demountable lid and inner capillary wall was created.

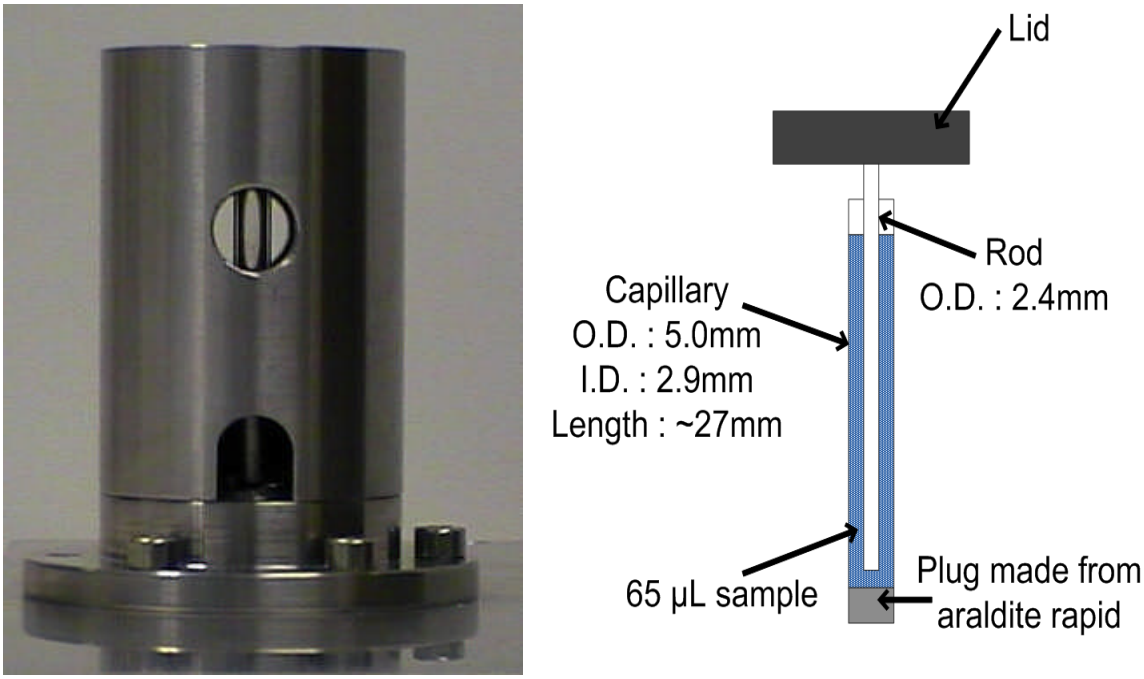

Figure 3.1.3 Micro-volume Couette LD cell and the schematic diagram showing the capillary and rod assembly.

The voltage applied to the motor that rotates the outer quartz cylinder is controlled electronically to allow the sample solution to be maintained with the highest possible degree of alignment without inducing turbulent flow and Taylor vortices. 3 V (corresponding to ~3000 rpm) was used unless otherwise mentioned. Extensive validation of this cell has been undertaken by R. Marrington (Marrington et al. 2005). The rotation speed, ω (rpm), can be converted to shear rate, G (s^{-1}), using the following equations:

$$G = \frac{dv_z}{dx} = \frac{2\pi R_o \omega}{60\left(R_o - R_i\right)}$$

where R_i and R_o are the radii of the inner and outer cylinders respectively.

3.1.4 Right-angle light scattering

Classical light scattering (also known as static or Rayleigh scattering) involves measuring the amount of light scattered by a solution at some angle relative to the incident light beam. Rayleigh scattering is the elastic scattering of light or other electromagnetic radiation by particles (*e.g.* proteins smaller than ~500 kDa) much smaller than the wavelength of the light. During elastic scattering, the scattered photons have the same energy (frequency) and wavelength as the incident photons, and the intensity of the scattered light is uniform in all directions. Therefore it is only necessary to measure scattering at a single angle (usually 90 degrees), and the excitation and emission wavelengths are set at the same.

The amount of Rayleigh scattering that occurs for a beam of light is dependent upon the size of the particles and the wavelength of the light. Specifically, the intensity of the scattered light varies as the sixth power of the particle size and varies inversely with the fourth power of the wavelength. So at a fixed wavelength, this "classical" light scattering provides a direct measure of particle size.

In this project, right-angle light scattering (90° angle light scattering) measurements were carried out to monitor the dynamics of FtsZ polymerization and depolymerization, which is based on the preliminary work of Mukherjee and Lutkenhaus (Mukherjee and Lutkenhaus 1999). The experiments were performed on a Perkin Elmer LS50B spectrofluorimeter under a time drive mode. The excitation and emission slits were set to 2.5 nm and data were collected every second until GTP depletion.

3.2 Colourimetric assay for the quantification of inorganic phosphate (P_i)

Colourimetric analysis is a method of determining the concentration of a chemical compound in a solution with the aid of a color reagent. The color being measured is proportional to the concentration of the substance being tested. Beer's Law is used to make this relationship quantitative. In the UV region, there is no visible color change but the principle is exactly the same, *i.e.* the change in the absorbance of the solution is measured.

The inorganic phosphate (P_i) released from GTP hydrolysis catalysed by FtsZ (§ 4.4) can be easily quantified employing a fast and sensitive colourimetric assay (figure 3.2). The method is based on an assay originally described by Webb (Webb 1992) and it consists of an enzymatic conversion by PNP (purine nucleoside phosphorylase) of the substrate MESG (2-amino-6-mercapto-7-methylpurine riboside) to ribose- 1-phosphate and 2-amino-6-mercapto-7-methlpurine in the presence of inorganic phosphate (P_i). The enzymatic conversion of MESG to ribose-1-phosphate and 2-amino-6-mercapto-7-methlpurine results in the shift of maximum absorption from 330 nm (substrate) to 360 nm (products). The change in absorption at 360 nm allows quantification of the inorganic phosphate consumed in the reaction. One of the main advantages of this assay is that the change in absorption at 360 nm allows quantification of P_i outside the absorbance envelope of most biological molecules.

EnzCheck® Phosphate Assay Kit (E-6646) was used to quantify P_i. (http://probes.invitrogen.com/media/pis/mp06646.pdf). The kit contains MESG substrate (6.3 mg, 20 µM), purine nucleoside phosphorylase (PNP) (two vials, each containing 50 U of lyophilized enzyme), 20× reaction buffer (10 mL of 1.0 M Tris-HCl, 20 mM $MgCl_2$, pH 7.5, containing 2 mM sodium azide) and phosphate standard (500 µL of 50 mM KH_2PO_4, containing 2 mM sodium azide). The reagents

were prepared and stored according to the manufacturer's directions. Upon receipt, the kit was stored at –20°C. A 1 mM stock solution of MESG was prepared by adding 20 ml of distilled water to the bottle containing MESG. After extensive mixing, the stock solution was aliquoted in 200 µl and kept at –20°C. Fresh aliquot(s) were thawed for every experiment. A 100 U/ml stock solution of PNP was prepared by adding 500 µl of distilled water to a vial, then store at 4 °C. The measurements were carried out at 25°C on a Cary 1E double beam UV-visible spectrophotometer unless otherwise mentioned.

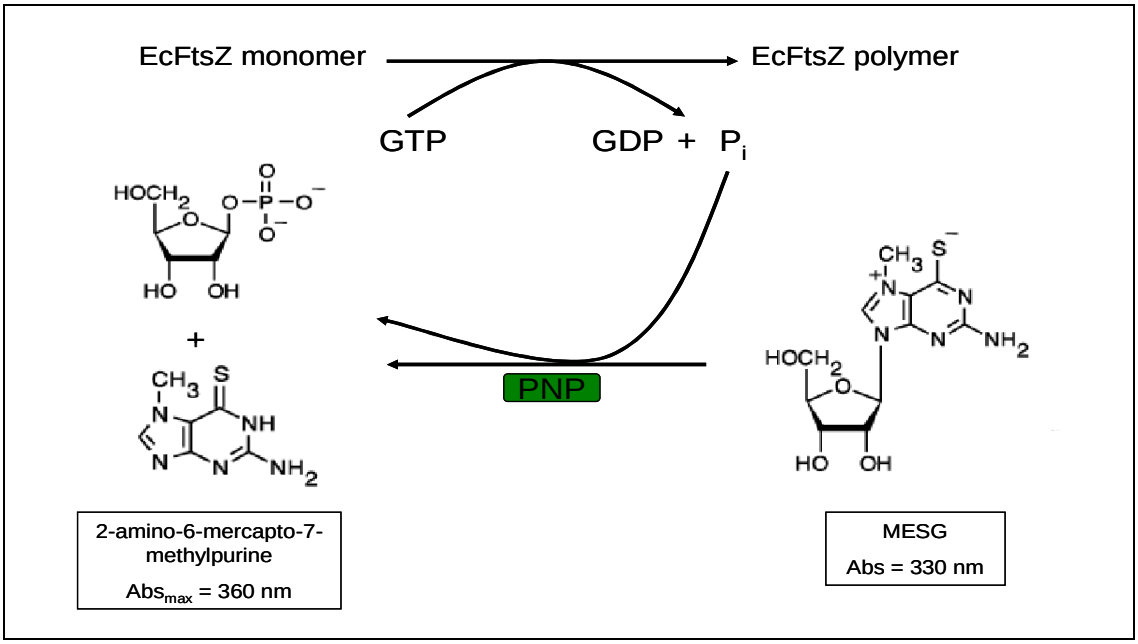

Figure 3.2 Schematic diagram of a simplified inorganic phosphate (P_i) release model following GTP hydrolysis catalysed by FtsZ and posterior enzymatic conversion of 2-amino-6-mercapto-7-methyl-purine riboside (MESG) to ribose-1-phosphate and 2-amino-6-mercapto-7-methylpurine by purine nucleoside phosphorylase (PNP). The change in absorption at 360 nm allows quantification of the inorganic phosphate produced in the hydrolysis reaction.

3.3 Analytical ultracentrifugation

Analytical ultracentrifugation (AUC) is a very versatile and powerful technique used for determining the molecular weight and the hydrodynamic and thermodynamic properties of a protein or other macromolecule. The ultracentrifuge is a centrifuge optimized for spinning a rotor at very high speeds, capable of generating acceleration as high as 2 to 3 million ×g (Moroz 1980). In an analytical ultracentrifuge, a sample being spun can be monitored in real time through an optical detection system, using UV/visible absorption and/or refractive index. This allows the operator to observe the sample concentration gradient as a function of radius in the applied centrifugal field.

The Beckman Coulter XL-I ultracentrifuge used in this project contains two optical detection systems: absorption optics in the UV/visible region and Rayleigh interference optics. The absorption optics system is based on the proportional relation between the concentration of the solute in a solution and its optical density (the Beer-Lambert Law). Most biological macromolecules absorb light in the near UV region. Nucleic acids have a very strong absorption around 260 nm, while proteins are characterised by an absorption peak close to 280 nm (§ 2.4.2.1 & § 2.5). The Rayleigh interference optics system can be applied to macromolecules that do not absorb significantly in the UV/visible range.

Two different types of experiments can be performed in an analytical ultracentrifuge: sedimentation velocity (SV) and sedimentation equilibrium (SE).

3.3.1 Sedimentation velocity experiments

Sedimentation velocity measures the rate at which molecules move in response to centrifugal force generated in a centrifuge. This sedimentation rate provides information about both the molecular mass and the shape of molecules. For a sedimentation velocity experiment, an initially uniform solution is placed in the cell

and a sufficiently high angular velocity is applied. The high centrifugal force depletes all the solute from the region nearest the center of the rotor, forming a boundary which moves toward the outside of the rotor. The rate of this movement of the boundary is measured by a series of scans at regular intervals using either absorbance or refractive index detection, typically 3 to 6 hours.

The rate at which the sedimentation boundary moves is a measure of the sedimentation coefficient of the solute. The sedimentation coefficient depends on the molecular weight (larger molecules sediment faster) and also on molecular shape. Unfolded proteins or one with highly elongated shapes will experience more hydrodynamic friction, and thus will have smaller sedimentation coefficients than a folded, globular protein of the same molecular weight.

In addition, the minimum width of the sedimentation boundary is related to the diffusion coefficient of the molecule; the presence of multiple species with similar sedimentation coefficients will cause the boundary to be broader than expected on the basis of diffusion alone.

Figure 3.3A shows a schematic diagram of a sedimentation velocity cell and the typical data from a sedimentation velocity experiment. Sedimentation velocity cells are cylindrical, and have a double-sector centerpiece. One sector is for loading sample, and the other is the reference sector and contains the solvent. The reference sector is filled slightly more than the sample sector so that the reference meniscus does not obscure the sample profile. Cells have upper and lower plane windows of optical grade quartz, which light can come through.

3.3.2 Sedimentation equilibrium experiments

Sedimentation equilibrium is used to measure protein molecular masses in solution and study protein-protein interactions. In a sedimentation equilibrium experiment

the sample is spun in an analytical ultracentrifuge at a speed high enough to force the protein toward the outside of the rotor, but not high enough to cause the sample to form a pellet. As the centrifugal force produces a gradient in protein concentration across the centrifuge cell, diffusion acts to oppose this concentration gradient. Eventually an exact balance is reached between sedimentation and diffusion, and the concentration distribution reaches equilibrium. This equilibrium concentration distribution across the cell is then measured while the sample is spinning, using either absorbance or refractive index detection. Generally, a sedimentation equilibrium experiment takes 24 hours, and several scans are recorded to try to ascertain that equilibrium has been reached (*e.g.* no difference has been observed from the consecutive two scans).

Sedimentation equilibrium distributions in the centrifugal field are characterized by Boltzmann distributions. The concentration distribution at equilibrium depends only on molecular mass, and is insensitive to the shape of the molecule. Furthermore, for proteins which self-associate to oligomers, or for mixtures of molecules that bind to one another, the overall distribution will also be in chemical equilibrium for the association process, and therefore will reflect the higher molecular weight of the associated states and their proportion in the sample.

Figure 3.3B shows a schematic diagram of a sedimentation equilibrium cell and the typical data from a sedimentation equilibrium experiment. The sedimentation equilibrium cell has 6 centerpieces. One row is for loading the sample, and the other is for reference containing only solvent. As is in the sedimentation velocity experiment, the reference columns are filled more than the sample columns, so that the reference meniscus does not obscure the sample profile. In the three sample centerpieces, the concentrations are varied, usually 0.25, 0.5 and 0.8 of absorbance at the selected wavelength.

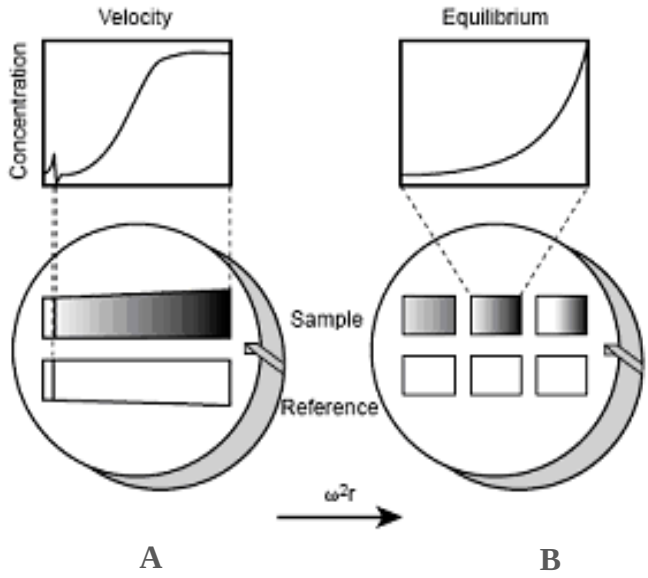

Figure 3.3 Typical cells and data from a sedimentation velocity experiment (A) and a sedimentation equilibrium experiment (B). The sample is rotated at high angular velocity that causes the solute moving towards the bottom of the cell. Reproduced from Cole and Hansen (Cole and Hansen 2000)

A major advantage of sedimentation velocity over sedimentation equilibrium is that experiments usually require only 4–6 hours, as opposed to the several days typical of sedimentation equilibrium. Thus sedimentation velocity can be used with samples that are too labile or unstable for sedimentation equilibrium. However, for interacting systems (proteins that reversibly self-associate or protein-protein complexes), the non-equilibrium nature of the measurement can lead to significant changes in species distributions over the course of an experiment. Thus it is generally more accurate to derive binding constants from sedimentation equilibrium data.

3.3.3 Analysis of the data

Coupled with appropriate software and data analysis methods, experiments performed *via* analytical ultracentrifugation are capable of rigorously determining

true solution sample size (molecular weight), and identifying the presence of different oligomerization states.

SEDFIT is the software used in this study, written at the National Institutes of Health in The United States (http://www.analyticalultracentrifugation.com/default.htm). This software programme is based on analytical and numerical algorithms to fit the Lamm equation (Lamm 1929) and/or the Svedverg equation (Svedverg 1940) in order to determine sedimentation coefficient and/or molar mass.

In sedimentation velocity, the sedimentation coefficient, *s*, of a particle is (Serdyuk, Zaccai and Zaccai 2007):

$$s = v / \omega^2 r = M\left(1 - \bar{v}\rho_0\right) / N_A f$$

where *v* is the velocity of the molecule, ω is the angular velocity of the rotor, *r* is the radial distance, *M* is the molecular mass, $\bar{v}$ is the partial specific volume of the solute, ρ_0 is the density of the solvent, N_A is Avogadro's number and *f* is the frictional coefficient.

In sedimentation equilibrium, the macromolecular concentration distribution between the meniscus at r_1 and point r_2 obeys an exponential law, called the second Svedberg equation (Serdyuk et al. 2007):

$$C\left(r_1\right) = C\left(r_2\right)\exp\left[\omega^2 M\left(1 - \bar{v}\rho_0\right)\left(r_1^2 - r_2^2\right) / 2RT\right]$$

where *C(r)* is the concentration gradient as a function of radius (*r*), *R* is the gas constant, *T* is the absolute temperature.

Density and viscosity can be either experimentally measured or calculated from the composition of the solvent. For most proteins under common experimental conditions, the effective partial specific volume can be predicted from the amino acid sequence, using for example the software SEDNTERP, written by Dr. John Philo (http://www.jphilo.mailway.com/download.htm). This software can also enable one to calculate the solvent density and viscosity containing common salts, buffering agents, and stabilizers such as sucrose, glycerol or mannitol.

Note: For some computers, this software only works in safe mode.

3.4 Dynamic light scattering

Dynamic light scattering (DLS), sometimes referred to as Photon Correlation Spectroscopy (PCS), is a technique that enables measurement of the size of the distribution profile of small particles in solution as long as the particles are small compared to the incident wavelength. Typical applications are size characterization of proteins, polymers and colloidal dispersions.

When a monochromatic and coherent source of light such as a laser with a known frequency hits small particles, the light is scattered in all the directions (Rayleigh scattering). Normally DLS is concerned with measurement of particles suspended within a liquid. If the particles or molecules are illuminated with an incident light beam, the intensity of the scattered light fluctuates at a rate that is dependent upon the size of the particles due to Brownian motion. Brownian motion is the random movement of particles due to the bombardment by the solvent molecules that surround them. The larger the particle, the slower the Brownian motion will be. Smaller particles with less inertia are “kicked” further by the solvent molecules and move more rapidly.

The velocity of the Brownian motion is defined by a property known as the translational diffusion coefficient (*D*). In dynamic light scattering, the speed at which the particles are diffusing due to Brownian motion is measured. This is done by measuring the rate at which the intensity of the scattered light fluctuates. These motion data are processed to derive a size distribution for the sample, where the size is given by the "hydrodynamic diameter", and refers to how a particle diffuses within a fluid. The diameter obtained by this technique is that of a sphere that has the same translational diffusion coefficient as the particle being measured.

The size of a particle is calculated from the translational diffusion coefficient by using the Stokes-Einstein equation:

$$d(H) = \frac{kT}{3\pi\eta D}$$

where *d(H)* = hydrodynamic diameter, *D* = translational diffusion coefficient, *k* = Boltzmann's constant, *T* = absolute temperature, η = viscosity.

The translational diffusion coefficient will depend not only on the size of the particle "core", but also on any surface structure, as well as the concentration and type of ions in the medium. In addition, an accurately known temperature is necessary for DLS because knowledge of the viscosity is required. The temperature also needs to be stable; otherwise convection currents in the sample will cause non-random movements of the molecule.

The advantage of using DLS is the possibility of analysing samples containing a broad distribution of species differing in molecular mass and to detect very small amounts of aggregate. In addition, it takes a short time to perform the experiment. One disadvantage of the technique is the lack of information on the shape of the

measured particles, which might give a false estimate of the molecular weight or size.

In this project, the DLS measurements were performed on the instrument Zetasizer Nano S (Malvern), equipped with a 5 mW He-Ne laser (633 nm). DLS was observed at a 173° scattering angle and a temperature of 25□°C, using the DTS2145-low volume glass cuvette (45 µl).

3.5 Electron microscopy

An electron microscope is a type of microscope that uses a particle beam of electrons to illuminate the specimen and produce a magnified image. Electron microscopes have a greater resolving power than a light-powered optical microscope, because electrons have wavelengths about 100,000 times shorter than visible light (photons) (Erni et al. 2009).

The transmission electron microscope (TEM) employed in this study is the original form of electron microscope that uses a high voltage electron beam transmitted through the specimen to create an image. The TEM works much like a slide projector. The beam of electrons is focused through the sample (the “slide”), and then projected onto the viewing screen, forming an enlarged image. The image obtained represents differences in electron scattering power of different regions of the sample. The darker areas of the image represent those areas of the sample that fewer electrons have been transmitted through (they are thicker or denser). The lighter areas of the image represent those areas of the sample that more electrons were transmitted through (they are thinner or less dense). The microscope must be under high vacuum, otherwise the electron beam would be scattered by the air.

The major technical drawback in using electron microscopy to image molecules is contrast. The electron density in the sample molecule is usually very similar to the

substrate or support film upon which it is mounted, so it can be hard to visualize against the background. Contrast can be enhanced by using heavy metal stains (with higher electron density), but this also tends to reduce the resolution of the image.

3.5.1 Sample preparation for EM

Specimen support

During imaging, the sample has to be kept free from drift. It is usually held on a carbon film that is placed on a grid. The grid has numerous holes large enough for the electron beam to travel through but small enough for the sample to form a fine film over the surface, covering the grid's holes.

Grids have been made of many different materials and of different mesh size. Most biological EM work is done on small (several millimeters) G400 copper grids, which have 400 meshes per square inch. On top of this grid, a thin layer of carbon is deposited by evaporating graphitic carbon onto it. Carbon is generally a hydrophobic substance. To make the surface more accessible to water and the suspended sample, the carbon needs to be made hydrophilic. This is accomplished by glow discharge. In order to glow discharge the carbon coated grids, the grids were placed carbon side up (noted in the box) onto a glass slide and put in the chamber of the glow discharge device (Emitech K100X) for 20 seconds at lower settings (10 mA, pale purple glow). When high voltage is applied between the cathode and anode at each end of the chamber that is filled with an inert gas at a certain pressure, the electron potential ionizes the gas within the chamber. These electrons then deposit on the carbon, giving the carbon film an overall hydrophilic surface.

Negative staining

Negative staining has been applied widely to the study of biological samples. It is a simple and rapid method for determining the overall morphology of a macromolecule and leads to high-contrast images.

The main constituents of biological molecules (oxygen, carbon and nitrogen) are not very electron dense and so do not interact strongly with the electron beam. The sample is therefore negatively stained by embedding it in an electron dense material, such as uranium or lead salt. In the electron micrograph, the sample appears as a light region surrounded by a dark background originating from the stains. The particle itself is not observed but its surrounding stain is. The sample structure is hence inferred by the distribution of the heavy stain and therefore has limited achievable resolution.

Methods

There are several methods for negative staining the sample. The method used in this study is described below.

5 µl of the sample mixture were placed onto the carbon side of the grid (glow discharged) for 1 minute and the sample was immediately stained by washing with seven drops of 1% UA (uranyl acetate) solution. The last two drops of the 1% UA solution was left for 20 seconds respectively before the excess liquid was gently blotted with a filter paper. Then the grid was allowed to dry in air and ready to be examined in the microscope.

The electron microscopy study of FtsZ polymers (§ 5.5 & § 6.5) has been done using this negative staining. The samples were then viewed by a JEOL 2011 transmission electron microscope.

CHAPTER 4 – THE TEST OF FtsZ QUALITY BY MEASURING ITS DYNAMIC ASSEMBLY REGULATED BY GTP#

4.1 Introduction

The cytoskeleton was previously thought to be a feature only of eukaryotic cells, but homologues to all the major proteins of the eukaryotic cytoskeleton have recently been found in prokaryotes (Shih and Rothfield 2006). FtsZ, which is a homolog of tubulin, was the first protein of the prokaryotic cytoskeleton to be identified, and plays important roles in cytokinesis. Like tubulin, FtsZ forms filaments in the presence of GTP, but these filaments do not group into tubules. During cell division, FtsZ is the first protein to move to the division site forming a ring called Z-ring, and is essential for recruiting other proteins that synthesize the new cell wall between the dividing cells (§ 1.1–1.2).

The discovery of the Z-ring raises intriguing biochemical questions such as its initial assembly, maintenance and disassembly, although it is likely that one of the major functions of the Z-ring is to recruit other proteins to the future division site. The polymerization of FtsZ has been successfully achieved in some laboratories, and it appears that FtsZ assembly dynamics are finely regulated and small changes in its assembly kinetics can result in large changes in the Z-ring structure (Lutkenhaus and Addinall 1997).

Similar to tubulin, FtsZ is a GTPase that polymerizes in a GTP-regulated manner into dynamic protofilaments in the presence of GTP. FtsZ assembly is coupled to GTP hydrolysis. GTP hydrolysis destabilizes FtsZ polymers, promoting disassembly into individual subunits. Once all of the GTP is converted to GDP, the polymers revert back to monomers (§ 1.1–1.2).

4.2 Objectives

In this chapter we report the results of investigating the dynamic behaviour of FtsZ polymerization *in vitro.* This is a way to test FtsZ quality and to determine whether the FtsZ produced for this work behaved in the same way as described in the literaturea. In the literature, FtsZ polymerization was reported to be affected by factors such as pH, K^+, and Mg^{2+}. We employed two major techniques, right-angle light scattering and GTPase assay to study FtsZ dynamic behavior, and to compare the results with literature data.

4.3 Expression and purification of EcFtsZ

EcFtsZ was expressed and purified as described above (§ 2.3.1). To overproduce FtsZ, *E. coli* competent cells B834 (DE3) were transformed with the plasmid DNA pETFtsZ, which contains an *ftsZ* open reading frame downstream of the high expression T7 promoter. LB containing 100 μg/ml ampicillin was inoculated with a fresh colony of the transformed B834 (DE3) and grown overnight with shaking at 37 °C. When the OD_{600} reached 0.3, IPTG was added to a final concentration of 1 mM, and the culture grown for another 3–4 hours. Cells were then harvested at 7,000 rpm at 4 °C and washed once with cold 10 mM Tris-HCl, pH 7.9, followed by another centrifugation.

From this step onward all operations were done at 4 °C unless otherwise noted. The cells were resuspended in 50 mM Tris-HCl, pH 7.9, 50 mM KCl, 1 mM EDTA and 10% glycerol (buffer A) prior to lysis by sonication. The resulting extract was then centrifuged at 10,000 g for 10 minutes to remove unbroken cells and debris and the supernatant was centrifuged then at 75,600 g for 90 minutes to remove the membrane fraction. The supernatant was then collected and fractionated with 30% ammonium sulfate (16.6 g / 100 ml of extract). The ammonium sulfate precipitate

was recovered by centrifugation at 20,000 × g for 10 minutes, resuspended in buffer A and dialyzed extensively against the same buffer.

The dialyzed sample was passed through a HiPrep 16/10 DEAE FF column, and washed with 5 bed volumes of buffer A and eluted with 200 ml of a 50 mM – 1 M KCl gradient at a flow rate of 0.2 ml/min. FtsZ was monitored during purification by SDS–PAGE, which is shown in figure 4.3. The heavy stained bands were at approximately 45 kDa and correspond to the overexpressed EcFtsZ protein. Lane 3 appeared as one major band with some contamination. The protein concentration was assayed with the Bio-Rad Assay reagent (§ 2.4.2.2).

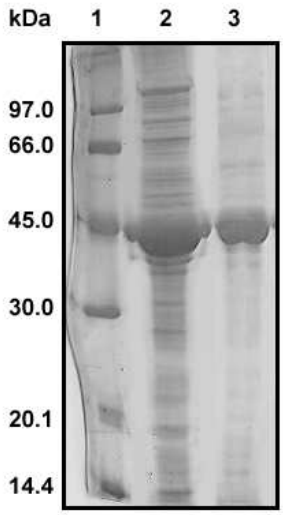

Figure 4.3 12% SDS-PAGE gel. Lane 1, protein marker; Lane 2, ammonium sulfate fraction of FtsZ, 5 µl of which was mixed with 5 µl of 5× loading buffer and loaded into the corresponding lane after denaturing at 95°C; Lane 3, FtsZ fraction from ion exchange column (DEAE-Sepharose), 3 µl of which was mixed with 5 µl of 5× loading buffer and loaded into the corresponding lane after denaturing at 95°C.

4.4 Analysis of FtsZ assembly by right-angle light scattering

Right-angle light scattering (or 90° angle light scattering) can be used to monitor the dynamics of FtsZ polymerization, steady state and depolymerization, based on the preliminary studies by Mukherjee and Lutkenhaus (Mukherjee and Lutkenhaus 1999). Results similar to those previously published were obtained for this batch of FtsZ.

For the standard polymerization assay, FtsZ to a final concentration of 71 μM was mixed with the polymerization buffer, which contains 50 mM MES-KOH (2-[N-Morpholino]ethane sulfonic acid), pH 6.5, 50 mM KCl, and 10 mM $MgCl_2$ at room temperature in an eppendorf tube. The solution was then transferred to the 0.3 cm path length fluorimeter cuvette (45 μL nominal volume). The cuvette was then placed in the cuvette chamber and the signal (a baseline) was collected for approximately 10 minutes. After the baseline had been obtained, the cuvette was removed and the polymerization reaction was initiated by the addition of GTP to a final concentration of 0.2 mM. The reaction mixture was gently stirred with a pipette tip and the cuvette was returned to the cuvette chamber for data collection. The delta light scattering, which is the change in light scattering after addition of GTP to the reaction media, is shown in the result, plotted as a function of time.

4.4.1 The cycle of FtsZ polymerization

As illustrated in figure 4.4.1, before GTP was added, the baseline of FtsZ in polymerization buffer was collected, which was defined as 0 in light scattering. After the addition of GTP, there was an increase in light scattering of approximately 60 units. This level remained constant for about 2 minutes, after which point the light scattering signal started to decrease, reaching the baseline value within 10 minutes.

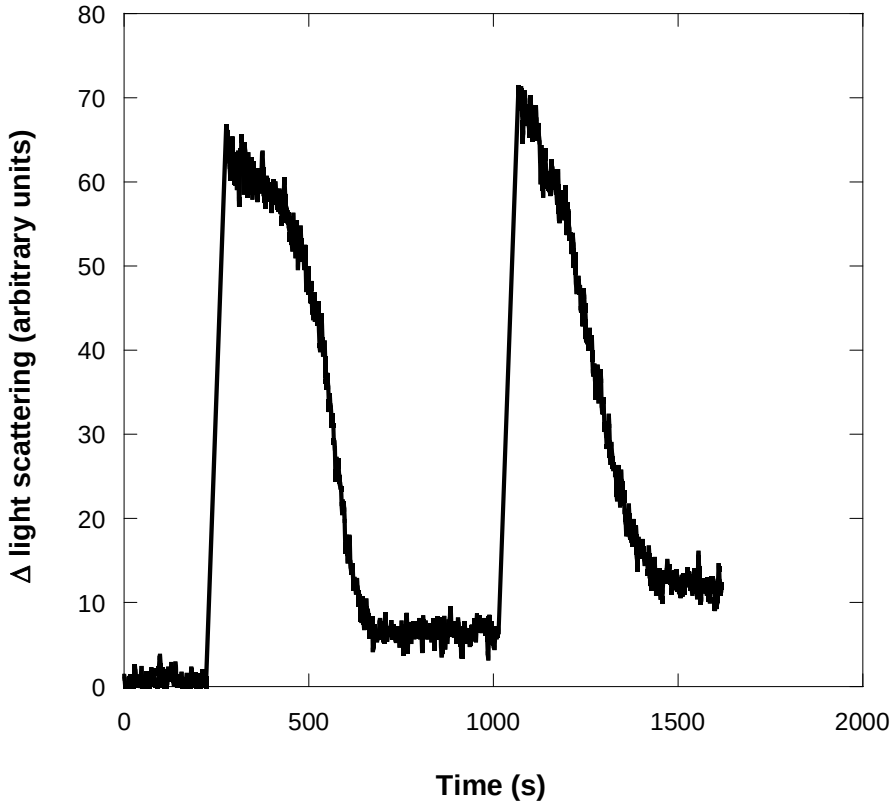

Figure 4.4.1 Assessment of the dynamic behaviour of FtsZ as observed by the increase and posterior decrease in light scattering. Polymerization was initiated by the addition of GTP (final concentration of 0.2 mM) to 71 μM FtsZ in 50 mM MES buffer pH 6.5, 50 mM KCl and 10 mM $MgCl_2$. Data were collected every second at room temperature in a 3 mm path length fluorescence cuvette (45 μL nominal volume) with excitation and emission wavelengths set at 540 nm. A cycle of polymerization can be initiated by the addition of 0.2 mM GTP after FtsZ was depolymerised.

The rapid increase in light scattering suggests that FtsZ undergoes rapid polymerization. After the rapid polymerization, it reaches a steady state, where excess GTP is being consumed. After the plateau, there is a rapid decrease in the light scattering which indicates the end of the steady-state phase. This is almost certainly due to GTP depletion, because of GTP hydrolysis, with consequent FtsZ

depolymerization. A cycle of FtsZ polymerization can be re-initiated readily after FtsZ depolymerization by the new addition of GTP to the reaction media. Interestingly, the disassembly of FtsZ did not induce the intensity of light scattering to go down to zero, possibly because some aggregation of FtsZ happened during the polymerization, which is not reversed.

4.4.2 FtsZ polymerization with different concentrations of FtsZ and GTP

Concentrations of FtsZ and GTP were also changed respectively to characterize FtsZ polymerization behaviour. Firstly, GTP to a final concentration of 0.2 mM was added into different concentrations of FtsZ in the polymerization buffer to start FtsZ polymerization.

It is known that light scattering is directly proportional to polymer mass and concentration (Wyatt 1993). From figure 4.4.2.1, we can see that when the FtsZ concentration was reduced from 71 to 43 μM, the increase in the light scattering being representative of FtsZ polymers reached approximately from 60 to 40 units after the addition of GTP. The amount of light scattered suggests that when there was plenty of FtsZ (71 μM), more FtsZ protofilaments were formed. The length of the steady-state period, where the polymer mass remains constant, increased from 3 to 6 minutes when the concentration of FtsZ decreased from 71 to 43 μM. That the steady-state time varied exactly inversely with the FtsZ concentration indicates that the increase of FtsZ concentration accelerates the rate of GTP consumption. After this stage, there was a net decrease in the light scattering due to complete GTP hydrolysis. These data suggested that GTP hydrolysis is dependent on FtsZ concentration.

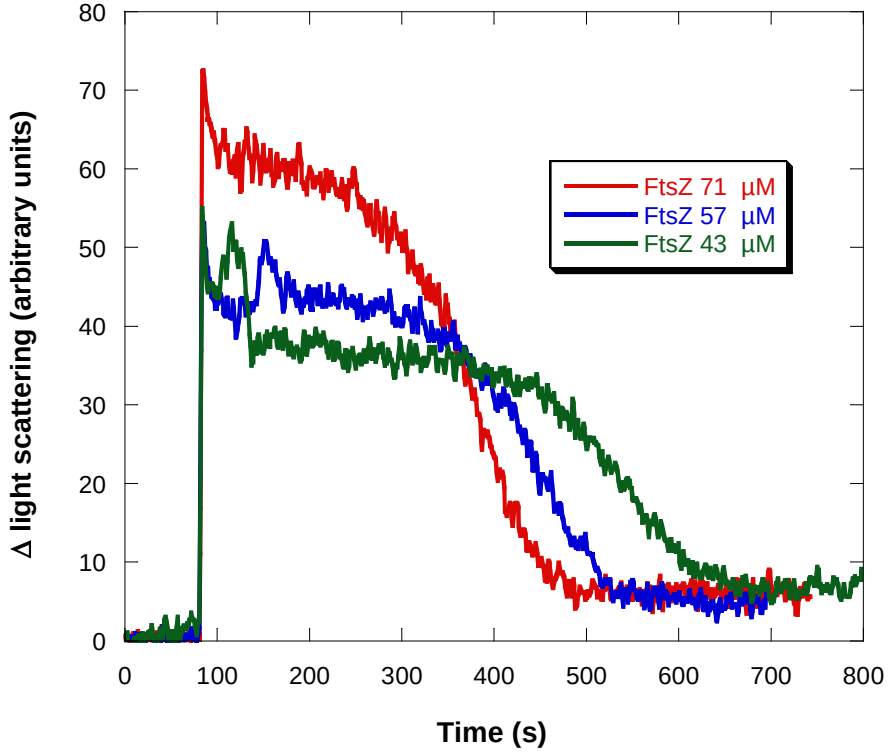

Figure 4.4.2.1 Assessment of the dynamic nature of FtsZ polymers at different concentrations as indicated by light scattering. Polymerization was initiated by the addition of GTP (final concentration of 0.2 mM) in 50 mM MES buffer pH 6.5, 50 mM KCl and 10 mM $MgCl_2$. Data were collected every second at room temperature in a 3 mm path length fluorimeter cuvette (45 µL nominal volume) with excitation and emission wavelengths set at 540 nm.

In another approach, we varied the GTP concentration to verify the above interpretation. Polymerization was initiated by adding GTP at different concentrations to reactions containing FtsZ at 71 µM. As shown in figure 4.4.2.2, after the addition of GTP, the light scattering increased to around 70 units. The initial change in light scattering was not noticeably affected by GTP concentration. After that, it was apparent that the steady-state period of FtsZ dynamics shortened dramatically when GTP was reduced to 0.1 mM. The length of the steady-state period decreased from 5 to 1 minute when the concentration of GTP was reduced

from 0.3 to 0.1 mM. These experiments suggested that the amount of GTP required for FtsZ polymerization is fixed for a certain amount of FtsZ, and the size/amount of FtsZ protofilaments formed is related to FtsZ concentration rather than GTP concentration. However, GTP influences the duration of FtsZ assembly, that is to say, the excess of GTP is helpful in maintaining the steady state phase of FtsZ dynamics.

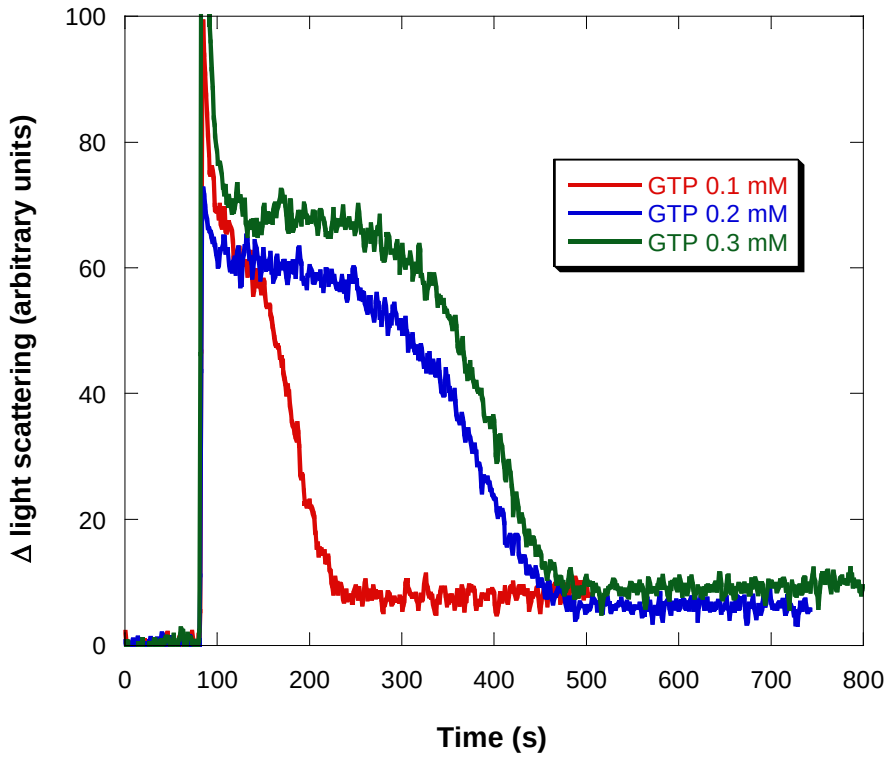

Figure 4.4.2.2 Assessment of the dynamic nature of FtsZ polymers by light scattering. Polymerization was initiated by adding GTP (at different concentrations as indicated) to 71 µM in 50 mM MES buffer pH 6.5, 50 mM KCl and 10 mM $MgCl_2$. Data were collected every second at room temperature in a 3 mm path length fluorimeter cuvette (45 µL nominal volume) with excitation and emission wavelengths set at 540 nm.

4.4.3 The effects of KCl on FtsZ polymerization

There are some factors which would affect FtsZ polymerization. Previous results (Mukherjee et al. 1993) have shown that the hydrolysis of GTP catalysed by FtsZ is affected by the KCl concentration. We obtained similar results to those previously published, which are reported in this section.

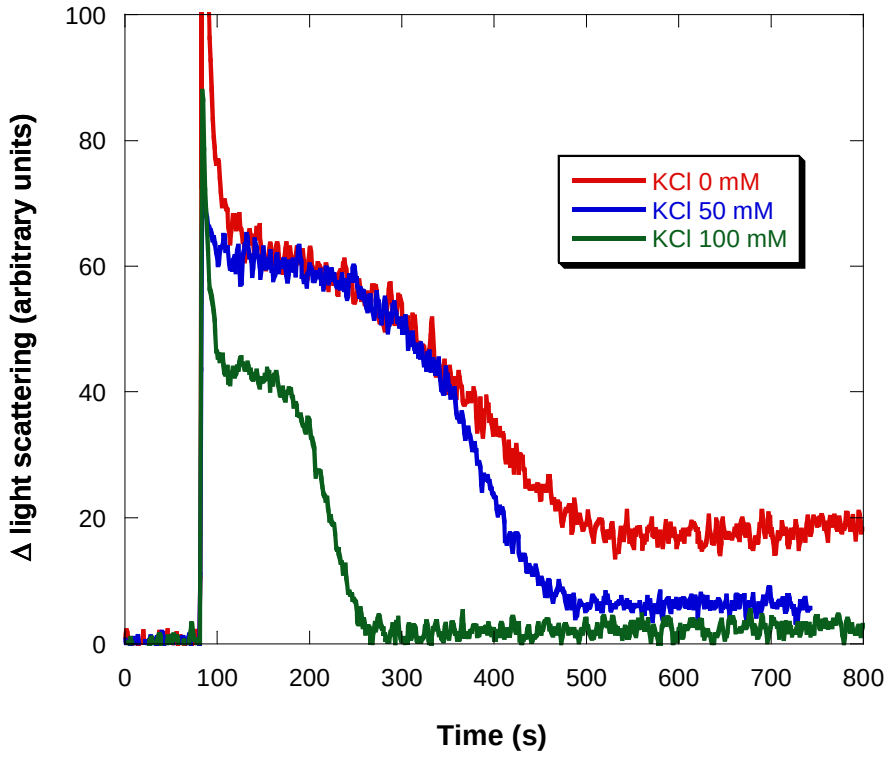

Figure 4.4.3 Effects of KCl concentration on FtsZ polymerization. Polymerization was initiated by the addition of GTP (final concentration of 0.2 mM) to 71 µM FtsZ in 50 mM MES buffer pH 6.5, 10 mM $MgCl_2$ and different concentrations of KCl as indicated. Data were collected every second at room temperature in a 0.3 cm path length fluorimeter cuvette (45 µl nominal volume). Excitation and emission wavelengths were set at 540 nm.

Polymerization was initiated by the addition of 0.2 mM GTP to 71 µM FtsZ in the polymerization buffer containing 50 mM MES pH 6.5, 10 mM $MgCl_2$ and varying concentrations of KCl. Figure 4.4.3 shows the initial increase in the light scattering

after the addition of GTP, and we find that the rate of GTP hydrolysis increases with increasing amounts of KCl between 0 and 100 mM. When KCl was absent, the increase in the light scattering reached approximately 60 units, and then it took 7 minutes before the light scattering stopped decreasing. In the end, the decrease in the light scattering did not reach the base level as 100 mM KCl did, which suggests that there may be FtsZ polymers still present. When 0.2 mM GTP was added to the FtsZ mixture containing 100 mM KCl, there was an initial increase in the intensity of light scattering, of approximately 40 units. This level started to decline after 2 minutes and reached zero after about 3 minutes. This experiment therefore demonstrates that KCl can accelerate the rate of GTP hydrolysis by FtsZ, though it is not essential for FtsZ polymerization. The effects of KCl on FtsZ's GTPase activity are further discussed below.

4.4.4 The effects of Mg^{2+} on FtsZ polymerization

The effects of varying the concentration of Mg^{2+} on the polymerization of FtsZ have also been studied. Figure 4.4.4 shows the results obtained. After the addition of GTP to a final concentration of 0.2 mM, an increase in light scattering was detected at all concentrations of Mg^{2+} examined, as well as in the absence of Mg^{2+}. The initial change in light scattering was directly correlated with the Mg^{2+} concentration. It increased significantly from approximately 10 to 100 units when the concentration of Mg^{2+} was raised from 0 to 20 mM, which indicates that Mg^{2+} is helpful in inducing FtsZ polymers, probably FtsZ bundles. After this initial increase, there was a constant value of the light scattering intensity for about 2 or 3 minutes before the light scattering started to rapidly decrease, when the concentration of Mg^{2+} is between 10 amd 20 mM. Importantly, in the complete absence of Mg^{2+}, this increase in the light scattering remained constant for as long as 45 minutes (data not shown), suggesting that FtsZ polymers formed but did not turn over. One possible explanation is that although Mg^{2+} is not required for GTP binding, it is essential for

GTP hydrolysis. The GTPase activity of the FtsZ in the presence or absence of Mg^{2+} is analysed in the following section.

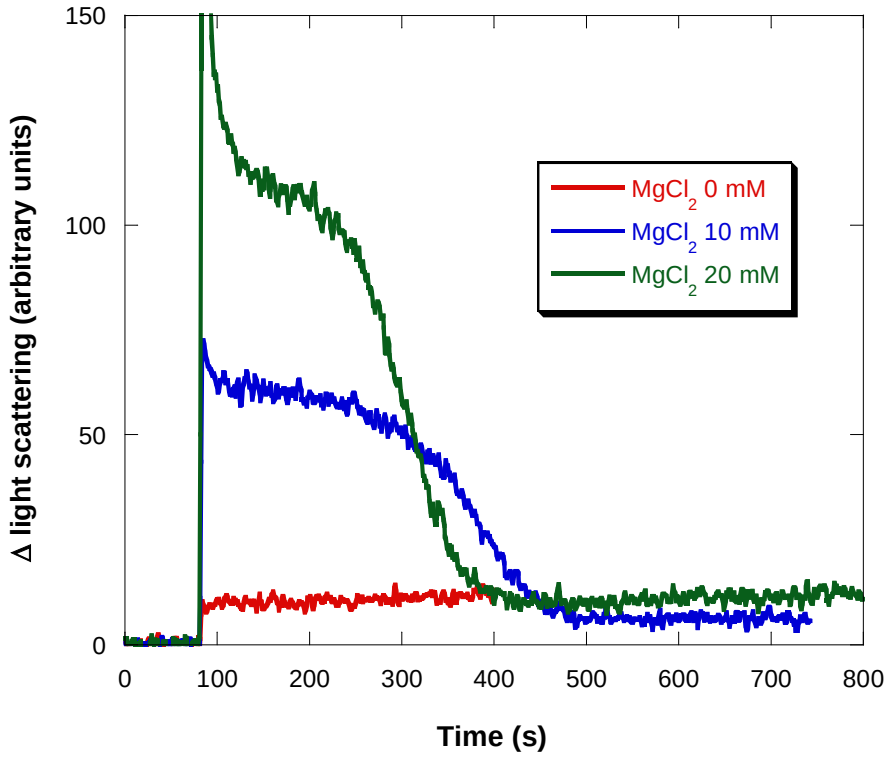

Figure 4.4.4 Effects of Mg^{2+} concentration on FtsZ polymerization. Polymerization was initiated by the addition of GTP (final concentration of 0.2 mM) to 71 µM FtsZ in 50 mM MES buffer pH 6.5, 50 mM KCl and different concentrations of KCl as indicated. Data were collected every second at room temperature in a 0.3 cm path length fluorimeter cuvette (45 µL nominal volume) with excitation and emission wavelengths set at 540 nm.

4.4.5 The effects of pH on FtsZ polymerization

FtsZ has been previously reported to polymerize over a broad pH range (Mukherjee 1999, Mukherjee and Lutkenhaus 1998). We have examined the effects of the pH on the formation of FtsZ polymers by light scattering, and similar results to those previously published were obtained.

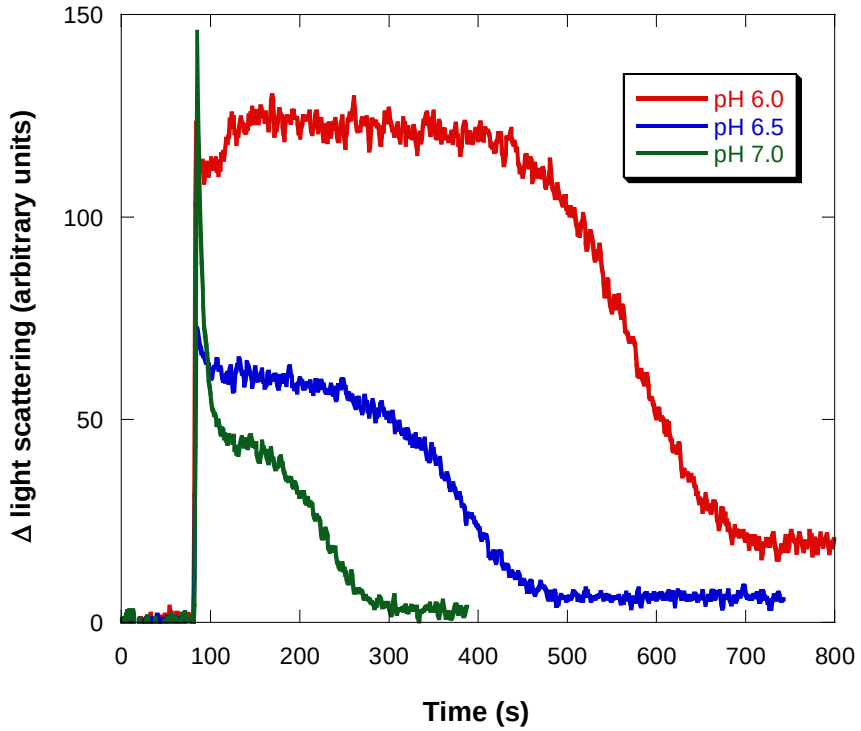

Figure 4.4.5 Effects of the pH on FtsZ polymerization. Polymerization was initiated by the addition of GTP (final concentration of 0.2 mM) to 71 µM FtsZ in 50 mM MES buffer of different pHs as indicated, 50 mM KCl and 10 mM $MgCl_2$. Data were collected every second at room temperature in a 0.3 cm path length fluorimeter cuvette (45 µL nominal volume) with excitation and emission wavelengths set at 540 nm.

Polymerization was initiated by the addition of 0.2 mM GTP to 71 µM FtsZ in the polymerization buffer containing 50 mM MES (altering the pH between 6.0 and 7.0), 50 mM KCl, and 10 mM $MgCl_2$. Figure 4.4.5 shows the GTP-dependent polymerization of FtsZ at three different pHs. It can be observed from the figure that an immediate increase of light scattering occurred upon addition of GTP at each pH studied, indicating FtsZ polymers were formed. However, the initial change in light scattering and the plateau region were different for the three pHs studied. At pH 7.0, the initial increase in the light scattering reached nearly 50 units, which increased significantly to 120 units when the pH is reduced down to 6.0. These differences in

the intensity of the light scattering could be explained by FtsZ bundling. At pH 6.0, the FtsZ easily forms bundled protofilaments, which would scatter more light and hence the light scattering intensity would obtain higher values. On the contrary, FtsZ mainly forms single protofilaments at pH 7.0, which scatter less light. In terms of the plateau region, the steady state period is approximately 6 minutes at pH 6.0, which is much longer than that of 1 minute at pH 7.0. This suggested that the rate of GTP hydrolysis is slower at lower pHs. This might because FtsZ bundling helps to stabilize the FtsZ polymers. Furthermore, it is also observed that the light scattering did not reach the base level at pH 6.0, suggesting there were FtsZ polymers still present. The GTPase activity of the FtsZ at different pHs is further analysed in the following section.

4.5 FtsZ's GTPase activity

The inorganic phosphate (P_i) released from the reaction of FtsZ catalysing the hydrolysis of GTP to GDP and P_i can be easily quantified employing a fast and continuous colourmetric assay that uses the dye MESG (2-amino-6-mercapto-7-methylpurine riboside). In the presence of P_i, the substrate MESG is converted enzymatically by PNP (purine nucleoside phosphorylase) to ribose-1-phosphate and 2-amino-6-mercapto-7-methylpurine. This conversion results in a spectrophotometric shift in maximum absorbance from 330 nm for the substrate to 360 nm for the product. The change in absorption at 360 nm allows quantification of the P_i consumed in the reaction. We can use this method as an indirect measure of FtsZ's GTPase activity.

The assay used here is a modification of that specified by the manufacturer (EnzCheck® Phosphate Assay Kit (E-6646), chapter 3). The kit contains MESG substrate, purine nucleoside phosphorylase (PNP), 20X reaction buffer, and phosphate standard. Instead of using the buffer supplied in the kit, we use our polymerization reaction buffer which contained 50 mM MES pH 6.5, 50 mM KCl

and 10 mM $MgCl_2$. A final concentration of 0.4 mM MESG instead of the 0.2 mM MESG recommended for the standard reaction was employed because we wanted to extend the linear range of the standard curve for inorganic phosphate to 200 µM, since we have used 200 µM GTP for the standard polymerization reaction (R. Pacheco-Gomez 2008, R. Pacheco-Gomez et al. 2011).

4.5.1 Standard curve for inorganic phosphate

Before the measurement of FtsZ's GTPase activity, we used the phosphate standard provided in the kit to generate the standard calibration curve for the inorganic phosphate assay. Different concentrations of phosphate standard from 0 to 250 µM were added to 0.4 mM MESG, 1 U/mL PNP and the polymerization reaction buffer (altering the pH between 6.0 and 7.5). The solution was then transferred to the 0.3 cm path length fluorimeter cuvette. After 10 minutes incubation at room temperature, the cuvette was placed in the cuvette chamber. The absorbance was then recorded respectively and the change in the absorbance at 360 nm was plotted as a function of the P_i concentration. The same procedure was followed for the different pHs studied in this project using MES as a buffer (pH 6.0, 6.5 and 7.0), and the results are shown in Table 4.5.1. The relative standard deviations (R.S.D.) of ΔA_{360} were between 1% and 3%, when the analysis was repeated for three times under the same conditions.

Table 4.5.1 ΔA_{360} after P_i addition to MES buffer at four different pHs (pH 6.0, pH 6.5, pH 7.0 and pH 7.5) for standard curve generation.

$[P_i]$ µM / **ΔA_{360}**	**0**	**50**	**100**	**150**	**200**	**250**
MES, pH 6.0	0	0.06	0.11	0.14	0.19	0.22
MES, pH 6.5	0	0.07	0.19	0.29	0.41	0.46
MES pH 7.0	0	0.16	0.31	0.45	0.59	0.71
MES pH 7.5	0	0.15	0.31	0.46	0.61	0.77

Figure 4.5.1 shows the change in the absorbance at 360 nm plotted as a function of the P_i concentration. We can observe the linear responses for all 4 pHs studied, which allows us to quantify directly the P_i released from the GTP catalysed by FtsZ. Besides, the standard calibration curves, for different concentrations of KCl or $MgCl_2$ were also studied; however, they almost remained the same (data not shown).

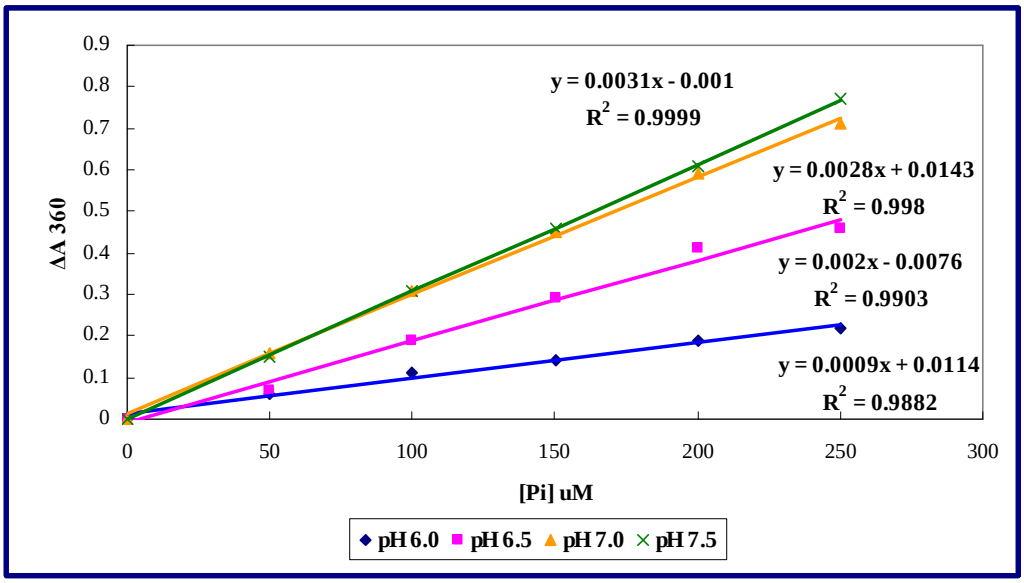

Figure 4.5.1 Change in absorbance at 360 nm plotted as a function of the P_i concentration.

4.5.2 Methods to detect FtsZ's GTPase activity

FtsZ catalyses the hydrolysis of GTP to GDP and P_i. The kinetics of P_i released continuously in this enzymatic reaction can be followed using the modified assay described above, in which FtsZ and GTP were added to generate P_i instead of the phosphate standard provided.

FtsZ to a final concentration of 11 μM was mixed with 0.4 mM MESG, 1 U/mL PNP and the polymerization buffer. Before adding GTP, it is important to examine reagents and enzymes for the possibility of P_i contamination. If there is no P_i

released from the enzyme and/or reagents, we should obtain a flat baseline for the absorbance at 360 nm. After such a baseline was obtained, A_{360} was zeroed, and the reaction started by the addition of 0.2 mM GTP. Then the absorbance at 360 nm was measured as a function of time until the reaction was complete. The data have been plotted and transformed to show the percentage of P_i released at any given time according to the calibration curves at the appropriate pH. 100% corresponds to complete hydrolysis of GTP to GDP, that is to say, if 0.2 mM phosphate was detected in the medium, it means 0.2 mM GTP completely converted to GDP.

4.5.3 Effects of KCl on FtsZ's GTPase activity

Light scattering results (§ 4.4.3) suggest that the hydrolysis of GTP is affected by the KCl concentration. The GTPase activity of FtsZ in different concentrations of KCl from 0 to 100 mM is reported in this section. FtsZ to a final concentration of 11 μM was mixed with 0.4 mM MESG, 1 U/mL PNP and the polymerization buffer, which contains 50 mM MES, pH 6.5, 10 mM $MgCl_2$ and varying concentrations of KCl. The reaction was initiated by the addition of 0.2 mM GTP at time 0. The results in figure 4.5.3 reveal that the GTPase activity is indeed affected by KCl as had been previously suggested by light scattering (§ 4.4.3).

Upon addition of GTP, P_i was released from the GTP hydrolysis catalysed by FtsZ, with a GTPase activity of 1.3 moles of GTP hydrolysed per mole of FtsZ per minute. Marrington *et al.* also measured GTPase activity of FtsZ under various buffer conditions (Marrington et al. 2004b). When the buffer contained 50 mM MES, pH 6.5, 50 mM KCl and 10 mM $MgCl_2$, the GTPase activity of FtsZ was found to be 1.8 mol mol^{-1} min^{-1}, which is a little higher than our result. This is probably because the real FtsZ concentration in the solution we made is somewhat lower than 11 μM, as indicated in the purification gel (figure 4.3).

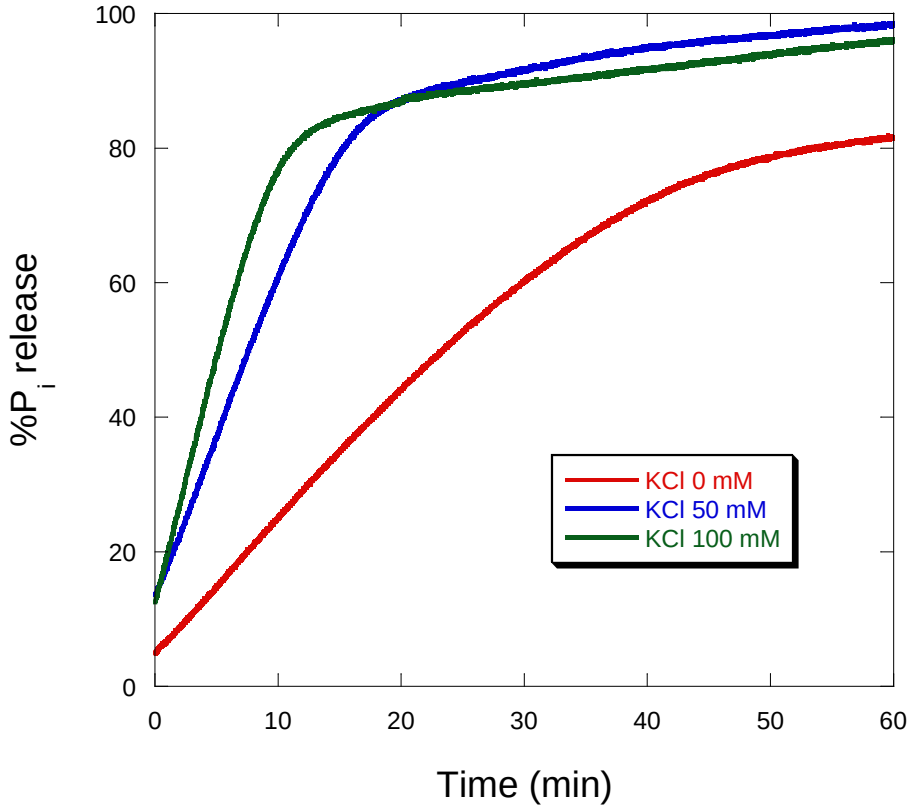

Figure 4.5.3 Effects of KCl on FtsZ's GTPase activity. The kinetics of P_i released from the enzymatic conversion of GTP to GDP catalysed by FtsZ in polymerization buffer which contained 50 mM MES buffer pH 6.5, 10 mM $MgCl_2$ and different concentrations of KCl as indicated was followed using a continuous colourmetric assay that measures ΔA_{360} between the substrate (MESG) and the products (ribose-1-phosphate and 2-amino-6-mercapto-7-methlpurine). Data were taken every 0.1 second for 60 minutes in a 0.3 cm path length cuvette (45 μL nominal volume) and transformed to show the percentage of P_i released at any given time.

In the experiment performed in the absence of KCl, we found that the P_i was released very slowly compared to the solutions which contained 50 mM KCl or 100 mM KCl. In the presence of 50 mM KCl or 100 mM KCl, the P_i release reached the end point, which corresponds to the maximum percentage of P_i released in the

reaction medium, within 20 or 12 minutes respectively. In the absence of KCl, the end point of P_i released was not reached within 60 minutes. Therefore it is demonstrated that KCl accelerating FtsZ depolymerization suggested by light scattering is due to the GTP hydrolysis being accelerated.

4.5.4 Effects of Mg^{2+} on FtsZ's GTPase activity

The effects of Mg^{2+} concentration ranging from 0 to 20 mM on FtsZ's GTPase activity are reported in this section.

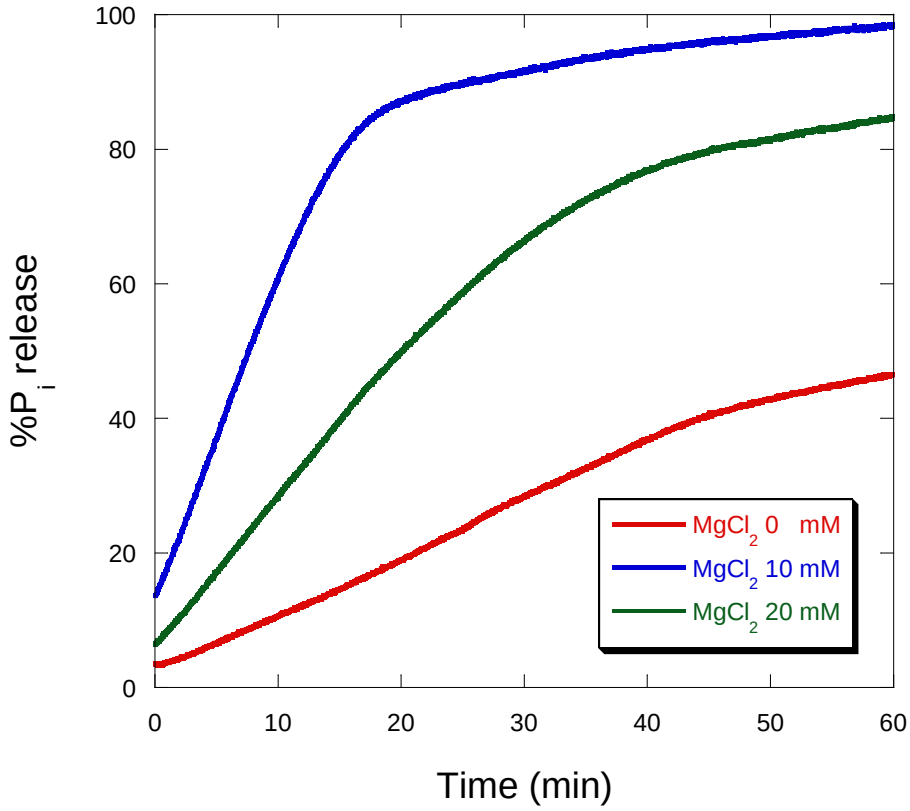

Fig.4.5.4 Effects of Mg^{2+} on FtsZ's GTPase activity. The kinetics of P_i released from the enzymatic conversion of GTP to GDP catalysed by FtsZ in polymerization buffer which contained 50 mM MES buffer pH 6.5, 50 mM KCl and different concentrations of $MgCl_2$ as indicated was followed using a continuous colourmetric assay that measures ΔA_{360} between the substrate (MESG) and the products (ribose-1-phosphate and

2-amino-6-mercapto-7-methlpurine). Data were taken every 0.1 second for 60 minutes in a 0.3 cm path length cuvette (45 μL nominal volume) and transformed to show the percentage of P_i released at any given time.

FtsZ to a final concentration of 11 μM was mixed with 0.4 mM MESG, 1 U/mL PNP and the polymerization buffer, which contains 50 mM MES, pH 6.5, 50 mM KCl, and varying concentrations of $MgCl_2$. The reaction was initiated by the addition of 0.2 mM GTP at time 0. As shown in figure 4.5.4, upon addition of GTP, P_i was released from the GTP hydrolysis catalysed by FtsZ. In the absence of Mg^{2+}, the rate of P_i released from GTP hydrolysis is the slowest, which agrees with the above light scattering results (§ 4.4.4). In 60 minutes, only approximately 45% of the total P_i was released into the reaction medium. In the presence of Mg^{2+}, however, the rate of GTP hydrolysis is faster at 10 mM Mg^{2+} than at 20 mM Mg^{2+}, whose turnover time of phosphate release was around 20 and 40 minutes respectively. These results indicate that a low concentration of Mg^{2+} is helpful to promote GTP hydrolysis catalysed by FtsZ, whereas too much Mg^{2+} may induce bundles that are not good for GTP hydrolysis.

4.5.5 Effects of pH on FtsZ's GTPase activity

Light scattering results (§ 4.4.5) also suggest that the pH has an important and big effect on the hydrolysis of GTP to GDP catalysed by FtsZ. The kinetics of P_i released at four different pHs (pH 6.0, pH 6.5, pH 7.0 and pH 7.5) in MES buffer were then measured. FtsZ to a final concentration of 11 μM was mixed with 0.4 mM MESG, 1 U/mL PNP and the polymerization buffer, which contains 50 mM MES at different pH, 50 mM KCl, and 10 mM $MgCl_2$. The reaction was initiated by the addition of 0.2 mM GTP at time 0, and the results are shown in figure 4.5.5. It can be observed that at different pHs, the P_i released reached approximately the same end point. At pH 6.0, approximately 90% of the P_i was released into the media within 40 minutes, whereas it took approximately 12 minutes to achieve this at pH

7.5. These data suggest that the hydrolysis is slower at pH 6.0, which might be due to the fact that FtsZ protofilaments easily to form bundles at lower pH (Mukherjee and Lutkenhaus 1999). The bundles are more stable than single protofilaments, and delay the release of phosphate from the hydrolysis of GTP to GDP catalysed by FtsZ.

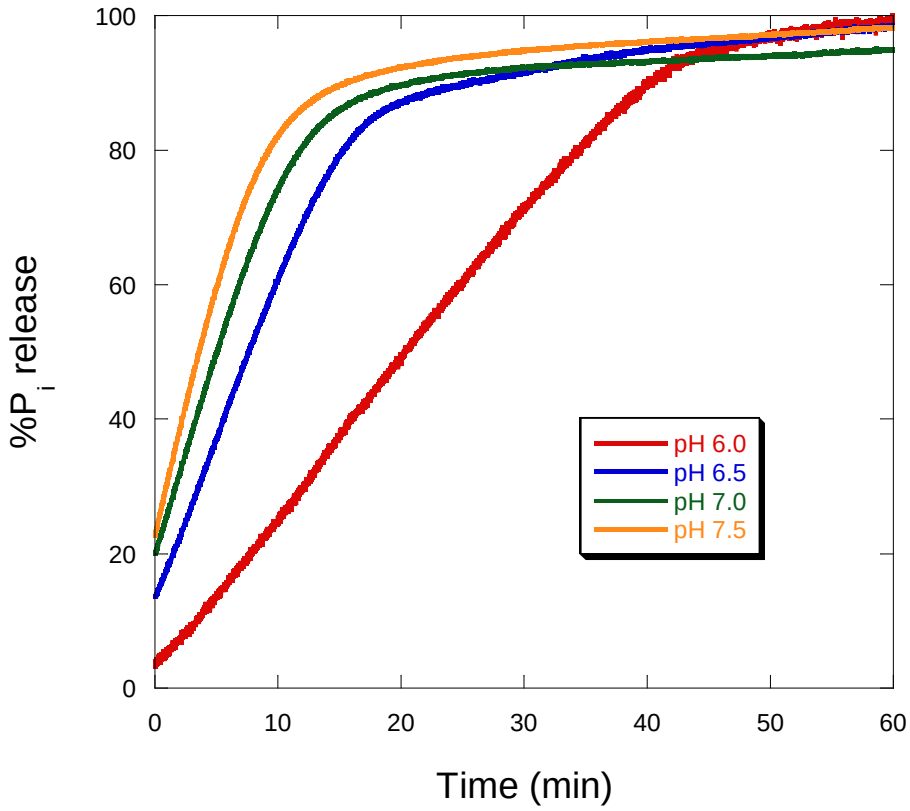

Figure 4.5.5 Effects of the pH on FtsZ's GTPase activity. The kinetics of P_i released from the enzymatic conversion of GTP to GDP catalysed by FtsZ at four different pHs using MES buffer was followed using a continuous colourmetric assay that measures ΔA_{360} between the substrate (MESG) and the products (ribose-1-phosphate and 2-amino-6-mercapto-7-methlpurine). Data were taken every 0.1 second for 60 minutes in a 0.3 cm path length cuvette (45 µL nominal volume) and transformed to show the percentage of P_i released at any given time.

4.6 Conclusions

Right-angle light scattering had been shown to be an effective method to monitor FtsZ dynamic assembly under a variety of conditions in preliminary studies by Mukherjee and Lutkenhaus (Mukherjee and Lutkenhaus 1999). In this chapter, right-angle light scattering was used to investigate FtsZ polymerization in real time to test FtsZ quality based on the comparison with literature data.

In the presence of GTP, FtsZ polymerizes into dynamic protofilaments, reaching a steady state by the time we began measurements. The disappearance of polymers follows after the GTP was consumed. However, a cycle of FtsZ polymerization can be re-initiated readily after FtsZ depolymerization by the new addition of GTP (Pacheco-Gomez *et al.* 2011).

At higher Mg^{2+} concentrations, there is a tendency for FtsZ protofilaments to align along the long axis to give bundles (Mukherjee and Lutkenhaus 1999, Pacheco-Gomez *et al.* 2011), suggested from the dramatic increase in the intensity of light scattered. This bundling is also affected by pH. From pH 6.0 – 7.5, our study revealed that FtsZ protofilaments also displayed increased bundling at acidic pH. By altering FtsZ, GTP, Mg^{2+}, KCl concentration or pH, we could manipulate the time for the persistence of the polymers, which coincides with the time when GTP was consumed.

Similar with the literature (Mukherjee and Lutkenhaus 1999, Pacheco-Gomez *et al.* 2011), we also found that Mg^{2+} is not required for FtsZ assembly, because the FtsZ polymers form in the absence of Mg^{2+}. Such polymers were very stable, however, indicating that Mg^{2+} is required for GTP hydrolysis leading the polymers to depolymerize.

The kinetics of P_i released from the GTP hydrolysis under different conditions have been further studied, which confirm and/or complement the light scattering results. In agreement with light scattering, KCl was found to be able to accelerate the rate of GTP hydrolysis. A Spanish group found that the presence of a K^+ ion at the GTP binding site allows the positioning of one water molecule that interacts with catalytic residues Asp235 and Asp238, which are also involved in the coordination sphere of K^+. This arrangement might favor dimer stability and GTP hydrolysis, and it explains why K^+ accelerates GTP hydrolysis (Mendieta *et al.* 2009).

In examining the effect of the Mg^{2+} concentration on FtsZ GTPase activity, we found that the rate of phosphate release is slower at 20 mM Mg^{2+} than at lower concentrations of Mg^{2+}. This suggests that although Mg^{2+} is required for GTP hydrolysis, the GTPase activity was enhanced at lower Mg^{2+} concentrations, resulting in a more rapid consumption of GTP. It is likely that at 20 mM Mg^{2+}, where the bundling is more noticeable, the increased bundling results in a slower turnover of FtsZ polymers, and also the reduction in the rate of GTP hydrolysis (Mukherjee and Lutkenhaus 1999, Pacheco-Gomez *et al.* 2011). Mg^{2+} is required for the hydrolysis of GTP, presumably because it binds the phosphates of the nucleotide. Also, Mg^{2+} was implicated in the association of FtsZ monomers, as well as oligomer formation, to enhance the lateral association (Mendieta *et al.* 2009, Rivas *et al.* 2000), so that at higher concentration of Mg^{2+}, the enhanced bundling reduces the FtsZ GTPase activity.

The hypothesis that increased bundling is associated with decreased GTPase activity is confirmed by the study at different pHs. At lower pH of 6.0, the protofilaments also tended to give bundles, and thus reduced the rate of GTP hydrolysis, and the FtsZ disassembly was much slower (Mukherjee and Lutkenhaus 1999, Pacheco-Gomez *et al.* 2011). Mendieta *et al.* consider that at lower pH values, the dimer interface is more stable, the GTPase activity is lower, and this might favour the filaments bundling. Besides, electrostatic interactions were thought to be

important for the assembly and bundling of FtsZ protofilaments by studying FtsZ assembly at different pH and/or ionic strength. Negative charge on the FtsZ protein increases with the increase in pH. Thus the inhibition of FtsZ assembly and bundling with the increase in pH is possibly due to an increase in the repulsion caused by the increase in the negative charge on FtsZ molecules (Beuria *et al.* 2006).

The very dynamic nature of FtsZ polymers observed *in vitro* could explain about how they are stabilized *in vivo* to some extent, since Z-rings once formed exist for some time before they are used in division (Addinall et al. 1996). The assembly of FtsZ protofilaments into bundles, however they are induced, decreases the dynamics of FtsZ polymers. Thus, any mechanism that causes association of protofilaments in *vivo* would contribute to their stability.

[#] In chapter 4, the real concentration of FtsZ was estimated to be 28% less, by comparison with the literature in the light of FtsZ's specific activity.

CHAPTER 5 -- YgfE ENHANCES FtsZ ASSEMBLY THROUGH BUNDLING[$]

5.1 Introduction

The recruitment of a number of accessory proteins to the Z-ring is also required for the progression and completion of cytokinesis. These accessory proteins regulate the dynamics of the Z-ring, and can be divided into inhibitors (SulA, MinC, EzrA) or promoters (ZipA, ZapA) of FtsZ polymerization. Since it seems increasingly likely that the formation of bundles through lateral associations between FtsZ polymers by promoters is critical to the function of the Z-ring, we are interested in studying such promoters.

ZapA, which was first found in *Bacillus subtilis*, is recruited to the divisome early by a direct interaction with FtsZ. ZapA induces bundling *in vitro* and stabilizes the Z-ring *in vivo*. It is also widely conserved among bacteria with apparent orthologs in many species. The *E. coli* ortholog is YgfE, exhibiting 11% identity and 34% similarity. The function of YgfE on FtsZ assembly remains largely uncharacterized however. Thus the focus of my project is on YgfE, with the purpose to understand how YgfE interacts with FtsZ and how YgfE promote FtsZ polymer association.

5.2 Objectives

In the literature, ZapA (YgfE) was reported to be able to induce FtsZ bundling and stabilize FtsZ polymers. In order to study how YgfE affects FtsZ polymerization we compared the effect of wild-type YgfE and a series of mutants. The mutant results are described in Chapter 6. They are generally consistent with the literature but we needed to be able to compare the wild type and mutants in exactly the same experiments. In this chapter, we report results from right-angle light scattering to

investigate the increase in polymer size and its dynamic behaviour in real time; linear dichroism (LD) to study the real-time backbone information of protofilaments and bundles; electron microscopy (EM) of negatively stained samples to characterize the FtsZ polymers induced by YgfE; and a colourimetric assay to measure the kinetics of inorganic phosphate (P_i) released from GTP hydrolysis catalysed by FtsZ in the presence of YgfE.

5.3 Expression and purification of EcYgfE

EcYgfE was expressed and purified as described above (§ 2.3.2). *E. coli* competent cells B834 (DE3) were transformed with the plasmid pETDuet-*ygfE*, allowing the production of an N-terminal six-histidine tagged (MGSSHHHHHH) protein YgfE in *E. coli*. Cells were grown at 37 °C in 1 litre of fresh LB medium containing 100 μg/ml ampicillin. Protein expression was induced by the addition of IPTG to a final concentration of 0.5 mM, when OD_{600} reached approximately 0.5. After another 3–4 hours growth, cells were harvested by centrifugation at 6400×g and resuspended in 25 mM HEPES pH 8.0, 1 M NaCl and 10 mM imidazole (buffer A).

The resuspended pellet was incubated on ice for 30 minutes with 2.5 mg/ml of chicken egg-white lysozyme prior to lysis by sonication in a MSE Soniprep device for 2 minutes with a minute pause interval. The sonicated extract was clarified by centrifugation at 50,000×g at 4°C and applied onto a Ni^{2+}-sepharose affinity column. After loading of the crude extract, the column was washed with ten column volumes of buffer A followed by a further ten column volumes of buffer B (25 mM HEPES, pH 8.0, 1 M NaCl and 100 mM imidazole). EcYgfE was finally eluted with ten column volumes of buffer C (25 mM HEPES pH 8.0, 1 M NaCl and 500 mM imidazole).

YgfE was monitored during purification by SDS–PAGE, which is shown in figure 5.3. The pure YgfE was then dialysed into buffer containing 50 mM Tris-HCl, pH

7.9, 50 mM KCl, 1 mM EDTA and 10% glycerol (the same buffer used for FtsZ). The protein concentration was assayed with the Bio-Rad Assay reagent (§ 2.4.2.2).

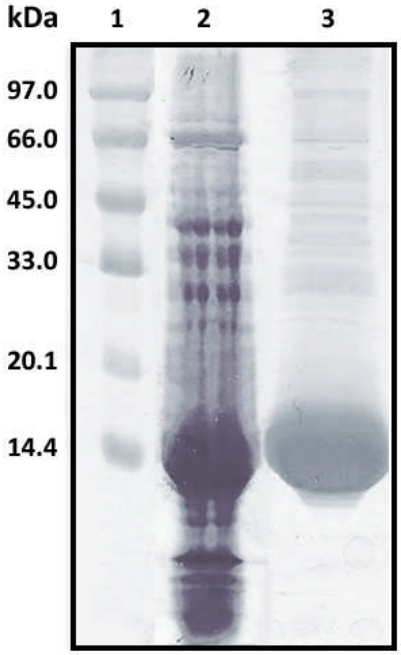

Figure 5.3 15% SDS-PAGE gel. Lane 1, protein mark. Lane 2, soluble crude cell lysates of *E. coli* B834 (DE3) transformed with pETDuet-*ygfE*. Lane 3, YgfE fractions eluted from the Ni^{2+}-sepharose affinity column in 500 mM imidazole gradient.

5.4 Analysis of YgfE-induced FtsZ polymer bundling by right-angle light scattering

Using right-angle light scattering we investigated how YgfE affects the amount of polymer and the stability of the FtsZ polymers, since light scattering signal corresponds to the average polymer size. Right-angle light scattering was measured at room temperature (~23°C) using a Perkin Elmer LS50B spectrofluorimeter with a 0.3 cm path length cuvette (45 μL nominal volume). The excitation and emission wavelengths were fixed at 550 nm, while excitation and emission slit widths were at 2.5 nm. Data were set to collect every second under the time-drive measurement.

Two different experiments were designed. (i) In the first experiment we determined the effects of YgfE at different concentrations on FtsZ preformed protofilaments. The light scattering was measured first adding GTP to FtsZ and then later adding different YgfE concentrations. This first experiment was designed to monitor bundling of preformed FtsZ protofilaments, since YgfE was added once the FtsZ protofilaments were preformed. (ii) In the second experiment, the light scattering was measured upon adding GTP to a premixed reaction medium of FtsZ and varying concentrations of YgfE. This second experiment was designed to probe FtsZ assembly when FtsZ and YgfE are present at the same time. With these two experiments together, we can get more information about the effects of YgfE on FtsZ assembly, and the results obtained are reported below.

5.4.1 Adding YgfE after FtsZ protofilaments were formed

In the first experiment, we show the effects of YgfE on preformed FtsZ protofilaments by right-angle light scattering. The reaction mixtures consisting of 11 μM FtsZ, 50 mM MES-KOH, pH 6.5, 10 mM $MgCl_2$, 50 mM KCl were prepared. After baseline collection, approximately 5 minutes, 0.2 mM GTP was added to initiate the polymerization reaction. Varying concentrations of YgfE were added last during the steady-state of FtsZ polymerization (the steady-state phase interpreted in the previous chapter), at approximately 3 minutes after the GTP addition. The control experiment in the absence of YgfE was also done which corresponds to FtsZ-YgfE ratio of 1:0.

The baseline is defined as the level of light scattering before GTP was added. The average of the baseline readings in each experiment was subtracted from all the values, and therefore we show the Δ or "jump" of light scattering measured. Zero time is defined to be the addition of GTP, so the first time-point is the point at GTP addition, and the initial light scattering signal corresponds to FtsZ protofilament formation.

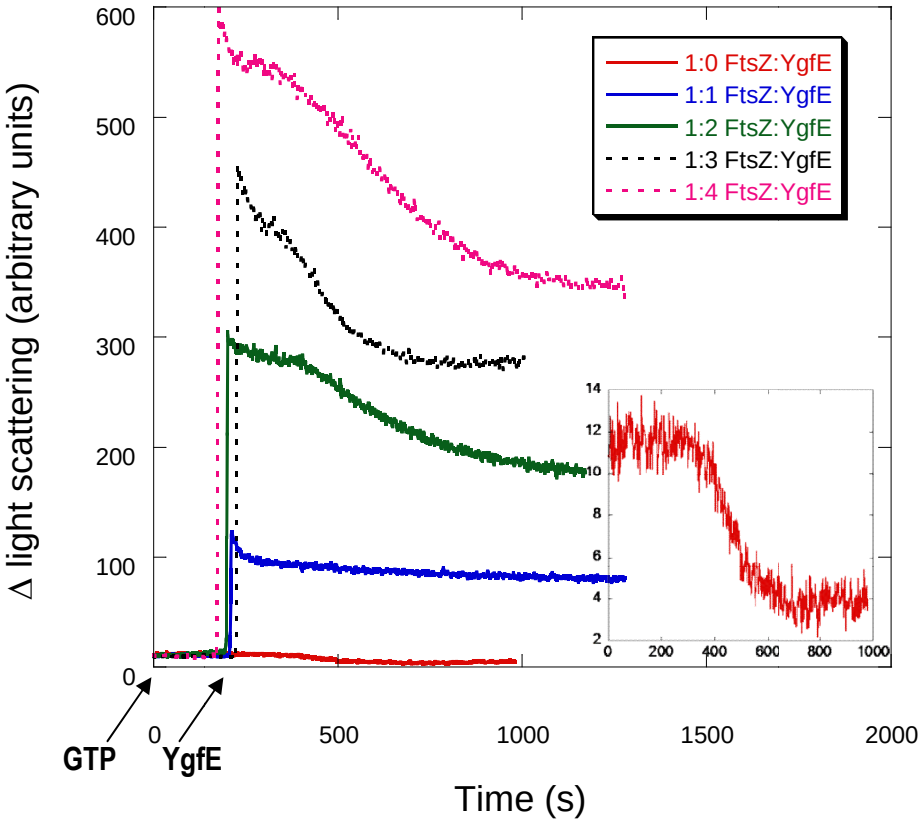

Figure 5.4.1 YgfE-induced polymer bundling detected by right-angle light scattering. FtsZ (11 μM in polymerization buffer) was mixed with GTP (0.2 mM) at time zero. YgfE at different concentrations (shown in graph) was added after protofilament formation (approximately 3 minutes). Excitation and emission wavelengths were set at 550 nm.

As can be observed from figure 5.4.1, the increase in light scattering after GTP addition and prior to YgfE addition reaches the same level (10 units) for all the different FtsZ-YgfE ratios indicating YgfE was added to identical protofilament preparations. Approximately 3 minutes after GTP addition, varying concentrations of YgfE (FtsZ-YgfE ratios from 1:1 to 1:4) were added. The addition of YgfE at different concentrations caused, in all cases, a great increase of the light scattering, with the highest increase as nearly 600 units. These increases were very fast and are proportional to the YgfE concentration added, suggesting that YgfE-induced FtsZ bundles were formed. Also, YgfE stabilises the FtsZ polymers as seen by the bigger

constant value of the Δ light scattering signal compared with the control experiment in the absence of YgfE. Under this condition, YgfE strongly promotes the bundling of FtsZ and prevents the disassembly of these bundles on a large time scale, which can be measured upto 6465 s, reaching the limitation of the instrument.

5.4.2 Adding GTP to premixed FtsZ and YgfE

In the second kind of experiment, we first studied the interaction between FtsZ and YgfE before adding GTP. The reaction mixtures consisting of 11 μM FtsZ, 50 mM MES-KOH, pH 6.5, 10 mM $MgCl_2$, 50 mM KCl were prepared. After baseline collection for approximately 5 minutes, varying concentrations of YgfE were added. The control experiment which is adding YgfE buffer to FtsZ instead of YgfE was also performed.

The baseline is defined as the level of light scattering of FtsZ on its own. The average of the baseline readings in each experiment was subtracted from all the values, and therefore we show the Δ light scattering measured. Zero time is defined to be the addition of YgfE or YgfE buffer.

As seen in figure 5.4.2.1, there is no change in light scattering upon adding YgfE buffer. However, when YgfE was added, the light scattering increased slightly with increasing concentrations of YgfE, and then remained constantly during measurements. We assume that the small increase of light scattering was due to YgfE attaching to FtsZ.

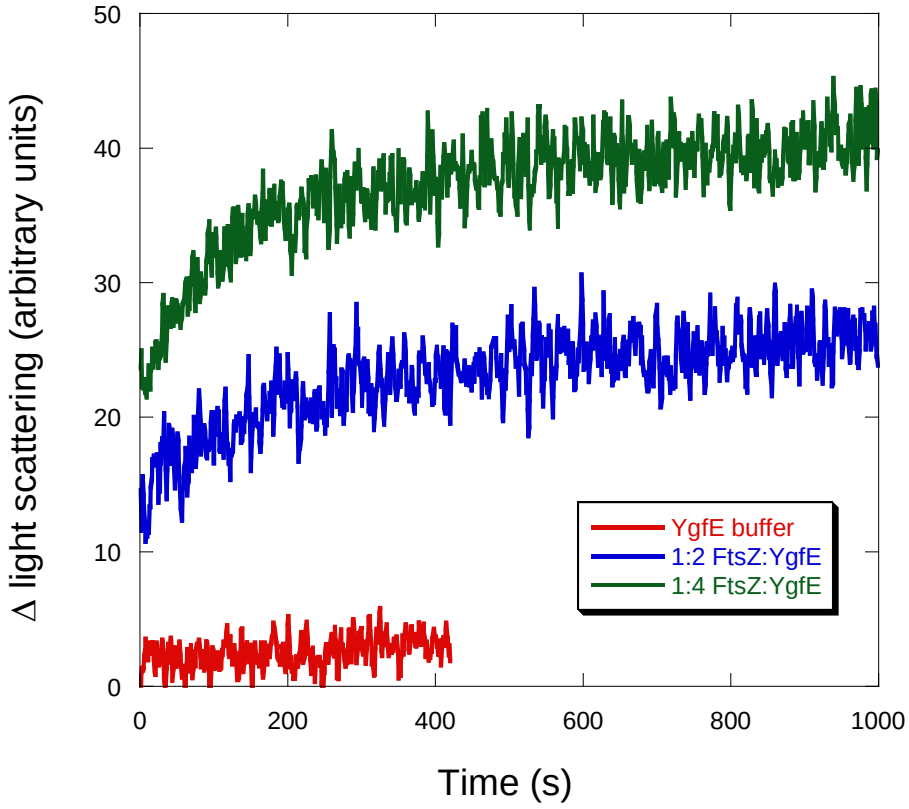

Figure 5.4.2.1 Interaction between FtsZ (11 μM in polymerization buffer) and YgfE/YgfE buffer (concentration as indicated in graph) without GTP detected by right-angle light scattering. Excitation and emission wavelengths were set at 550 nm.

In order to investigate the effects of YgfE on FtsZ polymerization with GTP, 0.2 mM GTP was then added to each mixture to start the polymerization and/or bundling reactions. Here the baseline is defined as the level of light scattering before adding GTP. Zero time is defined to be the addition of GTP.

After subtracting the baseline, we obtained figure 5.4.2.2, which measures the change in light scattering upon adding GTP last to premixed FtsZ and YgfE at different ratios. Compared with the control experiment (FtsZ-YgfE ratio as 1:0), the changes in light scattering after GTP addition when YgfE was present are higher,

and related to YgfE concentration, which means YgfE-induced bundles were also formed.

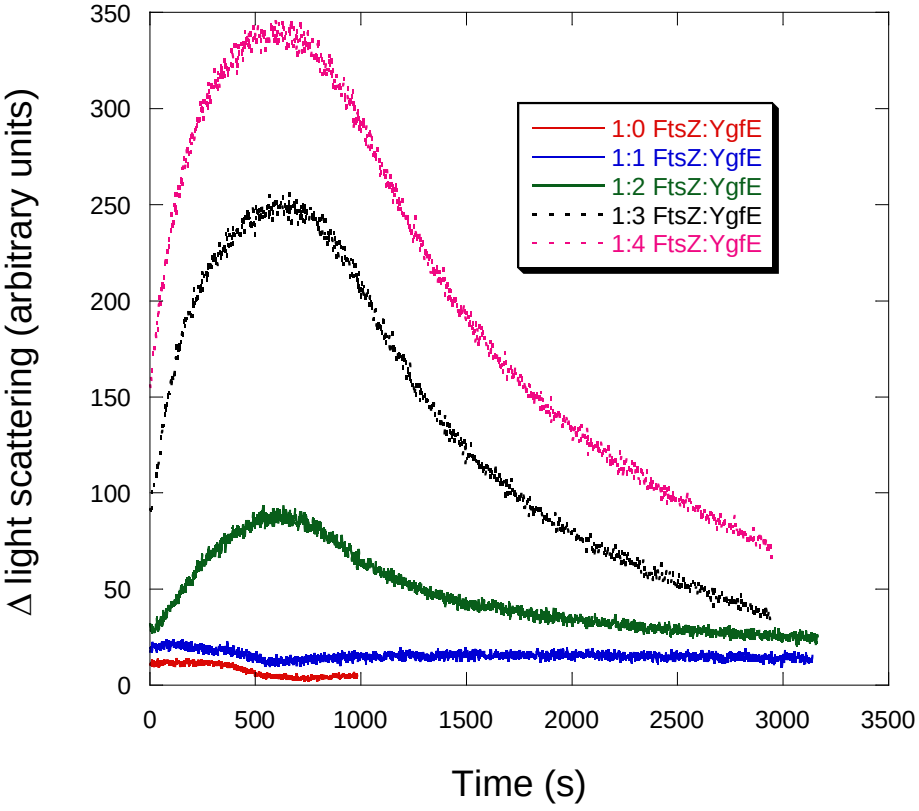

Figure 5.4.2.2 Effects of YgfE (concentration as indicated in graph) on FtsZ (11 μM in polymerization buffer) assembly when be premixed with FtsZ measured by right-angle light scattering. 0.2 mM GTP was added to the reaction medium at time zero. Excitation and emission wavelengths were set at 550 nm.

However, compared with adding YgfE onto preformed FtsZ protofilaments (figure 5.4.1), the dynamics of FtsZ in the intensity of light scattering has a different shape here. When FtsZ and YgfE were of equal concentration as 11 μM, the light scattering underwent a small increase, slightly bigger than that with FtsZ alone. This increase then remained constant for approximately 6 minutes before its decrease. For the other ratios (FtsZ -YgfE ratio from 1:2 to 1:4), the light scattering gradually

increased and reached to peak intensity at around 10 minutes, followed by a steep decrease to the baseline value within nearly 50 minutes. In addition, the peak values are also smaller in this experiment, almost half of the number in the previous experiment at each YgfE concentration.

These data suggest a more complicated process here, probably a competition between protofilament formation and bundling. Before longer FtsZ protofilments were formed, YgfE-induced FtsZ bundling happened. These short bundles were not stable enough, so GTP hydrolysis happened rapidly, causing FtsZ polymers to disassemble. Therefore the increase in light scattering is slower, the decrease is larger, and the peak value is also smaller. In order to get more stable FtsZ polymers, FtsZ protofilaments are suggested to be formed before YgfE-induced bundling.

5.5 Analysis of YgfE-induced FtsZ polymer bundling by linear dichroism

Linear dichroism (LD) gives information about orientation of the chromophores in the long fibres, and was employed in this section to continue to study the effects of YgfE on FtsZ assembly.

Two kinds of experiments were designed analogous to the right-angle light scattering experiments. (i) In the first experiment, we determined the effects of adding varying concentrations of YgfE to FtsZ preformed protofilaments. In this experiment, FtsZ protofilaments were formed by adding GTP and two LD scans later (approximately 3 minutes, still during the steady-state phase), different amounts of YgfE were added to the preformed protofilaments to initiate the bundling reaction we had seen in the light scattering experiments. (ii) In the second approach, premixed FtsZ and varying YgfE concentrations were added to the LD capillary. The polymerization/bundling reaction was started by adding GTP to the reaction medium last.

LD spectra were measured at room temperature (~23°C) using a Jasco J-815 circular dichroism spectrometer adapted for LD spectroscopy with a 65 μL nominal volume capillary. LD spectra were collected using the interval scan measurement programme within the Jasco software. This enabled collection of full wavelength scans from 350 to 190 nm every minute at a scanning speed of 100 nm min^{-1}.

The LD signal at 210 nm (LD_{210}) corresponds to the backbone of the FtsZ polymer and its intensity gives us an idea of the rigidity/flexibility of the polymer. Below 210 nm, the signal is not valid, because the high tension voltage (due to the sample absorption/scattering) is too high. Therefore we monitored LD_{210} in all cases.

5.5.1 Adding YgfE after FtsZ protofilaments were formed

In the first approach, we investigated the effect of adding varying concentrations of YgfE to preformed FtsZ protofilaments. The mixtures consisting of 11 μM FtsZ, 50 mM MES-KOH, pH 6.5, 10 mM $MgCl_2$, 50 mM KCl were prepared. A baseline was collected before initiation of the polymerization reaction with GTP, by measuring the LD spectrum with and without rotating of the LD cell. The difference between the two spectra results in a flat line around zero, consistent with there being nothing in solution oriented. After that, 0.2 mM GTP was added to initiate the polymerization reaction. Varying concentrations of YgfE were added 2 scans after the GTP addition. Zero time is defined to be the addition of GTP. The control experiment in the absence of YgfE was also conducted which corresponds to an FtsZ-YgfE ratio of 1:0. The comparison of LD_{210} (the LD signal at 210 nm) at different FtsZ-YgfE ratios are shown in figure 5.5.1.

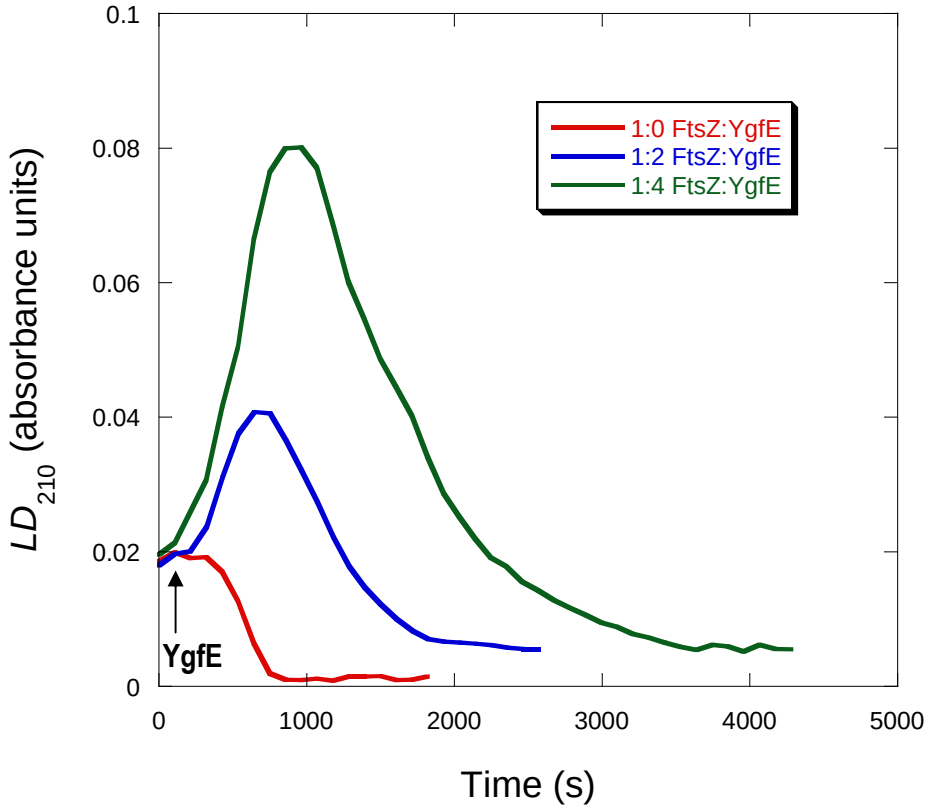

Figure 5.5.1 Comparison of the LD_{210} at different FtsZ-YgfE ratios. FtsZ (11 μM in polymerization buffer) and GTP (0.2 mM) were mixed at time zero. YgfE at different concentrations (shown in graph) was added after protofilament formation at approximately 3 minutes.

The LD_{210} signal corresponds to the orientation of the backbone of FtsZ polymer. Better oriented polymers give a bigger LD_{210}. As can be seen in figure 5.5.1, there is a small increase, approximately 0.02 units in the LD_{210} signal, after GTP addition at time zero as a result of the growth of FtsZ protofilaments and them becoming oriented. The LD_{210} signal after GTP addition and prior to YgfE addition reaches the same level for all the different FtsZ-YgfE ratios indicated YgfE was added to identical protofilament preparations. YgfE was added after the second scan at approximately 3 minutes, which caused a bigger increase in the LD_{210} signal. This

increase could be attributed to the bundling effect of FtsZ protofilaments, which can be better oriented, and it also was related to YgfE concentrations, suggesting more bundles were formed with more YgfE. At a 1:2 ratio of FtsZ to YgfE, the peak LD_{210} reached to approximately 0.04 units, while this value even doubled when the FtsZ-YgfE ratio was 1:4. In addition, in the presence of YgfE, it took a long time for LD_{210} to decrease back to around zero indicating complete depolymerization. This time was approximately 12 minute, 30 minute and 60 minute respectively when the FtsZ-YgfE ratio was from 1:0 to 1:2 and to 1:4, which means FtsZ polymers became more stable when assembled into bundles.

5.5.2 Adding GTP to premixed FtsZ and YgfE

In the second kind of experiment, we chose to first study the interaction between FtsZ and YgfE before adding GTP. 11 μM FtsZ and varying concentrations of YgfE were premixed in the reaction medium consisting of 50 mM MES-KOH, pH 6.5, 10 mM $MgCl_2$ and 50 mM KCl. LD spectra were collected with and without rotating of the LD cell. The difference between pairs of spectra gave a flat line around zero in all cases. Although YgfE may attach to FtsZ, they cannot form long polymers, thus we cannot get an LD signal here.

Then 0.2 mM GTP was added to each mixture to start the polymerization and/or bundling reactions. The control experiment with no YgfE (1:0 FtsZ:YgfE) was performed as well. Zero time is defined to be the addition of GTP.

The comparison of LD_{210} at different FtsZ-YgfE ratios is shown in figure 5.5.2. Generally speaking, the results from the LD are similar to that from light scattering, which may further prove our hypothesis. Compared with the control experiment, we can see LD signal increase after GTP addition and decreases more slowly when YgfE was present, indicating the bundles were formed. Compared with the LD experiments performed previously, the increase in LD_{210} is not as dramatic as before.

In this approach, the peak LD_{210} reached to a little above 0.03 units, when FtsZ-YgfE ratio was 1:4, while at the same concentration of YgfE, the biggest LD_{210} reached to 0.08 units in the previous experiment. In addition, the time took for LD_{210} to decrease back to around zero is different. Although this time is longer than that in the absence of YgfE, it is still shorter than that in the other experiment. Therefore we are also observing a competition between protofilament formation and the bundling reaction, which affected the whole assembly process.

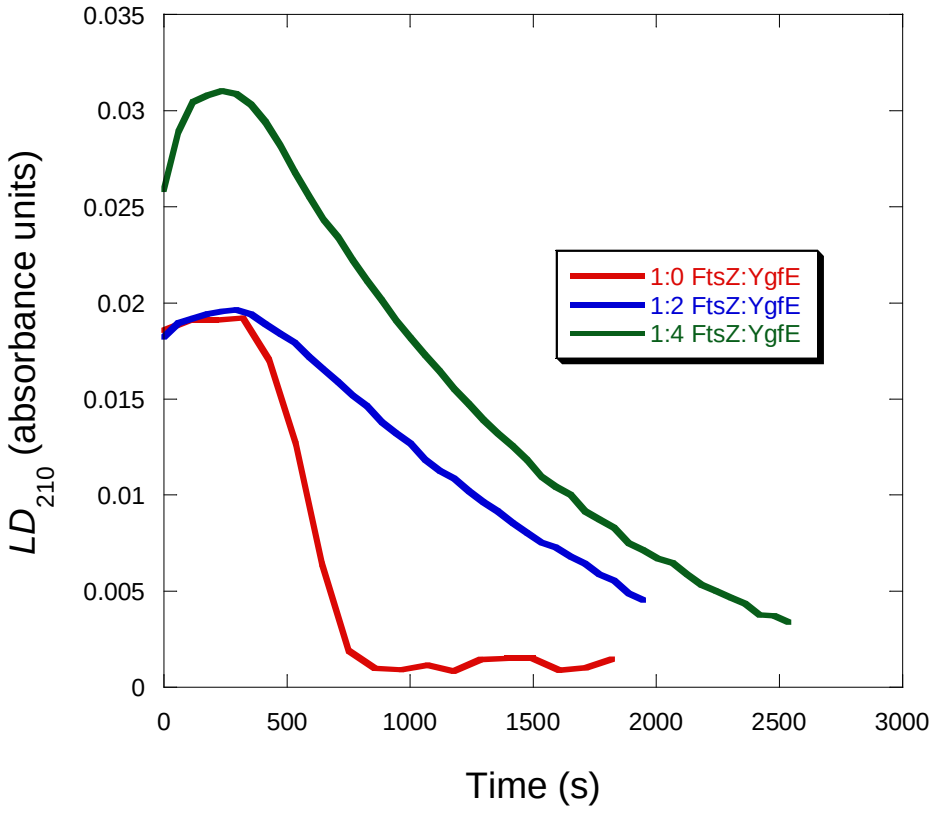

Figure 5.5.2 Comparison of the LD_{210} for premixed FtsZ (11 μM in polymerization buffer) and YgfE (concentration as indicated in graph). 0.2 mM GTP was added to the mixture to start the polymerization at time zero.

5.6 Visualization of the effects of YgfE on FtsZ assembly by electron microscopy

We examined the morphology of FtsZ polymers formed in the absence and presence of YgfE by negative stain electron microscopy using a JEOL 2011 transmission electron microscope.

In this section, the FtsZ-YgfE ratio was chosen as 1:4 since we believe much more YgfE could induce the large bundles that can be easily observed. Six samples were prepared and can be divided equally into two groups. The first group was designed to check whether FtsZ and YgfE have a direct interaction in the absence of GTP. First two samples were prepared as the control experiments for comparison purpose. 11 μM of FtsZ and 44 μM of YgfE were mixed respectively in the polymerization buffer consisting of 50 mM MES-KOH, pH 6.5, 10 mM $MgCl_2$ and 50 mM KCl. Then 11 μM of FtsZ and 44 μM of YgfE were mixed together in the polymerization buffer without adding GTP. The next group was designed to study the effects of YgfE on FtsZ polymerization. Control experiment was also done first. 0.2 mM GTP was added to 11 μM of FtsZ in the polymerization buffer to start the polymerization reaction. 3 minutes later, 3 μl of the sample mixture were then withdrawn for imaging. YgfE was included in the last two samples. 11 μM of FtsZ and 44 μM of YgfE were premixed in the polymerization buffer. 0.2 mM GTP was then added to start the polymerization reaction. 5 minutes later, 3 μl of the sample mixtures were then withdrawn for imaging. Lastly, 3 minutes after the GTP addition to FtsZ, 44 μM of YgfE was added to initiate the bundling reaction. 2 minutes later, the solution was 5 times diluted with water before imaging. Because too many bundles were obtained in this way, dilution was required. After that, 3 μl of the diluted solution were then withdrawn for imaging.

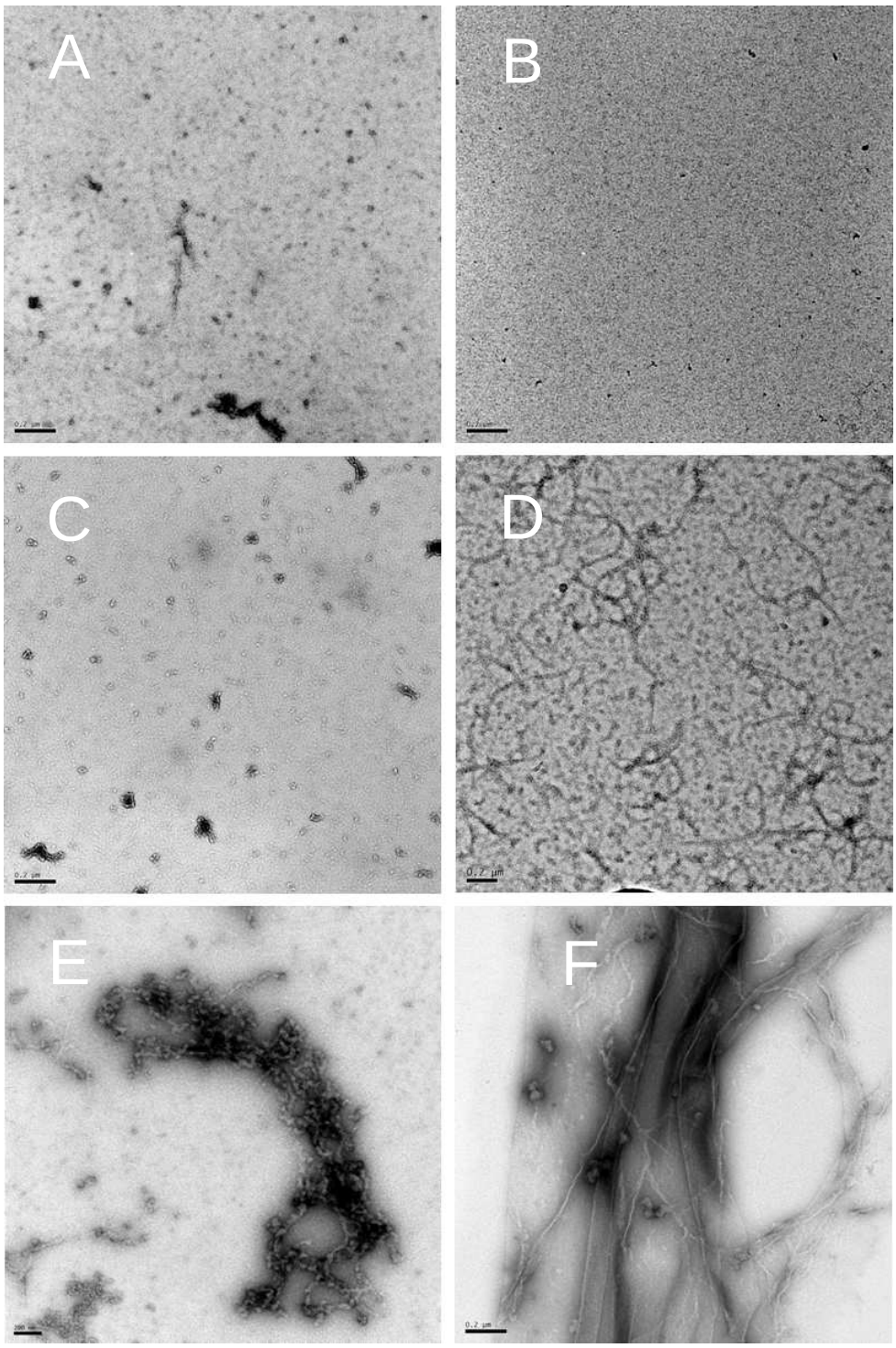

Figure 5.6 Electron microscopy of the products of FtsZ and YgfE. (A) FtsZ (11 μM) in polymerization buffer; (B) YgfE (44 μM) in polymerization buffer; (C) FtsZ (11 μM) and YgfE (44 μM) in polymerization buffer; (D) FtsZ (11 μM) mixed with GTP (0.2 mM); (E) 0.2 mM GTP was added into premixed FtsZ (11 μM) and YgfE (44 μM); (F) YgfE (44 μM) was added to FtsZ protofilaments, 3 minutes after the GTP (0.2 mM) addition to FtsZ (11 μM). The sample was then diluted 1:5 with water for imaging. Bars, 200 nm.

Figure 5.6 shows the images of each sample prepared. FtsZ and YgfE are monomeric or present as small oligomers in the absence of GTP as seen in figure 5.6A, B. Without GTP, YgfE seems to be able to bind to FtsZ to form bigger circle particles (figure 5.6C). In the presence of GTP and absence of YgfE, FtsZ formed mostly single-stranded protofilaments, or lateral associations of a few protofilaments (figure 5.6D). The addition of YgfE caused the bundling of the GTP-induced FtsZ protofilaments into large branched networks (figure 5.6E, F). However, the different ways of adding YgfE can result in different behaviour of bundling. When YgfE was added to preformed FtsZ protofilaments, we get more high-order YgfE-induced FtsZ bundles (figure 5.6F) than in the other way where GTP was added into premixed FtsZ and YgfE (figure 5.6E). When GTP was added into premixed FtsZ and YgfE, the formation of FtsZ protofilaments and bundles happened at the same time, thus the polymers obtained were a mess. However, when we added YgfE into FtsZ protofliaments, YgfE linked FtsZ protofilaments together, and formed ordered bundles.

The pictures from electron microscopy show clearly that YgfE can interact with FtsZ in the absence of GTP, and more importantly, adding YgfE into preformed FtsZ protofilaments can help to form more high-order bundles efficiently. All these results obtained are consistent with the hypothesis we proposed in the light scattering and LD sections.

5.7 GTPase assay

The inorganic phosphate (P_i) released from the hydrolysis of GTP to GDP catalysed by FtsZ is reported in this section. Investigating how P_i is released when both YgfE and FtsZ are present in the reaction medium may give us the idea of the interaction between FtsZ and YgfE from another perspective. The P_i release can be easily quantified employing a fast and continuous colourimetric assay. In the presence of P_i,

the substrate MESG is converted enzymatically by PNP to ribose-1-phosphate and 2-amino-6-mercapto-7-methlpurine. This conversion results in a spectrophotometric shift in the maximum absorbance from 330 nm for the substrate to 360 nm for the product. The change in absorption at 360 nm (ΔA_{360}) allows quantification of the P_i consumed in the reaction.

The measurements were carried out at room temperature (~23°C) in a Cary 1E double beam UV/Visible spectrophotometer with a 0.3 cm path length cuvette (45 μL nominal volume). The absorption at 360 nm was collected every 0.2 second at a scanning speed of 300 nm min^{-1}. Using the calibration curve reported in § 4.5.1, we then converted ΔA_{360} to the percentage of P_i released from the hydrolysis of GTP to GDP catalysed by FtsZ.

Before studying the effects of YgfE, we first checked that there was no P_i release from YgfE. A standard reaction was prepared in the absence of FtsZ. GTP was added later to the reaction media to check if there was any P_i released as the result of YgfE contamination or the hydrolysis of GTP to GDP by YgfE. We found there was no change in the absorption at 360 nm obtained as a function of time and thus we conclude that there was no P_i being released from YgfE contamination, and YgfE cannot catalyse GTP hydrolysis.

Two experiments were then designed as with right-angle light scattering and linear dichroism. (i) In the first experiment, FtsZ protofilaments were formed by adding GTP and 3 minutes after the reaction, different amounts of YgfE were added to the preformed protofilaments. We determined the effects of YgfE induced bundles on P_i release from the hydrolysis of GTP to GDP catalysed by FtsZ. (ii) In the second approach, premixed FtsZ and varying YgfE concentrations were prepared before adding GTP. We wanted to know how P_i was released when FtsZ protofilaments formation and bundling reaction was started at the same time.

In every single experiment, a baseline was collected before initiating the phosphate release reaction by the addition of GTP to examine reagents and enzymes for the possibility of P_i contamination. If there is no P_i contamination, we should obtain a flat baseline, which means no change at A_{360}. After a successful baseline had been obtained, the reaction was started by the addition of GTP.

5.7.1 Adding YgfE after FtsZ protofilaments were formed

In the first experiment, we investigated the effect of YgfE-induced bundles on P_i release from the hydrolysis of GTP to GDP catalysed by FtsZ. The reaction consisting of 11 μM FtsZ, 50 mM MES-KOH, pH 6.5, 10 mM $MgCl_2$, 50 mM KCl, 0.4 mM MESG and 1 U/mL PNP were prepared. After baseline collection, 0.2 mM GTP was added to initiate the phosphate release reaction. After 3 minutes, varying concentrations of YgfE (FtsZ-YgfE ratios from 1:1 to 1:4) were added to the reaction medium. The absorbance at 360 nm was obtained as a function of time, and then transformed to the percentages of P_i released from the hydrolysis of GTP to GDP catalysed by FtsZ, which are shown in figure 5.7.1. The control experiment in the absence of YgfE was also done which corresponds to an FtsZ-YgfE ratio of 1:0.

As can be observed from figure 5.7.1, approximately 90% of the P_i was released into the medium within 15 minutes when YgfE was absent. After GTP addition and prior to YgfE addition, the speed of phosphate released from the hydrolysis of GTP to GDP catalysed by FtsZ reaches the same level for all the different FtsZ-YgfE ratios. Approximately 3 minutes after GTP addition, varying concentrations of YgfE were added. It is observed that the rate of phosphate release decreased with more YgfE present, as well as the total amount of P_i realeased in the end. The end point of the reaction is as low as 55% of P_i release when 44 μM of YgfE was added, which indicates that some phosphate was never released in the presence of YgfE.

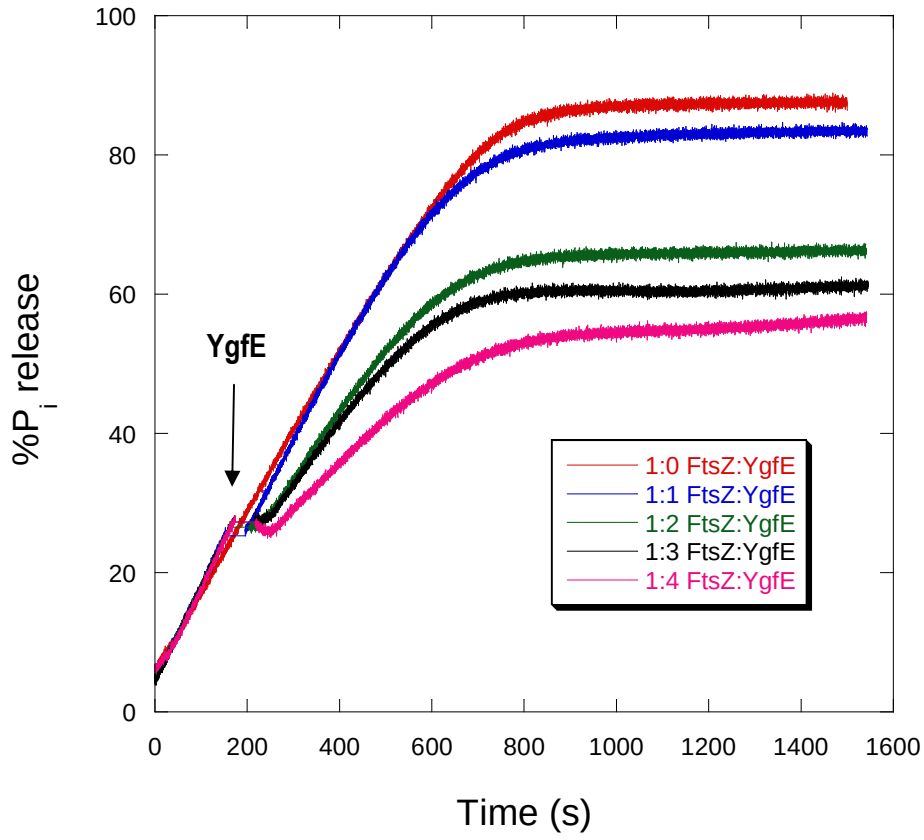

Figure 5.7.1 Effects of YgfE-induced bundles on FtsZ GTPase activity. FtsZ (11 μM in polymerization buffer) was mixed with GTP (0.2 mM) at time zero. YgfE at different concentrations (shown in graph) was added after protofilament formation (approximately 3 minutes).

Therefore, it can be concluded that YgfE is a potent inhibitor of FtsZ GTPase activity. We assume that YgfE induce the formation of FtsZ bundles to help stabilise FtsZ polymers, and then less GTP was free to hydrolyse, which caused small amounts of P_i to be released slowly. In addition or alternatively, the dense network of bundles may trap the P_i inside the subunits, making the GTP turnover slower.

5.7.2 Adding GTP to premixed FtsZ and YgfE

In the second approach, FtsZ and YgfE were premixed at different ratios from 1:0 to 1:4 in the reaction medium consisting of 11 μM FtsZ, 50 mM MES-KOH, pH 6.5, 50 mM KCl, 10 mM $MgCl_2$, 0.4 mM MESG and 1 U/mL PNP. 0.2 mM GTP was added last to the reaction medium. The P_i release as a consequence of the hydrolysis of GTP to GDP catalysed by FtsZ was measured as ΔA_{360}, and then transformed to the percentages of P_i release. Figure 5.7.2 shows the results obtained, giving the information of the effects of YgfE on FtsZ GTPase activity, when FtsZ protofilaments formation and bundling reaction happened at the same time.

As can be observed from figure 5.7.2, the rate of phosphate release from the hydrolysis of GTP to GDP is slower when YgfE was present (FtsZ-YgfE ratio from 1:2 to 1:4), and the amount of P_i released is also lower as the YgfE concentration increases. This shows that the FtsZ GTPase activity is inhibited upon the formation of FtsZ bundles induced by YgfE. However, this reduction of the rate and amount of P_i release is not as great as in the previous experiment when YgfE was added to the preformed FtsZ protofilaments. At the ratio 1:4 of FtsZ to YgfE, nearly 65% of the P_i was released within 25 minutes, whereas in the previous experiment only 55% of the P_i was found to be released during the same period at the same YgfE concentration. Especially for the equimolar addition of YgfE, there is little change observed in P_i release, unless more YgfE was added. This reduced effect on FtsZ's GTPase activity was also attributed to the competition mentioned above between FtsZ protofilaments formation and bundling. Dense bundles were formed effectively when adding YgfE to preformed FtsZ protofilaments, which can inhibit FtsZ's GTPase activity more significantly.

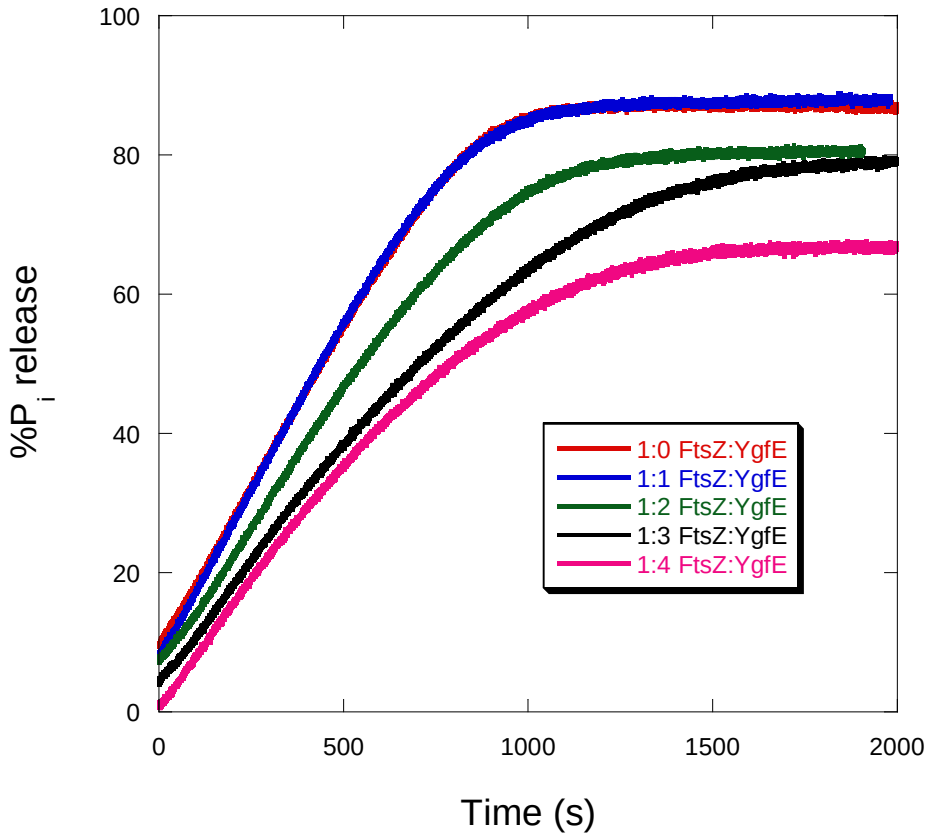

Figure 5.7.2 FtsZ's GTPase activity when FtsZ (11 μM in polymerization buffer) was premixed with YgfE (concentration as indicated in graph). 0.2 mM GTP was added to the mixture to start the reaction at time zero.

5.8 Conclusions

Recently, His-ZapA (YgfE) was shown not to be functional *in vivo.* As ZapA is a rather small protein of about 10 kDa, the addition of six histidine residues could affect the tetramerization and function of YgfE (Mohammadi *et al.* 2009). However, studying the effect of His-YgfE on FtsZ bundling *in vitro* can still give us some indication about how they could behave in *vivo*, although the remove of the His tag is needed for the further experiments.

In the most studies, ZapA (YgfE) has been reported to promote the bundling of FtsZ and stabilize the polymers (Gueiros-Filho and Losick 2002, Low *et al.* 2004, Small *et al.* 2007). Increasing pH (*e.g.* 7.5), and/or decreasing the concerntration of Mg^{2+} (*e.g.* 5 mM) was shown to enhance the dynamics of FtsZ bundles induced by ZapA (YgfE) (Mohammadi *et al.* 2009).

In this chapter, we did experiments under the condition of pH 6.5, 10 mM $MgCl_2$, and 50 mM KCl, which is the more optimal pH for FtsZ polymerization (chapter 4). We have also found that YgfE enhances the amount of FtsZ bundling as well as stabilizing the FtsZ polymers from both right-angle light scattering and LD. Those FtsZ bundles induced by YgfE have been visualised directly by electron microscopy. Besides, electron microscopy also suggested that without GTP, YgfE still can bind to FtsZ monomers to form small size of round oligomers. The tendency of the protofilaments to associate to form bundles resulted in a slower turnover of FtsZ polymers that resulted in a reduced rate of GTP hydrolysis. From studying the P_i released from the hydrolysis of GTP to GDP catalysed by FtsZ, we have found that YgfE is an inhibitor of FtsZ's GTPase activity.

The new protocol we introduced for this study was to design two different kinds of experiments, (i) adding YgfE to preformed FtsZ protofilaments and (ii) adding GTP to premixed FtsZ and YgfE, to compare the bundling effect of YgfE. When YgfE was added to preformed FtsZ protofilaments, YgfE was found to stabilize FtsZ bundles on a extremely long time scale (at least 6465 s) from right-angle light scattering. However, LD shows that FtsZ bundles disassembled completely around 3000 s, which suggestes that the signal detected by right-angle light scattering 3000 s is possibly due to the aggregation of protein.

When we started polymerization by adding GTP to premixed FtsZ and YgfE, the signal in both light scattering and LD increased, but this increase were much smaller and was not maintained as long as the previous way. Especially in the light scattering, we found that FtsZ bundles disassembled completely around 3000 s, instead of stabilizing as long as 6465 s. This could be explained by a competition between FtsZ protofilment-formation and YgfE-induced bundling. When FtsZ protofilments formation and bundling happens simultaneously, short bundles tend to be formed as soon as the formation of protofilments, and these short bundles are easy to disassemble, including not forming aggregation, compared with the long bundles. It also can be observed from electron microscopy that when YgfE was added into the preformed FtsZ protofilaments, the high-order YgfE-induced FtsZ bundles were formed, which can not be achieved by adding GTP into premixed FtsZ and YgfE. In addition, the decrease in the inhibition of YgfE on FtsZ's GTPase activity, which is associated with less effective FtsZ bundling in the case of adding GTP into premixed FtsZ and YgfE, is demonstrated from the phosphate release assay. Therefore, in order to obtain stable FtsZ bundles caused by YgfE efficiently, sufficient FtsZ protofilments should be formed before.

[$] In chapter 5 and 6, the real concentration of FtsZ was estimated to be 11% less, by comparison with the literature in the light of FtsZ's specific activity.

CHAPTER 6 -- EFFECTS OF YgfE MUTANTS ON THE POLYMERIZATION AND BUNDLING OF FtsZ[$]

6.1 Introduction

Lateral associations between FtsZ polymers, assisted by the accessory cell division proteins, are thought to be important for the function of the Z-ring *in vivo*. ZapA binds to the FtsZ polymer and, by an unknown mechanism, renders FtsZ filaments more stable and enhances bundling, a property believed to be connected to its dimeric or tetrameric nature (§ 1.3.1). The crystal structure of ZapA (figure 1.3.1), which is the orthologue of YgfE, revealed an anti-parallel tetramer that is composed of a pair of dimers which associate through extensive coiled-coil interactions along the C termini of the individual subunits (Low et al. 2004, Löwe, van den Ent and Amos 2004). In solution, the protein was shown being an equilibrium mixture of dimers and tetramers (Small *et al.* 2007).

In the previous chapter, we discussed the behavior of YgfE, a putative *E. coli* ZapA orthologue, on inducing FtsZ bundles. In order to further study how YgfE interacts with FtsZ, we then made a series of YgfE mutants, and the results obtained with these mutants are reported in this chapter.

6.2 Objectives

Since the ability of YgfE to induce FtsZ bundling was thought to be related to its dimeric or tetrameric nature, a number of YgfE mutants were generated with the aim of disrupting the dimer-dimer interface. In this chapter, we explore how YgfE affect FtsZ bundling by changing its oligomerization state.

In chapter 5, we saw that adding YgfE into preformed FtsZ protofilaments can produce FtsZ bundles more efficiently. We then chose to study the effect of YgfE

mutants on FtsZ bundling in the same way. Right-angle light scattering was used to investigate the increase in polymer size and its dynamic behaviour in real time; linear dichroism (LD) enables us to study the real-time changes in the protein backbones and side chains of protofilaments and bundles; electron microscopy (EM) of negatively stained samples characterizes the FtsZ polymers induced by YgfE and YgfE mutants; a colourimetric assay was used to measure the kinetics of inorganic phosphate (P_i) released from GTP hydrolysis catalysed by FtsZ in the presence of YgfE or YgfE mutant; and a sedimentation assay shows the interaction between FtsZ and YgfE mutant.

6.3 Characterization of YgfE mutants

In order to know how YgfE/ZapA interacts with FtsZ or how it stabilizes the polymer, a number of mutations of YgfE were made with the aim to disrupt the two dimer-dimer interfaces (A/C subunit interface and A/B subunit interface) shown in figure 6.3.1. Table 6.3.1 shows a list of the purified YgfE protein mutants.

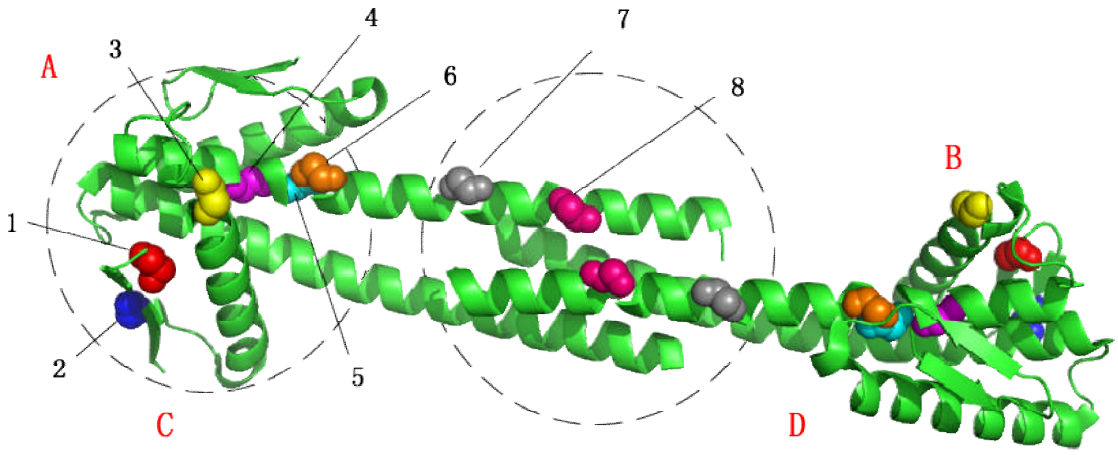

Figure 6.3.1 Crystal structure of tetrameric ZapA from *Pseudomonas aeruginosa* (Löwe et al. 2004) with the indication of the mutant positions. Tetrameric ZapA consists of four monomers (A, B, C, D). The mutations are as follows. (1) red: F11W (2) dark blue: V17E (3) yellow: L41Q (4) pink: L59Q (5) cyan blue: Y63W (6) orange: E64L (7) gray: Y75W (8) deep pink: I83E

Table 6.3.1 YgfE mutants with amino acid mutations exchanges and their character indicated. V17E for example denotes the valine at position 17 is replaced by a glutamic acid.

YgfE mutants[@]	Original side chain polarity	Position	Substitutent polarity	Remarks
YgfE–F11W	Phenylalanine (F), nonpolar hydrophobic	11	Tryptophan (W), nonpolar hydrophobic	None
YgfE–V17E	Valine (V), nonpolar hydrophobic	17	Glutamic acid (E), negatively charged hydrophilic	None
YgfE–L41Q	Leucine (L), nonpolar hydrophobic	41	Glutamine (Q), polar uncharged	None
YgfE–L59Q	Leucine (L), nonpolar hydrophobic	59	Glutamine (Q), polar uncharged	The protein precipitated as white flakes when it was dialysed in the storage buffer (buffer A).
YgfE–Y63W	Tyrosine (Y), polar uncharged	63	Tryptophan (W), nonpolar hydrophobic	None
YgfE–E64L	Glutamic acid (E), negatively charged hydrophilic	64	Leucine (L), nonpolar hydrophobic	The protein was either not overexpressed or overexpressed in the insoluble fraction of the cell lysate
YgfE–Y75W	Tyrosine (Y), polar uncharged	75	Tryptophan (W), nonpolar hydrophobic	None
YgfE–I83E	Isoleucine (I), nonpolar hydrophobic	83	Glutamic acid (E), negatively charged hydrophilic	Surface mutation in the coil region.

[@] All those mutants were kindly provided by Dr. Raul Pacheco-Gomez.

The assumption was that YgfE is mostly coiled-coils with a very small globular region. The residues which were either conserved (not as likely in a coiled region as in a globular region) or within regions very likely to be coiled-coils were then

chosen to be mutated accordingly - polar to non-polar, charged to non-charged or oppositely charged *etc.*

Analytical ultracentrifugation (AUC) sedimentation velocity experiments were also performed by Dr. Raul Pacheco-Gomez for all the YgfE and mutants as shown in figure 6.3.2. From the sedimentation coefficient, *S*, which depends directly on the mass of the particles, we found two mutants YgfE-I83E and YgfE-V17E were most different from the wild type YgfE in size, which indicates the oligomerization of those three proteins may be different.

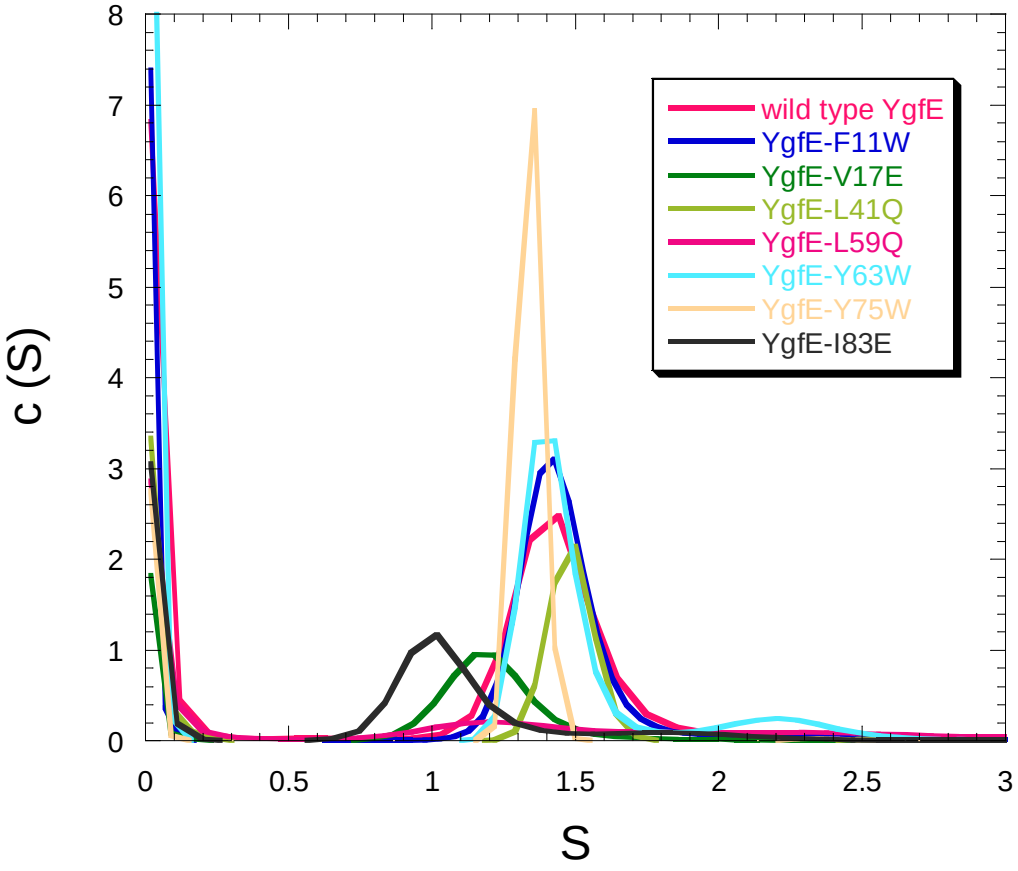

Figure 6.3.2 Sedimentation velocity study of YgfE and YgfE mutants by analytical ultracentrifugation (provided by Dr. Raul Pacheco-Gomez).

To ascertain whether the mutants were folded, far-UV circular dichroism spectra were measured on J-815 spectropolarimeter using a 1 mm pathlength cuvette. Figure

6.3.3 shows the CD spectra of wild type YgfE and the other two mutants YgfE-I83E and YgfE-V17E at each concentration of 100 μg/ml after a baseline (background spectrum measured in the absence of protein) subtraction. The negative peaks at 222 nm and 208 nm with separate maxima of similar magnitude exhibit a CD spectrum characteristic of an α-helix. It is demonstrated that in both cases the fold has not been significantly altered by the amino acid substitutions.

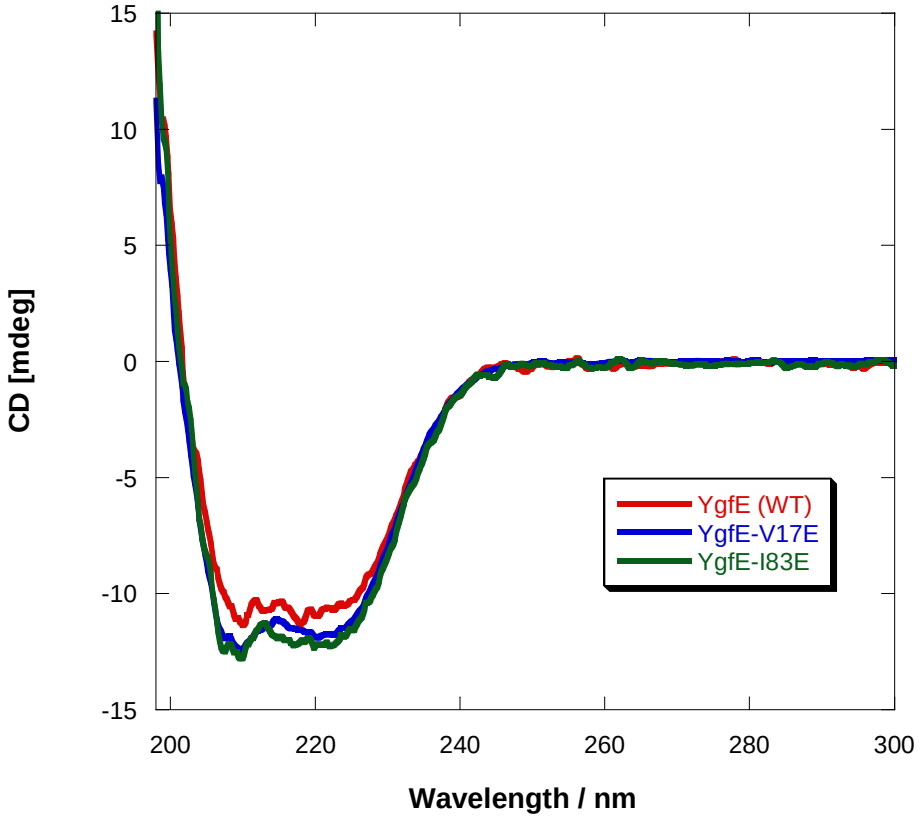

Figure 6.3.3 CD spectra of purified wild type YgfE and two mutants I83E and V17E at the same concentration (~100 μg/ml).

In order to obtain the exact oligomerization states of these three proteins, wild type YgfE, YgfE-I83E and YgfE-V17E, AUC sedimentation equilibrium experiments

were performed. Different concentrations from 0.3 mg/ml to 1.5 mg/ml proteins were prepared, and run at three different speeds as indicated in figure 6.3.4.

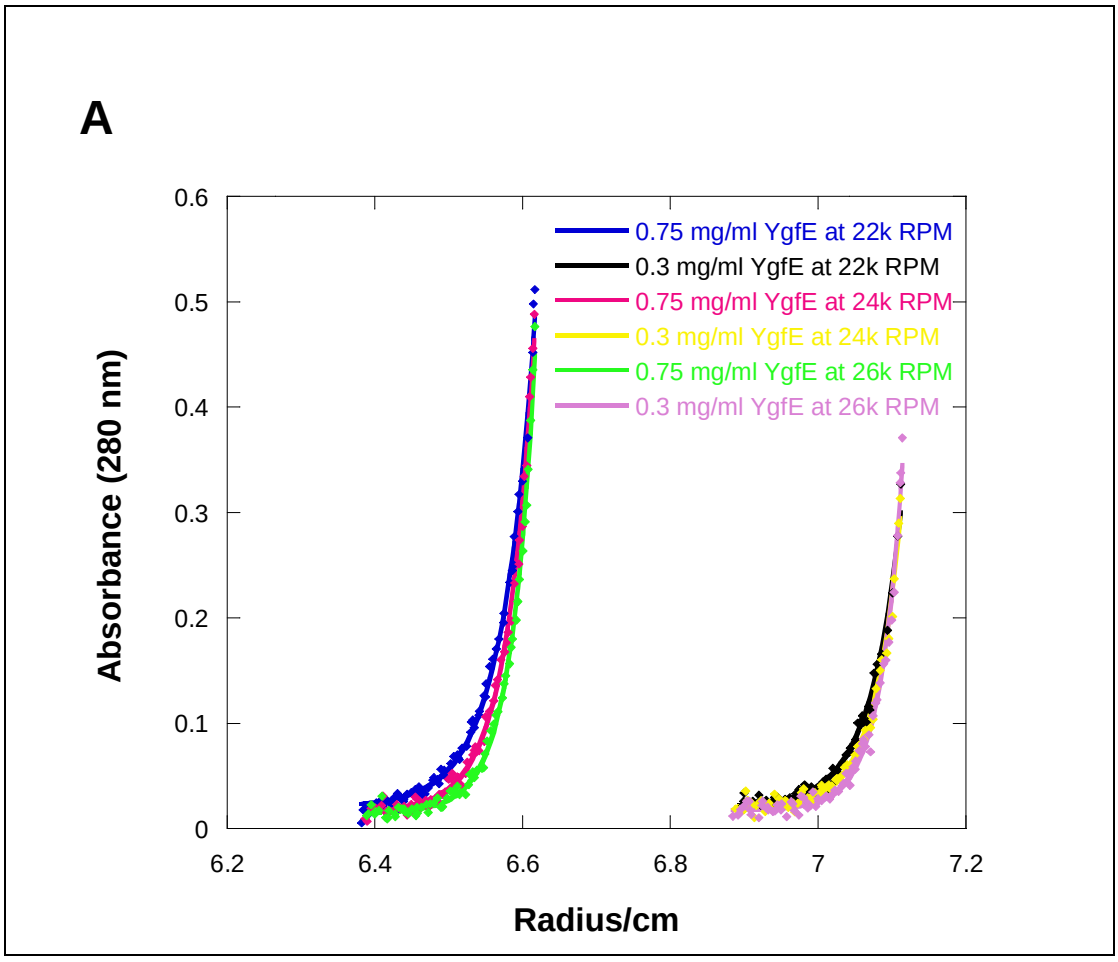

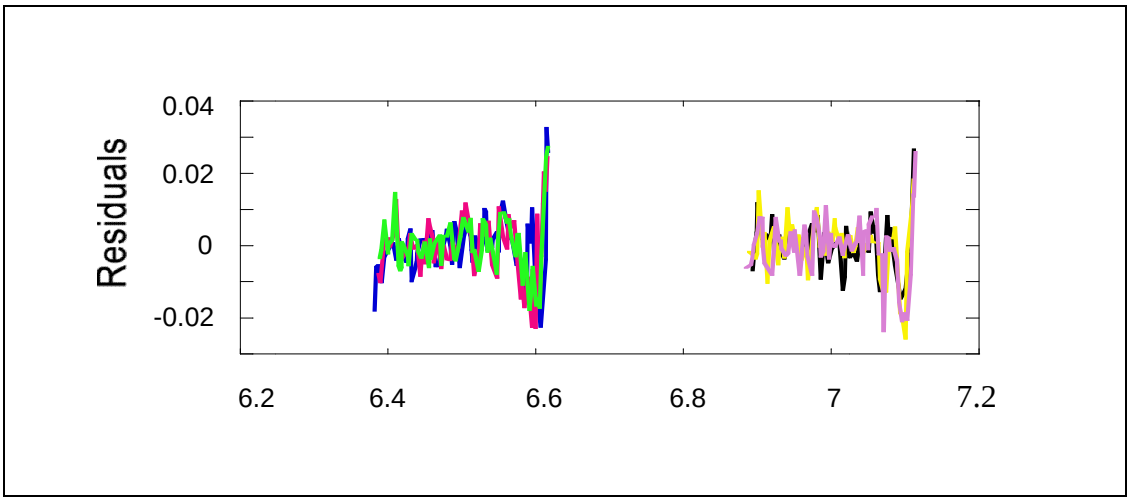

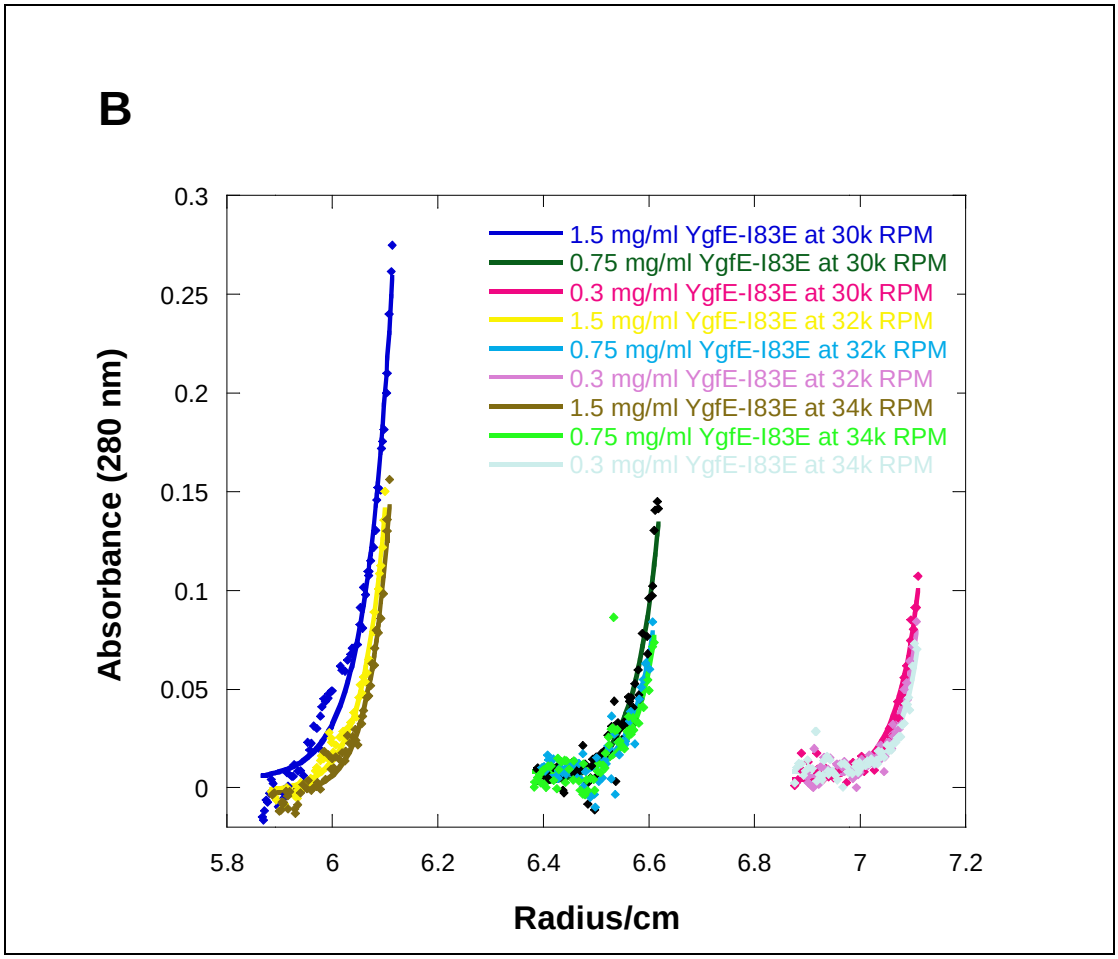
B
Absorbance (280 nm)
Radius/cm
1.5 mg/ml YgfE-I83E at 30k RPM
0.75 mg/ml YgfE-I83E at 30k RPM
0.3 mg/ml YgfE-I83E at 30k RPM
1.5 mg/ml YgfE-I83E at 32k RPM
0.75 mg/ml YgfE-I83E at 32k RPM
0.3 mg/ml YgfE-I83E at 32k RPM
1.5 mg/ml YgfE-I83E at 34k RPM
0.75 mg/ml YgfE-I83E at 34k RPM
0.3 mg/ml YgfE-I83E at 34k RPM
0.3
0.25
0.2
0.15
0.1
0.05
0
5.8
6
6.2
6.4
6.6
6.8
7
7.2

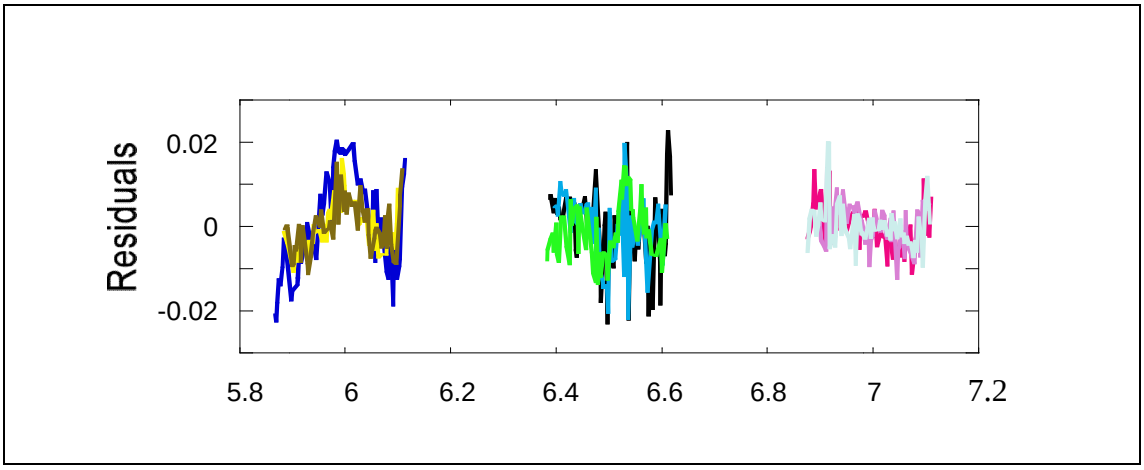
Residuals
0.02
0
-0.02
5.8
6
6.2
6.4
6.6
6.8
7
7.2

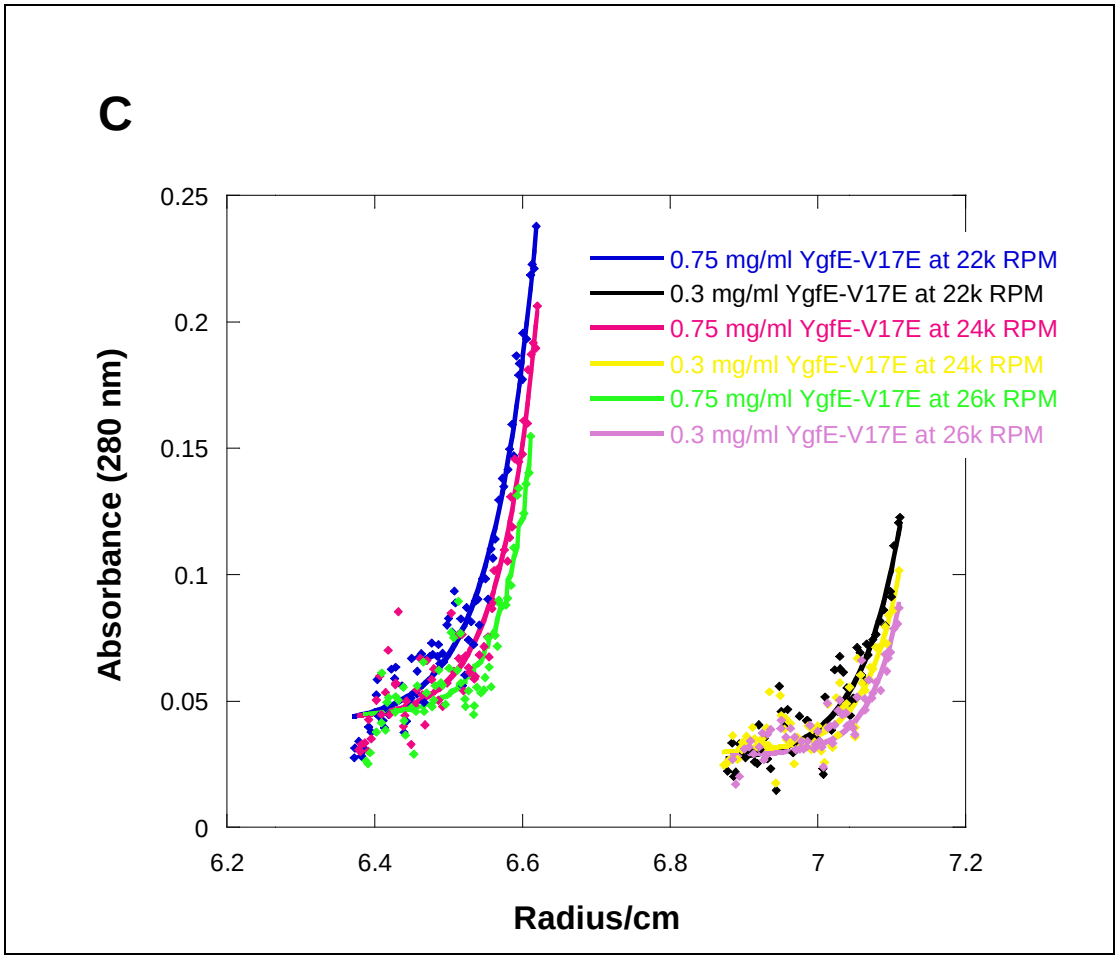

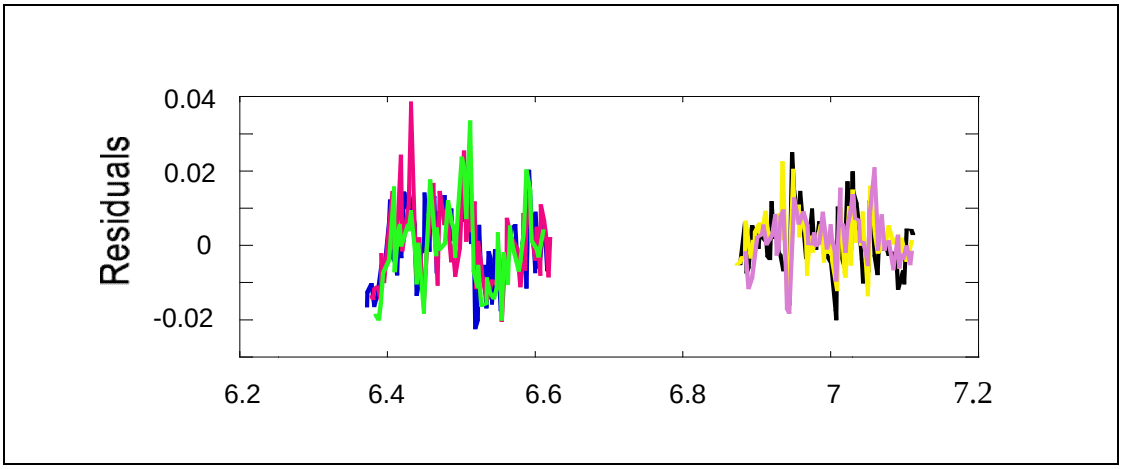

Figure 6.3.4 Sedimentation equilibrium study of YgfE and YgfE mutants by analytical ultracentrifugation. A: wild type YgfE; B: YgfE mutant I83E; C: YgfE mutant V17E.

According to the Svedberg equation (§ 3.3), the molecular weight and thus the oligomerization state was determined from the concentration distribution shown in table 6.3.2.

Table 6.3.2 Determination of molecular mass by sedimentation equilibrium analytical ultracentrifugation.

Sample	Expected monomer molecular mass (kDa)	Measured molecular mass (kDa)	Oligomerization state
YgfE (wild type)	14.4	55.2	tetramer
YgfE-I83E	14.4	26.3	dimer
YgfE-V17E	14.4	37.7	Mixture of tetramers and dimers

Previous results (Small *et al.* 2007) showed wild type YgfE being an equilibrium mixture of dimers and tetramers. Much higher concentrations were required to obtain similar results with the ZapA of *P. aeruginosa* (Low *et al.* 2004). Under the experimental conditions of our studies, we concluded that the wild type YgfE is a tetramer species, since the molecular mass was measured as 55.2 kDa, which is compatible with the expected mass of the protein tetramer (molecular weight of the YgfE monomer is 14.4 kDa). Mohammadi *et al.* also demonstrated that *E. coli* ZapA (YgfE) is a tetramer using equilibrium centrifugation (Mohammadi *et al.* 2009).

The mutant YgfE-I83E was concluded to be predominantly a dimer, since the molecular weight of purified YgfE-I83E in solution was given as 26.3 kDa, which is close to two times the predicted molecular weight of the YgfE monomer (14.4 kDa). The mutant YgfE-I83E is a surface mutation of the coiled-coil region and suggests disruption of the tetramer in favour of a dimer (figure 6.3.1). If one views the tetrameric YgfE as a dog bone, the YgfE-I83E is only half the bone. With regards to

the mutant YgfE-V17E, whose molecular weight appears to be 37.7 kDa, it is in equilibrium between a dimer and a tetramer.

We suspected the different oligomerization of YgfE in solution may have different effects on its ability to induce FtsZ bundling, which could help us to explore how YgfE interacts with FtsZ. Therefore, the two YgfE mutants, YgfE-I83E and YgfE-V17E were chosen for the more detailed studies below.

6.4 Right-angle light scattering analysis of FtsZ polymerization in the presence of YgfE mutants

Right-angle light scattering has shown that YgfE induces FtsZ bundling, and it could be employed in a continuous assay to study the effects of YgfE mutant on preformed FtsZ protofilaments. The experiments were performed as described in the previous chapter (§ 5.4.1). Briefly, the reaction mixtures consisting of 11 μM of FtsZ, 50 mM of MES-KOH, pH 6.5, 10 mM of $MgCl_2$, 50 mM of KCl were prepared. After baseline collection of approximately 5 minutes, 0.2 mM GTP was added to initiate the polymerization reaction. Varying concentrations of YgfE mutant (FtsZ-YgfE ratios from 1:1 to 1:4) were added last during the steady-state phase of the FtsZ polymerization, at approximately 3 minutes after the GTP addition. The control experiments in the presence of wild type YgfE and in the absence of YgfE that were performed in the pervious chapter are also shown here for comparison (figure 6.4). The baseline is defined as the level of light scattering before GTP was added. Zero time is defined to be the addition of GTP.

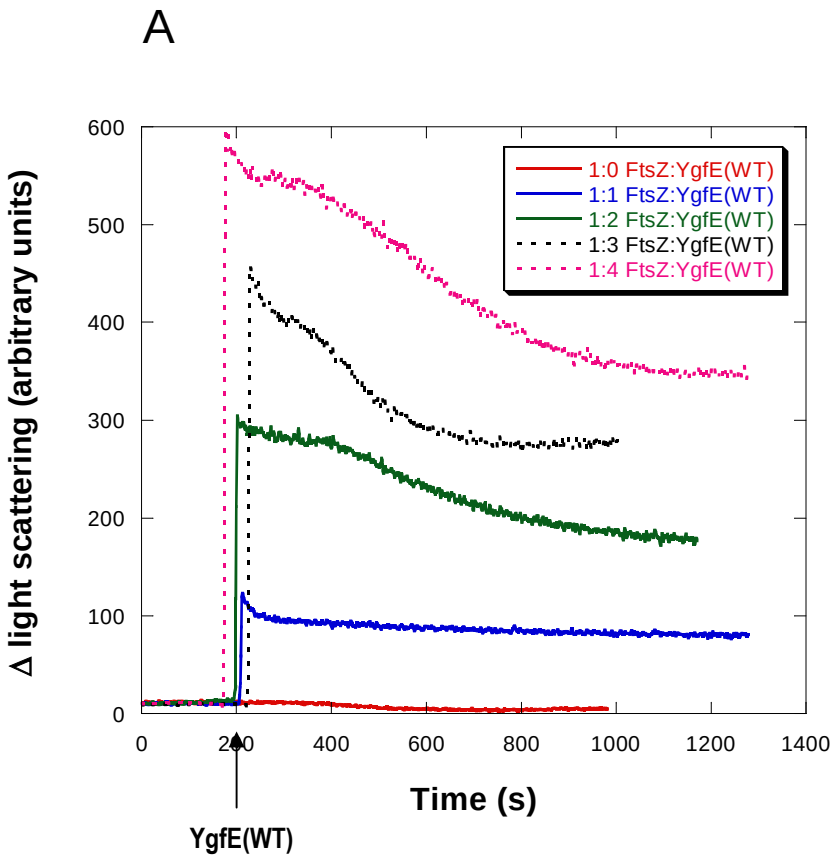
A
Δ light scattering (arbitrary units)
Time (s)
YgfE(WT)
1:0 FtsZ:YgfE(WT)
1:1 FtsZ:YgfE(WT)
1:2 FtsZ:YgfE(WT)
1:3 FtsZ:YgfE(WT)
1:4 FtsZ:YgfE(WT)

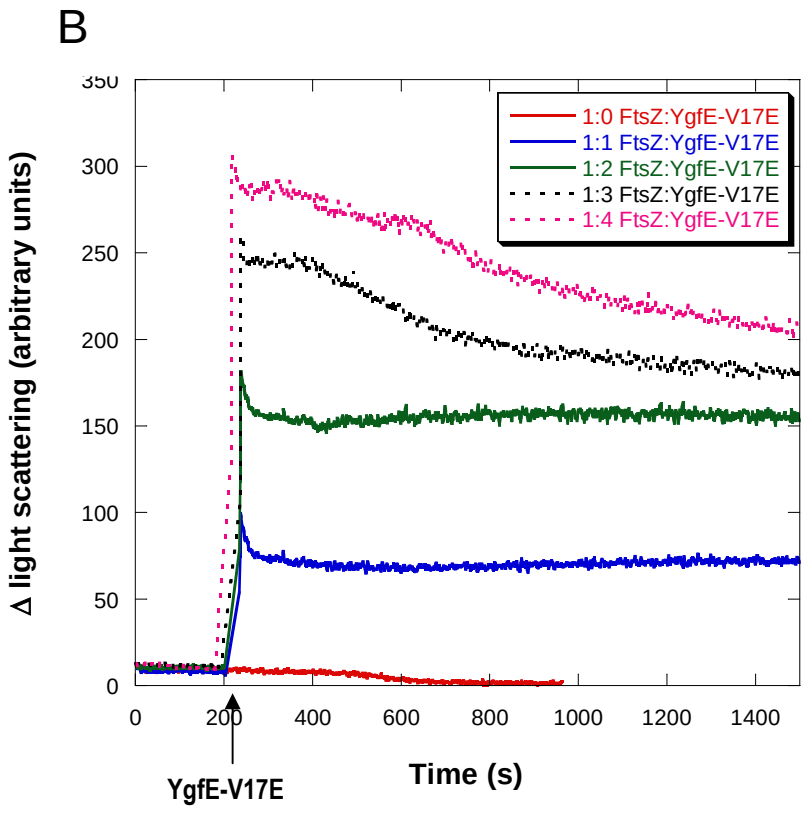
B
Δ light scattering (arbitrary units)
Time (s)
YgfE-V17E
1:0 FtsZ:YgfE-V17E
1:1 FtsZ:YgfE-V17E
1:2 FtsZ:YgfE-V17E
1:3 FtsZ:YgfE-V17E
1:4 FtsZ:YgfE-V17E

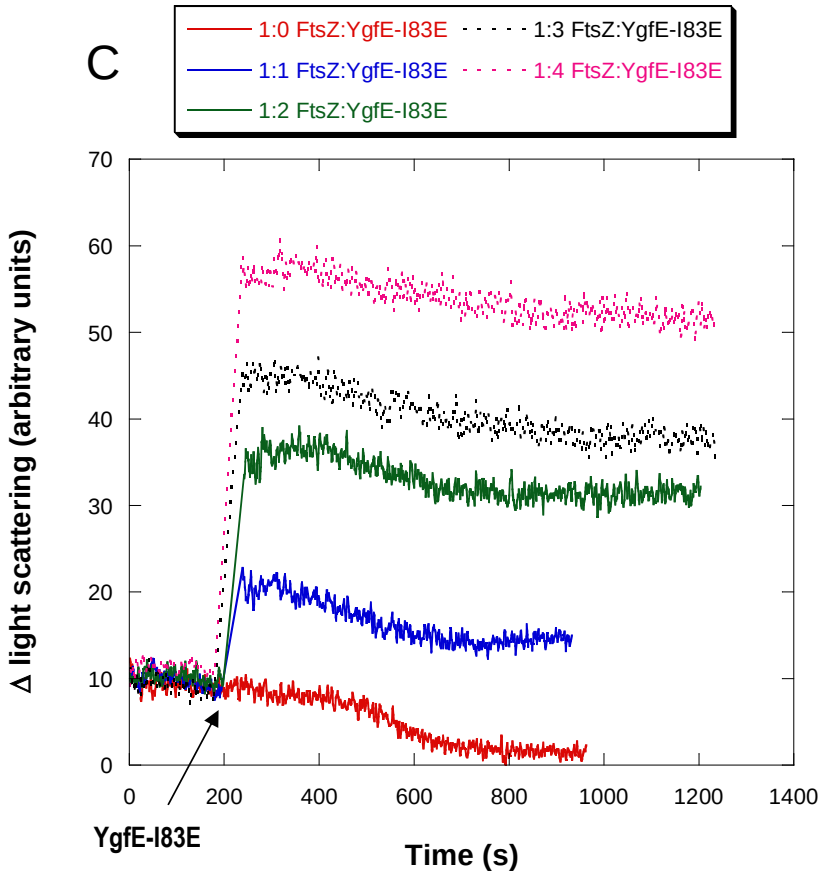

Figure 6.4 The effects of YgfE and YgfE mutants on FtsZ preformed protofilaments proved by right-angle light scattering. FtsZ (11 μM in polymerization buffer) was mixed with GTP (0.2 mM) at time zero. Different types of YgfE at different concentrations (shown in graph) were added after protofilament formation (approximately 3 minutes). Excitation and emission wavelengths were set at 550 nm.

As shown in figure 6.4, in almost all the ratios studied, the addition of wild type YgfE caused the largest increase in light scattering, nearly 600 units when FtsZ-YgfE ration reached 1:4, which indicates the formation of most FtsZ bundles. The increase induced by YgfE-V17E is intermediate while that induced by YgfE-I83E is the slightest. At the same ratio 1:4 of FtsZ to YgfE, the increase was approximately 300 and 60 units respectively for YgfE-V17E and YgfE-I83E. We thereby conclude that the ability of YgfE to induce effective FtsZ bundling is related to YgfE's propensity to form tetramers, since wild type YgfE exists as a tetramer; YgfE-I83E is a dimer, and YgfE-V17E is somewhat in between.

In addition, we can observe that FtsZ polymers are stabilised in the presence of YgfE-V17E since its light scattering increases significantly as does the wild type YgfE. For YgfE-I83E, interestingly, if we subtract the end point data from all the values, we found that the light scattering change was the same for all the concentrations studied. Therefore we assume the very slight increase induced by YgfE-I83E was contributed by YgfE-I83E itself attaching to FtsZ instead of forming FtsZ bundles.

6.5 Linear dichroism analysis of FtsZ polymerization in the presence of YgfE mutants

Linear dichroism studies also have shown that YgfE can induce FtsZ bundling, and we continue to report the results from LD studying the effects of YgfE mutant on preformed FtsZ protofilaments. LD provides more information than light scattering and helps us to confirm whether the small increase in light scattering is due to bundling or simply aggregation. Bundling and aggregation are indistinguishable in light scattering.

The experiments were performed as described in the previous chapter (§ 5.5). Briefly, the mixtures consisting of 11 μM of FtsZ, 50 mM of MES-KOH, pH 6.5, 10 mM of $MgCl_2$, 50 mM of KCl were prepared. A baseline was collected before initiation of the polymerization reaction with GTP by measuring the LD spectrum with and without rotating of the LD cell. The difference of both spectra is a flat line around zero as expected, since there being nothing in solution being oriented without GTP. After that, 0.2 mM of GTP was added to initiate the polymerization reaction. Varying concentrations of YgfE mutants (FtsZ-YgfE ratios from 1:0 to 1:4) were added after 2 scans, roughly 3 minutes after the GTP addition. Zero time is defined to be the addition of GTP. The comparison of LD_{210} at different FtsZ-YgfE ratios is shown in figure 6.5.

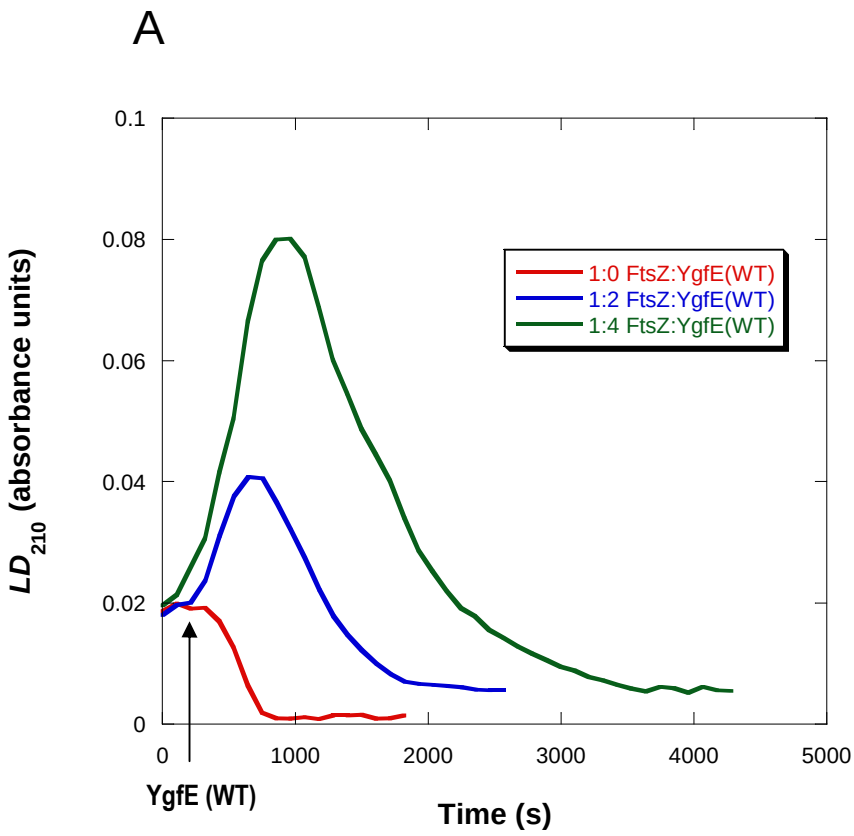
A
0.1
0.08
0.06
0.04
0.02
0
LD_{210} (absorbance units)
1:0 FtsZ:YgfE(WT)
1:2 FtsZ:YgfE(WT)
1:4 FtsZ:YgfE(WT)
0
1000
2000
3000
4000
5000
YgfE (WT)
Time (s)

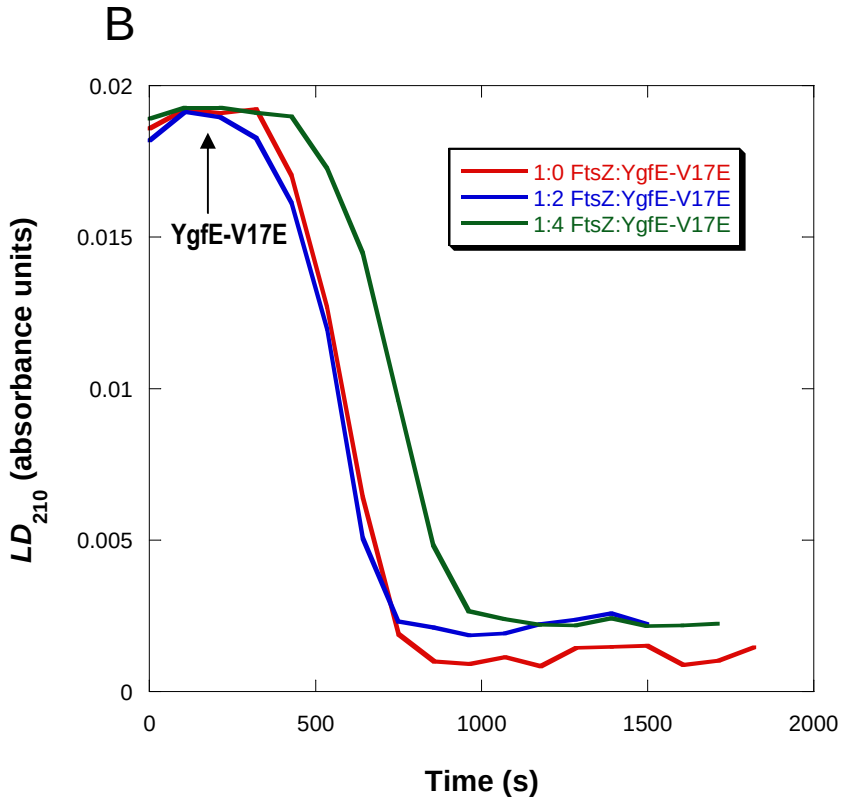
B
0.02
0.015
0.01
0.005
0
LD_{210} (absorbance units)
1:0 FtsZ:YgfE-V17E
1:2 FtsZ:YgfE-V17E
1:4 FtsZ:YgfE-V17E
YgfE-V17E
0
500
1000
1500
2000
Time (s)

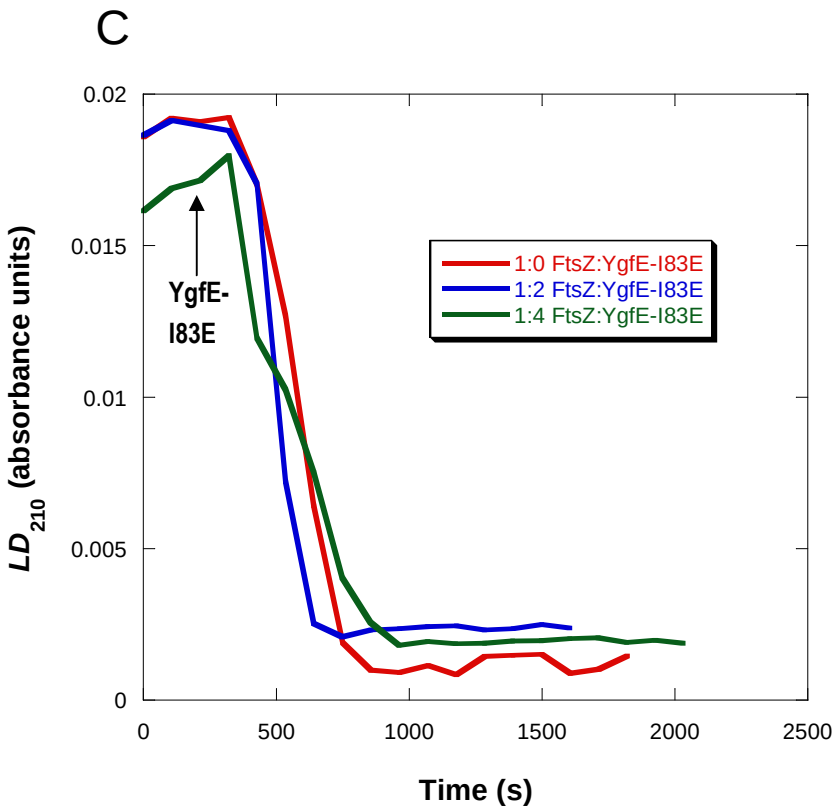

Figure 6.5 Comparison of the LD_{210} at different FtsZ-YgfE ratios. FtsZ (11 μM in polymerization buffer) was mixed with GTP (0.2 mM) at time zero. Different types of YgfE at different concentrations (shown in graph) were added after protofilament formation (approximately 3 minutes).

In figure 6.5, the control experiments in the presence of wild type YgfE and in the absence of YgfE that were performed in the pervious chapter are also included for comparison. Wild type YgfE obviously caused the greatest increase in LD signal at 210 nm, and the polymers obtained were the most stable as seen from the time of the LD signal lasted. This means wild type YgfE has the strongest ability to promote FtsZ bundling. When it comes to YgfE-V17E, we can only see the FtsZ polymers were stabilised a little longer, approximately 4 minutes longer at the 1:4 ratio of FtsZ toYgfE-V17E, compared with the data obtained in the absence of YgfE. We suspect this effect resulted from formation of a few FtsZ bundles. As for YgfE-I83E,

however, it made little or no difference in the LD signal at 210 nm, which means it does not help to form FtsZ bundles.

Consistent with the right-angle light scattering results, the ability of YgfE to promote FtsZ bundling is related to its state in solution. Wild type YgfE, which is a tetramer, induce the most effective FtsZ bundles, and next comes mutant YgfE-V17E. Mutant YgfE-I83E, however, as a dimer, is not able to induce the formation of FtsZ bundles.

6.6 Visualization of the effect of YgfE on FtsZ protofilaments by electron microscopy

We examined the morphology of FtsZ polymers formed in the presence of YgfE mutants by negative stain electron microscopy using a JEOL 2011 transmission electron microscope.

A 1:4 FtsZ-YgfE ratio was chosen for EM. 11 μM of FtsZ were incubated in the polymerization buffer consisting of 50 mM MES-KOH, pH 6.5, 10 mM $MgCl_2$ and 50 mM KCl. At 3 minutes of GTP addition, 44 μM of the two YgfE mutants was added into the mixture respectively. 2 minutes later, 3 μl of the sample mixtures were then withdrawn for imaging. Pictures are shown in figure 6.6, and for comparison, the pictures in the presence of wild type YgfE and in the absence of YgfE are also included.

As seen in figure 6.6, in the presence of GTP and absence of YgfE, FtsZ formed mostly single-stranded protofilaments, or lateral associations of a few protofilaments (figure 6.6A). The addition of wild type YgfE induces the thickest bundles (figure 6.6B). YgfE-V17E has similar effects to wild type YgfE (figure 6.6C), but the bundles formed are not as large as those induced by wild type YgfE. After adding YgfE-I83E, we see almost only FtsZ protofilamets on the picture (figure 6.6D).

However, there are some little dark dots on FtsZ protofilamets, which are assumed to be YgfE-I83E, are attached to FtsZ, but cannot bridge two adjacent FtsZ protofilaments.

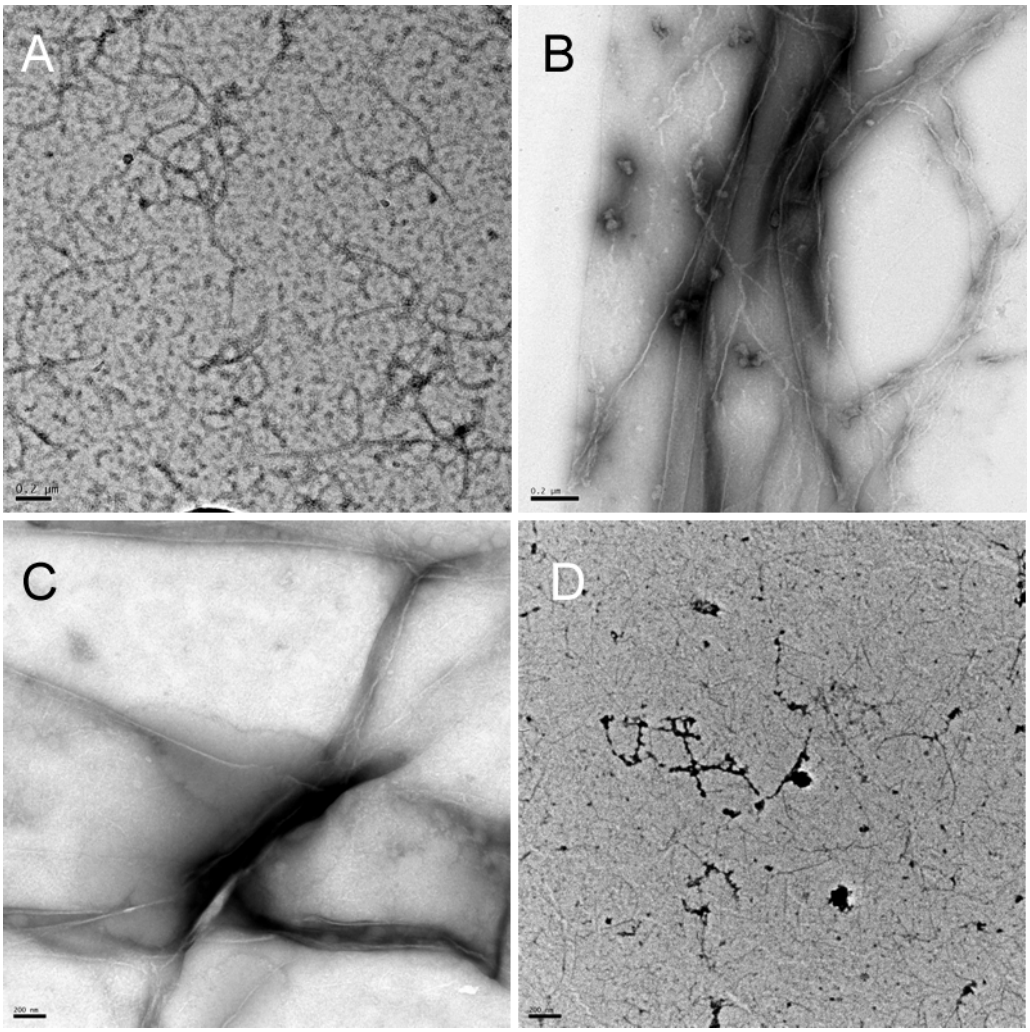

Figure 6.6 Electron microscopy of the products of FtsZ and diffent types of YgfE. (A) FtsZ (11 μM in polymerization buffer) mixed with GTP (0.2 mM); (B) YgfE (44 μM) was added to FtsZ protofilaments, 3 minutes after the GTP (0.2 mM) addition to FtsZ (11 μM). The sample was then diluted 1:5 with water for imaging. (C) YgfE-V17E (44 μM) was added to FtsZ protofilaments, 3 minutes after the GTP (0.2 mM) addition to FtsZ (11 μM). (D) YgfE-I83E (44 μM) was added to FtsZ protofilaments, 3 minutes after the GTP (0.2 mM) addition to FtsZ (11 μM). Bars, 200 nm.

Employing transmission electron microscopy, we confirmed our hypothesis from light scattering and linear dichroism. As a tetramer, wild type YgfE has the strongest ability to induce FtsZ bundling. As a dimer, although YgfE-I83E can bind to FtsZ, it cannot bring two FtsZ protofilaments together. YgfE-V17E behaves in an intermediate fashion. We thus believe the ability of YgfE to make FtsZ bundles depends on the percentage of tetramer present.

6.7 GTPase assay

The effects of YgfE mutants on FtsZ GTPase activity is reported in this section. Basically the principle of the experiment is the same as that used in FtsZ chapter (§ 4.5), employing a fast and continuous colourimetric assay to measure the P_i released from GTP hydrolysis catalysed by FtsZ.

6.7.1 Calibration curve for inorganic phosphate

In this study, A Jsaco V-660 UV-Vis spectrophotometer was used, thus a new calibration curve with phosphate standard was re-generated. As described in § 4.5.1, different concentrations of phosphate standards from 0 to 250 µM were added to 0.4 mM MESG, 1 U/mL PNP and the polymerization reaction buffer, pH 6.5. The solution was then transferred to the 3 mm path length fluorimeter cuvette after 10 minutes incubation at room temperature. The absorbance was then recorded and the change in the absorbance at 360 nm was plotted as a function of the P_i concentration (figure 6.7.1.1). From this figure, we can observe the linear responses of the ΔA_{360} to the P_i concentration, which will allow us to quantify directly the P_i released from the GTP catalysed by FtsZ.

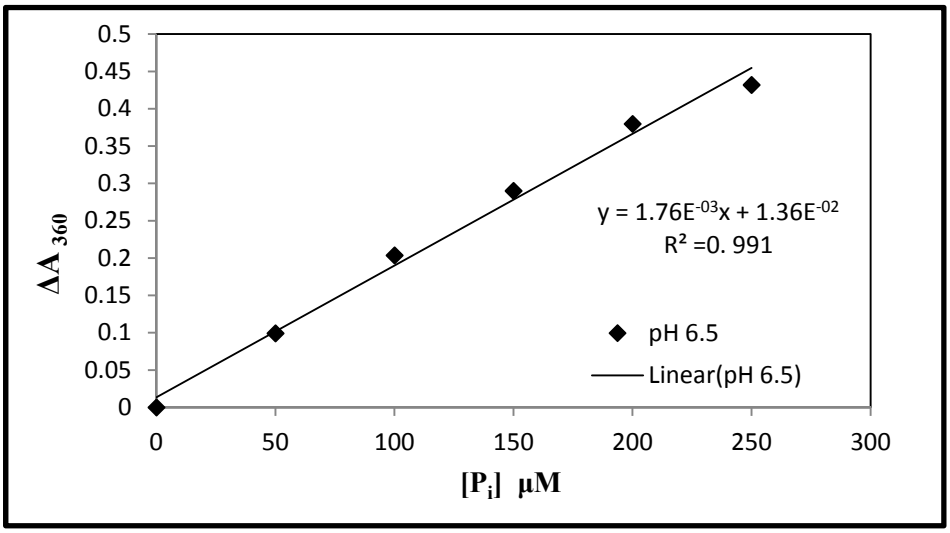

Figure 6.7.1.1 Change in absorbance at 360 nm plotted as a function of the P_i concentration. The absorbance was collected on the Jsaco V-660 UV-Vis spectrophotometer, using a 3 mm path length fluorimeter cuvette.

However, when the mutant YgfE-V17E was studied, a small amount of precipitation was observed when YgfE-V17E, $MgCl_2$ and GTP were mixed. In order to measure the absorbance, the solution had to be stirred during the measurements. As the LD cell (a mirco-volume 65 µL capillary) can be rotated, and there is also a spare channel for UV measurement on the Jasco J-815 circular dichroism spectrometer adapted for LD spectroscopy, we then explored the possibilty of measuring LD and UV simultaneously.

A calibration curve experiment with phosphate standard was first employed to test the performance. Different concentrations of phosphate standard from 0 to 250 µM were added to 0.4 mM MESG, 1 U/mL PNP and the polymerization reaction buffer, pH 6.5. The solution was then transferred to the mirco-volume capillary after 10 minutes incubation at room temperature. LD and absorbance spectra were collected using the spectrum measurement programme within the Jasco software. This enabled collection of full wavelength scans from 500 to 300 nm at a scanning speed of 200 nm min^{-1}. The absorbance at 360 nm was plotted as a function of the P_i concentration shown in figure 6.7.1.2. The linear responses of the ΔA_{360} to the P_i

concentration were observed in the figure, which shows that accurate UV absorbance measurments can be achived while the LD is being measured. This method as well as the calibration curve was thus used to quantify the P_i released from the GTP catalysed by FtsZ in the presence of the YgfE mutant V17E.

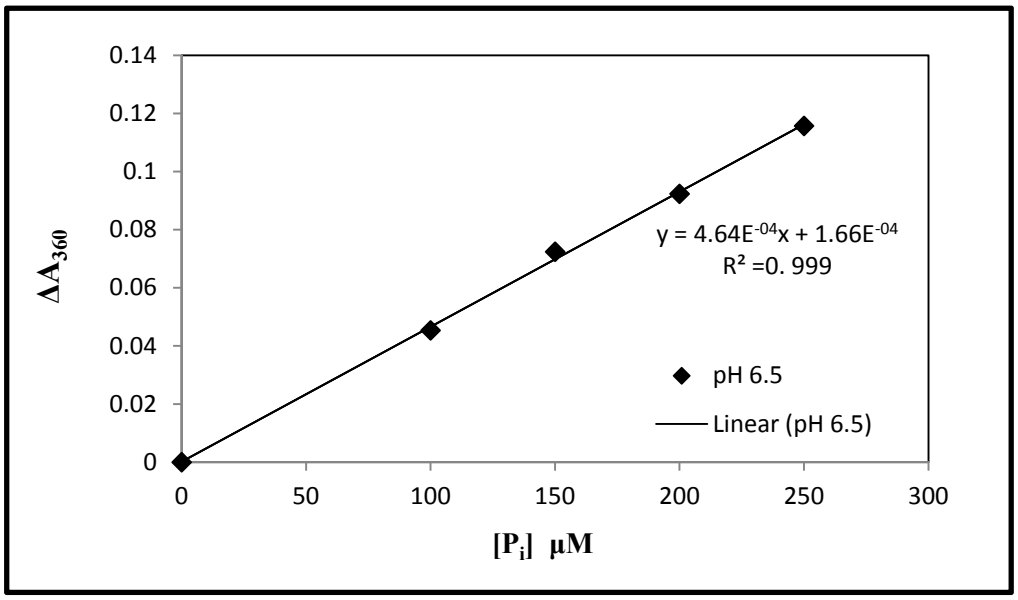

Figure 6.7.1.2 Change in absorbance at 360 nm plotted as a function of the P_i concentration. The absorbance was collected on the J-815 circular dichroism spectrometer adapted for LD spectroscopy, using a mirco-volume 65 μL capillary with 0.5 mm path length.

6.7.2 Effects of YgfE mutants on FtsZ's GTPase activity

In order to detect the P_i released from GTP hydrolysis catalysed by FtsZ in the presence of YgfE mutants, FtsZ, GTP, and YgfE mutants were added to generate the P_i instead of using the phosphate standard provided. For YgfE-I83E, we employed a time course measurement on the Jasco V-660 UV-Vis spectrophotometer to collect the absorption at 360 nm every 0.5 second after the addition of GTP. On the other hand, in the presence of YgfE-V17E, we used the interval scan measurement programme for the Jasco J-815 collecting both LD and absorbance of full wavelength scans from 500 to 300 nm at a scanning speed of 200 nm min^{-1} continuously until no phosphate was produced.

Before adding all of the FtsZ, GTP and YgfE into the media, we firstly checked that there was no P_i released when GTP was added into the mutants YgfE-I83E or YgfE-V17E alone. Then the reaction consisting of 11 μM of FtsZ, 50 mM of MES-KOH, pH 6.5, 10 mM of $MgCl_2$, 50 mM of KCl, 0.4 mM of MESG and 1 U/mL of PNP was prepared. A baseline was also collected before initiating the phosphate release reaction by adding GTP to make sure there was no P_i released from all the enzyme and/or reagents.

After such a baseline collection, GTP to a final concentration of 0.2 mM was added to start the phosphate release reaction. After 3 minutes, varying concentrations of YgfE mutants (FtsZ-YgfE ratios from 1:0 to 1:4) were added to the reaction medium. The absorbance at 360 nm was obtained as a function of time, and then transformed to the percentages of P_i released from the hydrolysis of GTP to GDP catalysed by FtsZ. For the mutant YgfE-V17E, the absorbance was corrected against light scattering induced by precipitation before transforming it to the percentages of P_i release. Figure 6.7.2 shows the effects of YgfE mutants on FtsZ's GTPase activity.

As we know from the previous chapter, wild type YgfE is a potent inhibitor of FtsZ's GTPase activity. YgfE stabilises FtsZ polymers when it assemble into bundles, and then less P_i is released. From figure 6.7.2, we see that YgfE-V17E is also an inhibitor of FtsZ's GTPase activity, reducing and slowing down the P_i release, but by less than that of wild type YgfE. As seen in figure 6.7.2A, the amount of P_i release was reduced by almost half after the addition of wild type YgfE at a 4:1 molar ratio to FtsZ. When the same concentration of YgfE-V17E was added into a solution of FtsZ, it resulted in approximately 20% less P_i released from GTP hydrolysis (figure 6.7.2B). YgfE-I83E, however, had little effect on FtsZ GTPase activity (figure 6.7.2C).

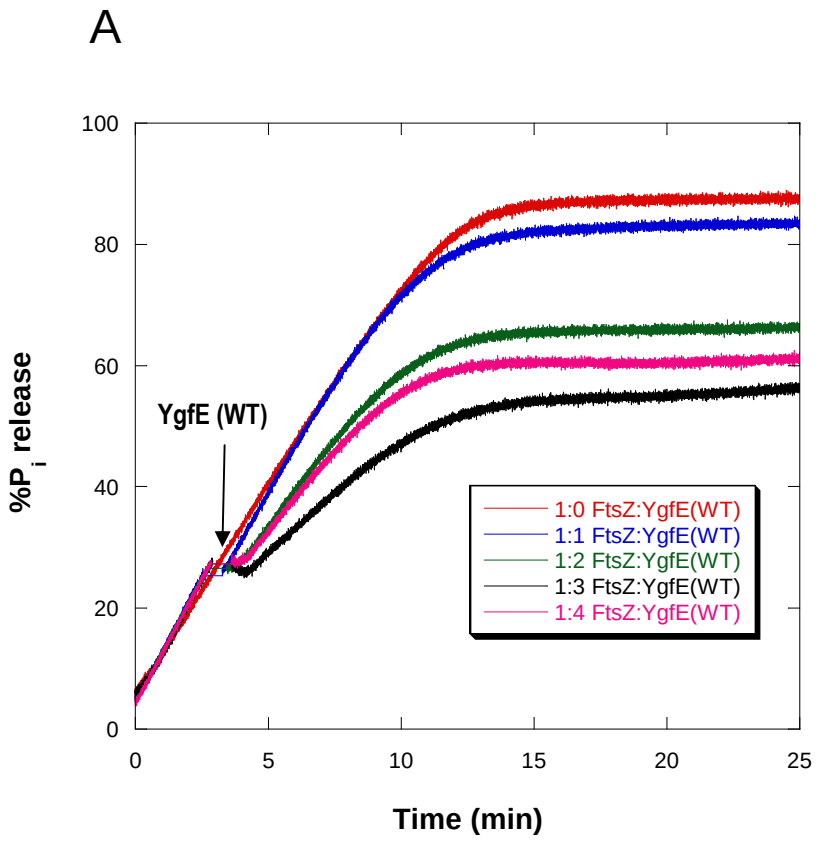
A
100
80
60
40
20
0
%P$_i$ release
YgfE (WT)
1:0 FtsZ:YgfE(WT)
1:1 FtsZ:YgfE(WT)
1:2 FtsZ:YgfE(WT)
1:3 FtsZ:YgfE(WT)
1:4 FtsZ:YgfE(WT)
0
5
10
15
20
25
Time (min)

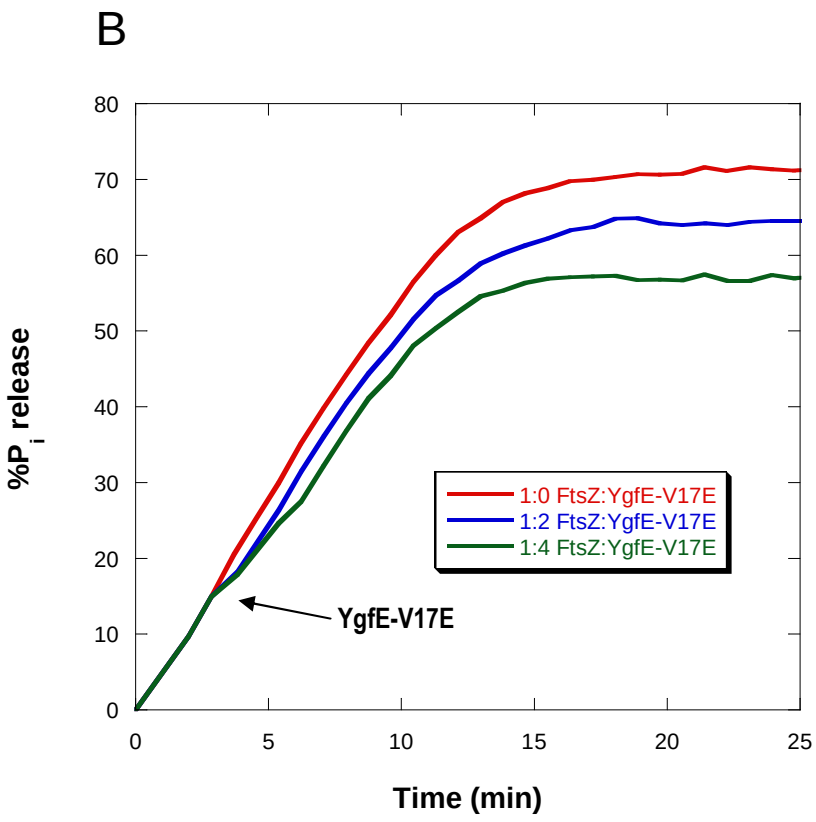
B
80
70
60
50
40
30
20
10
0
%P$_i$ release
1:0 FtsZ:YgfE-V17E
1:2 FtsZ:YgfE-V17E
1:4 FtsZ:YgfE-V17E
YgfE-V17E
0
5
10
15
20
25
Time (min)

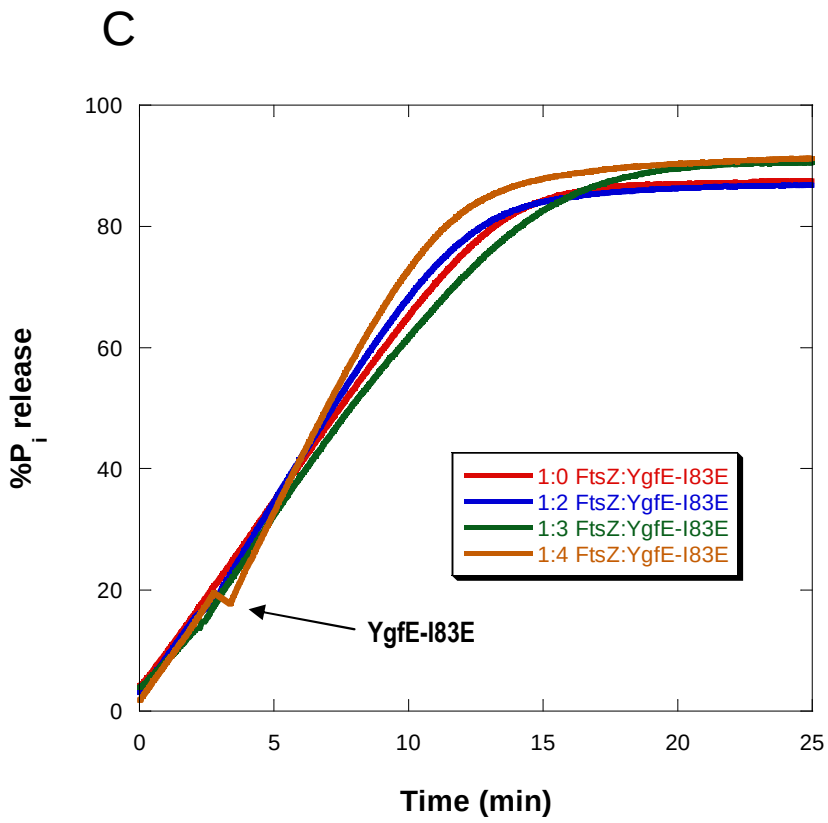

Figure 6.7.2 Effects of YgfE and YgfE mutants on FtsZ GTPase activity. FtsZ (11 μM in polymerization buffer) was mixed with GTP (0.2 mM) at time zero. Different types of YgfE at different concentrations (shown in graph) were added after protofilament formation (approximately 3 minutes). Experiments A, B and C were performed on Cary 1E double beam UV/Visible spectrophotometer, Jasco J-815 circular dichroism spectrometer and Jasco V-660 UV-Vis spectrophotometer respectively.

Again, we found that the ability of YgfE to inhibit FtsZ GTPase activity is related to its form in solution. Being a tetramer, wild type YgfE is the most potent inhibitor. The second place comes to the mutant YgfE-V17E, which exists presumably as a tetramer/ dimer equilibrium. As a dimer, however, the mutant YgfE-I83E can not inhibit FtsZ GTPase activity. These results confirm the right-angle light scattering and LD data in reverse. The YgfE which is capable of inducing FtsZ bundles and stabilising FtsZ polymers has the same ability to inhibit FtsZ GTPase activity.

6.8 The binding of YgfE-I83E to FtsZ protofilaments

6.8.1 Sedimentation assay

Using a sedimentation assay, we wanted to investigate whether the mutant YgfE-I83E can bind to FtsZ even though it does not induce FtsZ bundling, as concluded from light scattering. Through ultracentrifugation, the large polymers go down to the bottom, and can be separated to identify the proteins by SDS-PAGE.

A ratio of 1:2 for FtsZ and YgfE was chosen for the experiment, and control experiments with YgfE or FtsZ on their own were also performed. 800 µl reaction mixtures consisting of 22 µM of wild type YgfE, 22 µM of YgfE-I83E, 11 µM of FtsZ, 11 µM of FtsZ and 22 µM of wild type YgfE, 11 µM of FtsZ and 22 µM of YgfE-I83E were prepared respectively in the polymerization buffer of 50 mM of MES-KOH, pH 6.5, 10 mM of $MgCl_2$, and 50 mM of KCl. Immediately after addition of GTP (2.5 mM), the centrifugation was performed at 80,000 RPM, 20°C for 10 minutes. In order to retain FtsZ in polymeric form throughout, we added a large excess of GTP, instead of 0.2 mM as normal. After that, 80 µl of 50 mM Tris, pH 8, was used to resuspend each pellet. Samples from both supernatant and pellet were analysed by 15% SDS-PAGE.

The gel is shown in figure 6.8.1 labeled with supernatant (S) and pellet (P). When YgfE (either wild type or I83E) was mixed with GTP, there is no YgfE observed in the pellet (lanes 1 and 4), which means GTP can not bind to YgfE to form polymers. When FtsZ was mixed with GTP, FtsZ was observed in the pellet (lane 2P or lane 5P) indicates that FtsZ protofilaments were formed in the presence of GTP. Wild type YgfE helps to form FtsZ bundles, and both FtsZ and YgfE (lane 3P) can be seen in the pellet, when GTP was added into premixed FtsZ and YgfE. Similarly, we can find almost the same amount of both YgfE-I83E and FtsZ in the pellet (lane 6P) after the addition of GTP into premixed FtsZ and YgfE-I83E, which suggests that

the mutant YgfE-I83E did attached to FtsZ protofilaments, although it does not induce FtsZ bundling.

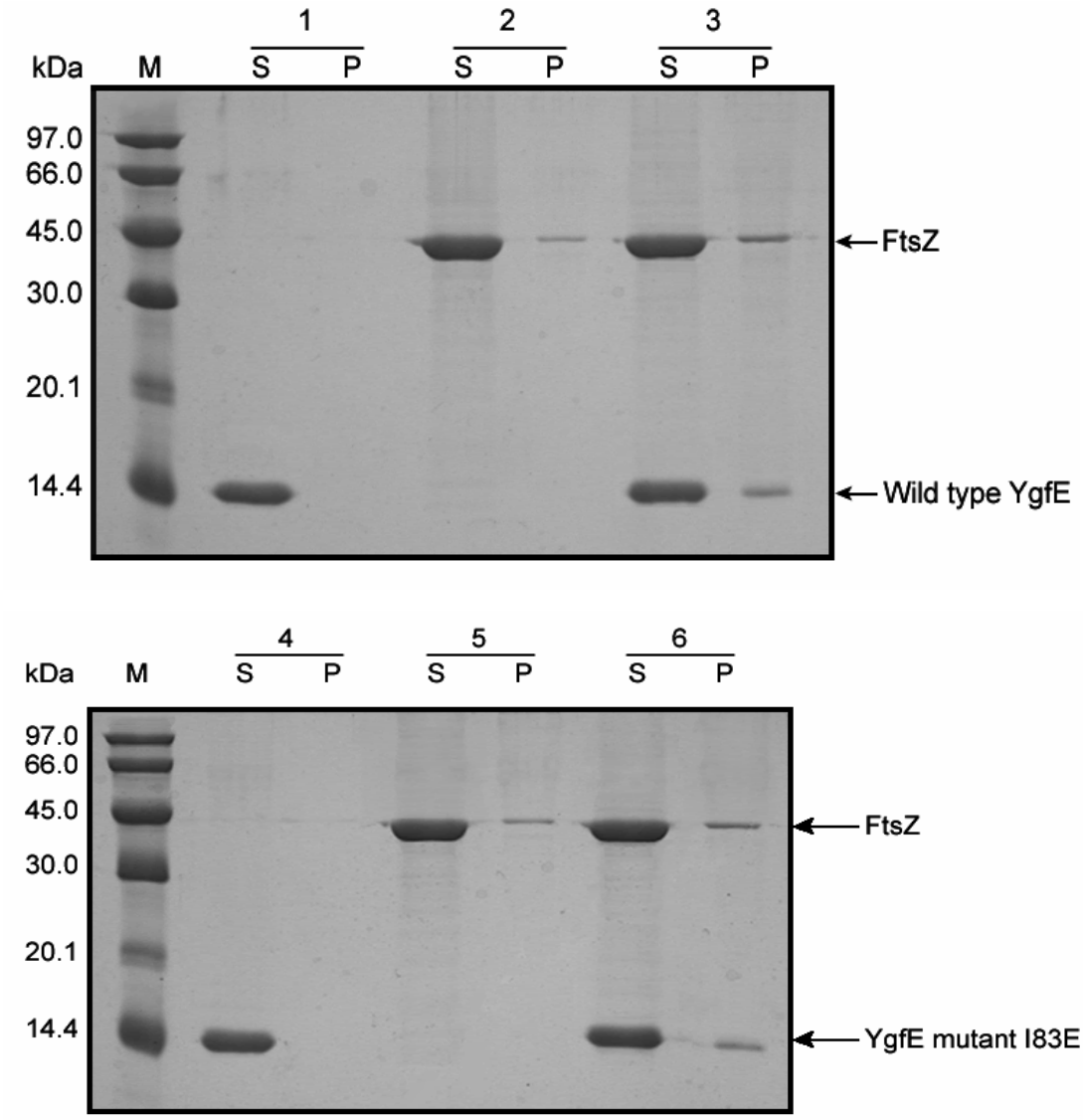

Figure 6.8.1 15% SDS-PAGE gel. M is marked for protein marker; S and P are marked for supernatant and pellet respectively. Where present, FtsZ and YgfE were at 11 μM and 22 μM in polymerization buffer (50 mM MES-KOH, pH 6.5, 10 mM $MgCl_2$ and 50 mM KCl). (1) wild type YgfE + GTP, (2) FtsZ + GTP, (3) FtsZ + wild type YgfE + GTP, (4) YgfE mutant I83E + GTP, (5) FtsZ + GTP, (6) FtsZ + YgfE mutant I83E + GTP.

6.8.2 Dynamic light scattering

The dynamic light scattering was used to determine sizes of particles present in solution of mixtures of YgfE-I83E and FtsZ protofilaments. The particle size was measured using the DLS instrument Zetasizer Nano S (Malvern).

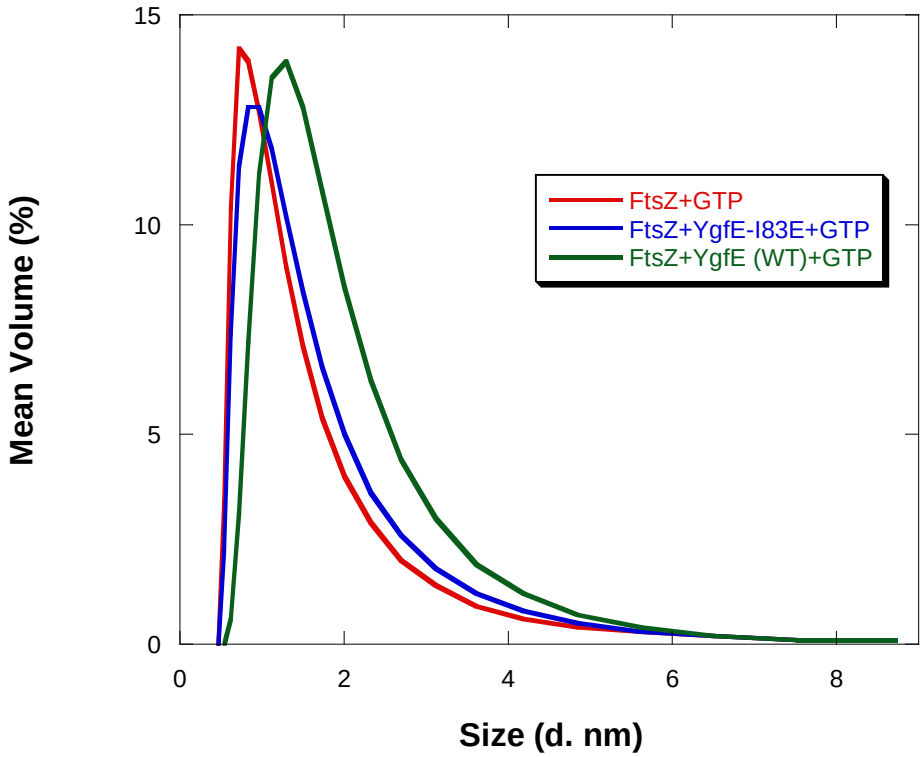

Figure 6.8.2 Volume particle size distributions obtained for different samples as indicated measured on a Nano S instrument using backscatter detection. 0.4 mM of GTP was added into the premixed solution to start the polymerization.

11 µM FtsZ and 44 µM of YgfE were premixed in the polymerization buffer consisting of 50 mM MES-KOH, pH 6.5, 10 mM $MgCl_2$ and 50 mM KCl. GTP to a final concentration of 0.4 mM, instead of 0.2 mM as normal, was added to start the polymerization, which prolongs the steady state time of FtsZ polymerization. Immediately after the addition of GTP, the solution was transferred to the

DTS2145-low volume glass cuvette, and the DLS was observed at a 173° scattering angle.

The volume particle size distributions obtained from DLS are shown in figure 6.8.2. FtsZ protofilmants gave a peak around 1 nm diameter, whereas the peak changed significantly to around 2 nm in the presence of wild type YgfE, which revealed that wild type YgfE enhanced the polymerization of FtsZ. When GTP was added into the premixed solution containing FtsZ and the mutant YgfE-I83E, the DLS peak was shifted right a little bit. These data suggested that FtsZ bundles like those induced by wild type YgfE were not formed upon addition of YgfE-I83E. However, YgfE-I83E did cause the DLS peak to shift slightly, suggesting it binds to FtsZ protofilaments. Thus the results are in agreement with the previous sedimentation assay, although the maxima in the peak size distribution do not necessarily correspond to the precise values of the actual diameter of each species, because the FtsZ polymers are long fibres rather than spheres.

6.8.3 Probing whether YgfE-I83E blocks FtsZ bundling by wild- type YgfE

Right-angle light scattering was continued to use to prove that the mutant YgfE-I83E is able to bind to FtsZ protofilments. 11 μM FtsZ and 44 μM of YgfE-I83E were premixed in the polymerization buffer consisting of 50 mM MES-KOH, pH 6.5, 10 mM $MgCl_2$ and 50 mM KCl. After baseline collection of approximately 5 minutes, GTP to a final concentration of 0.2 mM was added to initiate the polymerization, followed by the addition of 44 μM of wild type YgfE during the steady-state phase of the FtsZ polymerization, at approximately 3 minutes after the GTP addition.

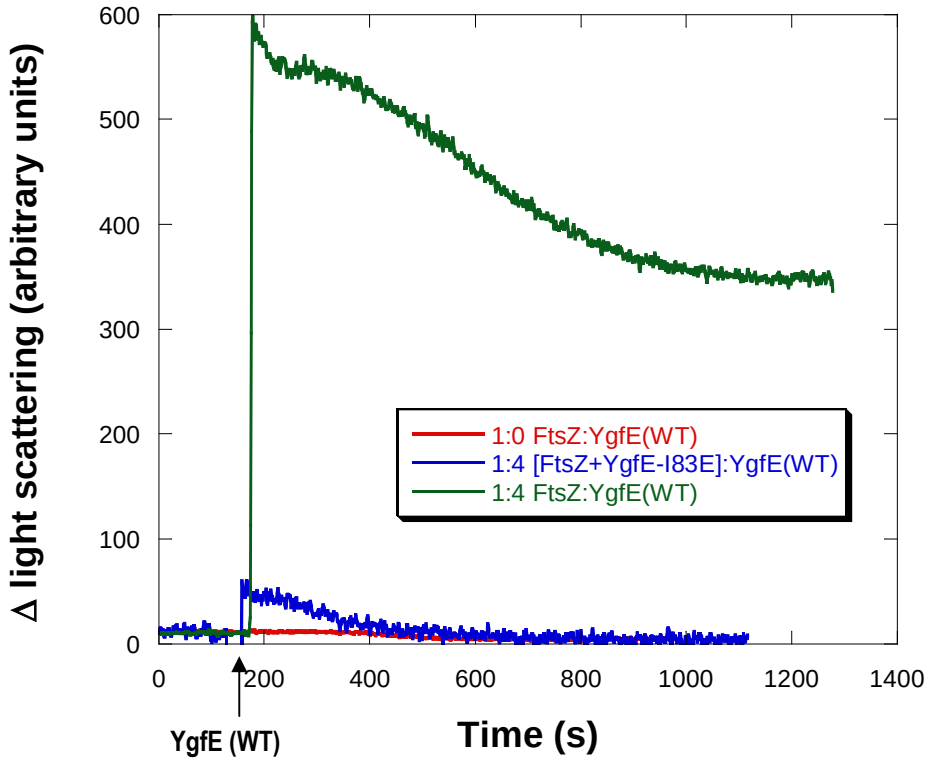

Figure 6.8.3 The block of FtsZ bundling by YgfE-I83E proved by right-angle light scattering. 11 μM of FtsZ and 44 μM of YgfE-I83E were premixed in the polymerization buffer, 44μM of wild type YgfE were added after FtsZ protofilament formation (approximately 3 minutes after 0.2 mM GTP addition at time zero). FtsZ polymerization on its own and adding wild type YgfE into FtsZ protofilaments containing no YgfE-I83E were also shown for comparison. Excitation and emission wavelengths were set at 550 nm.

Figure 6.8.3 shows the light scattering data obtained. After adding GTP into premixed FtsZ and YgfE-I83E, theres is a slight increase in the light scattering, which was identical to that by adding GTP into FtsZ alone, indicating only FtsZ protofilaments were formed. After that, wild type YgfE was added into FtsZ protofilaments containing YgfE-I83E, and a small increase in the light scattering (approximately 50 units) was observed, compared with the increase of 550 units that

was induced by adding wild type YgfE into FtsZ protofilaments on its own. Furthermore, this small increase in the light scattering rapidly decreased to zero within 4 minutes. The light scattering suggested that the wild type YgfE loses the abilty to induce FtsZ bundling in the presence of YgfE-I83E. This is presumably because YgfE-I83E binds to FtsZ protofilments and occupying the YgfE binding sites, therefore wild type YgfE is incapable of binding to FtsZ protofilments and thus induces the bundling.

6.9 Conclusions

In this chapter, we have investigated two kinds of YgfE mutants: YgfE-V17E and YgfE-I83E. Different YgfE mutants have different effects on FtsZ bundling. Through right-angle light scattering, LD, EM, and GTPase assays, we have found that wild type YgfE has the strongest effect, and we suspect this relates to its propensity to form tetramers. YgfE-I83E seems to be unable to induce FtsZ bundling, as it is preferentially a dimer with no evidence of tetramer formation in the AUC data. YgfE-V17E has an effect intermediate between the other two, consistent with it adopting both dimer and tetramer species in solution.

Although YgfE-I83E can not stimulate FtsZ assembly into bundles of protofilaments, YgfE-I83E does bind to FtsZ when present. It also blocks the bundling of FtsZ by wild type YgfE perhaps by taking up the entire binding site, so that no position is left for the wild type YgfE. Besides, YgfE-I83E doesn’t affect the GTPase activity of FtsZ, which means the reduction in GTPase activity is related to the formation of bundles instead of only YgfE binding. As for YgfE-V17E, we consider the ability of inducing FtsZ bundling depends on how many percentages of tetramers in V17E behaved. Therefore we suppose the ability of YgfE to promote the bundling of protofilaments could be the consequence of the bridging of FtsZ monomers between adjacent protofilaments. A model for the function of YgfE will be discussed in the conclusion chapter.

CHAPTER 7 -- CONTINUOUS CHANNEL FLOW LINEAR DICHROISM

7.1 Introduction

Linear dichroism (LD) is a differential polarised absorption spectroscopy technique in which molecules in a sample are oriented and then the difference in absorption of light polarised in orthogonal directions (one of which is the orientation direction) is determined. Thus it is the ideal technique for studying classes of long biomacromolecules for which it is intrinsically difficult to gain structural information using more commonly available structural characterisation techniques such as NMR and X-ray diffraction.

Different methods of LD sample presentation exist for different types of sample, for example stretched film for small molecules, flow orientation, squeezed gel and electric field orientation for larger molecules. For solution phase samples Couette flow orientation is most commonly used for the study of long biological macromolecules (§ 3.1.3).

In the chapter 5 and chapter 6, we have employed Couette flow LD to study the dynamics of FtsZ polymerization. However, the study of such time dependent interactions including enzyme kinetics, fiber assembly, or protein insertion into membranes, is limited by the time required to assemble and fill the cell. For currently available cells this process commonly takes about one minute, meaning that the first minute of any reaction cannot be easily measured using LD. Therefore we have developed a continuous channel flow-LD technique with the ability to record the very first seconds of the reactions including FtsZ polymerization.

7.2 Objectives

In order to improve the LD system for recording fast kinetics, we have designed a continuous channel flow-LD, based on a stopped-flow system. In the development process, three different flow cells were employed. The first one is an FC-20 open cuvette (BioLogic), the second is µ-Slide III$^{3\ in\ 1}$ channel slide (ibidi), and the last one is a custom-made channel slide with quartz window (kindly provided by Max Joseph, MOAC Doctoral Traning Center and the School of Engineering, the University of Warwick). The utility of the devices have been tested by measuring the alignment of known DNA, DNA-ligand systems, and the kinetics of DNA exonuclease I digestion of ct-DNA. The cell with the best performance was then used to study the FtsZ polymerization reaction.

7.3 Continuous channel flow–LD system based on SFM-300 stopped-flow device

The continous channel flow-LD has been developed based on the stopped-flow system. Stopped-flow is a frequently used technique for the study of the rapid chemical kinetics of a reaction in solution. Existing stopped flow systems are generally based on a configuration that uses a drive motor or air pressure to rapidly fire two solutions contained in separate drive syringes, together into a mixing device. The mixture then flows into the observation cell. Measurements are made once the sample enters the cell, an event that is triggered by the sample filling the stop syringe, a third syringe that is inline with the cell, and the plunger hitting a block, causing the flow to be stopped instantaneously. The reaction in the observation cell is monitored using a suitable spectroscopic method, such as absorbance, fluorescence or circular dichroism, and the change in the spectroscopic signal as a function of time is recorded.

However, the conventional stopped-flow system cannot be used to detect a linear dichroism signal, as it does not align the sample when measuring. In order to flow

the sample during measurement, an open flow cell was employed instead of using the cuvette cell blocked with a stop syringe. In the continuous channel flow-LD experiments, the sample is introduced into the cell still using the twin drive syringes and mixer arrangement, but with the drive system configured to deliver a known amount through the open flow cell, and then directly flow out as a waste. In the open cuvette cell where the LD signal is detected, the sample is being continuously flowed and aligned with the flow.

7.3.1 Instrument setup

The primary continuous channel flow-LD experiments were performed on a Bio-Logic MOS-450 spectrometer that is adapted for LD spectroscopy, to which a SFM-300 stopped-flow device is attached. This stopped-flow device is designed for both stopped-flow and continuous-flow experiments, whose configuration are shown in figure 7.3.1.1. In this configuration, two or three solutions can be mixed and injected into the cuvette. The stop syringe present in most conventional stopped-flow systems is absent, due to the movements of the syringes are completely controlled by the microprocessor. Thus this equipment is suitable for either stopped-flow or continuous-flow experiments.

In our study, the SFM-300 stopped-flow device was employed as a continuous channel flow-LD system without stopping the flow during measurement. In the FC-20 open-ended cuvette (figure 7.3.1.2), the sample is continuously flowed past the observation window, and gets aligned with the flow, which then gives the corresponding LD signal.

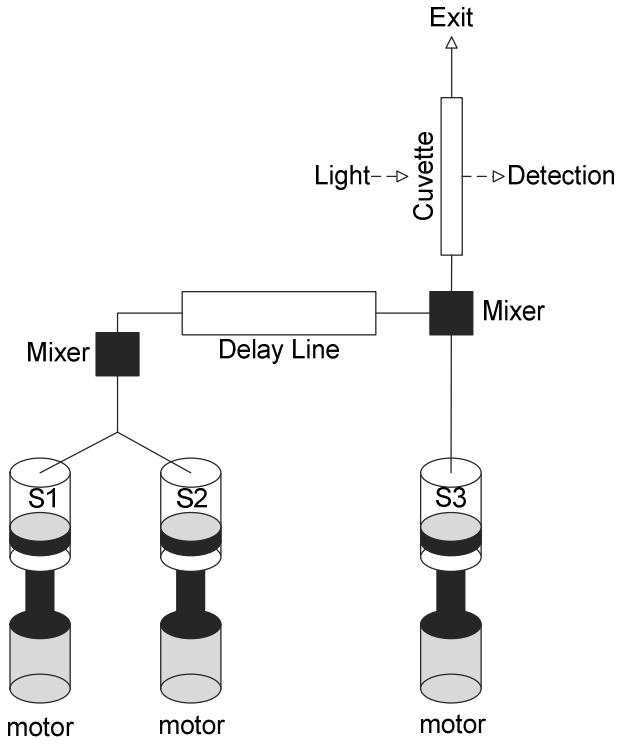

Figure 7.3.1.1 Configuration of the SFM-300 stopped-flow device. For the continuous channel flow-LD experiments, two or three solutions were mixed and injected into the cuvette without stopping the flow during measurement.

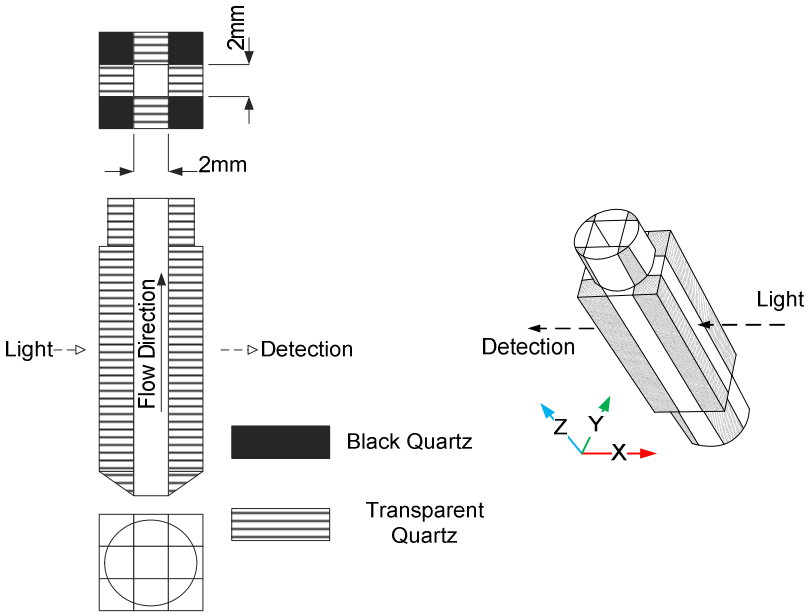

Figure 7.3.1.2 The schematic diagram of the FC-20 cuvette that is inserted into the SFM-300 stopped-flow device, where the xy-plane is horizontal and the z-axis points up.

7.3.2 Orientation of ct-DNA

In order to test the performance of this instrument, ct-DNA, a sample with a well defined LD spectrum (figure 7.3.2.1), was chosen.

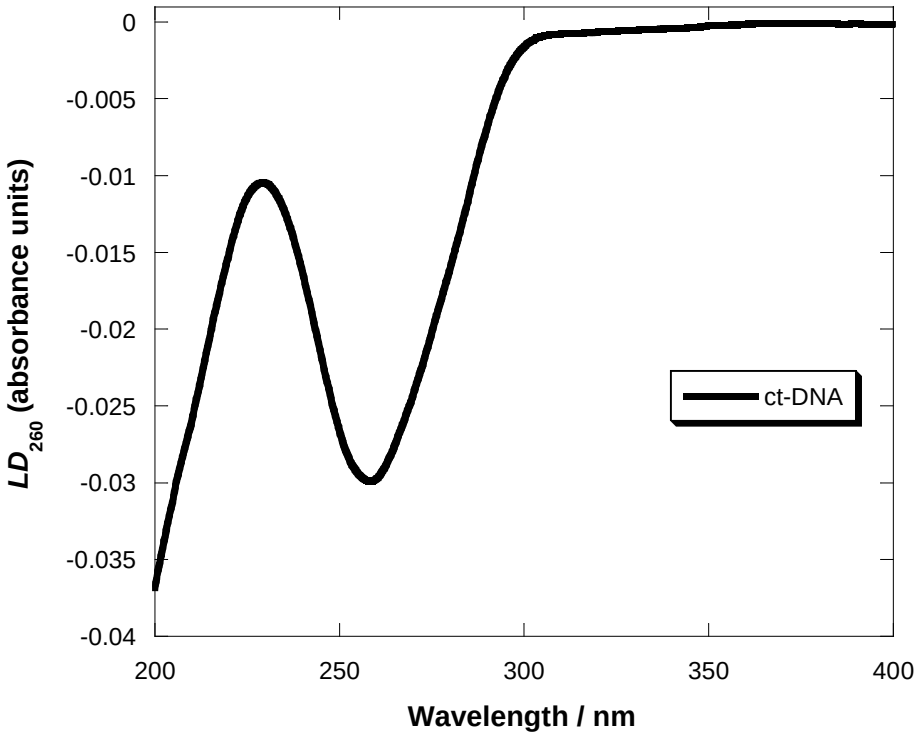

Figure 7.3.2.1 Normal Couette flow LD spectrum of ct-DNA (250 mM) in a capillary collected with a Jasco J-815 spectropolarimeter.

DNA is normally double stranded macromolecule, in which two polynucleotide chains are held together by weak thermodynamic forces. In the most common form of DNA (B-DNA), the double helix twists in a right-hand direction, and the conjugated π bonds of nucleotide bases (aromatic molecules) align perpendicular to the helix axis (Rodger 2008). In the normal Couette flow LD (§ 3.1.3), the orientation axis of DNA molecules, the helix axis, is parallel to the light beam. As the π-π transitions of the aromatic bases are all polarised within the plane of the

bases, whose absorbance is perpendicular to the helix axis and the light beam, we expect the LD spectrum to show a negative maximum at around 260 nm, which is very similar to an upside-down DNA absorbance spectrum as shown in figure 7.3.2.1. In some continuous channel flow experiments, where the geometry is inverted, we would expect to see a positive signal.

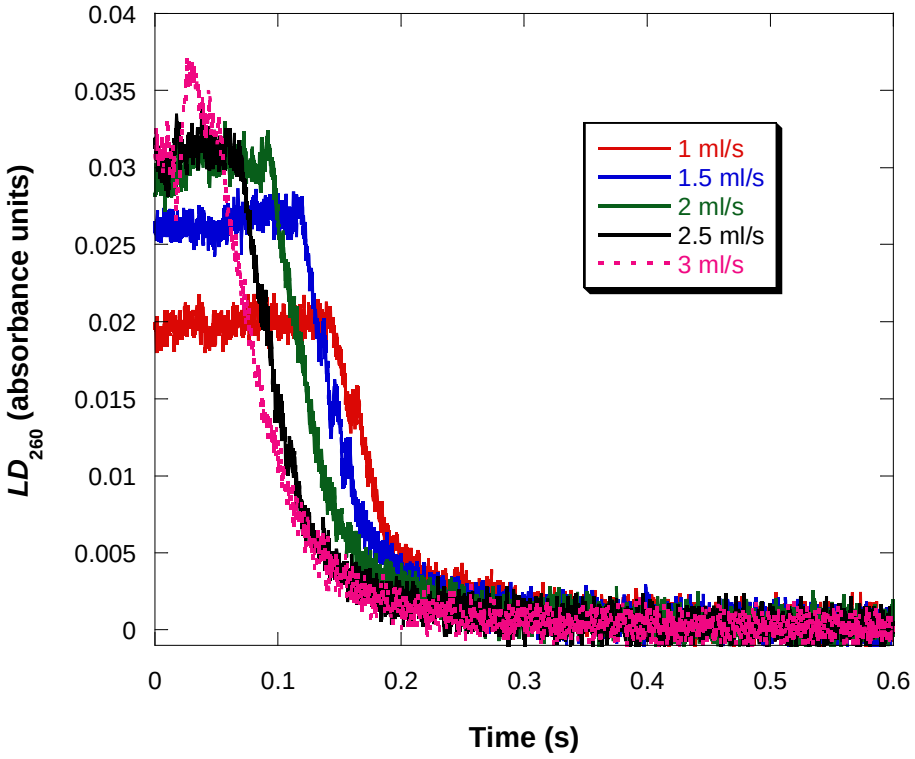

Figure 7.3.2.2 Continuous channel flow LD_{260} at different flow rates. 239 ul of 2.5 mM ct-DNA was injected to FC-20 cuvette using SFM-300 stopped-flow device.

To do the continuous channel flow-LD, all the syringes of the SFM were filled. A disposable plastic syringe containing 2 ml of 2.5 mM ct-DNA was attached to the syringe reservoir port. The SFM syringe was driven up and down several times to eliminate any bubbles in the SFM syringe and then the reservoir was filled. Each time, 239 µl of ct-DNA was injected at a flow rate ranging from 1 ml/s to 3.5 ml/s.

The LD signal at 260 nm was recorded under the transient recorder mode as shown in figure 7.3.2.2.

As shown in figure 7.3.2.2, ct-DNA shows a significant positive LD signal at 260 nm under the flow. The sign is positive as the DNA helix axis is perpendicular to the light beam under the continuous channel flow (figure 7.3.1.2), so the bases and their π-π^* transitions are parallel to the flow direction. After about 0.1 s of the steady state of LD, the signal decreased to zero due to the flow stopping. The slowest flow rate of 1 ml/s maintained the steady state LD signal the longest because it gave the longest flow time. The LD of ct-DNA is also related to the shear rate. The LD magnitude gradually increased from 0.02 to 0.03 units when the flow rate was increased from 1 ml/s to 2 ml/s. However, there was no further increase in the LD of ct-DNA when the flow rate was faster than 2 ml/s, and the signal even became noisier up to 3 ml/s. We think the phenomenon happened due to the onset of turbulence at high flow rates. In order to reduce turbulent flow a thin chip-based channel slide was employed as described in the following section. In addition, the thin flow chip enabled a higher shear rate so that both flow rate and sample concentration can be reduced, and less sample is required.

7.4 Continuous channel flow–LD system based on a μ-Slide III$^{3\ in\ 1}$ channel slide (ibidi)

A μ-Slide III $^{3\ in\ 1}$ flow kit, which contains the μ-Slide III$^{3\ in\ 1}$ channel slide that merges 3 separated liquids into one channel in a laminar flow, as well as the connectors and tubings, was purchased from ibidi (http://www.ibidi.de/products/disposables/S_8031X_SlideIII_3in1.html). A schematic diagram of the kit is shown in figure 7.4. The size of the tubing was not provided by the supplier. We measured an 18 cm of tubing and found it can be filled with 378.2 μl of water at room temperature. In the experiments, the spare inlet connections were blocked when not necessary.

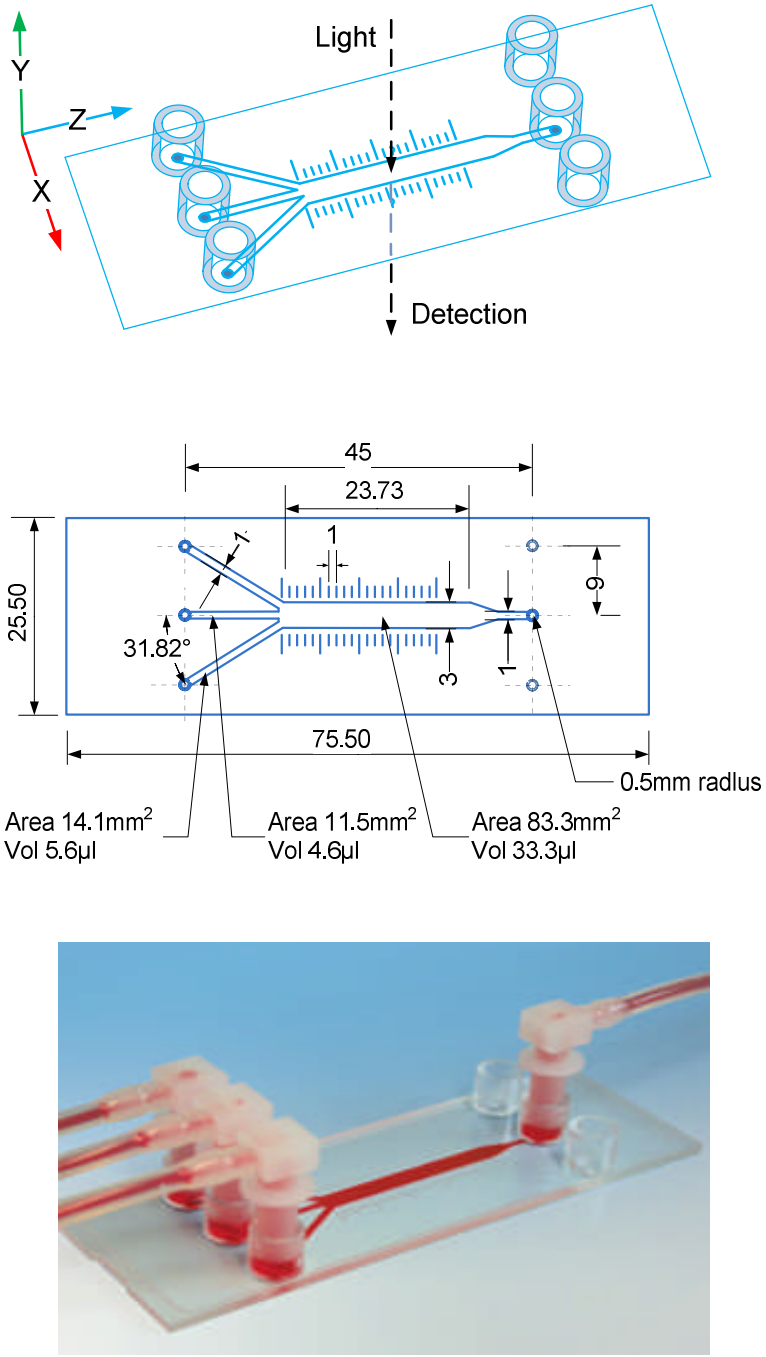

Figure 7.4 Schematic diagram of µ-Slide III$^{3\text{ in }1}$ channel slide, where the xy-plane is horizontal and the z-axis points up.

The principle of measurement is similar to that described in the above section. In order to get a continuous flow, the µ-Slide III$^{3\text{ in }1}$ flow cell was connected to a

disposable plastic syringe *via* tubing, and a syringe pump (Cole-Parmer®) was employed to push the sample in instead of using the commercial stopped-flow device. This pump accommodates dual syringes, and delivers a fixed amount of sample at a fixed flow rate under the "infuse only" mode. For observation, the flow cell was placed vertically in between the light and the detector of the Bio-Logic MOS-450 spectrometer that is adapted for LD spectroscopy (figure 7.4), so that the flow direction was perpendicular to the light beam.

Because the μ-Slide III$^{3\ in\ 1}$ channel slide was made of hydrophobic, uncoated plastic, it only gives a high degree of transparency at wavelengths higher than 300 nm. The performance was then tested by two DNA-ligand systems, both of which can give LD signals in the detection range.

7.4.1 DNA-ethidium bromide system

Ethidium bromide (EB) is a planar aromatic molecule that is often used as a DNA stain. The molecules intercalate (sandwich) between the DNA base pairs when bound to DNA. EB transitions are then oriented perpendicular to the DNA helix axis and so give the same sign of LD signals as DNA bases does. Figure 7.4.1.1 shows a normal Couette flow LD spectrum of DNA plus ethidium bromide collected with a Jasco J-715 spectropolarimeter (Dicko et al. 2008, Marrington et al. 2004a). The longest wavelength band of ethidium bromide when bound to DNA occurs at 516 nm; however, the maximum of the ethidium bromide band appears as long wavelength shoulder on the 260 nm DNA band.

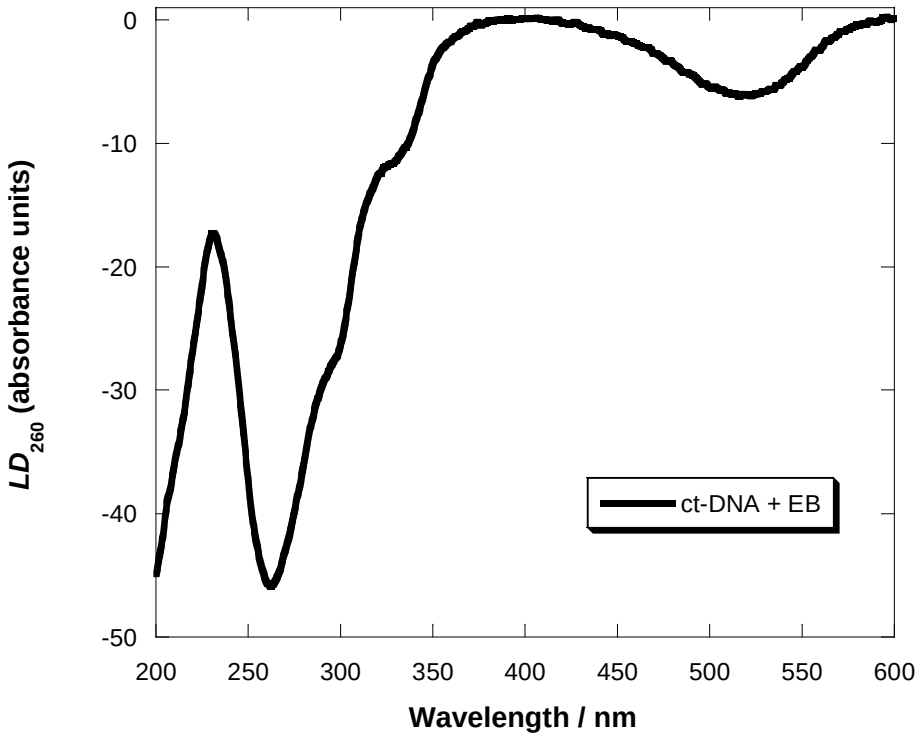

Figure 7.4.1.1 Normal Couette flow LD spectrum of ct-DNA (250 mM) plus ethidium bromide (EB, 25 mM) in a capillary collected with a Jasco J-715 spectropolarimeter.

To probe the full wavelength range that we anticipated would be usable from the μ-Slide III$^{3\ in\ 1}$ channel slide, the continuous flow-LD of ct-DNA plus ethidium bromide was measured from 300 nm to 600 nm, as the μ-Slide III$^{3\ in\ 1}$ channel slide only transmits wavelengths higher than 300 nm. 150 μl of a solution containing ct-DNA (250 μM) and ethidium bromide (25 μM) were injected at the flow rate of 500 μl/s, and the continuous flow-LD at different wavelengths from 300 nm to 600 nm are shown in figure 7.4.1.2.

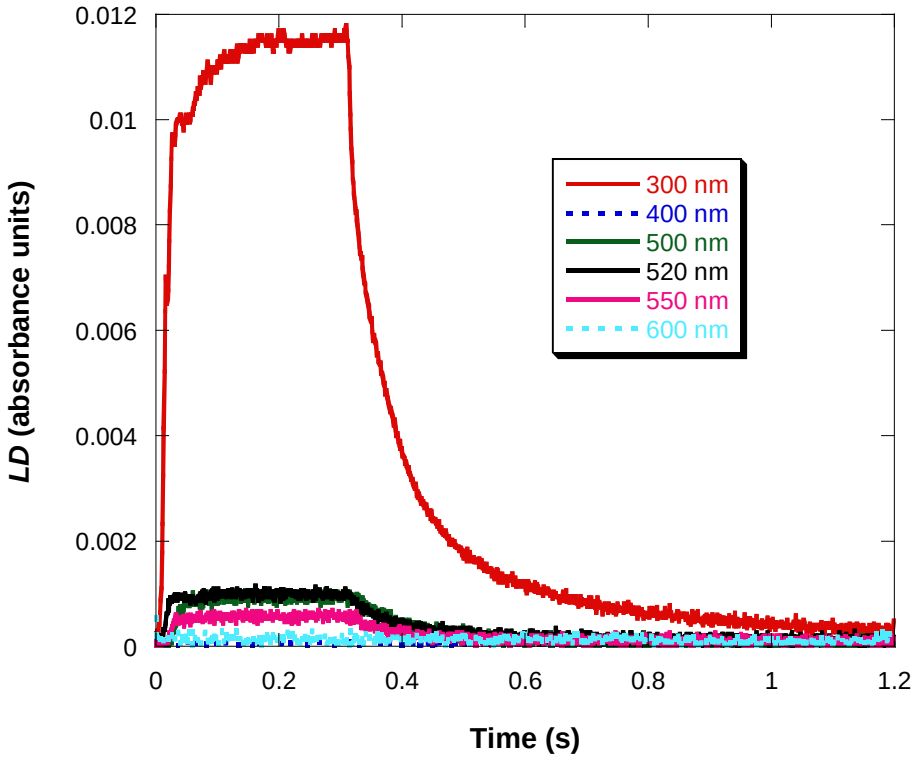

Figure 7.4.1.2 Continuous channel flow LD of a solution containing ct-DNA (250 μM) and ethidium bromide (25 μM) measured at different wavelengths. 150 μl of the solution was injected into the μ-Slide III$^{3\text{ in }1}$ channel slide at 500 μl/s flow rate at each wavelength.

Figure 7.4.1.2 shows the positive LD of ethidium bromide (due to the flow direction in the μ-Slide III$^{3\text{ in }1}$ channel slide being perpendicular to the polarization light beam, as is the DNA helix axis). The biggest LD of ethidium bromide when bound to DNA was measured at 300 nm, a small longer wavelength band occured from 500 to 550 nm, and no LD signal was observed at either 400 nm or 600 nm. These results agree with the LD spectrum of ct-DNA plus ethidium bromide measured in a microvolume Couette flow cell (figure 7.4.1.1).

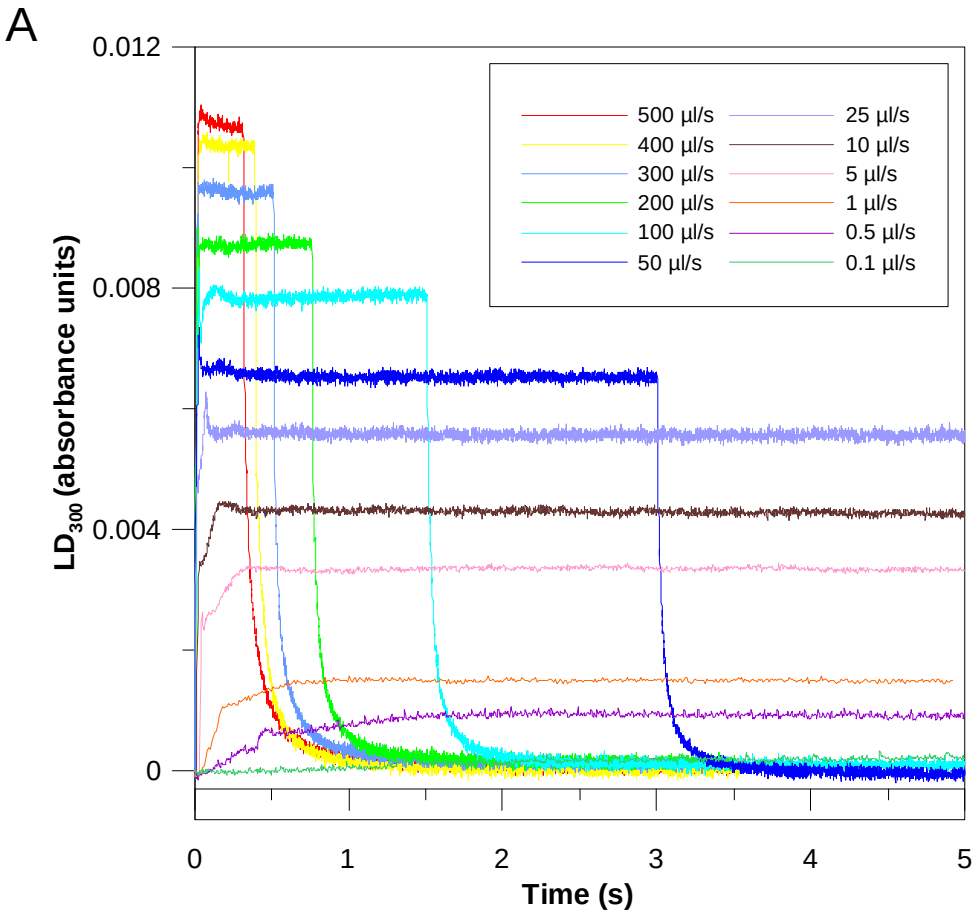

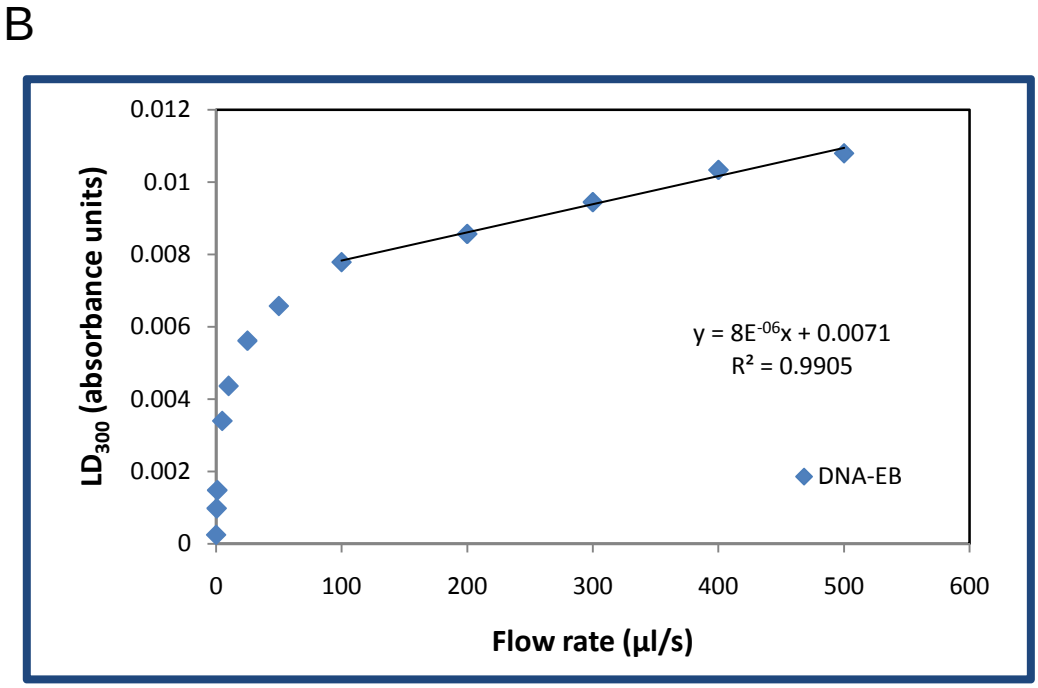

Figure 7.4.1.3 Continuous channel flow LD of a solution containing ct-DNA (250 µM) and ethidium bromide (25 µM) measured at 300 nm at different flow rate. 150 µl of the solution was injected into the µ-Slide III$^{3\text{ in }1}$ channel slide each time.

The relationship between LD and shear rate using the μ-Slide III$^{3\text{ in }1}$ channel slide was then studied. A solution containing 150 μl ct-DNA (250 μM) and ethidium bromide (25 μM) was injected at different flow rates, and data were collected at 300 nm. The magnitude of LD depends not only on concentration of the sample but also how fast the solution is flowing, because the faster speed will flow the molecules in better order, as long as the flow remains laminar. As shown in figure 7.4.1.3A, the LD of the DNA-ethidium bromide system dramatically decreased with the decline of flow rate. When the flow rate was 500 μl/s (the biggest rate provided by the syringe pump), the LD at 300 nm reached approximately 0.011 units; while the LD decreased to almost zero when the flow rate was as slow as 0.1 μl/s. When the LD of the steady state phase is plotted against flow rate, there is a good linear relationship, (in which the coefficient of determination R^2 equals to 0.9905) between LD and flow rate, when the flow rate is from 100 μl/s to 500 μl/s (figure 7.4.1.3B).

7.4.2 DNA-DAPI system

In addition to the DNA-ethidium bromide system, another DNA binding ligand system 4',6-diamidino-2-phenylindole (DAPI) was also employed to test the performance of the μ-Slide III$^{3\text{ in }1}$ channel slide. DAPI is a DNA groove binder, and the long axis of DAPI lies along the DNA minor groove making an angle of about 45° to the helix axis. Thus, its long axis polarized transition at 350 nm has an opposite LD signal from the DNA as show in figure 7.4.2.1 (Dicko et al. 2008, Marrington et al. 2004a).

The continuous flow LD of ct-DNA plus DAPI was then determined in the μ-Slide III$^{3\text{ in }1}$ channel slide at 350 nm. As the flow direction is perpendicular to the light beam in this experiment, we would expect a negative LD of DAPI at 350 nm.

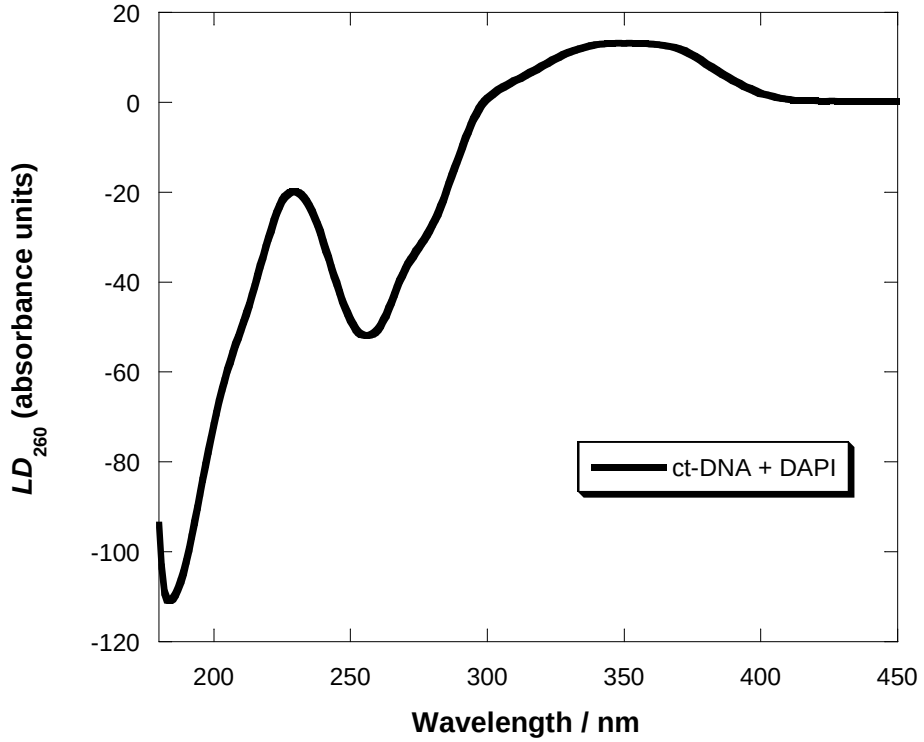

Figure 7.4.2.1 Normal Couette flow LD spectrum of ct-DNA (200 mM) plus DAPI (30 mM) in a capillary collected with a Jasco J-815 spectropolarimeter.

The 150 μl solution containing 50 μM of ct-DNA and 7.5 μM of DAPI was injected into the channel slide at different flow rates ranging from 100 μl/s to 500 μl/s. As illustrated in figure 7.4.2.2A, DAPI gave the expected negative LD signal, and the intensity decreased from approximately 0.008 to 0.0045 units with the decline of the flow rate. Also, LD and flow rate show a good linear relationship, in which the coefficient of determination R^2 equals to 0.996, when the flow rate is between 100 μl/s and 500 μl/s (figure 7.4.2.2B).

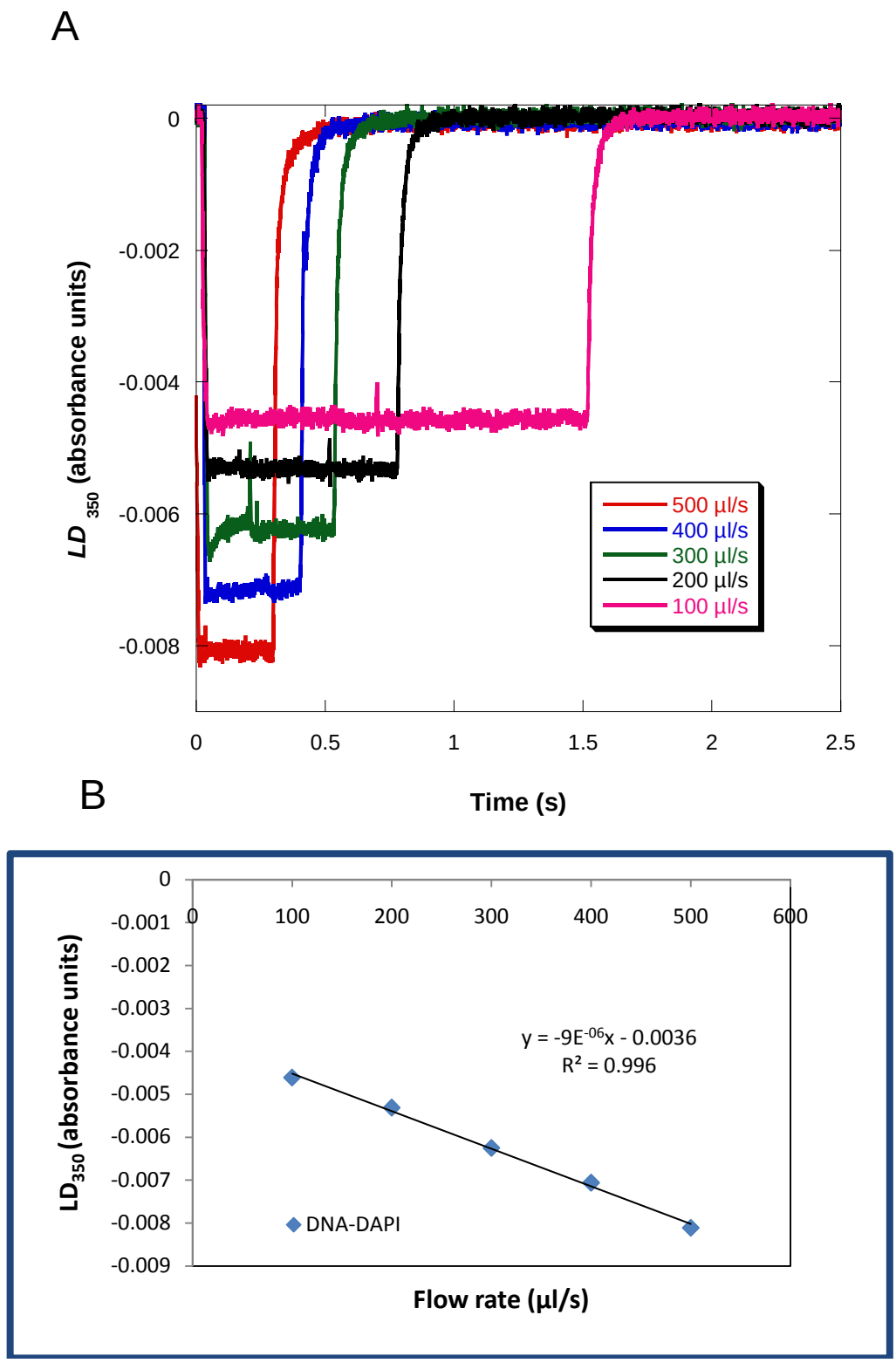

Figure 7.4.2.2 Continuous channel flow LD of a solution containing ct-DNA (50 µM) and DAPI (7.5 µM) measured at 350 nm at different flow rates. 150 µl of the solution was injected into the µ-Slide III$^{3\text{ in }1}$ channel slide each time.

In conclusion, the µ-Slide III$^{3\ in\ 1}$ channel slide shows a good performance for measuring continuous channel flow-LD of the orientation of DNA-ligand systems. However, due to the low transparency in the wavelength range lower than 300 nm, which is the important region for both DNA and proteins, the application of the µ-Slide III$^{3\ in\ 1}$ channel slide is very limited.

7.5 Continuous channel flow–LD system based on a custom-made channel slide with quartz window

In order to break the 300 nm limit for continuous channel flow–LD measurements, a custom-made one channel slide with quartz window was chosen to use. For the mixing of two solutions, a T-mixer was attached *via* tubing, in exacyly the same manner as that in the µ-Slide III $^{3\ in\ 1}$ flow kit. Figure 7.5 shows the pictures of the custom-made flow cell and a T-mixer.

A

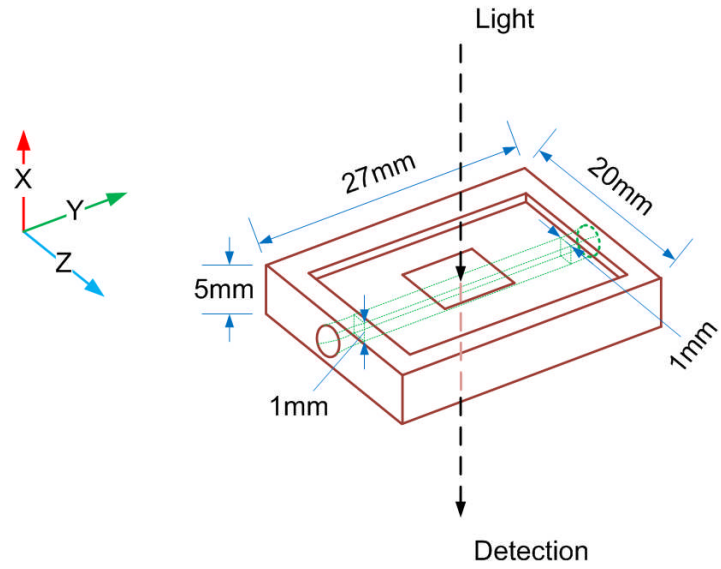

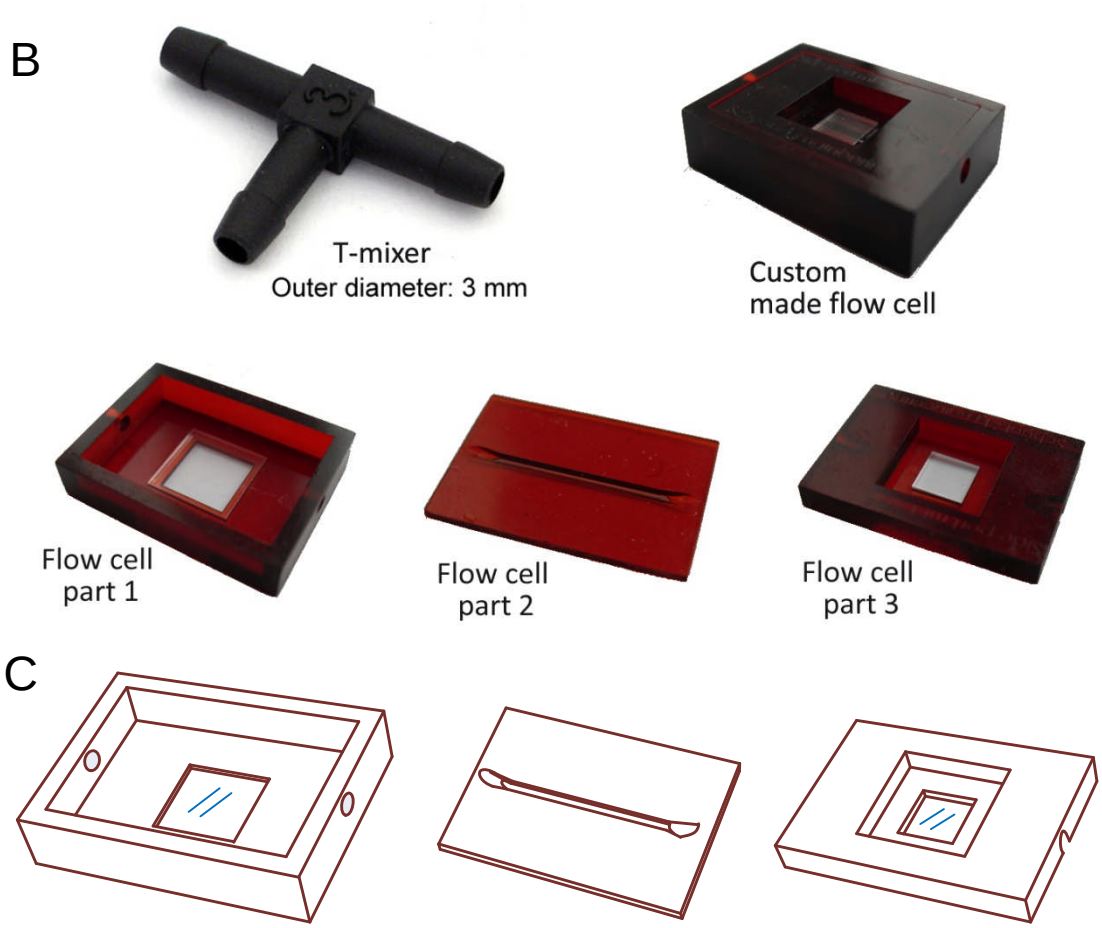

Figure 7.5 Pictures of the T-mixer and the custom-made one-channel slide attached with two quartz windows. The flow cell was assembled from three parts. Their schematic diagrams are shown on the top and bottom respectively, where the xy-plane is horizontal and the z-axis points up.

7.5.1 Orientation of ct-DNA

The orientation of ct-DNA on its own by continuous channel flow-LD was first measured at 260 nm without the T-mixer. 100 µl of ct-DNA (250 µM) was injected into the custom-made flow cell at different flow rates from 2 ml/min to 6 ml/min.

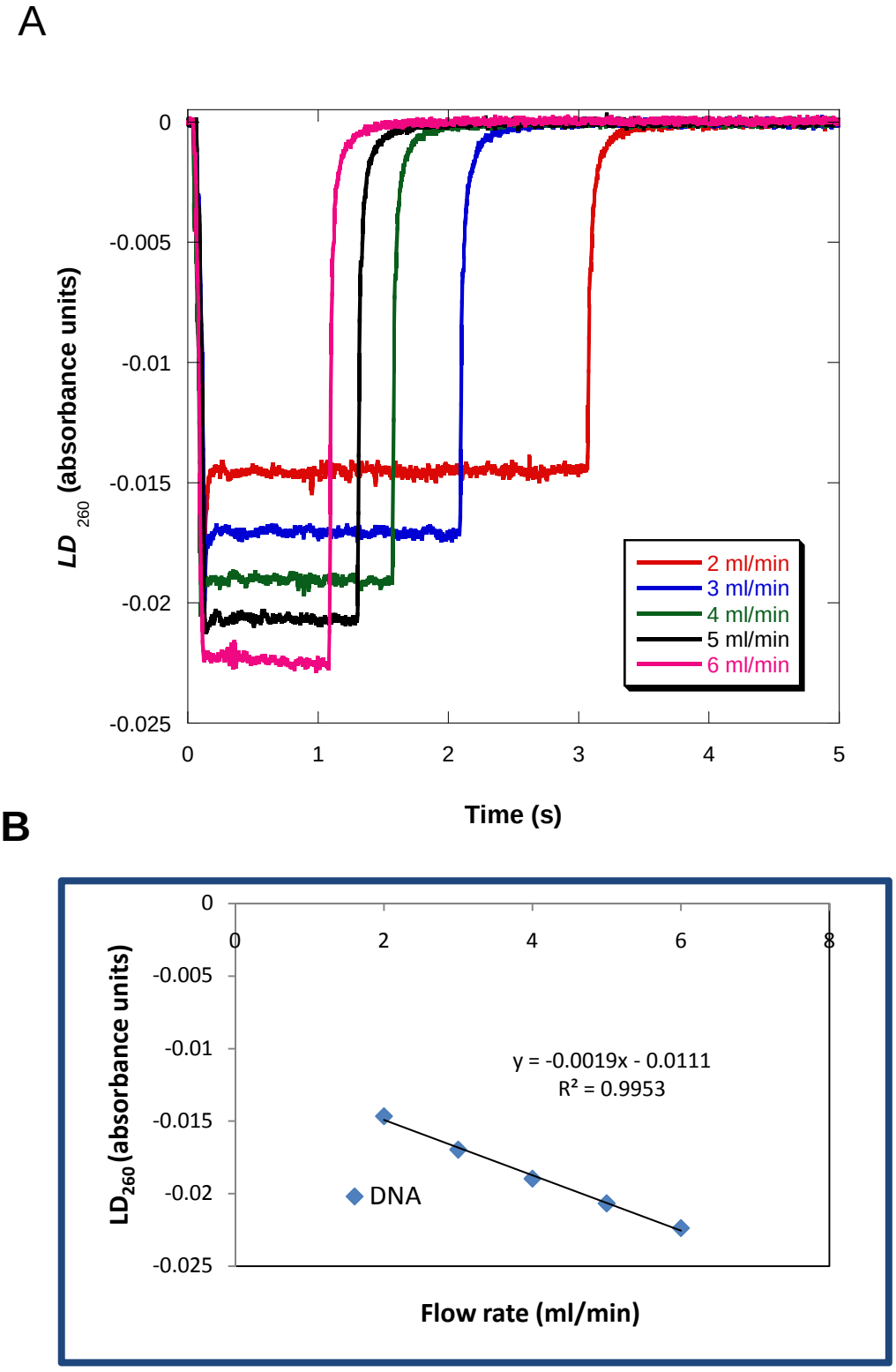

Figure 7.5.1.1 Continuous channel flow LD of ct-DNA (250 μM) measured at 260 nm at different flow rates from 2 ml/min to 6 ml/min. 100 μl of the solution was injected into into the custom-made flow cell each time.

As illustrated in figure 7.5.1.1A, ct-DNA shows a negative LD signal at 260 nm, due to the DNA helix axis being parallel to the light beam under the flow in this system (figure 7.5). As with the DNA-ethidium bromide in the μ-Slide III$^{3\ in\ 1}$ channel slide (figure 7.4.1.3), the ct-DNA in the custom-made flow cell also shows a dramtic decrease in LD with decline of flow rate. The linear relationship between LD and flow rate when the flow rate is between 2 ml/min and 6 ml/min is shown in figure 7.5.1.1B.

In addition to the possibility of measuring LD in the UV region, which can not be achieved with the μ-Slide III$^{3\ in\ 1}$ channel slide, the custom-made flow cell also shows a better behavior in flowing than the FC-20 open cuvette thanks to the reduction in the cross-sectional area of the channel from 4 mm^2 to 1 mm^2. The LD signal reached 0.02 units when 2.5 mM of ct-DNA flowed at 1 ml/s through the FC-20 open cuvette, whereas the same magnitude was achieved when 250 μM of the sample flowed at 5 ml/min (0.083 ml/s) through the custom-made flow channel. Both concentration and flow rate were reduced approximately by a factor of 10, which also resulted in a great reduction in the sample cost. Furthermore, a better signal to noise ratio can be obtained by using the custom-made flow cell.

To test the mixing, continuous channel flow-LD measurements were made by injecting two solutions (ct-DNA and water) simultaneously. Two 2 ml syringes containing 250 μM ct-DNA and water respectively were pushed simultaneously at the same speed, thus the DNA was diluted in the T-mixer and then flowed through the cell. The syringe pump was set to push 50 μl of each solution and results were compared with injecting DNA alone (figure 7.5.1.2).

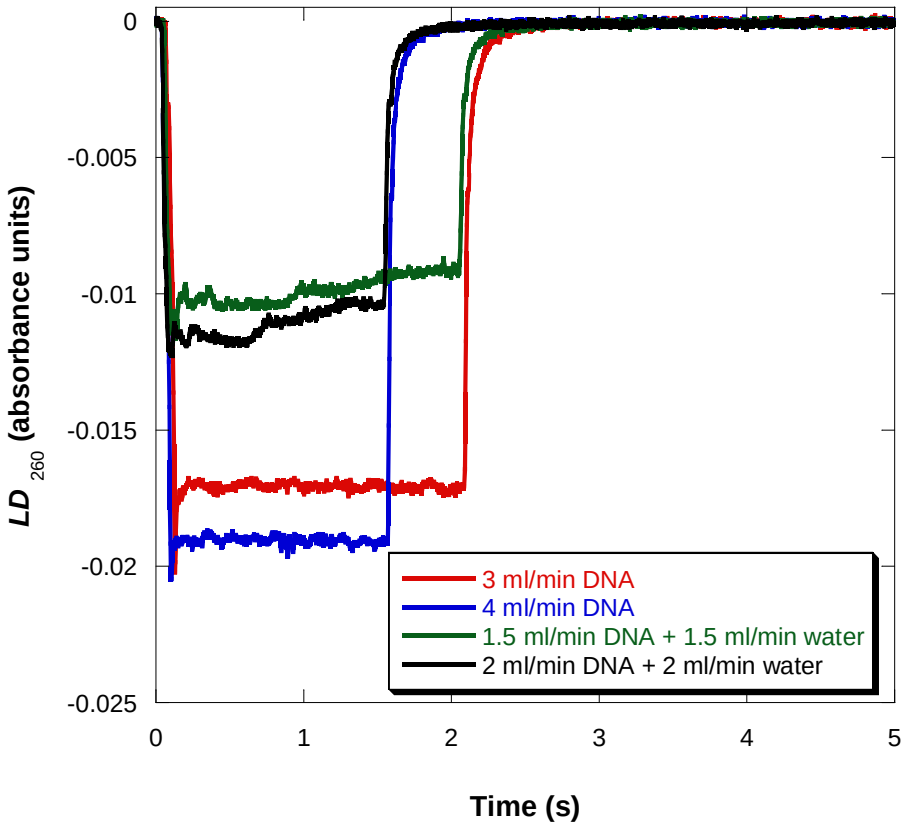

Figure 7.5.1.2 The comparision of injecting DNA mixed with water and DNA alone into the custom-made flow cell. 100 µl of 250 µM DNA on its own was injected at 3 and 4 ml/min respectively. When mixed with water, 50 µl of 250 µM DNA and 50 µl of water were set to be pushed simultaneously at 1.5 and 2 ml/min respectively. LD was measured at 260 nm.

When ct-DNA and water were injected at 1.5 ml/min simultaneously, the total flow rate at the detection cell was doubled to 3 ml/min. However, the concentration of ct-DNA was diluted 2-fold at the detection cell. Therefore the continuous channel flow LD would be expected as half of the signal when only ct-DNA was injected at 3 ml/min. From figure 7.5.1.2, we observe that when injecting DNA alone at 3 ml/min, the LD reached approximately –0.017 units, nearly double when DNA and water were injected at 1.5 ml/min. Similarly, the continuous channel flow LD from

injecting DNA alone at 4 ml/min is double that given by injecting ct-DNA and water simultaneously at 2 ml/min. These results suggest that the T-mixer attached is capable of effectively mixing two solutions in symmetrical 1:1 volume ratios over the range of flow rates we studied.

7.5.2 Kinetics measurments

Since the T-mixer allows the effective mixing of two solutions of reactants, the custom-made flow cell attached with the T-mixer was first used to detect the fast kinetics. The detection of a reaction process at different times was made by changing the length of the decay line from T-mixer to the detection flow cell. In order to record different dead time points, the solution left in the flow cell as well as the T-mixer was removed. When two solutions were ready to flow into the T-mixer, the solution injection and the data collection were started simultaneously. The time when we saw the first LD signal after a flat baseline of approximately zero, was the dead time of the system.

DNA exonuclease kinetics

An assay was then required where the signal produced is an LD signal that changes due to a change in alignment during the reaction to test the continuous channel flow LD system as a method to monitor fast kinetics. One such reaction is the enzymatic hydrolysis of DNA, a reaction in which DNA is degraded by DNase I to small fragments that have a greatly reduced or no LD signal (N'soukpoé-Kossi, Diamantoglou and Tajmir-Riahia 2008).

250 μM of ct-DNA and 0.73 μM of DNase I in the reaction buffer (50 mM Tris-HCl, pH 8.0, 1 mM Ca_2Cl, 1 mM $MgSO_4$) were stored separately in two syringes. Nine different lengths of decay line were used in this experiment, which monitored the reaction of DNA digestion from 1.9 s to 4.4 s. 300 μl of each solution was injected simultaneously at 1.5 ml/min for each decay line. Continuous channel

measured at 260 nm. Then the LD of the steady state phase was plotted against different reaction times to give the results below.

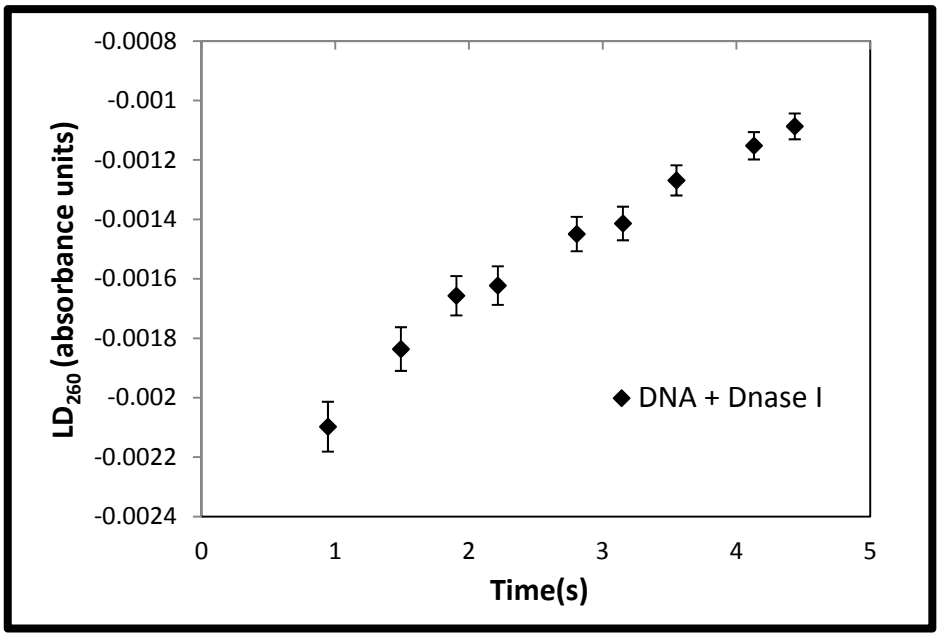

Figure 7.5.2.1 Continuous channel flow-LD system based on the custom-made flow cell was used to measure the rapid digestion of ct-DNA by DNase I. 250 μM of ct-DNA and 0.73 μM of DNase I was stored in two syringes separately. 300 μl of each solution was injected simultaneously at 1.5 ml/min for each decay line. LD was measured at 260 nm, and plotted against different reaction time.

As seen in figure 7.5.2.1, DNA shows a negative LD signal, as discussed in the previous section (§ 7.5.1). It is clear that the intensity of LD decreases signifiantly (from 0.0017 to 0.0011 units) over the 2.5 s of DNA digestion. Thus upon being mixed with DNase I, the LD signal of DNA at 260 nm diminishes indicating that the alignment of the DNA in the flow cell is reduced. This agrees with the expectation that the action of DNase I leads to the generation of progressively shorter DNA fragments which are less able to align and hence produce a less intense LD signal.

FtsZ assembly kinetics

Finally, the continuous channel flow-LD system based on the custom-made flow cell was used to study the early stages of FtsZ polymerization. 22 μM of FtsZ in the polymerization buffer (100 mM MES-KOH, pH 6.5, 20 mM $MgCl_2$, and 100 mM KCl) and 0.4 mM of GTP were stored separately in two syringes. 300 μl of each solution was injected simultaneously at 1.5 ml/min. Continuous channel flow LD was measured at 210 nm, which is the backbone region of FtsZ. The detection for the process of FtsZ polymerization at different time was made by changing the length of the decay line from T-mixer to the detection flow cell. Then the LD of the steady state phase subtracted by the value when the flow stopped was plotted against different reaction time, which is shown in figure 7.5.2.2.

Ten different lengths of decay line were used in this experiment. The FtsZ polymerization was measured from 0.6 s to 4.1 s. FtsZ polymers show positive LD, because the protein backbone axis is parallel to the light beam under the continuous flow (figure 7.5), and their π-π^* transitions are parallel to the flow direction.

Negative control experiments were also performed. When FtsZ was injected into the flow cell alone, there no LD signal was observed, indicating that only FtsZ polymers result in the positive LD signal at 210 nm.

It can be observed from figure 7.5.2.2 that the LD of FtsZ increased slightly (from 0 to 0.001 units) over the 4.1 s of the reaction, suggesting that FtsZ protofilaments were formed gradually. However, at 0.6 s, the earliest data point monitored, there was not much increase in LD, which is consistent with the previously reported lag phase (Chen et al. 2005). This lag lasted for 1 s before a significant increase in LD was observed. The minimal kinetic model of FtsZ polymerization outlined in the literature postulates three steps after addition of GTP to FtsZ. The first step in the assembly mechanism is activation of the FtsZ monomer, which is needed to account for the lag of nearly 1 s, followed by formation of a dimer nucleus and elongation

(Chen et al. 2005). The continuous channel flow shows us the early stages of FtsZ assembly. After that, there is a plateau and decrease in FtsZ polymerization which is already shown by either light scattering or Couette flow LD data.

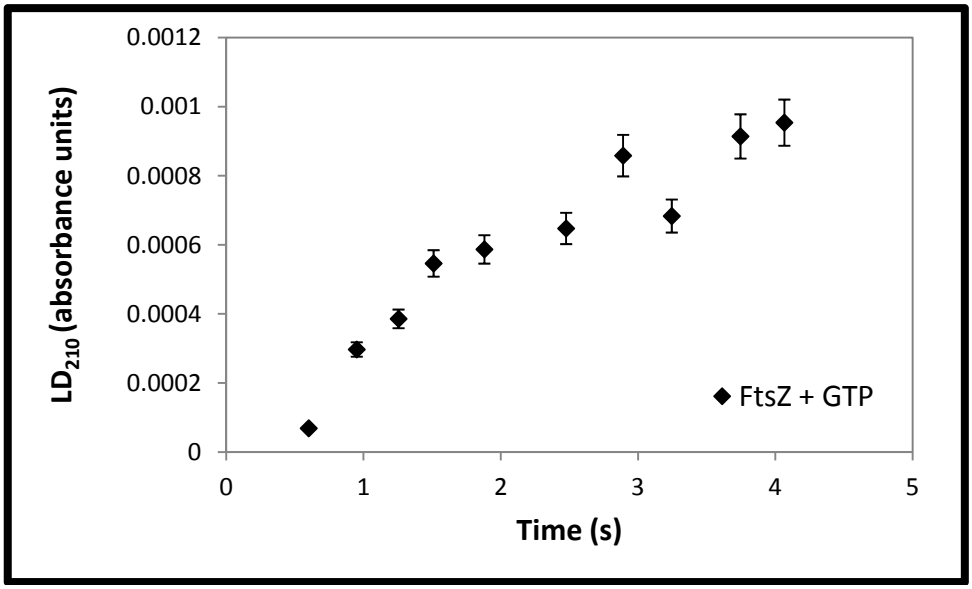

Figure 7.5.2.2 Continuous channel flow-LD system based on the custom-made flow cell was used to measure the polymerization of FtsZ. 22 μM of FtsZ in the polymerization buffer (100 mM MES-KOH, pH 6.5, 20 mM $MgCl_2$, 100 mM KCl) and 0.4 mM of GTP was stored in two syringes separately. 300 μl of each solution was injected simultaneously at 1.5 ml/min for each decay line. LD was measured at 210 nm, and plotted against different reaction time.

7.6 Conclusions

In this chapter a novel technique continuous channel flow LD has been described, which is an adpted stopped-flow system to record fast kinetics for reactions in which the alignment of long biomacromolecules changes. In the continuous channel flow-LD system, a known amount of sample is delivered into the open flow cell by a twin drive syringes and mixer arrangement, and then passed through the cell during the LD measurements. Thus the sample is continuously flowed and aligned with the flow in the detection cell, which then gives the corresponding LD signal.

Three flow cells, FC-20 open cuvette, μ-Slide III$^{3\ in\ 1}$ channel slide, and a custom-made channel slide with quartz window, have been tested, and we found that the custom-made channel slide gave the best performance as far as both sample flowing and dection range are considered. Compared with the μ-Slide III$^{3\ in\ 1}$ channel slide, the custom-made flow cell enables the detection down to UV region. On the other hand, the custom-made quartz window flow cell has a thinner channel than the commercial FC-20 cuvette. Therefore under a high shear rate, a better alignment of long molecules is obtained in the custom-made flow cell, which leads to a bigger LD signal. In addition, the signal to noise ratio is also improved and the sample cost is reduced due to both lower concentrations and slower flow rates required.

When we used the custom-made flow cell for kinetics measurements, it also gave us the best results. From the enzymatic hydrolysis of DNA by DNase I, which was monitored from 1.9 s to 4.4 s, we found that the action of DNase I leads to the generation of progressively shorter DNA fragments as seen from the reduced LD signal. More importantly, the continuous channel flow LD complements the study of FtsZ dynamics in the previous chapters. For the early stages of FtsZ polymerization, it was observed that the FtsZ protofilaments were formed gradually. At 0.6 s, the earliest data point monitored, there was not much increase in LD, which is consistent with a lag phase to activate the FtsZ monomer. This lag could last for 1 s before a significant increase in LD was observed. In addition to the the increase in the number of FtsZ protofilaments shown from the continuous channel flow LD, it will then reach a plateau where both aseembly and disassembly are balanced, followed by a net disassembly of FtsZ which has already been shown by either light scattering or Couette flow LD.

CHAPTER 8 -- CONCLUSIONS

8.1 Effects of Mg^{2+}, K^{+} and pH on FtsZ assembly

The FtsZ protein plays an essential role in regulating cell division in bacteria, which is related to its dynamic Z-ring. It has been postulated that the Z-ring is formed through self-assembly of FtsZ due to its GTPase activity. Studies have shown the dynamic behaviour of FtsZ *in vitro* (Mukherjee and Lutkenhaus 1999, Pacheco-Gomez *et al.* 2011), in which FtsZ properties change from assembling into protofilaments to maintaining the steady-state phase then to net disassembly of the protofilaments to monomers. Although the detailed mechanisms responsible for regulating FtsZ ring dynamics during the cell cycle have not yet been fully elucidated, some factors that influence FtsZ ring assembly and disassembly *in vitro* have been found.

For testing FtsZ quality, a traditional technique right-angle light scattering was used to study the GTP-dependent polymerization of FtsZ as well as its dynamic behaviour of polymerization, steady-state and depolymerization. Results similar to those in the literature have been found in this work. FtsZ polymerization was observed over a broad pH range from 6.0 to 7.5, although the most effective polymerization occurred at pH 6.5. For the standard polymerization assay, the reaction was initiated by the addition of GTP to a final concentration of 0.2 mM into the mixture containing 11 μM FtsZ and the polymerization buffer (50 mM MES-KOH, pH 6.5, 50 mM KCl, and 10 mM $MgCl_2$). Mg^{2+} is not required for FtsZ polymerization, however, it is required for GTP hydrolysis which leads to the polymers depolymerizing. At higher Mg^{2+} concentrations and/or acidic pH, there is a tendency for FtsZ protofilaments to align along the fibre axis to give bundles. Additionally, by changing the concentration of the reagents in the medium (GTP, FtsZ, Mg^{2+} and/or KCl), the time

for the persistence of the polymers, which coincides with the time when GTP is consumed changes.

Colourmetric assay was implemented to study the inorganic phosphate (P_i) released from the enzymatic hydrolysis of GTP to GDP catalysed by FtsZ. The phosphate released was detected using a spectroscopic coupled enzyme system which measured the difference in absorbance between the reagents and the products. The change in absorption at 360 nm allowed real time quantification of the inorganic phosphate consumed in the reaction. The effects of the pH, KCl and Mg^{2+} concentrations were all studied, and we found that the reduction in the rate of GTP hydrolysis could be attributed to an increase in the bundling effect as a result of changes in the polymerization conditions. It also revealed that GTP hydrolysis was not required for FtsZ assembly since the polymers formed in the absence of Mg^{2+} were very stable, but GTP hydrolysis was required for the depolymerization.

8.2 Model of the function of YgfE in FtsZ bundling

The very dynamic nature of FtsZ polymers observed *in vitro* could explain how they are stabilized *in vivo* to some extent, since the Z-ring has to persist for some time before they are used for cell division. The study shows that the assembly of protofilaments into bundles reduces the dynamics of FtsZ polymers, which might have a very important role in the stability of the polymers. Although FtsZ bundling could be induced by some factors such as the macromolecular crowding, multivalent cations including DEAE dextran, calcium, and magnesium, these effects are not as great as that cross-linked by some accessory cell division proteins.

One of the accessory proteins is YgfE, a putative *E. coli* ZapA orthologue. YgfE binds to FtsZ polymers, strongly promotes FtsZ polymer bundling and it is a potent inhibitor of the FtsZ's GTPase activity (Gueiros-Filho and Losick 2002, Low *et al.* 2004, Small *et al.* 2007). In order to study how YgfE affect FtsZ polymerization by

using its mutants, we performed the experiments on wild type YgfE first as the control, and also to check for consistency with published data.

Two different experiments were designed. In the first experiment, the bundling effects of YgfE were studied on preformed protofilaments. In the second experiment, the polymerization/bundling reaction was started by the addition of GTP into the premixed FtsZ and YgfE. Examination of the results obtained from both experiments suggested that YgfE enhances the amount of polymer and the stability of the polymers. However, the efficient polymer bundling activity of YgfE is exerted on preformed FtsZ protofilaments.

The crystal structure of YgfE is an anti-parallel tetramer with four globular domains, at each end of the coiled-coil stalk. In solution it mainly exists as a tetramer at the concentrations reported in our study as suggested by sedimentation equilibrium experiments of analytical ultracentrifugation. It was thought that YgfE binds directly with FtsZ and induces protofilaments to associate into large bundles, a property believed to be connected to its dimeric or tetrameric nature.

In order to gain a better understanding of the protein interactions that stabilise the FtsZ polymers, a series of YgfE mutants were produced with the aim to disrupt its tetramer structure. Among those mutants, YgfE-I83E was found to be dimeric and YgfE-V17E was in between a dimer and a tetramer, according to the sedimentation equilibrium experiments of analytical ultracentrifugation.

Right-angle light scattering, LD, EM, and the GTPase assay were used to study the bundling activity of the wild type YgfE and two other YgfE mutants: YgfE-V17E and YgfE-I83E, by adding YgfE onto preformed FtsZ protofilaments. The cross-linking interactions of YgfE onto FtsZ frotofilaments are believed to be related to its propensity to form tetramers. In according with this, wild type YgfE, as a tetramer, has been shown to have the strongest ability to induce FtsZ protofilaments

to associate into thick bundles. YgfE-I83E, as it is preferentially a dimer, seems to be unable to induce FtsZ bundling. The effect of YgfE-V17E is intermediate between the other two, consistent with it adopting both dimer and tetramer species in solution.

Whether the dimer YgfE-I83E could bind to FtsZ protofilaments was then investigated. Both sedimentation assay and dynamic light scattering suggested that YgfE-I83E is still able to bind to FtsZ, and it also blocks the bundling of FtsZ by occupying the entire binding sites. It is therefore clear that a tetramerisation of YgfE is not required for binding, and by inference it is likely that the association between two dimers of YgfE on different FtsZ fibres could underlie the mechanism of YgfE induced FtsZ fibre bundling with the extended tetramer bridging two FtsZ fibres. The FtsZ binding region of YgfE is in a region separate from the tetramerisation interface in the structure.

In the model proposed by Gueiros-Filho and Losick (Gueiros-Filho and Losick 2002), they considered that dimers of ZapA (YgfE) cross-link FtsZ monomers in adjacent protofilaments, thereby stabilizing the lateral interactions. However, in our studies, we find that the dimer cannot bridge two FtsZ protofilaments, and only the tetramer does. Therefore we present another model which is shown in figure 8.2

As a tetrameric dogbone-like protein, YgfE could attach two FtsZ protofilaments with either the same end (figure 8.2A) or the two opposite ends (figure 8.2B) of the “dog bone”. However, if the two FtsZ protofilaments were crosslinked by the same end of the dogbone shaped YgfE, the dimer YgfE-I83E should also have the ability to bridge two FtsZ protofilaments, which is not consistent with our experimental results. Therefore, we believe that YgfE binds two FtsZ protofilaments with its two opposite ends. In such a case, there are also two possibilities. YgfE might be able to bind in between FtsZ protofilaments (figure 8.2B2) as well as on top of a double filament (figure 8.2B1).

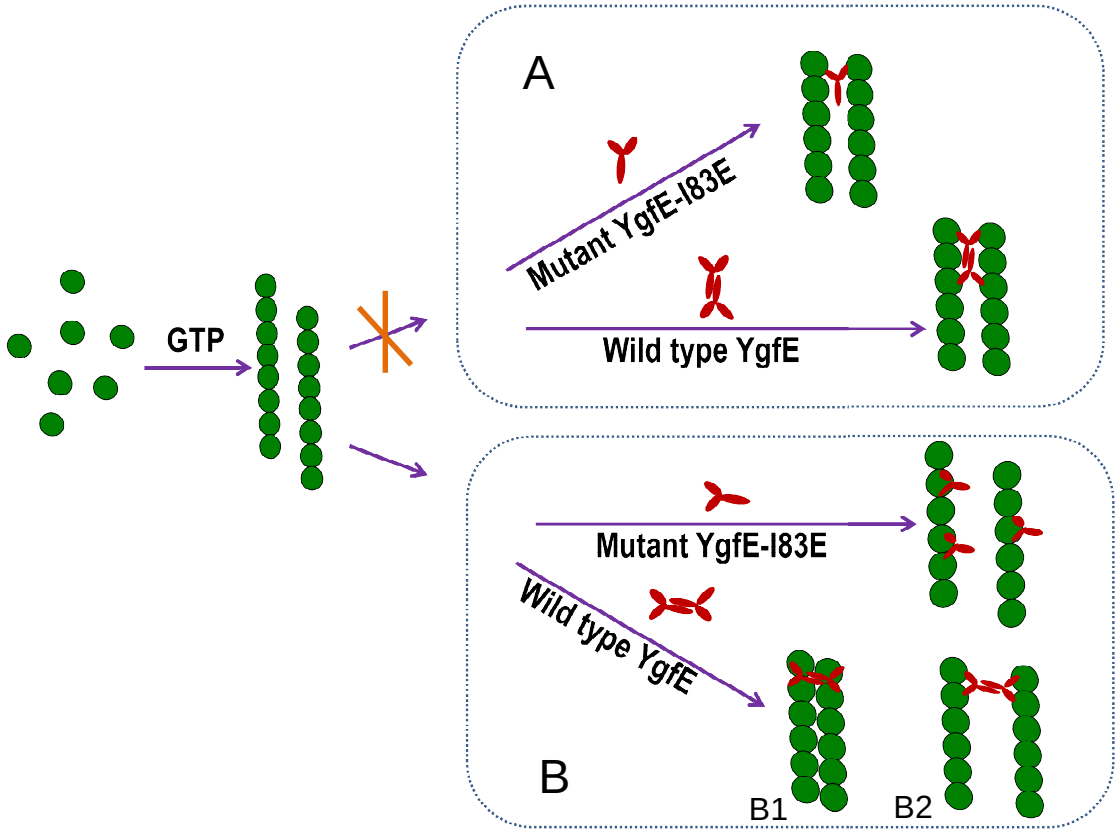

Figure 8.2 Model for the function of YgfE in FtsZ bundling. In the presence of GTP, FtsZ monomers polymerise into head-to-tail protofilaments, which then associate with each other laterally to form bundles with the bridging of wild type YgfE. The tetramer YgfE may attach two FtsZ protofilaments with the two opposite ends (B) of the "dog bone" but not with the same end (A), because the dimer mutant YgfE-I83E does not have the cross-link function. When crosslinking two FtsZ protofilaments with the two opposite ends, YgfE might be able to bind in between FtsZ protofilaments (B2) as well as on top of a double filament (B1). The binding in between filaments is more likely to have a function in bringing the filaments together. The green circles present FtsZ monomers molecules, the red bone-like shape presents the YgfE tetramer and the red half-bone like shape presents the dimer YgfE-I83E.

Mohammadi *et al.* found that the width of the parallel double FtsZ filaments is about 10.5 nm, and the distance from the middle of a double FtsZ filament to the next parallel double filament is 22 nm. If a YgfE tetramer binds in between FtsZ

filaments, the distance to be covered would be 11.5 nm, which more or less corresponds to the length of an YgfE tetramer, approximately 10 nm. Possibly, a YgfE tetramer is also able to bind on top of a double FtsZ filament from the distance detected, although His-YgfE might not because of steric hindrance due to the presence of the His tag and appears to cover a larger distance between two filaments (Mohammadi *et al.* 2009).

The binding in between filaments likely have a function in bringing the filaments together. Mohammadi *et al.* found that the magnitude of ZapA (YgfE) affecting the GTPase activity of FtsZ follows the same trend as that in the absence of YgfE. That is to say, FtsZ protofilaments are more readily bundle at pH 6.5 than at pH 7.5 and still more in the case of 10 mM $MgCl_2$ compared to 5mM $MgCl_2$ both in the presence and absence of YgfE. Besides, the filaments probably become more stable when they are annealed over a particular length. Since the FtsZ association is cooperative，a certain distance may be required for the continued action of YgfE superfluous (Mohammadi *et al.* 2009).

8.3 Continuous channel flow LD

In order to further study the FtsZ polymerization and bundling, the early stages of the reactions were deemed to be important. LD is a simple spectroscopy technique for structure characterization of long biomacromolecules in solutions, such as DNAs and assemblies of molecules into fibres (*e.g.* FtsZ polymers) as well as membrane-bound molecules. It can also help to distinguish aggregation compared with light scattering. However, the application is limited by the time required to assemble and fill the LD cell, approximately 45 s. For recording the very first seconds of the FtsZ polymerization as well as other fast reactions, a continuous channel flow-LD technique has been developed.

The continuous channel flow LD is based on a stopped-flow system, in which a known amount sufficient sample is delivered into the open flow cell with the twin drive syringes and mixer arrangement, and then continuously past through the cell. Therefore the sample is aligned with the flow in the detection cell, and gives the corresponding LD signal. The signal at different reaction time can be recorded by changing the decay line between the mixer and the observation cell. Three flow cells, FC-20 open cuvette, μ-Slide III$^{3\text{ in }1}$ channel slide, and a custom-made channel slide with quartz window, have been tested to build the best system. As far as both sample flowing and dection range are considered, the custom-made channel slide gave us the best performance. It not only can be used for the detection in the UV region but also offers the best alignment of the long molecules due to the thinnest channel. The improvement of alignment results in the growth of LD signal or the decrease of sample concentration.

Finally the custom-made flow cell was used for the continuous channel flow LD system to study the early stages of FtsZ polymerization. It was observed that the FtsZ protofilaments were formed gradually over the first 4 s of time. Before 1 s, there is likely a lag phase to activate the FtsZ monomer. The minimal kinetic model of FtsZ polymerization postulates three steps after addition of GTP to FtsZ: activation of the FtsZ monomer; formation of a dimer nucleus; and elongation.

8.4 Outlook and future challenges

FtsZ polymer dynamics are controlled during the cell cycle by a balanced network of positive- and negative-acting factors. The past few years have seen the discovery of many factors that are involved in Z ring formation and modulating polymer dynamics. The relatively recent identification of ZapA and YgfE in *E. coli* highlights the importance of non-essential proteins in cell division and their role in allowing cytokinesis to proceed.

Although the very promising results obtained during this study have allowed us to answer some of the basic questions, there are still some questions remaining unanswered. In particular, we are interested in answering questions such as the following. Where is the FtsZ binding site on YgfE? Will it be possible to obtain the crystal structure of a complex of both YgfE and FtsZ? What are the kinetics of protofilament formation? What is the geometry of protofilament formation?

An exhaustive understanding of FtsZ dynamics will very likely depend on an extension and/or development of the techniques currently being used. In this study we have developed a continuous channel flow LD system reducing the dead time of Couette flow LD from 45 s to less than 1 s, which is extremely helpful to study the kinetics of the early stages of FtsZ assembly. However, this channel flow LD system could be further improved in the aspect of tubing connection and mixer arrangement, so that more data points can be collected and more effective mixing can be obtained to facilitate better modeling of FtsZ polymerization.

Finally, we must remain cautious when drawing conclusions on the basis of the effects of *in vitro* experiments involving single accessory proteins on FtsZ polymers. In the cell, we also need to take into account the effects of membrane binding, the presence of numerous other regulatory proteins at the Z ring and the crowded nature of the cytoplasmic environment (Adams and Errington 2009). Further studies and new biochemical approaches both *in vivo* and *in vitro* are required to get a complete conclusion.

BIBLIOGRAPHY

Adams, D. W. & J. Errington (2009) Bacterial cell division: assembly, maintenance and disassembly of the Z ring. *Nature Reviews Microbiology,* 7, 642–653.

Addinall, S. G., E. F. Bi & J. Lutkenhaus (1996) FtsZ ring formation in *fts* mutants. *J. Bacteriol.,* 178, 3877–3884.

Addinall, S. G., K. A. Johnson, T. Dafforn, C. Smith, A. Rodger, R. Paco-Gomez, K. Sloan, A. Blewett, D. J. Scott & D. I. Roper (2005) Expression, purification and crystallization of the cell-division protein YgfE from *Escherichia coli*. *Acta Crystallogr. Sect. F Struct. Biol. Cryst. Commun.,* 61, 305–307.

Addinall, S. G. & J. Lutkenhaus (1996) FtsZ-spirals and -arcs determine the shape of the invagination septa in some mutants of *Escherichia coli*. *Molecular Microbiology,* 22, 231–237.

Anderson, D. E., F. J. Gueiros-Filho & H. P. Erickson (2004) Assembly dynamics of FtsZ rings in *Bacillus subtilis* and *Escherichia coli* and effects of FtsZ-regulating proteins. *J. Bacteriol.,* 186, 5775–5781.

Beer, A. (1852) Bestimmung der Absorption des rothen Lichts in farbigen Flüssigkeiten (Determination of the absorption of red light in colored liquids). *Annalen der Physik und Chemie,* 86, 78–88.

Beuria, T. K., J. H. Shah, M. K. Santra, V. Kumarb, D. Panda (2006) Effects of pH and ionic strength on the assembly and bundling of FtsZ protofilaments: A possible role of electrostatic interactions in the bundling of protofilaments. Int. J. Biol. Macromol., 40, 30-39.

Bi, E. & J. Lutkenhaus (1991) FtsZ ring structure associated with the division in *Escherichia coli*. *Nature*, 354, 161–164.

Bi, E. & J. Lutkenhaus (1993) Cell division inhibitors SulA and MinCD prevent formation of the FtsZ ring. *J. Bacteriol.,* 175, 1118–1125.

Bradford, M. M. (1976) A Rapid and Sensitive Method for the Quantitation of Microgram Quantities of Protein Utilizing the Principle of Protein-Dye Binding. *Anal. Biochem.,* 72, 248–254.

Bramhill, D. & C. M. Thompson (1994) GTP-dependent polymerization of *Escherichia coli* FtsZ protein to form tubules. *Proc. Natl. Acad. Sci. USA*, 91, 5813–5817.

Caplan, M. R. & H. P. Erickson (2003) Apparent cooperative assembly of the bacterial cell division protein FtsZ demonstrated by isothermal titration calorimetry. *J. Biol. Chem.,* 278, 13784–13788.

Chen, Y., K. Bjornson, S. D. Redick & H. P. Erickson (2005) A rapid fluorescence assay for FtsZ assembly indicates cooperative assembly with a dimer nucleus. *Biophys. J.,* 88, 505–514.

Chen, Y. & H. P. Erickson (2005) Rapid in vitro assembly dynamics and subunit turnover of FtsZ demonstrated by fluorescence resonance energy transfer. *J. Biol. Chem.,* 280, 22549–22554.

Chung, K. M., H. H. Hsu, H. Y. Yeh & B. Y. Chang (2007) Mechanism of regulation of prokaryotic tubulin-like GTPase FtsZ by membrane protein EzrA. *J. Biol. Chem.,* 282, 14891–14897.

Cole, J. L. & J. C. Hansen (2000) Analytical Ultracentrifugation as a contemporary biomolecular research tool. *Journal of Biomolecular Techniques,* 10, 163–176.

Cordell, S. C., E. J. Robinson & J. Löwe (2003) Crystal structure of the SOS cell division inhibitor SulA and in complex with FtsZ. *Proc. Natl Acad. Sci. USA,* 100, 7889–7894.

Couette, M. (1890) Etudes sur le frottement des liquides. *Ann. Chim. Phys.,* 6, 433–510.

Dai, K. & J. Lutkenhaus (1992) The proper ratio of FtsZ to FtsA is required for cell division to occur in *Escherichia coli*. *J. Bacteriol.,* 174, 6145–6151.

Dajkovic, A., G. Lan, S. X. Sun, D. Wirtz & J. Lutkenhaus (2008a) MinC spatially controls bacterial cytokinesis by antagonizing the scaffolding function of FtsZ. *Curr. Biol.,* 18, 235–244.

Dajkovic, A. & J. Lutkenhaus (2006) Z ring as executor of bacterial cell division. *J. Mol. Microbiol. Biotechnol.,* 11, 140–151.

Dajkovic, A., A. Mukherjee & J. Lutkenhaus (2008b) Investigation of regulation of FtsZ assembly by SulA and development of a model for FtsZ polymerization. *J. Bacteriol.,* 190, 2513–2526.

Davis, B. J. (1964) Disc electrophoresis. II. Method and application to human serum proteins. *Ann. N.Y. Acad. Sci.,* 121, 404–427.

de Boer, P., R. Crossley & L. Rothfield (1992) The essential bacterial cell-division protein FtsZ is a GTPase. *Nature,* 359, 254–256.

de Boer, P. A., W. R. Cook & L. I. Rothfield (1990) Bacterial cell division. *Annu. Rev. Genet.,* 24, 249–274.

de Pereda, J. M., D. Leynadier, J. A. Evangelio, P. Chacon & J. M. Andreu (1996) Tubulin secondary structure analysis, limited proteolysis sites, and homology to *ftsZ*. *Biochemistry,* 35, 14203–14215.

den Blaauwen, T., N. Buddelmeijer, M. E. Aarsman, C. M. Hameete & N. Nanninga (1999) Timing of FtsZ Assembly in *Escherichia coli*. *J. Bacteriol.,* 181, 5167–5175.

Dicko, C., M. R. Hicks, T. R. Dafforn, F. Vollrath, A. Rodger & S. V. Hoffmann (2008) Breaking the 200 nm Limit for Routine Flow Linear Dichroism Measurements Using UV Synchrotron Radiation. *Biophys J.,* 95, 5974–5977.

Din, N., E. M. Quardokus, M. J. Sackett & Y. V. Brun (1998) Dominant C-terminal deletions of FtsZ that affect its ability to localize in Caulobacter and its interaction with FtsA. *Mol. Microbiol.,* 27, 1051–1063.

Donnelly, R. J. (1991) Taylor-Couette flow: the early days. *Phys. Today,* Nov, 32–39.

Erickson, H. P. (1995) FtsZ, a prokaryotic homolog of tubulin? *Cell,* 80, 367–370.

Erickson, H. P. (1997) FtsZ, a tubulin homologue in prokaryote cell division. *Trends Cell Biol.,* 7, 362–367.

Erickson, H. P. (1998) Atomic structures of tubulin and FtsZ. *Trends Cell Biol.,* 8, 133–137.

Erickson, H. P. (2001) The FtsZ protofilament and attachment of ZipA — structural constraints on the FtsZ power stroke. *Curr. Opin. Cell Biol.,* 13, 55–60.

Erickson, H. P. (2009) Modeling the physics of FtsZ assembly and force generation. *PNAS,* 106, 9238–9243.

Erickson, H. P. & D. Stoffler (1996) Protofilaments and rings, two conformations of the tubulin family conserved from bacterial FtsZ to α, β, and γ tubulin. *J. Cell Biol.,* 135, 5–8.

Erickson, H. P., D. W. Taylor, K. A. Taylor & D. Bramhill (1996) Bacterial cell division FtsZ assembles into prtofilaments sheets and minirings, structural homologs of tubulin polymers. *Proc. Natl. Acad. Sci.,* 93, 519–523.

Erni, R., M. D. Rossell, C. Kisielowski & U. Dahmen (2009) Atomic-Resolution Imaging with a Sub-50-pm Electron Probe. *Phys. Rev. Lett.,* 102, 4 pages.

Errington, J., R. A. Daniel & D. J. Scheffers (2003) Cytokinesis in bacteria. *Microbiol. Mol. Biol. Rev.,* 67, 52–65.

Feucht, A., I. Lucet, M. D. Yudkin & J. Errington (2001) Cytological and biochemical characterization of the FtsA cell division protein of Bacillus subtilis. *Mol. Microbiol.,* 40, 115–125.

Gilson, P. R. & P. L. Beech (2001) Cell division protein FtsZ: running rings around bacteria , chloroplasts and mitochondria. *Res. Microbiol.,* 152, 3–10.

Glockner, F. O., M. Kube, M. Bauer, H. Teeling, T. Lombardot, W. Ludwig, D. Gade, A. Beck, K. Borzym, K. Heitmann, R. Rabus, H. Schlesner, R. Amann & R. Reinhardt (2003) Complete genome sequence of the marine planctomycete Pirellula sp. strain 1. *Proc. Natl. Acad. Sci. USA,* 100, 8298–8303.

González, J. M., M. Jiménez, M. Vélez, J. Mingorance, J. M. Andreu, M. Vicente & G. Rivas (2003) Essential cell division protein FtsZ assembles into one monomer-thick ribbons under conditions resembling the crowded intracellular environment. *J. Biol. Chem.,* 278, 37664–37671.

González, J. M., M. Vélez, M. Jiménez, C. Alfonso, P. Schuck, J. Mingorance, M. Vicente, A. P. Minton & G. Rivas (2005) Cooperative behavior of Escherichia coli cell-division protein FtsZ assembly involves the preferential cyclization of long single-stranded fibrils. *Proc. Natl Acad. Sci. USA,* 102, 1895–1900.

Gueiros-Filho, F. J. & R. Losick (2002) A widely conserved bacterial cell division protein that promotes assembly of the tubulin-like protein FtsZ. *Genes Dev.,* 16, 2544–2556.

Haeusser, D. P., R. L. Schwartz, A. M. Smith, M. E. Oates & P. A. Levin (2004) EzrA prevents aberrant cell division by modulating assembly of the cytoskeletal protein FtsZ. *Mol. Microbiol.,* 52, 801–814.

Hale, C. A. & P. A. J. de Boer (1997) Direct binding of FtsZ to ZipA, an essential component of the septal ring structure that mediates cell division in *E. coli*. *Cell,* 88, 175–185.

Hale, C. A. & P. A. J. de Boer (1999) Recruitment of ZipA to the septal ring of Escherichia coli is dependent on FtsZ and independent of FtsA. *J. Bacteriol.,* 181, 167–176.

Hale, C. A., A. C. Rhee & P. A. J. de Boer (2000) ZipA-induced bundling of FtsZ polymers mediated by an interaction between C-terminal domains. *J. Bacteriol.,* 182, 5153–5166.

Haney, S. A., E. Glasfeld, C. Hale, D. Keeney, Z. He & P. de Boer (2001) Genetic analysis of the Escherichia coli FtsZ-ZipA interaction in the yeast two-hybrid system. *J. Biol. Chem.,* 276, 11980–11987.

Harry, E. J., J. Rodwell & R. G. Wake (1999) Co-ordinating DNA replication with cell division in bacteria: a link between the early stages of a round of replication and mid-cell Z ring assembly. *Mol. Microbiol.,* 33, 33–40.

Hayashi, I., T. Oyama & K. Morikawa (2001) Structural and functional studies of MinD ATPase: implications for the molecular recognition of the bacterial cell division apparatus. *EMBO J.,* 20, 1819–1828.

Haydon, D. J., N. R. Stokes, R. Ure, G. Galbraith, J. M. Bennett, D. R. Brown, P. J. Baker, V. V. Barynin, D. W. Rice, S. E. Sedelnikova, J. R. Heal, J. M. Sheridan, S. T. Aiwale, P. K. Chauhan, A. Srivastava, A. Taneja, I. Collins, J. Errington & L. G. s. a. a. Czaplewski (2008) An inhibitor of FtsZ with potent and selective anti-staphylococcal activity. *Science,* 321, 1673–1675.

Higashitani, A., N. Higashitani & K. Horiuchi (1995) A cell division inhibitor SulA of Escherichia coli directly interacts with FtsZ through GTP hydrolysis. *Biochem. Biophys. Res. Commun.,* 209, 198–204.

Higashitani, A., Y. Ishii, Y. Kato & K. Horiuchi (1997) Functional dissection of a celldivision inhibitor, SulA, of *Escherichia coli* and its negative regulation by Lon. *Mol. Gen. Genet,* 254, 351–357.

Hirota, Y., A. Ryter & F. Jacob (1968) Thermosensitive mutants of *E. coli* affected in the process of DNA synthesis and cell division. *Cold Spring Harbor Symp. Quant. Biol.,* 33, 677–694.

Hsieh, C. W., T. Y. Lin, H. M. Lai, C. C. Lin, T. S. Hsieh & Y. L. Shih (2010) Direct MinE-membrane interaction contributes to the proper localization of MinDE in *E. coli*. *Mol. Microbiol.,* 75, 499–512.

Hu, Z., A. Mukherjee, S. Pichoff & J. Lutkenhaus (1999) The MinC component of the division site selection system in Escherichia coli interacts with FtsZ to prevent polymerization. *Proc. Natl Acad. Sci. USA,* 96, 14819–14824.

Hu, Z. L., E. P. Gogol & J. Lutkenhaus (2002) Dynamic assembly of MinD on phospholipid vesicles regulated by ATP and MinE. *Proc. Natl. Acad. Sci. USA,* 99, 6761–6766.

Huang, J., C. Cao & J. Lutkenhaus (1996) Interaction between FtsZ and inhibitors of cell division. *J. Bacteriol.,* 178, 5080–5085.

Huisman, O. & R. D'Ari (1981) An inducible DNA replicationcell division coupling mechanism in *E. coli*. *Nature,* 290, 797–799.

Huisman, O., R. D'Ari & S. Gottesman (1984) Cell-division control in Escherichia coli: specific induction of the SOS function SfiA protein is sufficient to block septation. *Proc. Natl Acad. Sci. USA,* 81, 4490–4494.

IUPAC (1997) Compendium of Chemical Terminology, 2nd ed. (the "Gold Book"). Online corrected version: (2006) "absorbance" (http://goldbook.iupac.org/A00028.html).

Johansson, L. B. A. & A. Davidsson (1985) Analysis and Application of Linear Dichroism on Membranes—Description of a Linear Dichroism Spectrometer. *J. Chem. Soc., Faraday Trans. 1,* 81, 1375–1388.

Johnson, W. C. J. (1990) Protein secondary structure and circular dichroism: A practical guide. *Proreins Sfruct. Funcf. Genet.,* 7, 205–214.

Jones, M. N. (1992) Surfactant interactions with biomembranes and proteins. *Chem. Soc. Rev.,* 21, 127–136.

Justice, S. S., J. Garcia-Lara & L. I. Rothfield (2000) Cell division inhibitors SulA and MinC/MinD block septum formation at different steps in the assembly of the *Escherichia coli* division machinery. *Mol. Microbiol.,* 37, 410–423.

Krebs, J. E., E. S. Goldstein & S. T. Kilpatrick (2009) Lewin's GENES X. Jones & Bartlett Publishers.

Kuchibhatla, A., J. Bellare & D. Panda (2011) Cationic lipid enhances assembly of bacterial cell division protein FtsZ: A possible role of bacterial membrane in FtsZ assembly dynamics. *International Journal of Biological Macromolecules,* 49, 737–741.

Laemmli, U. K. (1970) Cleavage of structural proteins during the assebmyl of the head of the bacteriophage T4. *Nature,* 227, 680–685.

Lambert, J. H. (1760) Photometria sive de mensura et gradibus luminis, colorum et umbrae [Photometry, or, On the measure and gradations of light, colors, and shade] (Augsburg ("Augusta Vindelicorum"), Germany: Eberhardt Klett,

Lamm, O. (1929) Die Differentialgleichung der Ultrazentrifugierung. *Ark. Mat. Astr. Fys.,* 21B, 1–4.

Lan, G., B. R. Daniels, T. M. Dobrowsky, D. Wirtz & S. X. Sun (2009) Condensation of FtsZ filaments can drive bacterial cell division. *PNAS,* 106, 121–126.

Levin, P. A., I. G. Kurtser & A. D. Grossman (1999) Identification and characterization of a negative regulator of FtsZ ring formation in *Bacillus subtilis*. *Proc. Natl. Acad. Sci. USA,* 96, 9642–9647.

Levin, P. A. & R. Losick (1996) Transcription factor Spo0A switches the localization of the cell division protein FtsZ from a medial to a bipolar pattern in Bacillus subtilis. *Genes & Development,* 10, 478–488.

Li, Z., M. J. Trimble, Y. V. Brun & G. J. Jensen (2007) The structure of FtsZ filaments in vivo suggests a forcegenerating role in cell division. *EMBO J.,* 26, 4694–4708.

Lin, D.-H., P. A. Levin & A. D. Grossman (1997) Bipolar localization of a chromosome partition protein in *Bacillus subtilis*. *Proc. Natl. Acad. Sci. USA,* 94, 4721–4726.

Liu, Z., A. Mukherjee & J. Lutkenhaus (1999) Recruitment of ZipA to the division site by interaction with FtsZ. *Mol. Microbiol.,* 31, 1853–1861.

Low, H., M. C. Moncrieffe & J. Löwe (2004) The Crystal Structure of ZapA and its Modulation of FtsZ Polymerisation. *J. Mol. Biol.,* 341, 839–852.

Lu, C., J. Stricker & H. P. Erickson (1998) FtsZ from *Escherichia coli, Azotobacter vinelandii*, and *Thermotoga maritima*—quantitation, GTP hydrolysis, and assembly. *Cell Motil. Cytoskelet.,* 40, 71–86.

Lu, C. L., M. Reedy & H. P. Erickson (2000) Straight and curved conformations of FtsZ are regulated by GTP hydrolysis. *J. Bacteriol.,* 182, 164–170.

Lutkenhaus, J. (1993) FtsZ ring in bacterial cytokinesis. *Mol. Microbiol.,* 9, 403–409.

Lutkenhaus, J. & S. G. Addinall (1997) Bacterial cell division and the Z ring. *Annu. Rev. Biochem.,* 66, 93–116.

Löwe, J. & L. A. Amos (1998) Crystal structure of the bacterial cell-division protein FtsZ. *Nature,* 391, 203–206.

Löwe, J. & L. A. Amos (1999) Tubulin-like protofilaments in Ca^{2+}-induced FtsZ sheets. *EMBO J.,* 18, 2364–2371.

Löwe, J., F. van den Ent & L. A. Amos (2004) Molecules of the bacterial cytoskeleton. *Annu. Rev. Biophys. Biomol. Struct.,* 33, 177–198.

Ma, X., D. Ehrhardt & W. Margolin (1996) Collocalization of cell division proteins Ftsz and FtsA to cytoskeletal structures in living *Escherichia coli* cells by using green fluorescent protein. *Proc. Natl. Acad. Sci.,* 93, 12998–13003.

Ma, X. & W. Margolin (1999) Genetic and functional analyses of the conserved C-terminal core domain of *Escherichia coli* FtsZ. *J. Bacteriol.,* 181, 7531–7544.

Mallock, A. (1888) Determination of the viscosity of water. *Proc. R. Soc. Lond.,* 45, 126–132.

Mallock, A. (1896) Experiments on fluid viscosity. *Phil. Trans. R. Soc. Lond., Ser., A,* 187, 41–56.

Margolin, W. (2000) Themes and variations in prokaryotic cell division. *FEMS Microbiol. Rev.,* 24, 531–548.

Margolin, W. (2005) FtsZ and the division of prokayotic cells and organelles. *Nature Reviews Molecular Cell Biology,* 6, 862–871.

Marrington, R., T. R. Dafforn, D. J. Halsall, J. I. Macdonald, M. Hicks & A. Rodger (2005) Validation of new microvolume Couette linear dichroism cells. *Analyst,* 130, 1608–1616.

Marrington, R., T. R. Dafforn, D. J. Halsall & A. Rodger (2004a) Micro-Volume Couette Flow Sample Orientation for Absorbance and Fluorescence Linear Dichroism. *Biophys. J.,* 87, 2002–2012.

Marrington, R., E. Small, A. Rodger, T. R. Dafforn & S. G. Addinall (2004b) FtsZ Fiber Bundling Is Triggered by a Conformational Change in Bound GTP. *J. Biol. Chem.,* 279, 48821–48829.

Mendieta, J., A. I. Rico, E. López-Viñas, M. Vicente, J. Mingorance, & P. Gómez-Puertas (2009) Structural and Functional Model for Ionic (K+/Na+) and pH Dependence of GTPase Activity and Polymerization of FtsZ, the Prokaryotic Ortholog of Tubulin. J. Mol. Biol., 390, 17-25.

Mileykovskaya, E. & W. Dowhan (2005) Role of membrane lipids in bacterial division-site selection. *Current Opinion in Microbiology*, 8, 135–142.

Mingorance, J., G. Rivas, M. Vélez, P. Gómez-Puertas & M. Vicente (2010) Strong FtsZ is with the force: mechanisms to constrict bacteria. *Trends in Microbiology*, 18, 348–356.

Mingorance, J., S. Rueda, P. Gomez-Puertas, A. Valencia & M. Vicente (2001) *Escherichia coli* FtsZ polymers contain mostly GTP and have a high nucleotide turnover. *Mol. Microbiol.,* 41, 83–91.

Mingorance, J., M. Tadros, M. Vicente, J. M. González, G. Rivas & M. Vélez (2005) Visualization of single Escherichia coli FtsZ filament dynamics with atomic force microscopy. *J. Biol. Chem.,* 280, 20909–20914.

Moffatt, B. A. & F. W. Studier (1986) Use of Bacteriophage T7 RNA Polymerase to Direct Selective High-level Expression of Cloned Genes. *J. Mol. Biol.,* 189, 113-130.

Mohammadi, T., G. E. J. Ploeger, J. Verheul, A. D. Comvalius, A. Martos, C. Alfonso, J. van Marle, G. Rivas & T. den Blaauwenet (2009) The GTPase activity of Escherichia coli FtsZ determines the magnitude of the FtsZ polymer bundling by ZapA *in vitro*. *Biochemistry*, 48, 11056-11066.

Moroz, P. E. (1980) Microanalytical ultracentrifuge. *Rev. Sci. Instrum.,* 51, 1247–1252.

Mukherjee, A., C. Cao & J. Lutkenhaus (1998) Inhibition of FtsZ polymerization by SulA, an inhibitor of septation in *Escherichia coli*. *Proc. Natl. Acad. Sci. USA*, 95, 2885–2890.

Mukherjee, A., K. Dai & J. Lutkenhaus (1993) *Escherichia coli* cell division protein FtsZ is a guanine nucleotide binding protein. *Proc. Natl. Acad. Sci. USA,* 90, 1053–1057.

Mukherjee, A. & J. Lutkenhaus (1994) Guanine nucleotide-dependent assembly of FtsZ into filaments. *Journal of Bacteriology*, 176, 2754–2758.

Mukherjee, A. & J. Lutkenhaus (1998) Dynamic assembly of FtsZ regulated by GTP hydrolysis. *EMBO J.*, 17, 462–469.

Mukherjee, A. & J. Lutkenhaus (1999) Analysis of FtsZ assembly by light scattering and determination of the role of divalent metal cations. *J. Bacteriol.*, 181, 823–832.

Nogales, E., K. H. Downing, L. A. Amos & J. Lowe (1998a) Tubulin and FtsZ form a distinct family of GTPases. *Nat. Struct. Biol.,* 5, 451–458.

Nogales, E., S. G. Wolf & K. H. Downing (1998b) Structure of the αβ tubulin dimer by electron crystallography. *Nature,* 391, 199–203.

Nordén, B. (1978) Applications of linear Dichroism Spectroscopy. *Appl. Spectrosc. Rev.*, 14, 157–248.

N'soukpoé-Kossi, C. N., S. Diamantoglou & H. A. Tajmir-Riahia (2008) DNase I – DNA interaction alters DNA and protein conformations. *Biochem. Cell Biol.*, 86, 244–250.

Ohashi, T., C. A. Hale, P. A. de Boer & H. P. Erickson (2002) Structural evidence that the P/Q domain of ZipA is an unstructured, flexible tether between the membrane and the C-terminal FtsZ-binding domain. *J. Bacteriol.,* 184, 4313–4315.

Oliva, M. A., S. C. Cordell & J. Löwe (2004) Structural insights into FtsZ protofilament formation. *Nature Struct. Mol. Biol.,* 11, 1243–1250.

Oliva, M. A., S. Huecas, J. M. Palacios, J. Martin-Benito, J. M. Valpuesta & J. M. Andreu (2003) Assembly of archaeal cell division protein FtsZ and a GTPase-inactive mutant into double-stranded filaments. *J. Biol. Chem.,* 278, 33562–33570.

Oliva, M. A., D. Trambaiolo & J. Löwe (2007) Structural Insights into the Conformational Variability of FtsZ. *J. Mol. Biol.,* 373, 1229–1242.

Ornstein, L. (1964) Dis electrophoresis. I. Background and theory. *Ann. N.Y. Acad. Sci.*, 121, 321–349.

Osawa, M., D. E. Anderson & H. P. Erickson (2008) Reconstitution of contractile FtsZ rings in liposomes. *Science,* 320, 792–794.

Osawa, M. & H. P. Erickson (2005) Probing the domain structure of FtsZ by random truncation and insertion of GFP. *Microbiology,* 151, 4033–4043.

Osteryoung, K. W. (2001) Organelle fission in eukaryotes. *Curr. Opin. Microbiol.,* 4, 639–646.

Pace, C. N., F. Vajdos, L. Fee, G. Grimsley & T. Gray (1995) How to measure and predict the molar absorption coefficient of a protein. *Protein Sci.,* 4, 2411–2423.

Pacheco-Gomez, R. (2008) Structural studies and assembly dynamics of the bacterial cell division protein FtsZ. MOAC Doctoral Training Centre. Warwick University. PhD.

Pacheco-Gomez, R., D. I. Roper, T. R. Dafforn & A. Rodger (2011) The pH dependence of polymerization and bundling by the essential bacterial cytoskeltal protein FtsZ. *PLoS One,* 6, e19369.

Panno, J. (2005) The Cell: Evolution of the First Organism. Facts on File.

Pichoff, S. & J. Lutkenhaus (2002) Unique and overlapping roles for ZipA and FtsA in septal ring assembly in *Escherichia coli*. *EMBO J.,* 21, 685–693.

Pichoff, S. & J. Lutkenhaus (2005) Tethering the Z ring to the membrane through a conserved membrane targeting sequence in FtsA. *Mol. Microbiol.,* 55, 1722–1734.

Pogliano, J. (2008) The bacterial cytoskeleton. *Curr. Opin. Cell Biol.,* 20, 19-27.

Popp, D., M. Iwasa, A. Narita, H. P. Erickson & Y. Maéda (2009) FtsZ condensates: an in vitro electron microscopy study. *Biopolymers,* 91, 340–350.

Quardokus, E. M. & Y. V. Brun (2002) DNA replication initiation is required for midcell positioning of FtsZ rings in *Caulobacter crescentus*. *Mol. Microbiol.,* 45, 605–616.

Raskin, D. M. & P. A. de Boer (1997) The MinE ring: an FtsZ-independent cell structure required for selection of the correct division site in *E. coli*. *Cell,* 91, 685–694.

Raskin, D. M. & P. A. de Boer (1999a) MinDE dependent pole-to-pole oscillation of division inhibitor MinC in *Escherichia coli. J. Bacteriol.,* 181, 6419–6424.

Raskin, D. M. & P. A. de Boer (1999b) Rapid pole-to-pole oscillation of a protein required for directing division to the middle of *Escherichia coli*. *Proc. Natl Acad. Sci. USA,* 96, 4971–4976.

Raychaudhuri, D. (1999) ZipA is a MAP-Tau homolog and is essential for structural integrity of the cytokinetic FtsZ ring during bacterial cell division. *EMBO J.*, 18, 2372–2383.

Raychaudhuri, D. & J. T. Park (1992) *Escherichia coli* cell-division gene *ftsZ* encodes a novel GTP-binding protein. *Nature*, 359, 251–254.

Raymond, A., S. Lovell, D. Lorimer, J. Walchli, M. Mixon, E. Wallace, K. Thompkins, K. Archer, A. Burgin & L. Stewart (2009) Combined protein construct and synthetic gene engineering for heterologous protein expression and crystallization using Gene Composer. *BMC Biotechnology*, 9, 37–51.

Regamey, A., E. J. Harry & R. G. Wake (2000) Mid-cell Z ring assembly in the absence of entry into the elongation phase of the round of replication in bacteria: coordinating chromosome replication with cell division. *Mol. Microbiol.*, 38, 423–434.

Reichmann, M. E., S. A. Rice, C. A. Thomas & P. Doty (1954) A further examination of the molecular weight and size of desoxypentose nucleic acid. *J. Am. Chem. Soc.,* 76, 3047–3053.

Rivas, G., A. López, J. Mingorance, M. J. Ferrándiz, S. Zorrilla, A. P. Minton, M. Vicente & J. M. Andreu (2000) Magnesium-induced linear self-association of the FtsZ bacterial cell division protein monomer. The primary steps for FtsZ assembly. *J. Biol. Chem.*, 275, 11740–11749.

Rodger, A. (1993) Linear dichroism. *Methods Enzymol.*, 226, 232–258.

Rodger, A. (2008) How to study DNA and proteins by linear dichroism spectroscopy. *Science Progress*, 91, 377–396.

Rodger, A. & B. Nordén (1997) Circular dichroism and linear dichroism. Oxford University Press.

Rodger, A., J. Rajendra, R. Marrington, M. Ardhammar, B. Nordén, J. D. Hirst, A. T. B. Gilbert, T. R. Dafforn, D. J. Halsall, C. A. Woolhead, C. Robinson, T. J. T. Pinheiro, J. Kazlauskaite, M. Seymour, N. Perez & M. J. Hannon (2002) Flow oriented linear dichroism to probe protein orientation in membrane environments. *Phys. Chem. Chem. Phys.*, 4, 4051–4057.

Romberg, L. & P. A. Levin (2003) Assembly dynamics of the bacterial cell division protein FtsZ: Poised at the edge of stability. *Annu. Rev. Microbiol.*, 57, 125–154.

Romberg, L. & T. J. Mitchison (2004) Rate-limiting guanosine 5 -triphosphate hydrolysis during nucleotide turnover by FtsZ, a prokaryotic tubulin homologue involved in bacterial cell division. *Biochemistry*, 43, 282–288.

Romberg, L., M. Simon & H. P. Erickson (2001) Polymerization of Ftsz, a bacterial homolog of tubulin.Is assembly cooperative? *J. Biol. Chem.*, 276, 11743–11753.

Rosenberg, A. H., B. N. Lade, D. S. Chui, S. W. Lin, J. J. Dunn & F. W. Studier (1987) Vectors for selective expression of cloned DNAs by T7 RNA polymerase. *Gene.*, 56, 125–135.

Rothfield, L., S. Justice & J. Garcia-Lara (1999) Bacterial cell division. *Annu. Rev. Genet.*, 33, 423–448.

Rueda, S., M. Vicente & J. Mingorance (2003) Concentration and assembly of the division ring proteins FtsZ, FtsA, and ZipA during the *Escherichia coli* cell cycle. *J. Bacteriol.*, 185, 3344–3351.

Scheffers, D. J., J. G. de Wit, T. den Blaauwen & A. J. Driessen (2001) Substitution of a conserved aspartate allows cation-induced polymerization of FtsZ. *FEBS Lett.*, 494, 34–37.

Scheffers, D. J., J. G. de Wit, T. den Blaauwen & A. J. Driessen (2002) GTP hydrolysis of cell division protein FtsZ: evidence that the active site is formed by the association of monomers. *Biochemistry*, 41, 521–529.

Serdyuk, I. N., N. R. Zaccai & J. Zaccai (2007) Methods in molecular biophysics: Structure, Dynamics, Function-Chapter D4 Analytical ultracentrifugation. Cambridge University Press.

Shen, B. & J. Lutkenhaus (2009) The conserved C-terminal tail of FtsZ is required for the septal localization and division inhibitory activity of MinC(C)/MinD. *Mol. Microbiol.,* 72, 410–424.

Shih, Y. L. & L. Rothfield (2006) The bacterial cytoskeleton. *Microbiol. Mol. Biol. Rev.,* 70, 729–754.

Shiomi, D. & W. Margolin (2007) The C-terminal domain of MinC inhibits assembly of the Z ring in *Escherichia coli. J. Bacteriol.,* 189, 236–243.

Small, E. & S. G. Addinall (2003) Dynamic FtsZ polymerization is sensitive to the GTP to GDP ratio and can be maintained at steady state using a GTP-regeneration system. *Microbiology,* 149, 2235–2242.

Small, E., R. Marrington, A. Rodger, D. J. Scott, K. Sloan, D. Roper, T. R. Dafforn & S. G. Addinall (2007) FtsZ Polymer-bundling by the *Escherichia coli* ZapA Orthologue, YgfE, Involves a Conformational Change in Bound GTP. *J. Mol. Biol.,* 369, 210–221.

Sossong, T. M., M. R. Brigham-Burke, P. Hensley & K. H. Pearce (1999) Self-activation of guanosine triphosphatase activity by oligomerization of the bacterial cell division protein FtsZ. *Biochemistry,* 38, 14843–14850.

Stricker, J., P. Maddox, E. D. Salmon & H. P. Erickson (2002) Rapid assembly dynamics of the Escherichia coli FtsZ-ring demonstrated by fluorescence recovery after photobleaching. *Proc. Natl. Acad. Sci. USA,* 99, 3171–3175.

Studier, F. W., A. H. Rosenberg, J. J. Dunn & J. W. Dubendorff (1990) Use of T7 RNA polymerase to direct expression of cloned genes. *Methods Enzymol.,* 185, 60–89.

Suefuji K, R. Valluzzi & D. RayChaudhuri (2002) Dynamic assembly of MinD into filament bundles modulated by ATP, phospholipids, and MinE *Proc. Natl. Acad. Sci. USA,* 99, 16776–16781.

Sugimoto, S., K. Yamanaka, S. Nishikori, A. Miyagi, T. Ando & T. Ogura (2010) AAA+ chaperone ClpX regulates dynamics of prokaryotic cytoskeletal protein FtsZ. *J. Biol. Chem.,* 285, 6648–6657.

Sun, Q. & W. Margolin (1998) FtsZ Dynamics during the Division Cycle of Live *Escherichia coli* Cells. *J. Bacteriology,* 180, 2050–2056.

Svedverg, T., & K. D. Pederson (1940) The Ultracentrifuge, Oxford University Press, London.

Szeto, T. H., S. L. Rowland, L. I. Rothfield & G. F. King (2002) Membrane localization of MinD is mediated by a C-terminal motif that is conserved across eubacteria, archaea, and chloroplasts. *Proc. Natl. Acad. Sci. USA,* 99, 15693–15698.

Trusca, D. & D. Bramhill (2002) Fluorescent assay for polymerization of purified bacterial FtsZ cell-division protein. *Anal. Biochem.,* 307, 322–329.

Trusca, D., S. Scott, C. Thompson & D. Bramhill (1998) Bacterial SOS checkpoint protein SulA inhibits polymerization of purified FtsZ cell division protein. *J. Bacteriol.,* 180, 3946–3953.

Vaughan, S., B. Wickstead, K. Gull & S. G. Addinall (2004) Molecular evolution of FtsZ protein sequences encoded within the genomes of archaea, bacteria, and eukaryota. *J. Mol. Evol.,* 58, 19–29.

Wang, X. & J. Lutkenhaus (1993) The FtsZ protein of Bacillus subtilis is localized at the division site and has GTPase activity that is dependent upon FtsZ concentration. *Mol. Microbiol.,* 9, 435–442.

Weart, R. B. & P. A. Levin (2003) Growth rate dependent regulation of medial FtsZ ring formation in *Bacillus subtilis*. *J. Bacteriol.,* 185, 2826–2834.

Webb, M. R. (1992) A continuous spectrophotometric assay for inorganic phosphate and for measuring phosphate release kinetics in biological systems. *Proc. Natl. Acad. Sci. USA,* 89, 4884–4887.

Weiss, D. S. (2004) Bacterial cell division and the septal ring. *Mol. Microbiol.,* 54, 588–597.

White, E. L., L. J. Ross, R. C. Reynolds, L. E. Seitz, G. D. Moore & D. W. Borhani (2000) Slow polymerization of Mycobacterium tuberculosis FtsZ. *J. Bacteriol.,* 182, 4028–4034.

Wilson, C. M. (1979) Studies and critique of Amido Black 10B, Coomassie Blue R, and Fast Green FCF as stains for proteins after polyacrylamide gel electrophoresis. . *Ana. Biochem.,* 96, 263–278.

Wilson, C. M. (1983) Staining of proteins on gels: Comparison of dyes and procedures. *Methods on Enzymology,* 91, 236–247.

Wyatt, P. J. (1993) Light scattering and the absolute characterization of macromolecules. *Anal. Chim. Acta,* 272, 1–40.

Yu, X. C. & W. Margolin (1997) Ca^{2+}-mediated GTP-dependent dynamic assembly of bacterial cell division protein FtsZ into asters and polymer networks *in vitro*. *EMBO J.*, 16, 5455–5463.

APPENDIX: PAPER SUBMITTED

Tetramerisation of ZapA is required for FtsZ bundling

Xi Cheng[†‡], Raúl Pacheco-Gómez[*‡], Matthew R. Hicks[*,†], Corinne J. I. Smith[§], David Roper[§], Stephen Addinall[†], Alison Rodger[†], Tim R. Dafforn[*]

[*]School of Biosciences, University of Birmingham, Edgbaston, Birmingham, West Midlands, B15 2TT UK.

[†]Department of Chemistry, University of Warwick, Coventry, Warwickshire, CV4 7AL UK.

[§]Department of Biological Sciences, University of Warwick, Coventry, Warwickshire, CV4 7AL UK.

Page Heading Title: Tetramerisation of ZapA is required for FtsZ bundling

[‡]These authors contributed equally to the work.

Corresponding Author: Dr Timothy R. Dafforn, School of Bioscience, University of Birmingham, Edgbaston, Birmingham, West Midlands B15 2TT. UK. Tel. +44 121 4145881, Fax +44 121 414 5925, Email: t.r.dafforn@bham.ac.uk

Abstract

Prokaryotic cell division is a highly orchestrated process requiring the formation of a wide range of biomolecular complexes. Perhaps the most important of these being formed by the prokaryotic tubulin homolog FtsZ, a polymer-forming GTPase. FtsZ assembles into a ring (the Z-ring) on the inner surface of the inner membrane at the site of cell division. The Z-ring then acts as a recruitment site for at least ten other proteins which form the division apparatus. One of these proteins, ZapA, acts to enhance lateral associations between FtsZ fibres to form larger bundles. Previously we have expressed, purified, and crystallised ZapA and demonstrated that it exists as a tetramer. We also showed that ZapA binds to FtsZ polymers, strongly promoting their bundling, while inhibiting of their GTPase activity by inducing conformational changes in bound nucleotide. In this study we investigate the importance of the tetramerisation of ZapA on function. We generate a number mutant forms of ZapA with the aim of disrupting the dimer:dimer interface. We show that one of these mutants I83E is fully folded and binds to FtsZ but is a constitutive dimer. Using this mutant we show that tetramerisation is a requirement for both FtsZ bundling, and GTPase modulation activities.

Keywords: FtsZ, ZapA, Cytokinesis, Linear Dichroism, Fibre, Bundling, Tetramerisation

INTRODUCTION

FtsZ is a ubiquitous bacterial protein that acts as a foundation for the molecular assemblies that underpin cell wall and membrane remodelling during cytokinesis [1, 2]. Structural and phylogenic studies of FtsZ have shown that it is related to the cytoskeletal protein tubulin [3]. Like tubulin, FtsZ can be induced to polymerise upon addition of GTP leading to the formation of unbranched FtsZ fibres [4, 5]. In bacterial cells, FtsZ monomers associate together during division to form a fibrous ring on the inner surface of the inner membrane at the cellular midpoint [6, 7]. The ultrastructure of the FtsZ ring is thought to be made up of individual FtsZ fibres bundled together to produce the scaffold for a much larger macromolecular structure. This larger structure involves a number of other proteins including integral membrane proteins (FtsI, FtsQ, FtsL, FtsN, ZipA, FtsW and FtsK) as well as soluble factors (FtsA) [8, 9]. These proteins form a complex set of interactions which have been delineated using both two hybrid methods [10-12] and spectroscopic methods [13]. The bundling of FtsZ has been shown to be induced by a number of factors including divalent cations, guanine nucleotide derivatives and crowding agents [14-19], although it is thought that under physiological conditions co-proteins such as ZapA and ZipA control FtsZ bundling [15, 20-22]. Although, interestingly ZapA deletion strains show no observable phenotype [23].

A number of studies have shown that ZapA induces bundling of FtsZ [24-26]. The *E. coli* ZapA (also known as YgfE) gene codes for a 12.6 KDa peptide chain that associates to form a dimer of dimers [24-26]. The crystal structure of *Pseudomonas Aerugenosa* ZapA [24] shows that the protein folds into a two domain structure [24].

The N-terminal domain is globular and is hypothesised to contain the FtsZ binding region [25]. The C-terminus domain is mainly α-helical and seems to perform 2 functions. Firstly it mediates interactions between dimers of ZapA while at the same time the extended nature of this domain ensures that the globular domains of each dimer are kept spatially separate. This separation of FtsZ binding regions is thought to underlie the FtsZ bundling function. A recent study has made elegant use of electron microscopy to suggest that ZapA links FtsZ polymers like rungs link the uprights of a ladder [25].

Our own work has examined the molecular events that occur upon binding of ZapA to FtsZ [26]. We have used linear dichroism spectroscopy (LD) to probe the configuration and conformation of GTP bound to ZapA. We have shown that ZapA induces a change in GTP conformation similar to that induced by high levels of divalent cations [26, 27]. This conformational rearrangement seems to distort the active site of FtsZ leading to an observed decrease in GTP hydrolysis [25, 26]. However at that time it was not possible to determine whether this conformation rearrangement was the result of a direct interaction between ZapA and the FtsZ active site, or whether it was indirectly as a result of FtsZ bundling itself altering FtsZ active site conformation.

In this work we aimed to produce mutant forms of ZapA that are unable to form a tetramer. The resulting mutant forms of ZapA are used to gain an understanding of the molecular interactions that stabilise the ZapA dimer. In addition a constitutively dimeric ZapA is used to prove that ZapA tetramerisation is required for FtsZ bundling and GTPase inhibition.

EXPERIMENTAL

MATERIALS AND METHODS

Chemicals and reagents. All chemicals used were of analytical grade and only molecular grade biology water (0.1 µm filtered) or deionised water was used. Unless otherwise stated, the providers were: Sigma-Aldrich (USA), Calbiochem (USA), Fisher Scientific (USA), Fluka Chemika (Germany) or Helena Biosciences (UK).

Purification of *Escherichia coli* FtsZ

Escherichia coli FtsZ was overproduced and purified following the method described by Mukherjee and Lutkenhaus [28]. However, some modifications were introduced: the pooled, dialysed ion-exchange DEAE-Sepharose column fractions were subject to a 20% ammonium sulfate precipitation that removes the acetate kinase activity from the FtsZ preparation and the last chromatography step was omitted. Instead, the 20% ammonium sulfate precipitation fraction was further purified by a further ion-exchange chromatography on DEAE-Sepharose.

Production of ZapA mutants DNA

Site directed mutations where introduced into the ZapA gene using the Quikchange® methodology (Stratagen, La Jolla, US). The gene was then introduced into the pETDuet-1 expression vector containing an N-terminal six-histidine tag. The gene sequences within these constructs were confirmed by DNA sequencing.

Overproduction and purification of *E. coli* ZapA

E. coli Zap A was overproduced and purified using the methods detailed previously by Small *et al.* [26].

Linear Dichroism

LD measurements were performed using the same equipment setup as our previous study [29]. Briefly, all measurements were made at room temperature using either a Jasco J-715 or J-815 spectropolarimeter adapted for *LD* spectroscopy. Samples were aligned in the light beam using a custom made Couette cell (Crystal Precision Optics, Rugby) and consists of a cylindrical cross section sleeve with a removable quartz capillary (sealed at one end with Araldite Rapid) held centrally with respect to its circular face by a rubber “O”-ring. An annular gap of ~0.25 mm between the quartz rod suspended from the demountable lid and inner capillary wall was created. The rod and the centre of the capillary were aligned so that the capillary was able to rotate freely. The sample (25–60 µL) was placed into the capillary and the lid and rod were then lowered into position. Upon rotation of the capillary (the rod remains stationary) a shear force is induced across the sample. The cylindrical sleeve has two windows for the light to pass through to make contact with the sample. The voltage applied to the motor that rotates the outer quartz cylinder is controlled electronically to allow the sample solution to be maintained with the highest possible degree of alignment. Data were collected using an interval scan measurement program that was available within the Jasco software. This enabled single full wavelength scans from 350–190 nm to be collected every minute at a scanning speed of 200 nm min^{-1}, data pitch 0.5 seconds and thus the monitoring of the kinetics of polymerisation across the whole wavelength spectrum. Baselines of

data collected after depolymerisation of FtsZ were subtracted from all spectra. It should be noted that the data collected can at this stage only be interpreted qualitatively rather than quantitatively. The time taken to load and assemble the capillary *LD* unit and start of the analysis (dead time) was about 60 seconds.

Circular Dichroism

Circular Dichroism data were collected in either a Jasco J715 or J815 spectropolarimeter. Samples were prepared in rectangular demountable quartz cells with appropriate pathlengths for the experiment being undertaken. Scans were made between 300 nm and 190 nm with a band width of 1 nm and scan speed of 100 nm/min. An average of 16 scans were taken for each experiment and a background spectrum (measured in the absence of protein) subtracted.

Analytical Ultracentrifugation (AUC)

Samples of ZapA were centrifuged at 40,000 rpm at 4 ^{o}C for 16 hours in an 8 cell An-50 Ti rotor in a Beckman XLI analytical ultracentrifuge. Migration of the protein during centrifugation was monitored by measuring the distribution of absorbance at 220 nm across the sample in the centrepiece at 200 consecutive time points. These data were then analysed using SEDFIT [30, 31] using a c(s) model. Molecular masses were calculated using a c(M) model. Protein partial specific volumes, buffer viscosities and densities were all calculated using SEDNTERP.

Dynamic Light Scattering

Electron Microscopy

We examined the morphology of FtsZ polymers formed in the absence and presence of ZapA by negative stain electron microscopy. 5 microlitres of the sample mixture (44 μM ZapA and/or 11 μM FtsZ) were deposited onto a glow-discharged carbon grid for 1 minute and the sample blotted and stained with 1% uranyl acetate solution. The grids were then imaged in a JEOL 2011 200 KV transmission electron microscope equipped with a LaB6 filament at 10,000 X magnification.

GTPase assay

The experiment was performed using an EnzChek® Phosphate Assay Kit (Invitrogen, USA) based on manufacturer's instructions from Invitrogen. The sample was prepared as described in the results. The mixture was then incubated at 25 °C for 10 minutes and placed into a 0.5 cm cuvette. The change in absorbance that results from the production of phosphate was then measured using a Jasco V-550 spectrometer at room temperature, and the wavelength was set up at 360 nm. The Abs_{360} was zeroed before adding 0.2 mM GTP into the sample.

Right-angle light-scattering assay

Right-angle light-scattering (90^o angle light scattering) measurements were carried out based on the assay used in our previous study [27]. FtsZ polymerization and subsequent steady state and depolymerization were measured by 90^o angle light scattering at room temperature (~25 ^oC) using a Perkin Elmer LS50B spectrofluorimeter. The excitation and emission wavelengths set at 450 nm unless

otherwise stated and the excitation and emission slit widths were set at 2.5 nm. For the standard polymerization assay, FtsZ to a final concentration of 11 μM was incubated at 25 ^{o}C in 50 mM MES-KOH (2-[N-Morpholino]ethane sulfonic acid) (altering the pH between 6.0-7.0 depending on the reaction), 50 mM KCl, and 10 mM $MgCl_2$ (polymerization buffer) for 15 minutes. FtsZ in the polymerization buffer was then added to the 0.3 cm path length fluorimeter cuvette (50 μL nominal volume). The cuvette was then placed in the fluorimeter at RT and a baseline was collected for approximately 10 minutes. The polymerization reaction was then initiated by the addition of 0.2 mM GTP. The reading at time zero is the first reading after the cuvette was returned to the chamber following nucleotide addition. The elapsed time for the nucleotide addition step was between 10 and 20 seconds and data points were collected every second.

Pelleting assay

800 μl reaction mixtures were made up in polymerisation buffer, 50 mM MES-KOH, pH 6.5, 10 mM $MgCl_2$, and 50 mM KCl. A final concentration of 2.5 mM GTP was added to the mixture to induce FtsZ polymerisation. This concentration of GTP is in excess of that required to maintain FtsZ in is fibrillar form throughout the pelleting experiments. FtsZ fibres and associated proteins were then sedimented by centrifuging in a TLA 100.2 rotor at 220,000*xg*, at 20°C for 10 minutes. The supernatant was then removed and any pellet resuspended in 80 μl of 50 mM TrisHCl, pH 8. Samples from both supernatant and pellet were then analysed by 15% SDS-PAGE.

RESULTS

Design of dimeric ZapA

In order to ascertain whether the formation of tetramer of ZapA is a prerequisite for FtsZ fibre bundling a number of point mutations were made in the *ZapA* gene to perturb the dimer:dimer interface (see table 1). These mutations were designed using a homology model of ZapA based on the X-ray crystal structure of *Pseudomonas aeruginosa* ZapA [24] a close relative of *E. coli* ZapA. Each mutation was chosen on the basis that it formed part of one of the two dimer interfaces. We defined these interfaces as being:

1) The C-terminal coiled coil dimerisation interface: the interface formed in the middle of ZapA structure made up of two pairs of coiled coils. Disruption of this interface would lead to a dimer with an intact globular head.

2) The coiled coil: globular head dimerisation interface: this interface is made up of the N-terminus of one α-helix from one monomer and the globular head region of another. Disruption of this interface would lead to a dimer connected only by the central C-terminal coiled coil region.

Examination of the inter-subunit contacts of the amino acids in these two interfaces provided 8 candidate positions for point mutations at positions 11, 17, 41, 59, 63, 64, 75 and 83. Two of these are in the coiled coil dimerisation region and 6 in the coiled coil: globular head dimerisation region. To disrupt these interfaces amino acid substitutions were chosen that either reduced the hydrophobicity of the region (V17E, L41Q, L59Q, I83E) or increased the size of the residue (F11W, Y63W, Y73W) or removed a potential charge:charge interaction (E64L). In each case the

substitution was designed to alter the interface enough to disrupt the oligomerisation without disrupting the underlying structure of the protein.

Production of Mutant ZapA

Each mutant gene was inserted into the pETDuet vector which contained a hexa-histidine tag on the N-terminal in order to aid purification. After induction with IPTG all but one of the proteins expressed well, E64L failing to express in all attempts. Examination of the solubility of the remaining proteins showed that a second mutant, L59Q was prone to significant precipitation and was excluded from further study. The remaining 6 proteins were purified using immobilised metal ion chromatography to produce a samples with >90% purity in all cases (an example of the purification of WT ZapA is shown in figure 2a).

To ascertain whether the mutants were folded, far-UV circular dichroism spectra were measured (an example of the data for WT and I83E ZapA is shown in figure 2b). These show that in all cases the fold has not been significantly altered by the amino acid substitutions a result that is confirmed by later AUC experiments.

Oligomerisation of ZapA Mutants

The oligomerisation state of each ZapA mutant protein was measured using sedimentation velocity analytical ultracentrifugation Wild type ZapA has a sedmentation coefficient of 1.5 S which is consistent with a tetrameric state of ZapA. Examination of these data for each of the mutant proteins shows that 4 (F11W, L41Q, Y63W, Y73W) had sedimentation coefficients close to that for the WT indicating that in each of these cases the tetrameric structure remained (see figure

3). Two of the mutations showed significant divergence from that of the WT, with sedimentation coefficients of 1.2S and 1S for V17E and I83E respectively. In order to determine the masses of the I83E and V17E mutants to a higher degree of precision each protein was subjected to sedimentation equilibrium analysis (data not shown). These studies showed that only data from I83E fitted to that expected for a dimer of ZapA, whereas data from V17E was more consistent with a model describing a dimer:tetramer equilibrium.

From these data it is clear that only the I83E mutation has induced dissociation of the ZapA tetramer to form a dimer and it is therefore this mutant form that is used for the rest of the study.

Effect of I83E on FtsZ fibre formation

The key aim of this study is to determine whether the tetrameric structure of ZapA is a requirement for its FtsZ fibre bundling function. To test this hypothesis dimeric ZapA (I83E) was subjected to a series biophysical studies that analysed its ability to bundle fibres. In each experiment the concentration of FtsZ was kept close to that found in the cell (approx. 5μM) [32].

FtsZ Co-pelleting assay

Our previous studies of ZapA function [26] and those of others [24] have used ultracentrifugation to sediment FtsZ fibres and any bound proteins, ZapA in this case, in order to demonstrate an interaction between the two proteins. If our hypothesis is correct, that a ZapA dimer should still bind to FtsZ, then such a pelleting assay should still result in the co-sedimentation of ZapA. Whereas, if the mutations have

disrupted the structure of ZapA to a greater degree, then no sedimentation should be observed. Examination of the results of the experiment (Figure 4) shows that, like WT ZapA, I83E ZapA does preferentially co-sediment with FtsZ indicating that the interaction site between FtsZ and ZapA remains intact. It is also clear that significant amounts of FtsZ and ZapA remain in solution during the experiment. This suggests that in this experimental format the FtsZ fibres are not efficiently sedimented at the G used in the experiment. However this does not effect the observation that both WT and mutant ZapA proteins co-associate with FtsZ.

Dynamic light scattering

To further confirm that I83E was interacting with FtsZ dynamic light scattering (DLS) experiments were carried out. Samples of WT and I83E were mixed with FtsZ and the size of the resulting complex measured (Table 2). These data shown that for FtsZ alone a size is determined which is very close to that predicted for the FtsZ monomer. The addition of WT ZapA increases the size of the complex which has dimensions close to that expected for one ZapA tetramer and one FtsZ. In contrast the complex between I83E ZapA and FtsZ seems to be larger than that of WT alone but smaller than the WT complex. The dimensions of this complex is consistent with those of a dimeric ZapA in complex with one FtsZ monomer (i.e. half the size of the WT ZapA:FtsZ complex). Taken together these data confirm that I83E can form a complex with FtsZ while providing insights that confirm the FtsZ ladder with ZapA rungs model.

Right angled light scattering

We have shown previously that right angled light scattering provides a good measure of both FtsZ polymerisation [26] and ZapA induced FtsZ fibre bundling. Upon addition of GTP to FtsZ the light scattering signal shows a characteristic response, increasing very rapidly, then reaching a plateau before returning to baseline when the GTP supply is exhausted (see figure 5). The addition of WT ZapA at a range of stoichiometries (from 1:1 to 1:4 FtsZ:ZapA) to the reaction has the effect of significantly increasing the maximal light scattering encountered during the reaction, while also increasing the time that the high level of light scattering persists. By contrast, the addition of the I83E mutant (stoichiometries ranging from 1:1 to 1:4 ftsZ:ZapA) to FtsZ during a comparable experiment leads to no change in the light scattering response when compared to FtsZ alone. This indicates that I83E is no longer able to induce bundling of FtsZ fibres.

Linear dichroism

Our previous studies have pioneered the use of linear dichroism spectroscopy to monitor both FtsZ fibre morphology and formation kinetics [26, 27]. Measurements of the kinetics of FtsZ fibre formation show a very similar trace to that observed for light scattering (see figure 6). This is the result of the fibres produced during the experiment aligning in shear flow, and hence becoming “visible” to LD, the monomeric units of FtsZ remaining invisible. We have previously shown that the addition of ZapA crosslinks the FtsZ fibres increasing their rigidity leading to an increase in intensity of the LD signal. Measurement of the LD signal changes in a reaction that contains both FtsZ and I83E (at 1:2 and 1:4 FtsZ:ZapA stoichometries)

shows minimal signal enhancement or shape change again indicating that the mutant does not bundle FtsZ.

Effect of I83E on FtsZ fibre morphology

Electron microscopy has been used by ourselves [26, 27] and others [24] to examine changes in the morphology of FtsZ during fibre formation and bundling. In these studies monomeric FtsZ and tetrameric ZapA appear as roughly spherical particles (Figure 7A & B). Examination of a sample containing both ZapA and FtsZ but without GTP shows the formation of slightly larger particles perhaps the product of ZapA:FtsZ complexes (Figure 7C). Incubation of FtsZ with GTP in the absence of ZapA leads to the formation of fine fibres (Figure 7D) which thicken upon the inclusion of wildtype ZapA (Figure 7E). However addition of I83E to FtsZ under the same conditions shows no significant change in FtsZ bundling (Figure 7E). This agrees with the observation that I83E does not alter either light scattering or LD of FtsZ fibres.

Effect of I83E on the GTPase activity of FtsZ

The FtsZ fibre form is sustained by the presence of GTP which binds between FtsZ monomers in the polymer acting like a “glue” holding the monomers within the fibre together. However FtsZ also acts as a GTPase, hydrolysing GTP and hence reducing the amount of free GTP in solution. While the GTP concentration is maintained above a critical concentration, FtsZ forms a complex with the GTP leading to the propagation of a polymeric form. Ourselves [26] and others have

observed that ZapA does not simply induce FtsZ bundling, but it also reduces the rate at which FtsZ hydrolyses GTP [26] (figure 8). This reduction in GTP hydrolysis rate was thought to be either a direct result of the interaction of ZapA with the FtsZ catalytic machinery or the influence of the FtsZ bundling induced by ZapA. In the presence of I83E we are able to show only a modest depression in the rate of phosphate release and hence hydrolysis of GTP by FtsZ (at stoichiometries of 1:2 and 1:4 FtsZ:ZapA) (figure 8). The equivalent experiment with WT ZapA substituted for the mutant shows a larger reduction in phosphate release compared to the mutant. This correlates well with observations from light scattering and LD which show that the length of time that FtsZ remains in the fibre form for a given amount of GTP is not increased in the presence of I83E ZapA. Whereas for WT ZapA the FtsZ fibre form is sustained as the GTPase activity of FtsZ is inhibited reducing the rate of GTP hydrolysis and hence allowing the GTP concentration to be maintained above the threshold required to support FtsZ polymerisation.

DISCUSSION

This study examined the influence of the oligomerisation state of ZapA on its function as an FtsZ bundling agent. Previous studies of *E. coli and Pseudomonas aerugenosa* ZapA [24, 26] have shown that both proteins exist in a dimer:tetramer equilibrium. Low *et al.* [24] propose that this equilibrium may be shifted towards tetramer when ZapA is bound to FtsZ. An examination of the X-ray crystal structure of the ZapA dimer clearly shows the potential for a dimer:dimer interface, which would lead to a protein assembly with two globular domains separated by an extended coiled coil domain. It therefore seemed likely that the association between two dimers of ZapA on different FtsZ fibres could underlie the mechanism of ZapA induced FtsZ fibre bundling with the extended tetramer bridging two FtsZ fibres. However the presence of a ZapA dimerisation equilibrium in solution has made it difficult to explicitly conclude that such a mechanism is correct.

To determine whether this mechanism is correct we set out to produce a mutant form of ZapA where the tetramerisation equilibrium is firmly in favour of dimeric ZapA. By mutating the dimer:dimer interface we were able to produce a form of ZapA (I83E) which under experimental conditions only exists as a dimer. The site of the I83E mutation in the coiled coil region of ZapA provides some information on the forces that hold the ZapA tetramer together making it clear that, the coiled coil domain of ZapA is essential to maintaining ZapA tetramer. It is also clear that this interaction is a relatively dynamic one as it only required a single amino acid substitution to completely abrogate the interaction. Examination of the secondary structure of the I83E showed that although the dimer:dimer interaction was disrupted the protein still remains folded.

The production of a constitutive ZapA dimer allowed us to probe a number of aspects of ZapA function. Firstly, FtsZ co-pelleting assays show that I83E ZapA is still able to bind to FtsZ. This shows for the first time that ZapA tetramerisation is not a prerequisite for FtsZ binding. These data are backed up the DLS experiments which show that both ZapA proteins form complexes with FtsZ. It is therefore clear that a tetramerisation of ZapA is not required for binding, and by inference it is likely that the FtsZ binding region of ZapA is in a region separate from the tetramerisation interface in the structure.

Our second observation is that dimeric ZapA does not induce bundling of FtsZ. This is a clear confirmation of previously hypothesised models [24-26] that indicate that ZapA tetramers bridge FtsZ fibres leading to fibre bundling. The work also adds weight to recent work that proposes that ZapA not only bundles but acts to crosslink and stabilise FtsZ fibres *in vitro* [33] helping to drive the helix to ring transition of the FtsZ polymer [34] . Recent work by Mohammadi *et al.* [25] has suggested that the histidine tagged form of ZapA (like that used here) can, in some instances, influence the interaction with FtsZ. In their study they suggest that ZapA has 4 FtsZ binding sites with one ZapA dimer binding to adjacent FtsZ monomers in a fibre and that addition of histidine tags to ZapA can block one of these sites. However it is clear that even in this single occluded site state WT ZapA can still bundle FtsZ. The observations of Mohammadi *et al.* [25] therefore do not alter the observation in this study that dimeric ZapA cannot bundle FtsZ. Thereby making the observations included in this work relevant to the *in vivo* situation. In our previous work both on FtsZ [27] alone and FtsZ [26] in the presence of ZapA we have shown that the GTPase activity of the FtsZ can be modulated by the binding of cofactors. In the former study we showed that the GTPase activity could be depressed in the

presence of small molecules, with particular reference to divalent cations like Ca^{2+}. We also showed that fibre bundling was coincident with this reduction in activity. In a second study we showed the ZapA could also produce the same FtsZ fibre bundling alongside a reduced GTP hydrolysis rate. However in both studies we were unable to establish whether these changes in fibre lateral association were directly linked to changes in GTPase activity. The development of a dimer-only mutant of ZapA (I83E) allows us to understand in more detail the inter-relationship between fibre bundling and GTPase activity. Examination of the results from work shows that although the dimeric ZapA is able to bind to FtsZ it no longer induces a change in the GTPase activity. This suggests strongly that it is lateral association of FtsZ fibres that drives the decrease in FtsZ GTPase activity. A logical extension of this work would also indicate that divalent cations are able to alter GTPase activity by inducing FtsZ bundling. These observations have implications for our understanding of the FtsZ fibre formation process *in vivo*. It is clear from this work that FtsZ has evolved to modulate its own GTPase rate and hence its persistence in the polymeric state as a function of lateral association. ZapA is able to enhance the formation of lateral association stabilising the fibre structure both mechanically and kinetically, by virtue of the decrease in GTPase activity.

Taken together this study has produced the first ZapA to be a constitutive dimer and has used this reagent to clarify the mechanism of both ZapA induced FtsZ fibre bundling and bundling induced GTPase suppression.

Tables and figures

Table 1

Point Mutation	Predicted position in structure	Purification	Oligomerisaton state
F11W	Coiled coil: Globular head Dimerisation region	Yes	Tetramer
V17E	Coiled coil: Globular head Dimerisation region	Yes	Dimer:Tetramer
L41Q	Coiled coil: Globular head Dimerisation region	No	-
L59Q	Coiled coil: Globular head Dimerisation region	Yes	Tetramer
Y63W	Coiled coil: Globular head Dimerisation region	Yes	Tetramer
E64L	Coiled coil: Globular head Dimerisation region	Yes	Tetramer
Y75W	Coiled Coil tetramerisation region	Yes	Tetramer
I83E	Coiled Coil tetramerisation region	Yes	Dimer

Table 2

Protein	Diameter from DLS (angstroms)	Model Configuration	Diameter from Model (angstroms)
FtsZ	70		50
FtsZ:WT ZapA	130		120
FtsZ:I83E ZapA	90		80

Figure 1 Sequence alignment of *E. coli* ZapA (Top) and *P. Aeruginosa* ZapA (Bottom) (identical residues shown in bold). Arrows show the position of mutants.

Figure 2 a) 15% SDS-PAGE gel. Lane 1, molecular mass standard; Lane 2, ZapA eluted from the Ni^{2+}-sepharose affinity column using a 0-500 mM imidazole gradient. B) CD spectra of purified WT (solid line) and I83E ZapA (dashed line).

Figure 3 The results of sedimentation velocity experiments of WT (solid line) and mutants I83E (dashed line) and V17E (dotted line) ZapA (44 μM) in polymerisation buffer (50 mM MES-KOH, pH 6.5, 10 mM $MgCl_2$ and 50 mM KCl) showing the dimeric nature of I83E.

Figure 4 15% SDS-PAGE gel where M is marked for protein marker; S and P are marked for supernatant and pellet respectively. Where present, FtsZ and ZapA were at 11 μM and 22 μM in polymerization buffer (50 mM MES-KOH, pH 6.5, 10 mM $MgCl_2$ and 50 mM KCl). (1) wild type ZapA + GTP, (2) FtsZ + GTP, (3) FtsZ + wild type ZapA + GTP, (4) ZapA mutant I83E + GTP, (5) FtsZ + GTP, (6) FtsZ + ZapA mutant I83E + GTP.

Figure 5 Right angled light scattering measurements of ZapA induced bundling of FtsZ. Experiment carried out by preincubating ZapA (11μM, 22μM, 33μM, 44 μM) with FtsZ (11 μM) in polymerisation buffer (50 mM MES-KOH, pH 6.5, 10 mM $MgCl_2$ and 50 mM KCl) and then initiating with the addition of GTP. Changes in the light scattered by the sample is then measured as a function of time. A) The upper trace demonstrates the increase in light scattering observed when WT ZapA is added to

FtsZ. All other traces overlay one another at the bottom of the graph. B) shows an expanded view of A) focusing on the behaviour of FtsZ alone and FtsZ with I83E ZapA at the same concentrations as for WT ZapA showing that there is no significant difference between light scattering changes FtsZ with I83E and FtsZ alone.

Figure 6 LD measurements of ZapA induced bundling of FtsZ alone (solid line) with WT ZapA (22μM (grey small dash), 44 μM (grey large dash)) and I83E (22μM (black small dash), 44 μM (black large dash)). The experiment was carried out by preincubating WT ZapA or I83E ZapA (22μM, 44 μM) with FtsZ (11 μM) in polymerisation buffer (50 mM MES-KOH, pH 6.5, 10 mM $MgCl_2$ and 50 mM KCl) and then initiating polymerisation with the addition of 0.2 mM GTP. The change in LD signal at 210 nm versus time was then monitored.

Figure 7. Measurement of GTPase activity of FtsZ alone (solid black line) and in the presence of WT (grey lines) and I83E (black dashed lines) ZapA on FtsZ GTPase. These data show that the addition of I83E ZapA has no effect on FtsZ GTPase activity in contrast to the reduction in activity induced by the presence of WT ZapA. FtsZ (11 μM) was mixed with either WT or I83E ZapA (22 μM, 44 μM) in polymerisation buffer (50 mM MES-KOH, pH 6.5, 10 mM $MgCl_2$ and 50 mM KCl). 0.2 mM GTP was then added to the reaction medium and the release of phosphate resulting from FtsZ mediated GTP hydrolysis was measured as a difference in absorbance at 360 nm between the reagents and the products. Each data set has been expressed as a percentage of the final equilibrium value.

Figure 8 Electron microscopy of the products of FtsZ and ZapA. (A) 11 μM FtsZ in polymerisation buffer; (B) 44 μM ZapA in polymerisation buffer; (C) 11 μM FtsZ and 44 μM ZapA in polymerisation buffer; (D) 11 μM FtsZ in the presence of 0.2 mM GTP; (E) 0.2 mM GTP was added into premixed 11 μM FtsZ and 44 μM WT ZapA; (F) 0.2 mM GTP was added into premixed 11 μM FtsZ and 44 μM I83E ZapA; each sample was then 5 times diluted with water for imaging. Bars, 200 nm.

Figure 1

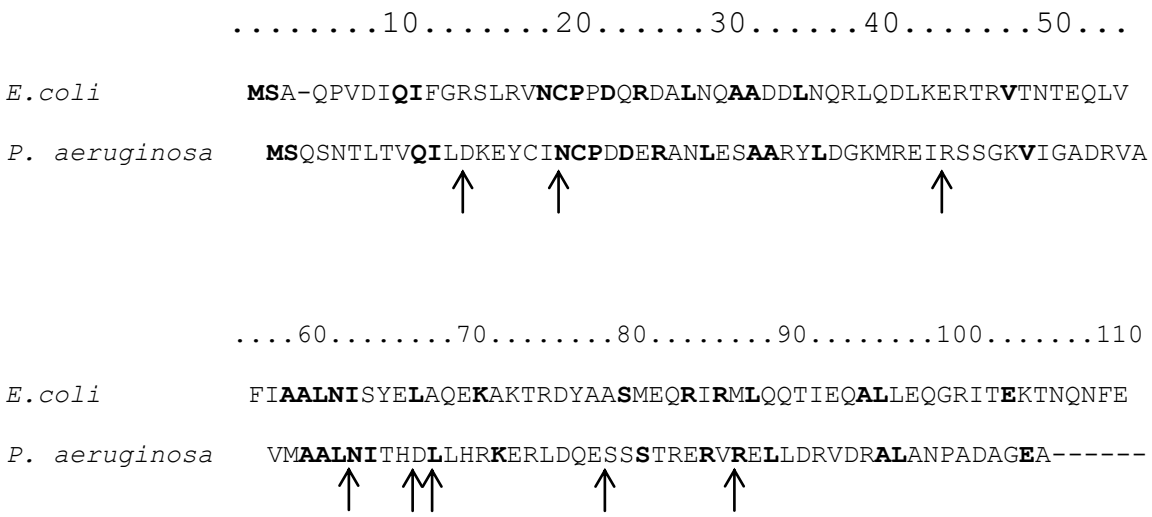
.....10.....20.....30.....40.....50...
E.coli MSA-QPVDIQIFGRSLRVNCPPDQRDALNQAADDLNQRLQDLKERTRVTNTEQLV
P. aeruginosa MSQSNTLTVQILDKEYCINCPDDERANLESAARYLDGKMREIRSSGKVIGADRVA
....60.....70.....80.....90.....100.....110
E.coli FIAALNISYELAQEKAKTRDYAASMEQRIRMLQQTIEQALLEQGRITEKTNQNFE
P. aeruginosa VMAALNITHDLLHRKERLDQESSSTRERVRELLDRVDRALANPADAGEA------

Figure 2

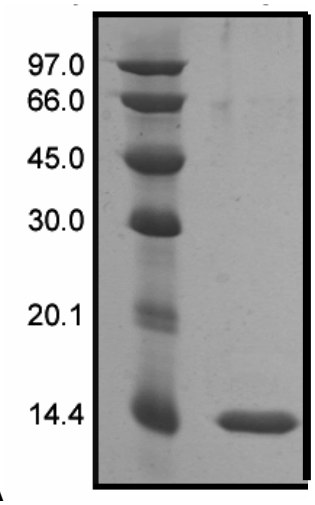
97.0
66.0
45.0
30.0
20.1
14.4

A

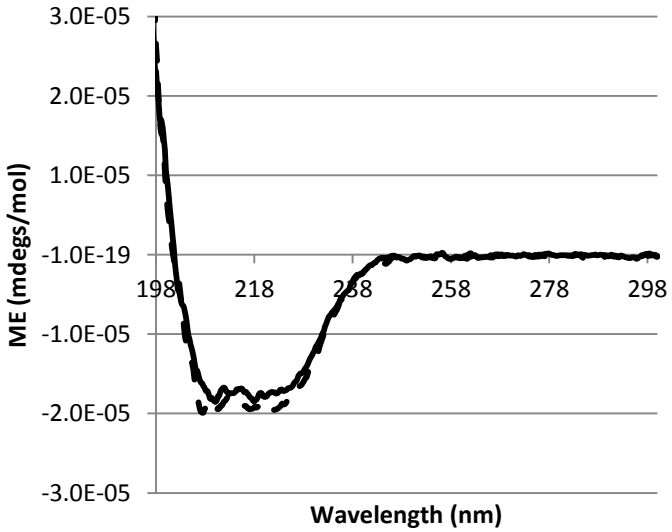
3.0E-05
2.0E-05
1.0E-05
-1.0E-19
-1.0E-05
-2.0E-05
-3.0E-05
ME (mdegs/mol)
198
218
238
258
278
298
Wavelength (nm)

B

Figure 3

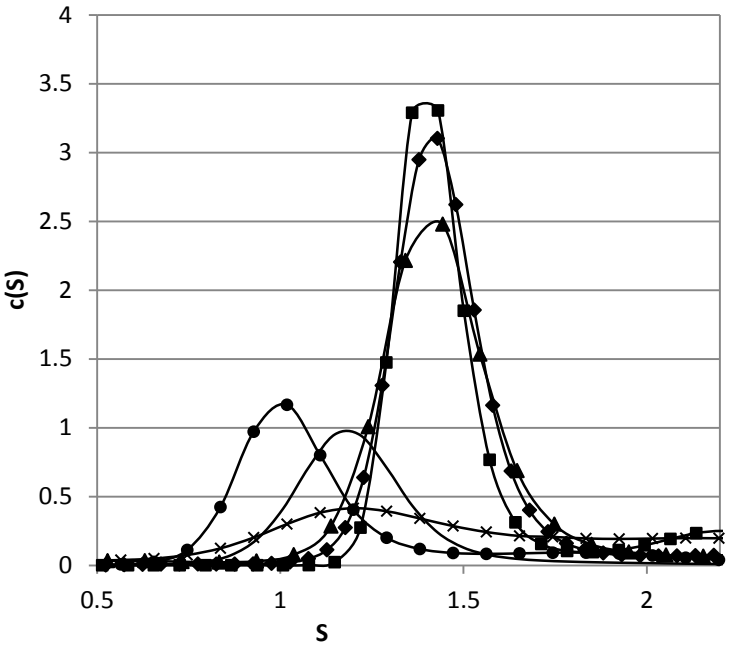

Figure 4

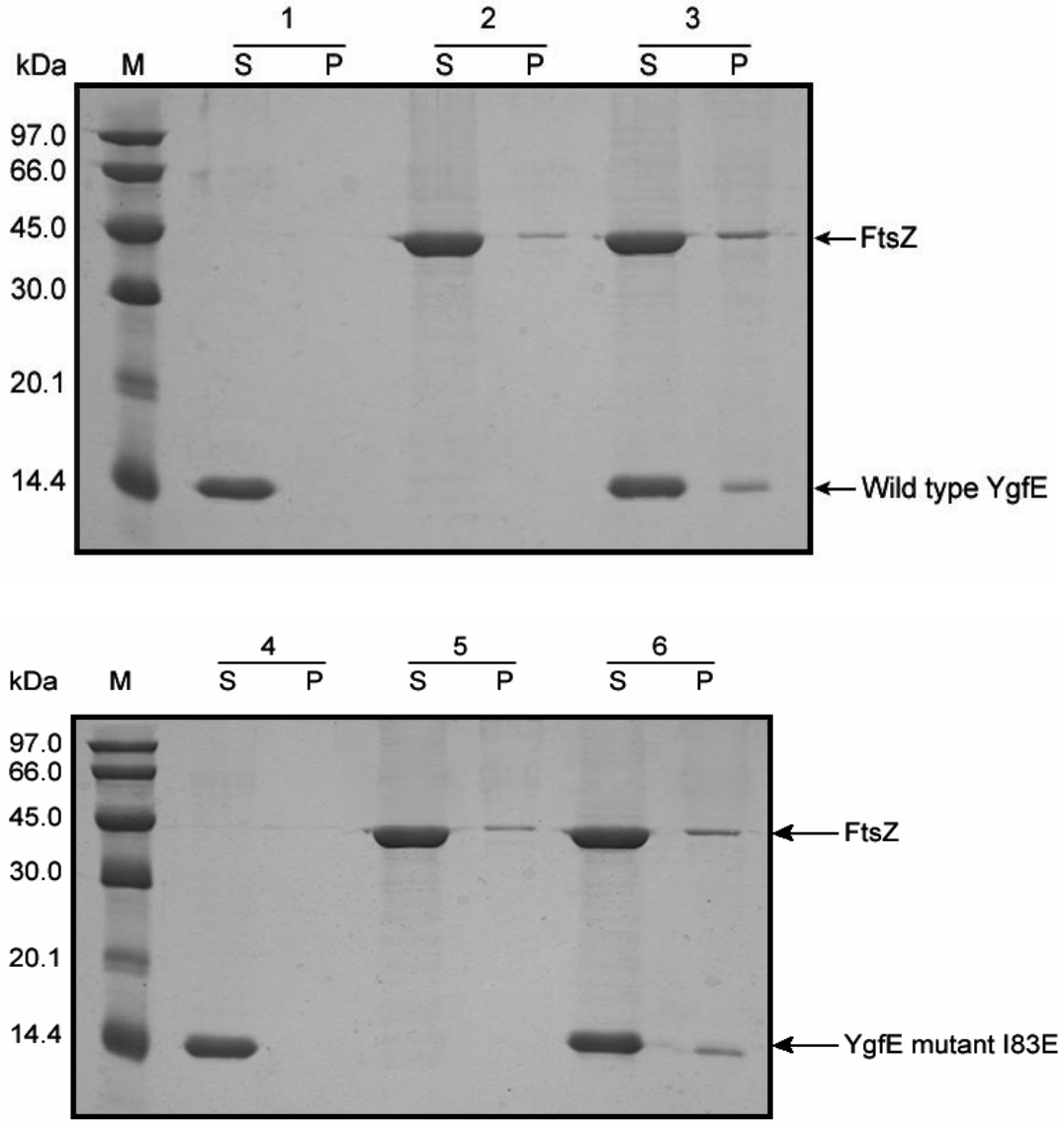
1
2
3
kDa
M
S
P
S
P
S
P
97.0
66.0
45.0
30.0
20.1
14.4
FtsZ
Wild type YgfE
4
5
6
kDa
M
S
P
S
P
S
P
97.0
66.0
45.0
30.0
20.1
14.4
FtsZ
YgfE mutant I83E

Figure 5

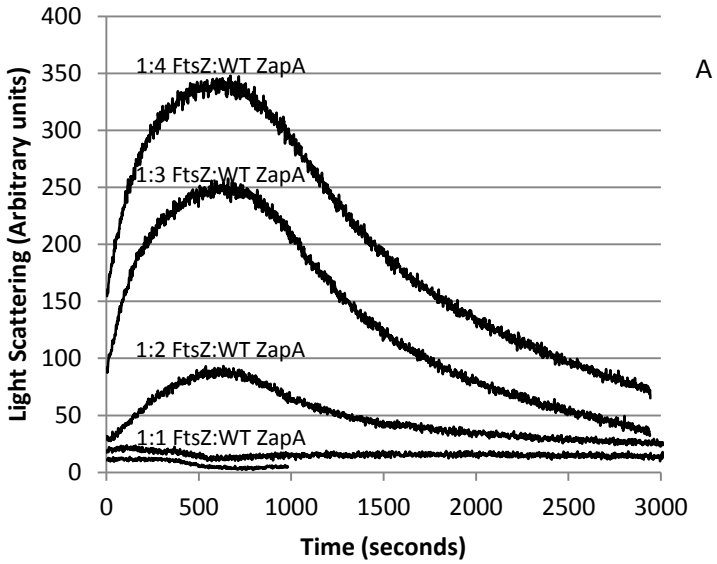
400
350
300
250
200
150
100
50
0
Light Scattering (Arbitrary units)
1:4 FtsZ:WT ZapA
1:3 FtsZ:WT ZapA
1:2 FtsZ:WT ZapA
1:1 FtsZ:WT ZapA
0
500
1000
1500
2000
2500
3000
Time (seconds)

A

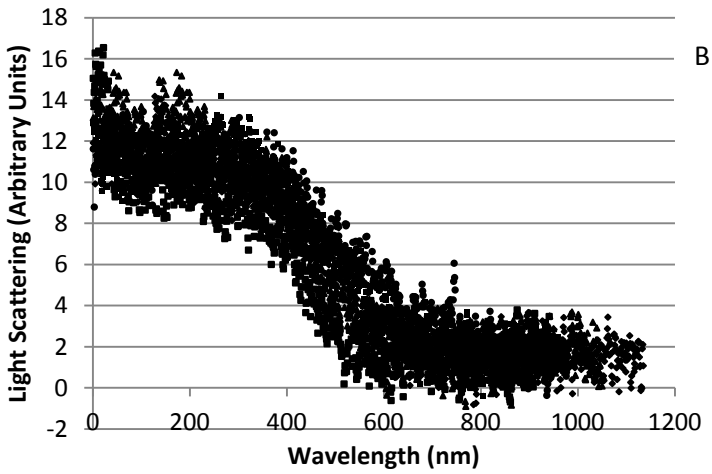
18
16
14
12
10
8
6
4
2
0
-2
Light Scattering (Arbitrary Units)
0
200
400
600
800
1000
1200
Wavelength (nm)

B

Figure 6

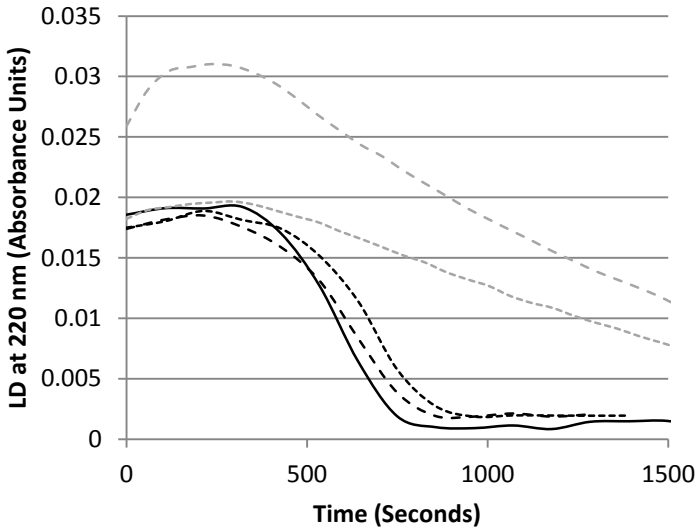
0.035
0.03
0.025
0.02
0.015
0.01
0.005
0
LD at 220 nm (Absorbance Units)
0
500
1000
1500
Time (Seconds)

Figure 7

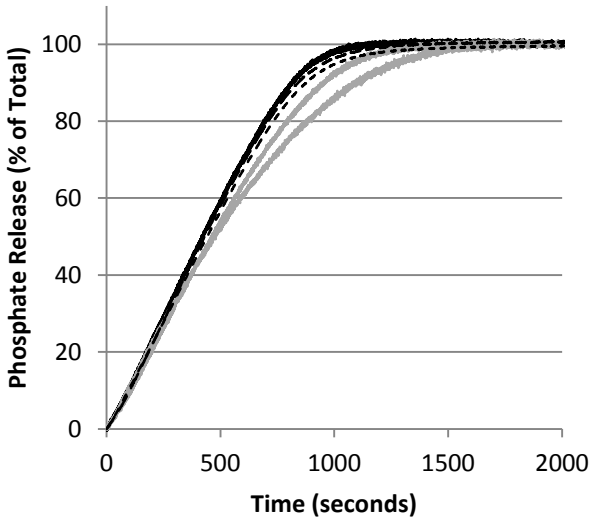
Phosphate Release (% of Total)
100
80
60
40
20
0
0
500
1000
1500
2000
Time (seconds)

E

E

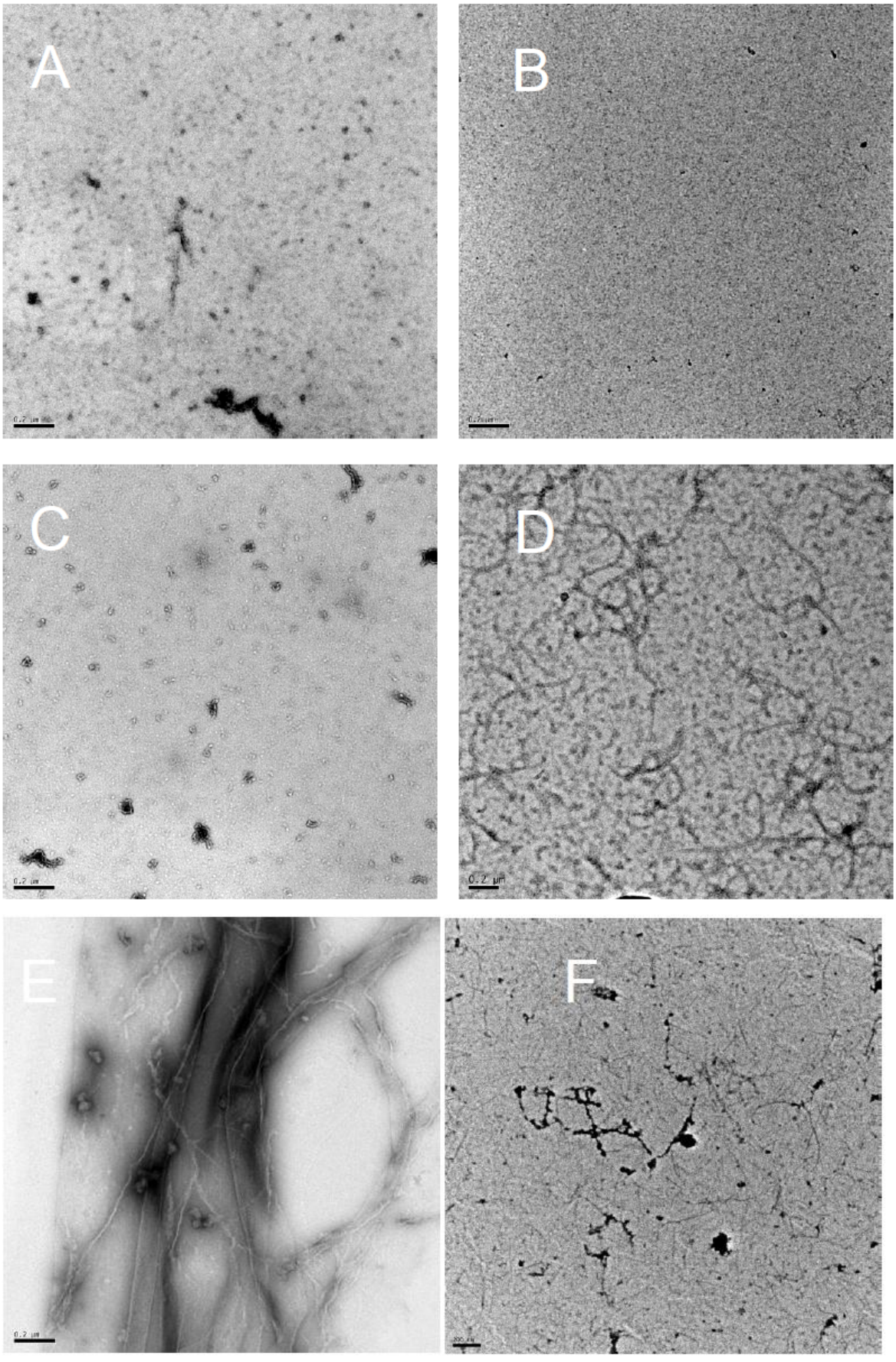
A
B
C
D
E
F

References

1. Adams, D.W. and J. Errington, *Bacterial cell division: assembly, maintenance and disassembly of the Z ring.* Nat. Rev. Microbiol, 2009. **7**(9): p. 642-53.
2. Margolin, W., *Sculpting the bacterial cell.* Curr Biol, 2009. **19**(17): p. R812-22.
3. Addinall, S.G. and B. Holland, *The tubulin ancestor, FtsZ, draughtsman, designer and driving force for bacterial cytokinesis.* J. Mol. Biol., 2002. **318**(2): p. 219-36.
4. Romberg, L. and P.A. Levin, *Assembly dynamics of the bacterial cell division protein FTSZ: poised at the edge of stability.* Ann. Rev. Microbiol., 2003. **57**: p. 125-54.
5. Romberg, L. and T.J. Mitchison, *Rate-limiting guanosine 5'-triphosphate hydrolysis during nucleotide turnover by FtsZ, a prokaryotic tubulin homologue involved in bacterial cell division.* Biochemistry, 2004. **43**(1): p. 282-8.
6. Bramhill, D. and C.M. Thompson, *GTP-dependent polymerization of Escherichia coli FtsZ protein to form tubules.* Proc. Natl. Acad. Sci. U S A, 1994. **91**(13): p. 5813-7.
7. Mukherjee, A. and J. Lutkenhaus, *Guanine nucleotide-dependent assembly of FtsZ into filaments.* J. Bacteriol., 1994. **176**(9): p. 2754-8.
8. Goehring, N.W. and J. Beckwith, *Diverse paths to midcell: assembly of the bacterial cell division machinery.* Curr. Biol., 2005. **15**(13): p. R514-26.
9. Vicente, M. and A.I. Rico, *The order of the ring: assembly of Escherichia coli cell division components.* Mol. Microbiol., 2006. **61**(1): p. 5-8.
10. Di Lallo, G., et al., *Use of a two-hybrid assay to study the assembly of a complex multicomponent protein machinery: bacterial septosome differentiation.* Microbiology, 2003. **149**(Pt 12): p. 3353-9.
11. Karimova, G., N. Dautin, and D. Ladant, *Interaction network among Escherichia coli membrane proteins involved in cell division as revealed by bacterial two-hybrid analysis.* J. Bacteriol., 2005. **187**(7): p. 2233-43.
12. Wang, X., et al., *Analysis of the interaction of FtsZ with itself, GTP, and FtsA.* J. Bacteriol., 1997. **179**(17): p. 5551-9.

13. Alexeeva, S., et al., *Direct interactions of early and late assembling division proteins in Escherichia coli cells resolved by FRET.* Mol. Microbiol., 2010. **77**(2): p. 384-98.
14. Gonzalez, J.M., et al., *Essential cell division protein FtsZ assembles into one monomer-thick ribbons under conditions resembling the crowded intracellular environment.* J. Biol. Chem., 2003. **278**(39): p. 37664-71.
15. Gueiros-Filho, F.J. and R. Losick, *A widely conserved bacterial cell division protein that promotes assembly of the tubulin-like protein FtsZ.* Genes. Dev., 2002. **16**(19): p. 2544-56.
16. Mukherjee, A. and J. Lutkenhaus, *Dynamic assembly of FtsZ regulated by GTP hydrolysis.* EMBO J., 1998. **17**(2): p. 462-9.
17. Mukherjee, A. and J. Lutkenhaus, *Analysis of FtsZ assembly by light scattering and determination of the role of divalent metal cations.* J. Bacteriol., 1999. **181**(3): p. 823-32.
18. Rivas, G., J.A. Fernandez, and A.P. Minton, *Direct observation of the enhancement of noncooperative protein self-assembly by macromolecular crowding: indefinite linear self-association of bacterial cell division protein FtsZ.* Proc. Natl. Acad. Sci. U S A, 2001. **98**(6): p. 3150-5.
19. Small, E. and S.G. Addinall, *Dynamic FtsZ polymerization is sensitive to the GTP to GDP ratio and can be maintained at steady state using a GTP-regeneration system.* Microbiology, 2003. **149**(Pt 8): p. 2235-42.
20. Hale, C.A. and P.A. de Boer, *Recruitment of ZipA to the septal ring of Escherichia coli is dependent on FtsZ and independent of FtsA.* J. Bacteriol., 1999. **181**(1): p. 167-76.
21. Hale, C.A., A.C. Rhee, and P.A. de Boer, *ZipA-induced bundling of FtsZ polymers mediated by an interaction between C-terminal domains.* J. Bacteriol., 2000. **182**(18): p. 5153-66.
22. Liu, Z., A. Mukherjee, and J. Lutkenhaus, *Recruitment of ZipA to the division site by interaction with FtsZ.* Mol. Microbiol., 1999. **31**(6): p. 1853-61.
23. Anderson, D.E., F.J. Gueiros-Filho, and H.P. Erickson, *Assembly dynamics of FtsZ rings in Bacillus subtilis and Escherichia coli and effects of FtsZ-regulating proteins.* J. Bacteriol., 2004. **186**(17): p. 5775-81.
24. Low, H.H., M.C. Moncrieffe, and J. Lowe, *The crystal structure of ZapA and its modulation of FtsZ polymerisation.* J. Mol. Biol., 2004. **341**(3): p. 839-52.
25. Mohammadi, T., et al., *The GTPase activity of Escherichia coli FtsZ determines the magnitude of the FtsZ polymer bundling by ZapA in vitro.* Biochemistry, 2009. **48**(46): p. 11056-66.
26. Small, E., et al., *FtsZ polymer-bundling by the Escherichia coli ZapA orthologue, YgfE, involves a conformational change in bound GTP.* J. Mol. Biol., 2007. **369**(1): p. 210-21.
27. Marrington, R., et al., *FtsZ fiber bundling is triggered by a conformational change in bound GTP.* J. Biol. Chem., 2004. **279**(47): p. 48821-9.
28. Mukherjee, A. and J. Lutkenhaus, *Purification, assembly, and localization of FtsZ.* Methods Enzymol., 1998. **298**: p. 296-305.
29. Marrington, R., et al., *Micro-volume couette flow sample orientation for absorbance and fluorescence linear dichroism.* Biophys. J., 2004. **87**(3): p. 2002-12.
30. Dam, J. and P. Schuck, *Sedimentation velocity analysis of heterogeneous protein-protein interactions: sedimentation coefficient distributions c(s) and asymptotic boundary profiles from Gilbert-Jenkins theory.* Biophys. J., 2005. **89**(1): p. 651-66.
31. Schuck, P., *Size-distribution analysis of macromolecules by sedimentation velocity ultracentrifugation and lamm equation modeling.* Biophys. J., 2000. **78**(3): p. 1606-19.
32. Rueda, S., M. Vicente, and J. Mingorance, *Concentration and assembly of the division ring proteins FtsZ, FtsA, and ZipA during the Escherichia coli cell cycle.* Journal of bacteriology, 2003. **185**(11): p. 3344-51.
33. Dajkovic, A., et al., *Cross-linking FtsZ polymers into coherent Z rings.* Mol. Microbiol., 2010. **78**(3): p. 651-68.
34. Monahan, L.G., A. Robinson, and E.J. Harry, *Lateral FtsZ association and the assembly of the cytokinetic Z ring in bacteria.* Mol. Microbiol., 2009. **74**(4): p. 1004-17.